To the Graduate Council:

I am submitting herewith a dissertation written by Timothy L. Davis entitle "Stratigraphy, Structure, and Metamorphism of a Crystalline Thrust Terrane, Western Inner Piedmont, North Carolina". I have examined the final copy of this dissertation for form and content and recommend that it be accepted in partial fulfillment of the requirements for the degree of Doctor of Philosophy, with a major in Geology.

Robert D. Hatcher, Jr., Major Professor

We have read this dissertation
and recommend its acceptance:

William M. Dunne

Theodore C. Labotka

Carl J. Remenyik

Accepted for the Council:

Associate Vice Chancellor
and Dean of the Graduate School

LITHOSTRATIGRAPHY, STRUCTURE, AND METAMORPHISM OF A CRYSTALLINE THRUST TERRANE, WESTERN INNER PIEDMONT, NORTH CAROLINA

A Dissertation

Presented for the

Doctor of Philosophy

Degree

The University of Tennessee, Knoxville

Timothy L. Davis

May, 1993

To the consummate teacher, my father
Michael E. Davis

ACKNOWLEDGMENTS

Acknowledgments and sincere thanks are extended to the many people that have been involved with or affected by this study, and by my tenure as Ph.D. student at The University of Tennessee. I have attempted to include all to those that have contributed to this endeavor, but here offer heartfelt apologies to those people I may have inadvertently forgotten.

Sincere gratitude goes to my major advisor, Dr. Robert D. Hatcher Jr., for his guidance, patience, and financial support through this project. I also thank Bob for all of the opportunities for professional development that he afforded me and other " Hatchery" students (e.g., field trips, short courses, meetings). Most of all, however, I thank Bob for treating me as a colleague, and welcoming my ideas and opinions concerning various aspects of southern Appalachian geology. I look forward to continued collaboration.

I thank all the other "Hatchery" students and staff (Beth, Peter, Angang, Mike, Greg, Mark, Janet, Jeff, John, Don, and Nancy) for being such an excellent crowd with whom to work, complain, and commiserate. Don McClanahan and Nancy Meadows are given special thanks for their assistance and putting up with the rest of us during hectic times before professional meetings and other deadlines. Former post-doc, John Tabor is greatly acknowledged for providing invaluable expertise and focus to this dissertation and his assistance in the field.

I would like to thank the other members of my dissertation committee, Drs. Bill Dunne and Ted Labotka in the Department of Geological Sciences for their insight and assistance during the course of this study. Bill Dunne is given special thanks for his assistance with the techniques and interpretations of quartz c-axis fabrics in high grade rocks. Dr. Carl Remenyik, Department of Engineering Science and Mechanics is thanked his insightful comments and for agreeing to serve on my committee at a late date. I also extend sincere appreciation to my colleagues at the North Carolina Geological Survey for their patience during the final phases this project.

Financial support for this project was provided by National Science Foundation grant EAR – 9004604 awarded to Drs. R. D. Hatcher, Jr., and J. R. Tabor. This work was also supported by student research grants from the Southeastern Section of the Geological Society of America, Sigma Xi, and the Professors Honor Fund, Department of Geological Sciences, University of Tennessee. The Graduate School at The University of Tennessee is also thanked for a International Travel Grant that assisted with my travel to the John Ramsay Meeting in Zurich, Switzerland.

I thank the numerous friends Sally and I have made a UT (the list is too long) who have made this experience enjoyable and bearable. Above all, are Jeff (Chief) and Kelly Connelly, who have shared the "graduate school thing" with us both at Bowling Green and UT. On behalf of the Chief and myself, I apologize (fingers crossed) to all those people we have tormented along the way. We have truly enjoyed entertaining ourselves at your expense! Forgive us – for we know not what we do! To all, we look forward to maintaining these friendships and would welcome a visit or reunion at any time. Chris Olson and Ian Richards are thanked for their yeoman efforts in shooting slides for my dissertation defense.

To all of my family, especially Mom and Dad, I thank you for your unwavering love and encouragement that you have always given to me. I am very fortunate to have the support of such a wonderful family, no matter how strange they may be! I hope now that this project is completed that we can see more of each other.

Finally, I thank my wife and best friend, Sally, for her constant encouragement, love, and support (mental, physical, and financial) during this tedious process. Sally deserves my most special thanks and love for putting many aspects of her life, and ours together, on hold to see me through this endeavor; a true sacrifice for one with such a dynamic personality. For this, I am truly fortunate and will always be grateful. I look forward to the next brush stroke. I also give thanks to Sally's (my extended) family for their constant encouragement. I know they often wondered about what adventure I was leading her on over the past several years.

ABSTRACT

The geology of the western Inner Piedmont of North Carolina, from knowledge gained in an area called the Columbus Promontory, is characterized by a stack of crystalline thrust sheets. In this study the stratigraphic, structural, and metamorphic development of this crystalline thrust terrane was examined.

The lithostratigraphic framework of the Columbus Promontory is divisible into four distinct and mappable rock units that include the Henderson Gneiss, Sugarloaf gneiss, Poor Mountain Formation, and the Mill Spring complex. This lithostratigraphic framework helps define three crystalline thrust sheets within the Columbus Promontory herein, called the Tumblebug Creek, Sugarloaf Mountain, and Mill Spring thrust sheets. Rocks of the Poor Mountain Formation and Mill Spring complex are similar to lithostratigraphic units recognized elsewhere in the southern Appalachian eastern Blue Ridge and Inner Piedmont. Similarities in physical stratigraphy indicate that the Poor Mountain Formation and Mill Spring complex rocks are representatives of two regionally extensive (Virginia to Alabama) lithostratigraphic sequences that record deep– to shallow–water deposition along the Laurentian margin and include: a lower sequence consisting of Lynchburg–Ashe–Tallulah Falls–Mill Spring–Sandy Springs/New Georgia–type rocks, and an upper sequence consisting of Evington–Alligator Back–Coweeta–Chauga River/Poor Mountain–Jackson's Gap/Ropes Creek–type rocks. By analogy to these rocks, the Poor Mountain Formation and Mill Spring complex are also interpreted as part of the deep-water facies rocks deposited along the Laurentian margin. Including the rocks of the Columbus Promontory into this regionally correlative lithostratigraphy further supports previous interpretations (Hatcher, 1978a, 1989) that the same lithostratigraphy occurs in the eastern Blue Ridge and Inner Piedmont. In addition, this correlation also supports the interpretation (Hatcher, 1978a, 1989) that the same rock units occur on both sides of the Brevard fault zone and suggests that this

feature, although recognized as a major structural discontinuity, does not represent a terrane boundary.

Amphibolite comprises a significant component of the lithostratigraphy of the Columbus Promontory and is intercalated with other lithostratigraphic units of the Poor Mountain Formation and Mill Spring complex. Because relict igneous textures, sedimentary features, and contact relationships have been destroyed by high grade regional metamorphism and transposition, a whole–rock geochemical approach was undertaken to determine the protolith as well as fractionation trends, and possible paleotectonic settings. Niggli trends, AFM relationships, and normative mineralogy suggest an igneous protolith for amphibolite in both stratigraphic units, which was tholeiitic basalt. Covariation diagrams indicate that both suites are fractionated and that the trends can be explained by fractionation of olivine, plagioclase, clinopyroxene, garnet, and magnetite. This assemblage is similar to the low–pressure fractionation sequence commonly observed in mid–ocean ridges and suggests the Columbus Promontory amphibolites are MORB. Zr/Nb, Y/Nb ratios further define the suite as N–type MORB, with a possible P–type MORB component. Other tectonomagmatic discriminant diagrams employed in this study indicate a correlation of the Columbus Promontory suite primarily with ocean–floor basalts, but also indicate some island–arc influence. The possibility of mixed N– and P–type MORB components suggests extrusion of these basalts along a mid–ocean ridge adjacent to a mantle plume, whereas the combination of MORB and island–arc characteristics indicate a back–arc basin setting. In either case, an oceanic setting is indicated for the Columbus Promontory suite. These observations further support the interpretation that the Poor Mountain Formation, Mill Spring complex, and correlative rock units in the eastern Blue Ridge and Inner Piedmont were deposited, at least partly, on oceanic crust.

The dominant structure of the western Inner Piedmont of North Carolina, South Carolina, and northeast Georgia is a stack of penetratively deformed ductile to semi–brittle crystalline thrust sheets. The structural development of this part of the Inner Piedmont is examined herein using

data from crystalline thrust sheets in the Columbus Promontory in North Carolina, and the Tamassee area in adjacent South Carolina and NE Georgia. Structural analysis in both areas reveals a regionally consistent, five–phase deformation history. Although the western Inner Piedmont is polydeformed (D_1 to D_5), the D_2 and D_3 episodes were the most important and represent a deformation continuum. D_2 was penetrative and synchronous with the principal (Acadian?) metamorphic event in the western Inner Piedmont. D_3 generally represents late– to post–peak final emplacement of thrust sheets as coherent masses. The emplacement history and internal deformation of this crystalline thrust complex involved coeval $D_2 - D_3$ orogen–parallel (SW–directed) displacement within the westernmost Inner Piedmont and Brevard fault zone and orogen–oblique (W– directed) displacement in thrust sheets in the Inner Piedmont. Importantly, this geometry indicates that early (middle Paleozoic) Brevard fault zone motion was kinematically linked to the crystalline thrust sheets in the adjacent Inner Piedmont. It is proposed that these dominant flow paths (W and SW directed) in the foreshortening crust were driven by large–scale transpression or oblique convergence during the amalgamation of the crystalline southern Appalachians. S_2 mylonitic foliation is the most characteristic and kinematically important structural element within the Inner Piedmont. S_2 also strongly controlled development of other $D_2 - D_3$ structural elements in the western Inner Piedmont. Internal deformation and variations in orientation, kinematics, and geometry of $D_2 - D_3$ structural features are interpreted to result from gradients of flow within S_2. This resulted in a partitioned thrust–wrench transport parallel to the plane of S_2 mylonitic foliation driven by larger–scale tectonic processes. These observations indicate that S_2 is a regionally extensive shear surface along which extensive $D_2 - D_3$ displacement occurred and suggests the Inner Piedmont represents a region of crustal–scale shear.

The metamorphic history, and the relationship between metamorphism and deformation in the thrust sheets of the Columbus Promontory are best recorded by pelitic schist within the Sugarloaf Mountain thrust sheet. The Sugarloaf Mountain sheet thrust rocks of the Poor

Mountain Formation and upper Mill Spring complex over the Henderson Gneiss and other rocks of the western Inner Piedmont. Pelitic schist in the Sugarloaf Mountain thrust sheet contain a sillimanite–muscovite assemblage that is characteristic of thrust sheets throughout the western Inner Piedmont (e.g., Alto allochthon, Six Mile thrust sheet). Metamorphic textures and mineral zoning suggest sillimanite growth was the result of continuous reactions involving both garnet consumption and garnet growth following the metamorphic peak. These relationships also suggest that this sillimanite–muscovite assemblage is a post–peak rather than a prograde or peak metamorphic assemblage. Metamorphic textures and microstructural analysis indicate that growth of the sillimanite–muscovite was synkinematic with development of microstructures related to emplacement of the Sugarloaf Mountain thrust sheet. The implication of these observations is that emplacement of the Sugarloaf Mountain thrust sheet occurred along the retrograde portion of the P–T path followed by these rocks. Qualitative constraints on the nature of this retrograde P–T path, gained from field criteria, petrographic observations, mineral zoning and geothermobarometric estimates, indicate a general path of decompression and cooling, but with episodes of near isobaric cooling.

TABLE OF CONTENTS

CHAPTER PAGE

I. INTRODUCTION 1

II. LITHOSTRATIGRAPHY OF THE COLUMBUS PROMONTORY, WESTERN INNER PIEDMONT, NORTH CAROLINA 15

Introduction 15

Lithostratigraphic Framework of the Columbus Promontory 16

Previous Work 16

Proposed Stratigraphic Framework 17

Structural Significance 18

Field and Petrographic Characteristics of Lithostratigraphic Units 21

Henderson Gneiss 21

Sugarloaf Gneiss 34

Poor Mountain Formation 35

Amphibolite–hornblende gneiss 38

Garnet–mica schist 38

Quartzite–amphibolite 42

Mill Spring Complex 46

Upper Mill Spring complex 49

Lower Mill Spring complex 53

Regional Relationships 55

Correlation of Stratigraphic Units 55

Depositional Environment and Tectonic Implications 63

III. GEOCHEMISTRY OF AMPHIBOLITE FROM THE COLUMBUS PROMONTORY, WESTERN INNER PIEDMONT, NORTH CAROLINA 68

Introduction 68

Sampling and Analytical Techniques 69

Whole–rock Approach and Limitations 69

Protolith—Para vs. Orthoamphibolitic Nature 74

Fractionation Trends 78

Paleotectonic Setting 90

Constraints 90

Possible Paleotectonic Settings 91

Regional Consideration....103
IV. DEFORMATION HISTORY, KINEMATICS, AND PARTITIONING OF COEVAL OROGEN–OBLIQUE (E–W) AND OROGEN–PARALLEL (NE–SW) DUCTILE DEFORMATION, WESTERN INNER PIEDMONT, CAROLINAS AND NE GEORGIA....108
Introduction....108
Deformation History....113
D_1 Deformation....114
D_2 Deformation....114
D_3 Deformation....117
D_4 –D_5 Deformation....117
D_2 and D_3 Structures....120
D_2 Structures....120
Foliation....120
Folds....124
Faults....127
Lineation....129
Quartz c–axis fabrics....134
D_3 Structures....138
Folds....138
Faults....138
Discussion....139
Kinematics of Orogen–Parallel and Orogen–Oblique Deformation....139
Development and Kinematic Importance of the S_2 Mylonitic Foliation....145
V. METAMORPHIC AND MICROSTRUCTURAL DEVELOPMENT OF SILLIMANITE–BEARING PELITIC SCHIST IN THE SUGARLOAF MOUNTAIN THRUST SHEET, COLUMBUS PROMONTORY, WESTERN INNER PIEDMONT, NORTH CAROLINA....152
Introduction....152
General Characteristics of Metamorphism....155
Mineral Assemblage....155
Metamorphic Zone and Isograds....156
Metamorphic Conditions....157

Microstructure Defined By Assemblage A_1 160
Composite–Planar Fabrics 160
Garnet Porphyroblasts 166
Petrography and Chemistry of Mineral Phases in Assemblage A_1 166
Sampling and Analytical Techniques 166
Mineral Phases 171
Garnet 171
Garnet Zoning 171
Biotite 174
Plagioclase 177
Muscovite 177
Sillimanite 177
Quartz 184
Ilmenite 184
Petrogenesis of Assemblage A_1 184
Reaction Relationships 184
Geothermobarometry 191
Techniques 191
Results 194
Qualitative Constraints on the P–T Path During Emplacement of the Sugarloaf Mountain Thrust Sheet 196
VI. CONCLUSIONS 201
REFERENCES CITED 207
APPENDICES 224
APPENDIX A. STRUCTURAL DATA 225
APPENDIX B. ELECTRON MICROPROBE DATA 238
VITA 245

LIST OF TABLES

2–1. Modal analyses of the Henderson Gneiss from the Columbus Promontory. 25
2–2. Modal analyses of granitic gneiss within the Henderson Gneiss in the Columbus Promontory. 31
2–3. Modal analyses of the Sugarloaf Gneiss in the Columbus Promontory 36
2–4. Modal analyses of Poor Mountain schist from the Columbus Promontory.....41
2–5. Modal analyses of Poor Mountain amphibolite from the Columbus Promontory 45
2–6. Modal analyses of biotite gneiss–metagraywacke of the upper Mill Spring complex.....52
2–7. Modal analyses of porphyroclastic biotite gneiss–metagraywacke of the lower Mill Spring complex 54
2–8. Modal analyses of amphibolite of the lower Mill Spring complex.....56
3–1. XRF analyses of Poor Mountain amphibolite from the Columbus Promontory.....72
3–2. XRF analyses of lower Mill Spring complex amphibolite from the Columbus Promontory 73
5–1. Mineral compositions and estimated temperature and pressures for pelitic schist of the Sugarloaf Mountain thrust sheet.....192

LIST OF FIGURES

1–1. Tectonic subdivisions of the southern Appalachians showing the location of the Columbus Promontory (CP) 2
1–2. Geologic map (a) and cross section (b) of the Columbus Promontory 6
1–3. U.S. Geological Survey Eros Data Center radar mosaic (near range) of the southeast corner of the Knoxville 1° x 2° sheet that shows high relief of the Columbus Promontory 8
1–4. Index to topographic quadrangles included as part of the Columbus Promontory 11
2–1. Conceptual stratigraphic and structural model (cross section) for rock units in the Columbus Promontory (Inner Piedmont) and the adjacent eastern Blue Ridge 19
2–2. Outcrop belt of Henderson Gneiss in the western Inner Piedmont of North and South Carolina 22
2–3. Classification of igneous rocks from the Columbus Promontory based on modal compositions 26
2–4. Mosaic of field photographs of the Henderson Gneiss and Sugarloaf gneiss and a photomicrograph of the Henderson Gneiss 28
2–5. Mosaic of field photographs of the Tumblebug creek thrust, hand sample of the Poor Mountain amphibolite, and photomicrograph of the Poor Mountain amphibolite 32
2–6. Mosaic of photographs showing field exposure and hand sample of the Sugarloaf Mountain thrust, photomicrograph of the Sugarloaf Mountain thrust, and photomicrograph of garnet–mica schist of the Poor Mountain Formation 39
2–7. Quartz–feldspar–mica diagram comparing composition of metasedimentary rocks of the Columbus Promontory 43
2–8. Photo mosaics of exposures of Mill Spring complex rocks along Interstate 26 between the Green River and Columbus, North Carolina 47
2–9. Mosaic of photographs and photomicrographs of rocks of the Mill Spring complex 50

2–10. Proposed regional stratigraphic correlation of metasedimentary rocks of the eastern Blue Ridge and Inner Piedmont, including rocks of the Poor Mountain Formation and Mill Spring complex of the Columbus Promontory 58
2–11. Schematic cross section of the Laurentian margin showing the proposed depositional setting and regional relationship of stratigraphic units discussed in this chapter 65
3–1. Location of Columbus Promontory amphibolite samples selected for whole–rock XRF analysis 70
3–2. Niggli mg–c–(al–alk) and AFM plots for amphibolites of the Columbus Promontory. 76
3–3. Harker–type covariation diagrams using TiO_2 as index of fractionation 79
3–4. Harker–type diagrams using Zr as fractionation index 81
3–5. Covariation diagram using immobile trace elements (Nb, Y, Zr, and Ti) and minor element Cr 84
3–6. Covariation diagram of Al_2O_3 and TiO_2 vs. MgO 88
3–7. Tectonomagmatic discriminant diagrams showing MORB character of the Columbus Promontory amphibolites 93
3–8. Tectonomagmatic discriminant diagrams showing ocean–floor basalt characteristics of the Columbus Promontory suite 96
3–9. Cr vs. Ti and Cr vs. V tectonomagmatic discriminant diagrams 98
3–10. Ti vs V tectonomagmatic discriminant diagram 100
3–11. Regional variations of geochemical composition (Ti vs. Zr) and tectonic setting of amphibolites in the eastern Blue Ridge and Inner Piedmont 104
4–1. Geologic map (a) and cross section (b) of the western Inner Piedmont in the Tamassee area 109
4–2. Outcrop photographs of D_2–D_3 structures from the Columbus Promontory (a, b, e, and f) and Tamassee area (c and d) 115
4–3. Mosaic of photographs and photomicrographs of D_2 lineations and microstructures from the Columbus Promontory 118
4–4. Lower–hemisphere equal–area projections of structural data a) Tamassee area, and b) Columbus Promontory 121
4–5. Outcrop photographs of D_2 faults and folds from the Columbus Promontory 125

4–6. Distribution and orientation of mineral stretching lineations from the Tamassee area....130
4–7. Distribution and orientation of mineral stretching lineations from the Columbus Promontory....132
4–8. Contoured lower–hemisphere equal–area projections of quartz c–axis measurements from quartz–rich metagraywacke, quartz–rich pelitic schist, and quartzite in the Columbus Promontory....136
4–9. Schematic configuration of the thrust stacking and deformation sequence envisioned for the western Inner Piedmont....141
4–10. Diagrammatic sketch of S_2 mylonitic foliation plane modified after Ridley (1986) and Holdsworth (1990)....149
5–1. Distribution of Paleozoic metamorphic isograds in the southern Appalachian orogen....153
5–2. P–T grid showing inferred maximum metamorphic conditions for SMT pelites....158
5–3. Schematic representation of the geometric and kinematic relationship between S_2 foliation components: a)S_{2c};b) S_{2s}, and; c) S_{2e}....162
5–4. Photomicrographs of S_2 foliation components....164
5–5. Photomicrographs showing the morphology, optical zoning patterns, and shear textures of garnets....167
5–6. Location of pelitic schist samples analyzed by electron microprobe techniques....169
5–7. Compositional zoning profiles from garnets in pelitic schist of the Sugarloaf Mountain thrust sheet....172
5–8. X_{Ti} versus Fe/Fe + Mg in biotite for pelitic schists....175
5–9. Plot of plagioclase compositions....178
5–10. Photomicrographs of textural relationships between sillimanite and muscovite....180
5–11. Photomicrographs showing sillimanite morphology and textural relationship between fibrolitic sillimanite and garnet porphyroblasts....182
5–12. AFM diagrams plotted using method of Thompson (1957) and the rim compositions of garnet–biotite pairs....186
5–13. Petrogenetic grids showing possible retrograde P–T paths for pelites in the SMT....197

LIST OF PLATES

PLATE I. Geologic Map and Cross Sections of the Cliffield Mountain and Northern Saluda $7\frac{1}{2}$ Minute Quadrangles, Polk and Henderson Counties, North Carolina. .....IN POCKET

PLATE II. Station Location Map of the Cliffield Mountain and Northern Saluda $7\frac{1}{2}$ Minute Quadrangles, Polk and Henderson Counties, North Carolina.....IN POCKET

PLATE III. Geologic Map of the Columbus Promontory, Western Inner Piedmont, North Carolina.....IN POCKET

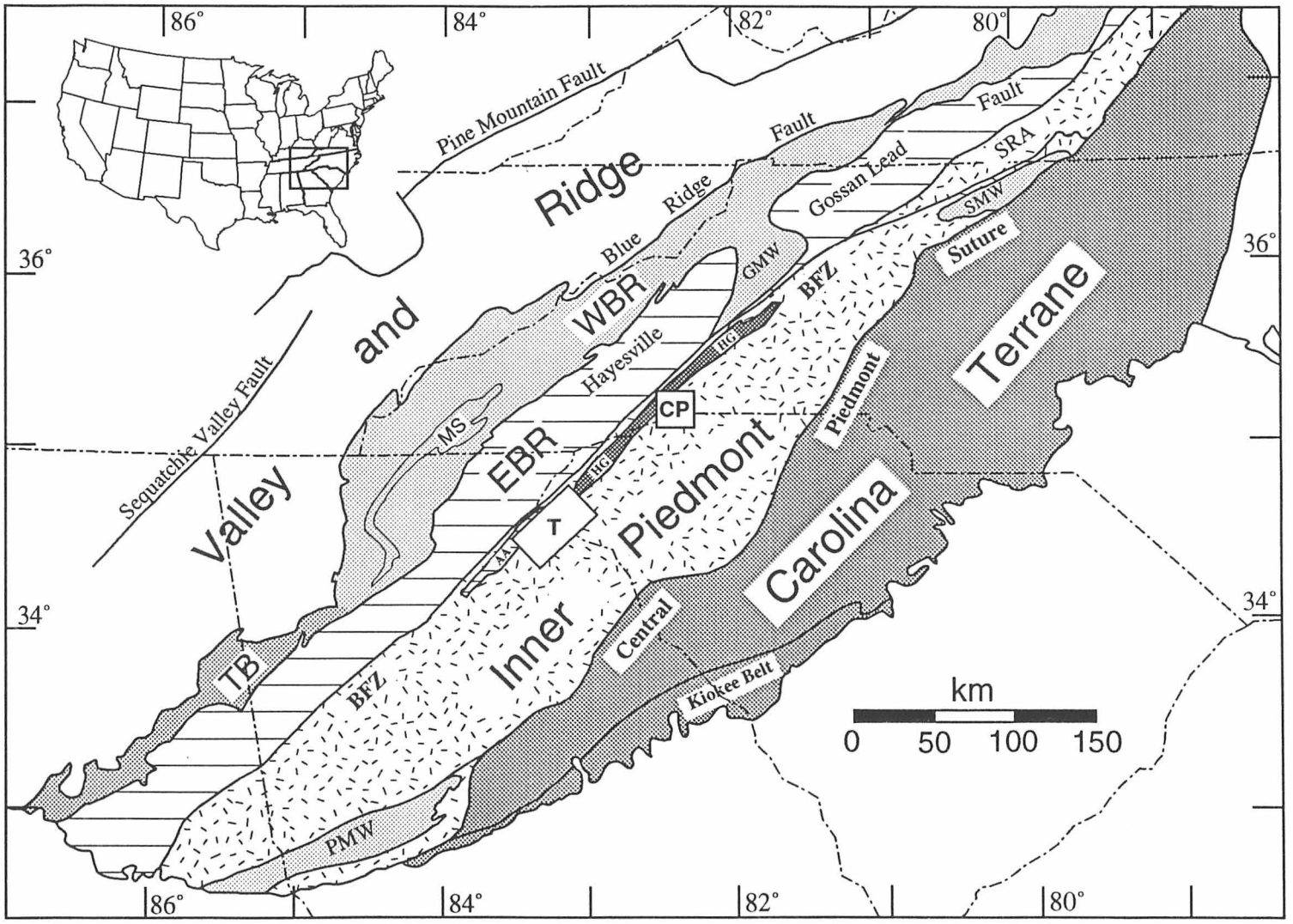
CHAPTER I

INTRODUCTION

The southern Appalachian orogen (Fig. 1–1) is subdivided into several tectonic regions that include from west to east the Valley and Ridge, Blue Ridge, Inner Piedmont, and Carolina Terrane (King, 1955; Hatcher, 1972, 1978a, 1987, 1989). The Inner Piedmont represents the high grade migmatitic core of the orogen originally defined by King (1955) as the highly deformed and metamorphosed terrane bounded on the northwest by the Brevard fault zone and on to the southeast by the Kings Mountain belt, later recognized to contain the central Piedmont suture (Hatcher and Zeitz, 1980; Hatcher, 1989; Hatcher and others, 1990). King's definition encompasses both the Inner Piedmont and the Chauga belt (Fig. 1–1), defined by Hatcher (1972) as a synclinorium within the western Inner Piedmont of South Carolina, which contains lower–grade rocks at higher structural and stratigraphic levels than the adjacent Blue Ridge and Inner Piedmont.

Inner Piedmont lithostratigraphy consists of an assemblage of high grade ortho– and paragneiss intruded by pre–, syn–, and postkinematic plutons. The protoliths of the Inner Piedmont rocks consisted presumably of immature quartzofeldspathic and pelitic sediments, and mafic volcanic rocks. Although no precise ages have been determined, regional lithostratigraphic correlation (Rankin, 1970, 1975; Hatcher, 1978a; 1987, 1989; Hatcher and Goldberg, 1990), and basement–cover relationships (Rankin 1975, Hatcher 1973, McConnell 1988, Stieve 1989), indicate they are probably Late Proterozoic or early Paleozoic. Correlation of the lithostratigraphy of the Inner Piedmont with that of the eastern Blue Ridge is one of the most controversial issue in the crystalline southern Appalachians (e.g., compare Hatcher, 1989; Hatcher and others, 1990; versus Horton and others, 1989; Rankin and others, 1989).

Figure 1–1. Tectonic subdivisions of the southern Appalachians showing the location of the Columbus Promontory (CP). Also shown is the Tamassee area (T) in the Inner Piedmont of South Carolina and NE Georgia discussed in Chapter IV.


86°
84°
82°
80°
36°
34°
Pine Mountain Fault
Ridge
and
Valley
Blue
Ridge
Fault
WBR
GMW
BFZ
Gossan Lead
SRA
Fault
SMW
Suture
Terrane
Piedmont
Carolina
Hayesville
HG
CP
MS
EBR
T
AA
Piedmont
Sequatchie Valley Fault
Inner
Central
Kiokee Belt
TB
BFZ
PMW
km
0 50 100 150

The Inner Piedmont of South Carolina and NE Georgia was subdivided by Griffin (1967, 1969, 1971a, 1974a, 1974b) into a stack of fold nappes including the Walhalla, Six Mile, and Anderson nappes. According to Griffin (1971a, 1974a), this nappe complex is characterized by kyanite–grade NW and SE flanks (kyanite–bearing) separated by a sillimanite–grade core. This nappe sequence was thought by Griffin (1971b) to be bordered to the west by a structurally higher and lower grade assemblage (Chauga belt) comprising suprastructure and *abscherungzone* (e.g., Haller, 1956) distinct from the higher grade infrastructure represented by the nappe sequence. Hatcher and Odom (1980) suggested a complex history of NW–directed pre–, syn–, and postmetamorphic thrusting in the Inner Piedmont. Studies by Lemmon (1973), Nelson and others (1987), Goldsmith and others (1988), Hopson and Hatcher (1988), Higgins and others (1988), Horton and McConnell (1990), Davis and others (1989, 1990a), and Tabor and others (1990) indicate the Inner Piedmont in the Carolinas and northeast Georgia is indeed composed of a crystalline thrust stack similar to the imbricate stacks of medium– to high–grade crystalline thrust sheets observed in Scandinavia (Gee, 1978; Gee and Sturt, 1983), in the Grenville province (Culshaw and others, 1988; Hanmer 1988), and in the Himalayas (Hubbard, 1989, Treolar and others, 1989).

Inner Piedmont thrust sheets are bounded to the northwest by the Brevard fault zone (Fig. 1–1), traceable 600 km from Alabama to Virginia. The Brevard fault zone separates the Blue Ridge from the Inner Piedmont (Reed and Bryant 1964), and has long been recognized as a major crustal break (Jonas, 1932, King, 1955, Reed and Bryant, 1964; Butler , 1971; Bryant and Reed, 1970; Bird and Dewey, 1970; Odom and Fullagar, 1973; Horton, 1974, 1982; Horton and Butler 1986; Hatcher, 1971b, 1972, 1978b, 1987, 1989). At least three major deformational events in the Brevard fault zone have been recognized: early thrusting (Jonas, 1932, Bentley and Neathery, 1970; Hatcher, 1971b, 1972; Stirewalt and Dunn , 1973; Roper and Justus, 1973); dextral strike slip (Reed and Bryant, 1964, Bobyarchik, 1984, Edelman and others, 1987; Evans and Mosher, 1986; and Bobyarchik and others, 1988); and brittle thrusting

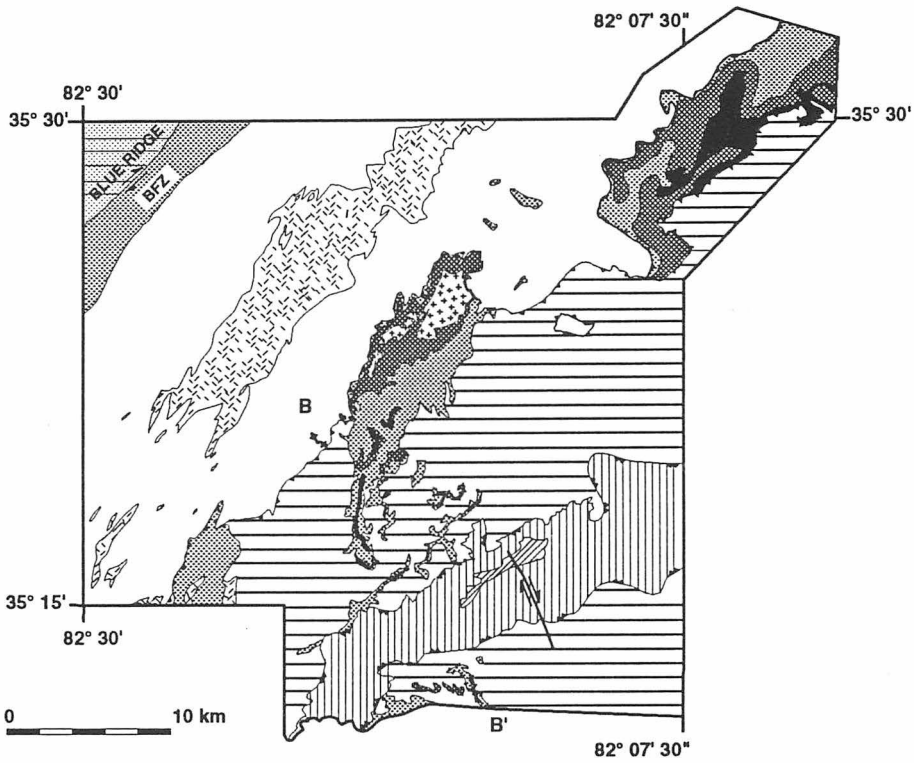
during the Rosman phase (Horton 1974, 1982; Horton and Butler, 1986, Edelman and others, 1987; Hatcher and others, 1989). Most studies have treated the structural development of the Brevard fault zone and the thrusting in the adjacent Inner Piedmont separately.

Metamorphism in the Inner Piedmont is generally characterized as part of a Barrovian sequence that includes prograde middle– to upper amphibolite facies event followed by a retrograde episode. The central part of the Inner Piedmont is in the sillimanite + muscovite zone, flanked by lower grade rocks of Chauga belt (garnet–staurolite) and Kings Mountain belt (Butler 1990). The age of metamorphism in the Inner Piedmont is not fully understood. Glover and others (1983), Hatcher (1987), and Butler (1990) have speculated that both Taconian and Acadian metamorphic episodes may have affected much of the Inner Piedmont.

Despite the general geologic understanding of the Inner Piedmont outlined above, this terrane remains one of the most poorly understood regions in the southern Appalachian orogen. This problem is not only the result of its complex geologic history, but also the result of the general lack of widespread detailed geologic mapping that resolves lithostratigraphic, structural, and metamorphic relationships, and few geochronological (either fossil or radiometric) constraints. The purpose of this study is a detailed examination of the lithostratigraphic, structural, and metamorphic development of a crystalline thrust complex within the western Inner Piedmont of North Carolina from an area herein called the Columbus Promontory. This complex contains three crystalline thrust sheets that include the Tumblebug Creek, Sugarloaf Mountain, and Mill Spring thrust sheets (Fig. 1–2; Plates I, II, III). Each thrust sheet contains a distinct lithostratigraphy, but records similar structural and metamorphic history.

The Columbus Promontory is located in a high relief (700–1000 m) area of Blue Ridge topography within the Inner Piedmont that produces continuity of outcrop atypical of the Inner Piedmont (Figs 1–3) and thus is an outstanding area for study of the complex geologic history of crystalline thrust sheet development in the Inner Piedmont. The Columbus Promontory, as defined here, extends from the Brevard fault zone approximately 40 km into the Inner Piedmont

Fig. 1–2. Geologic map (a) and cross section (b) of the Columbus Promontory. Unpatterned– Henderson Gneiss. cross hatch – 438 Ma granitic gneiss. crosses – Sugarloaf gneiss. black – Poor Mountain Formation quartzite. dark gray – Poor Mountain amphibolite. light gray – Poor Mountain pelitic schist. horizontal lines – Mill Spring complex migmatitic biotite gneiss – metagraywacke. vertical lines – Mill Spring complex migmatitic metagraywacke–amphibolite–amphibole gneiss. BFZ– Brevard fault zone; TCT– Tumblebug Creek thrust; SMT – Sugarloaf Mountain thrust; MST- Mill Spring thrust. Teethed lines are thrust faults (teeth on hanging wall) Map compiled from Lemmon 1973, unpublished data of Conley and Drummond (1975) and unpublished data of Davis (1987–1990), Tabor (1988–1990) and Yanagihara (1990–1992).


82° 07' 30"
82° 30'
35° 30'
35° 30'
BLUE RIDGE
BFZ
B
35° 15'
82° 30'
0
10 km
B'
82° 07' 30"

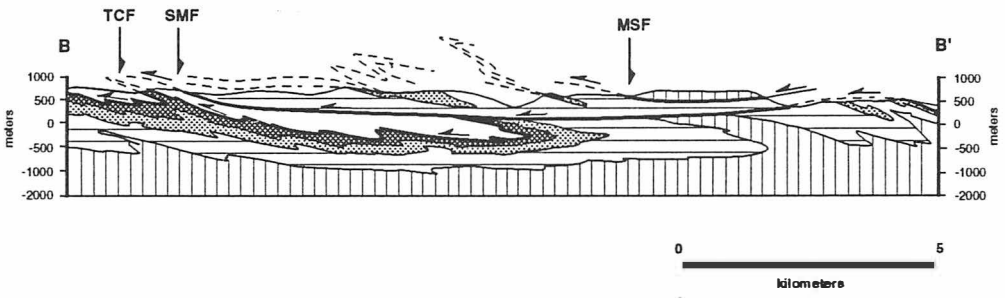
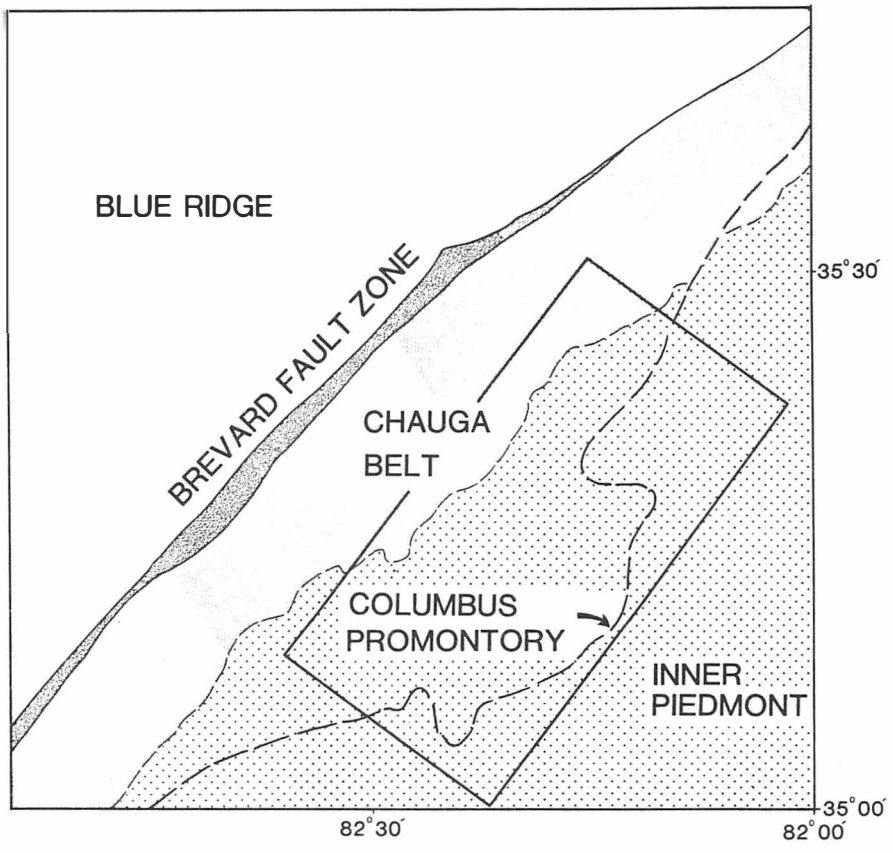

TCF
SMF
MSF
B
B'
1000
500
0
-500
-1000
-2000
meters
0
5
kilometers

Figure 1–3. U.S. Geological Survey Eros Data Center radar mosaic (near range) of the southeast corner of the Knoxville 1° x 2° sheet that shows the high relief of the Columbus Promontory. Diagram on the right outlines the area included in the Columbus Promontory.

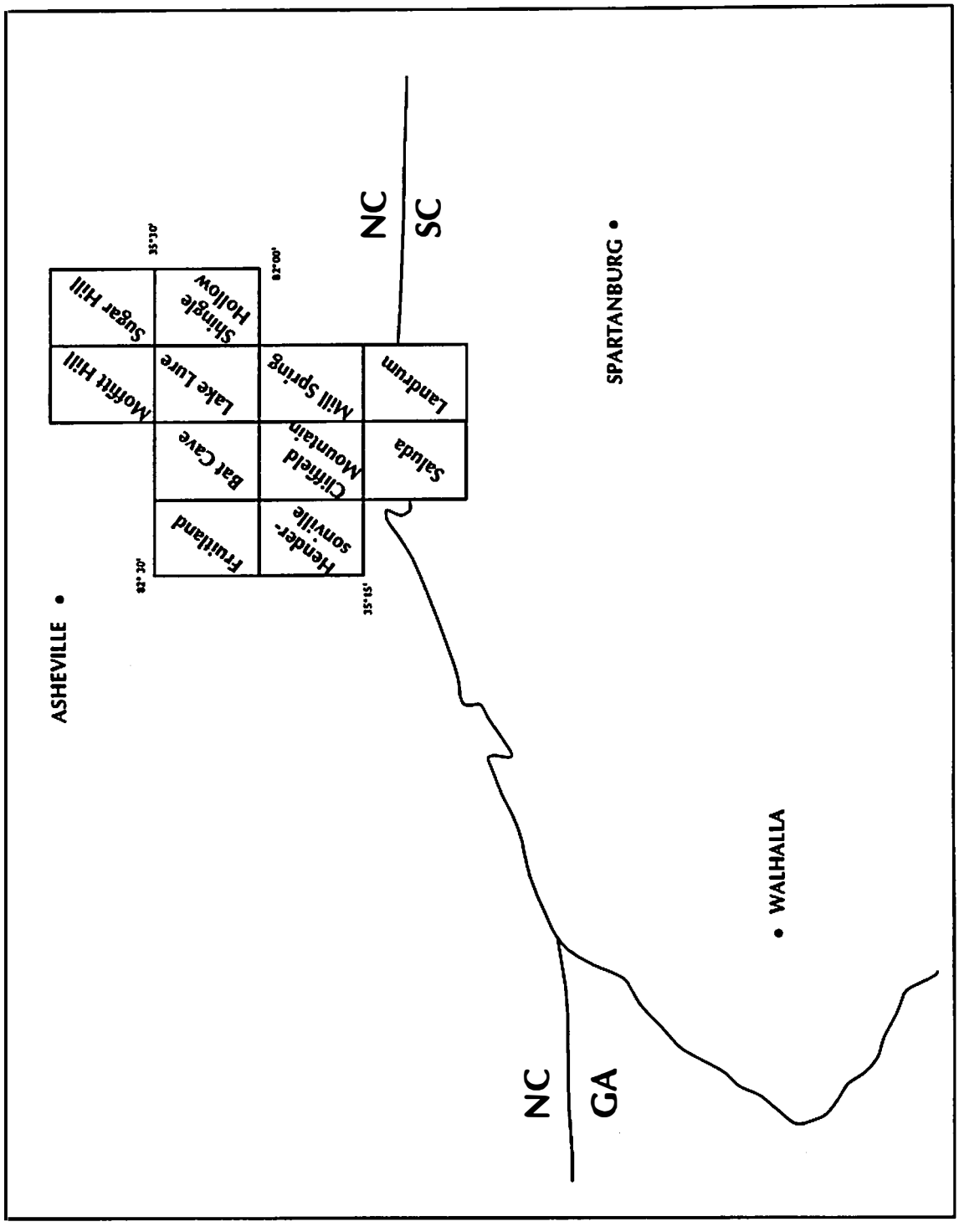



BLUE RIDGE
BREVARD FAULT ZONE
CHAUGA
BELT
COLUMBUS
PROMONTORY
INNER
PIEDMONT
35°30´
35°00´
82°30´
82°00´

(Figs. 1–1 and 1–3). This area encompasses seven $7\frac{1}{2}$ minute quadrangles including the Bat Cave, Cliffield Mountain, Fruitland, Hendersonville, Lake Lure, Mill Spring, and Saluda quadrangles (Fig. 1–4). The study area incorporates geologic features of both the Chauga belt of Hatcher (1972) and the parts of the high grade Inner Piedmont (Fig 1–1). The majority of data used to examine the lithostratigraphic, structural and metamorphic history of the Columbus Promontory comes from the Bat Cave, Cliffield Mountain, Hendersonville, Lake Lure, Mill Spring, and Saluda quadrangles. Data form the Fruitland quadrangle (Lemmon and Dunn, 1973b) was only used for the structural aspect of this study.

This study represents an integrated field, petrographic, and analytical investigation of rocks within the crystalline complex of the Columbus Promontory. Consequently , this investigation has resulted in a considerable amount of new geologic data for the Inner Piedmont, but also includes the compilation and incorporation of a significant amount of previous work. The field portion of the study involved 1:24,000 scale geologic mapping in the seven $7\frac{1}{2}$ minute quadrangles discussed above. The geologic mapping effort (shown in Plates I, II, and III) incorporates the results of my recent work, primarily in the Cliffield Mountain and Saluda quadrangles, with previous work of Lemmon (1973), and Lemmon and Dunn (1973a) in the Bat Cave, Fruitland (Lemmon and Dunn, 1973b) and Hendersonville (Lemmon, unpublished data) quadrangles, unpublished work of Conley and Drummond (1975) in Polk County, North Carolina, and the unpublished work of Tabor (1988–1990) in portions of the Mill Spring and Lake Lure quadrangles. Petrographic analysis involved examination of nearly two hundred thin sections from samples collected during the field portion of this study. These were used for modal estimations, microstructural analysis, quartz–c axis measurements, and determining metamorphic assemblages. Also included is this part of the study is the previous petrographic work (modal analysis) of Lemmon (1973). The analytical portion of the study included XRF analysis of amphibolite from the Poor Mountain Formation and the Mill Spring complex. Analytical

Figure 1–4. Index to topographic quadrangles included as part of the Columbus Promontory.


ASHEVILLE
SPARTANBURG
WALHALLA
NC
SC
NC
GA
Hender-sonville
Cliffield Mountain
Mill Spring
Landrum
Saluda
Fruitland
Bat Cave
Lake Lure
Mofitt Hill
Shingle Hollow
Sugar Hill
35°15'
35°20'
82°20'
82°00'

analysis also included electron microprobe analysis of polished minerals (thin sections) from samples of pelitic schist from the Poor Mountain Formation and Mill Spring complex.

In discussing the development of the crystalline thrust terrane present in the Columbus Promontory, this study is divided into four subject chapters (II, III. IV, and V). The major conclusions of this study are summarized in Chapter VI.

Chapter II addresses the lithostratigraphic framework within the crystalline thrusts sheets present in the Columbus Promontory. Also included in this chapter is a discussion of the regional correlation of rock units in the Columbus Promontory with other parts of the eastern Blue Ridge and the Inner Piedmont and the tectonic implications of these correlations. Chapter III continues with the stratigraphic theme, but focuses on the geochemical characteristics of the mafic rocks interleaved within the two dominant lithostratigraphic units (Poor Mountain Formation and Mill Spring complex) that are present in the study area. In this chapter I attempt to: 1) elucidate the protolith of the Poor Mountain and Mill Spring complex amphibolites; 2) determine fractionation trends, suggest possible plate tectonic settings from which the amphibolite were generated; and, 3) examine the regional relationships of mafic rocks in the crystalline southern Appalachians.

The focus of Chapter IV is on the deformational history and kinematics of emplacement of the crystalline thrust sheets in the western Piedmont of the Carolinas and NE Georgia. This chapter incorporates the results of my work in the Columbus Promontory with that of an area to the southwest in South Carolina and NE Georgia referred to as the Tamassee area (Fig. 1–1) that has been studied by Dr. R. D., Hatcher, Jr., and former students for over twenty years. In this chapter evidence is presented indicating that early SW–directed Brevard fault zone movement was synchronous and coupled with W–directed thrust sheet emplacement in the adjacent Inner Piedmont. It is suggested that this linked displacement, between the Brevard fault zone and ductile crystalline thrust sheets of the western Inner Piedmont, is the result of one a pre–Alleghanian orogeny transpressional or oblique convergence event in the crystalline southern

Appalachians. In addition, this chapter attempts to show the kinematic importance of the regionally extensive subhorizontal S_2 mylonitic foliation, which is the most characteristic structural element in the western Inner Piedmont, on thrust sheet emplacement and development of associated micro– and mesoscopic structures in this part of the Inner Piedmont.

Chapter V examines the metamorphic and microstructural development of sillimanite–muscovite bearing pelitic schist in the Poor Mountain Formation and Mill Spring complex within the Sugarloaf Mountain thrust sheet. This chapters examines the petrogenetic development of this assemblage, attempts to document the synkinematic relationship between deformation and metamorphism during thrust sheet emplacement in this area, and presents qualitative constraints on the P–T path related to emplacement of the Sugarloaf Mountain thrust sheet.

CHAPTER II

LITHOSTRATIGRAPHY OF THE COLUMBUS PROMONTORY, WESTERN INNER PIEDMONT, NORTH CAROLINA

INTRODUCTION

The lithostratigraphy of the Inner Piedmont represents one of the most poorly understood aspects of the geology of the crystalline southern Appalachian orogen. Mapping in the Inner Piedmont by Griffin (1969, 1971a, 1971b, 1974a, 1974b), Hatcher (1969, 1970, 1972, 1978b, 1987), Bentley and Neathery (1970), Conley and Henika (1973), Rankin and others (1973), Heyn (1984), Goldsmith and others (1988), Hatcher (1988), Hopson and Hatcher (1988), McConnell (1988), and Steltenpohl and others (1990) have helped to elucidate many aspects of Inner Piedmont stratigraphy, however, many questions remain unanswered. The internal stratigraphy of the Inner Piedmont has been resolved in detail in only a few areas including the Smith River allochthon (Conley and Henika, 1973), the Alto allochthon (Hatcher, 1978b; Hopson and Hatcher, 1988), west of the Sauratown Mountains (Heyn, 1984, 1988; Hatcher, 1988; McConnell, 1988), the Chauga belt of South Carolina (Hatcher, 1969, 1970; Hatcher and Acker, 1984), and adjacent to the Brevard fault zone in Alabama (Bentley and Neathery, 1970; Steltenpohl and others, 1990; Neilson and others, 1990a, 1990b). In the most general sense, Inner Piedmont stratigraphy consists of an assemblage of medium– to high–grade ortho– and paragneiss intruded by pre–, syn–, and postkinematic plutons. The protoliths of the Inner Piedmont rocks consisted predominantly of immature quartzofeldspathic and pelitic sediments, and mafic lavas.

The purpose of this chapter is to examine, in detail, Inner Piedmont lithostratigraphy exposed in the Columbus Promontory (Fig. 1–2; Plates I and III). In doing so, this chapter

has two primary objectives. The first objective is to propose a lithostratigraphic framework for the Columbus Promontory and describe the field and petrographic characteristics of rock units within this lithostratigraphic framework. The second objective of this chapter is to place the lithostratigraphic units of the Columbus Promontory into the regional (tectono–) lithostratigraphic framework of the crystalline southern Appalachians. The internal stratigraphy of the Columbus Promontory contains rock units and a lithostratigraphic sequence similar to those described elsewhere in the Chauga Belt, Inner Piedmont, and eastern Blue Ridge (e.g., Sloan, 1908; Shufflebarger, 1961; Bentley and Neathery, 1970; Hatcher, 1969, 1970, 1971a, 1971b; Rankin 1970, 1975; Conley and Henika, 1973 Hopson and Hatcher, 1988; Higgins and McConnell, 1978, and others). Consequently, this chapter also addresses possible regional correlations of the lithostratigraphy of the Columbus Promontory with other parts of the eastern Blue Ridge and the Inner Piedmont, and the tectonic implications of these correlations.

LITHOSTRATIGRAPHIC FRAMEWORK OF THE COLUMBUS PROMONTORY

Previous Work

Keith (1905, 1907), Reed and Bryant (1964), Stuckey and Conrad (1958), and Hadley and Nelson (1971) all identified the Henderson Granite (Keith, 1907) or Henderson Gneiss (Reed and Bryant, 1964) near the Columbus Promontory, but did not address the lithostratigraphy of the adjacent Inner Piedmont rocks. Hadley and Nelson (1971) broadly defined the lithostratigraphy of the Inner Piedmont east of the outcrop belt of the Henderson Gneiss as being composed of a sequence of paragneiss, schists and migmatite. Lemmon (1973, 1982), Lemmon and Dunn (1973a), and Conley and Drummond (unpublished, 1975) made the first major contributions to resolution of the internal

stratigraphy of the Columbus Promontory. Lemmon (1973) defined two rock units within the Henderson Gneiss outcrop belt, and was able to subdivide the overlying Inner Piedmont rocks into three mappable units as part of sequence he termed the Sugarloaf Mountain group contained in an unnamed thrust sheet. Conley and Drummond (unpublished, 1975) working south of Lemmon's area in Polk County, North Carolina, described a similar stratigraphic package they informally called the Tryon formation for the town of Tryon, North Carolina (Plates I, II, and III). In their Tryon formation, Conley and Drummond recognized rock units similar to those in the Sugarloaf Mountain group, but also included a thick biotite gneiss unit. Lemmon also recognized a thick biotite gneiss unit beneath the garnet-muscovite schist of his Sugarloaf Mountain group, but was unable to definitively determine the contact relationships between these two units. Conley and Drummond also defined a sequence of migmatitic granitic gneiss, amphibolite, and amphibole gneiss they informally termed the Mill Spring group for the town of Mill Spring, North Carolina (Plates I, II, and III).

Proposed Lithostratigraphic Framework

As noted above, Lemmon (1973) originally defined rocks of the Columbus Promontory as part of a lithostratigraphic unit he defined as the Sugarloaf Mountain group, but he also noted a similarity of these rocks to the Poor Mountain Formation recognized to the southwest in South Carolina (Sloan, 1907; Shufflebarger, 1961; Hatcher, 1969, 1970). Field criteria and petrologic data gathered during this study suggest that rocks of the Sugarloaf Mountain group (Lemmon, 1973) are similar or identical to those of the Poor Mountain Formation in South Carolina, and thus I prefer to designate rocks of the Sugarloaf Mountain group as correlatives of the Poor Mountain Formation. Lemmon (1973) also included a granitic gneiss at the top of Sugarloaf Mountain (Plate III) in his Sugarloaf Mountain group, however, because of its possible igneous origin, I prefer to designate this

granitic gneiss as distinct unit within the stratigraphy of the Columbus Promontory defined herein as the Sugarloaf gneiss. I include the thick biotite gneiss recognized by Lemmon (1973) beneath his Sugarloaf Mountain group, and the migmatitic gneiss and interlayered amphibolite, and amphibole gneiss (Mill Spring group Conley and Drummond (unpublished)), into a stratigraphic assemblage herein termed the Mill Spring complex. As will be discussed in greater detail below, the Mill Spring complex is subdivided into two units based on the relative abundance of mafic rocks. Thus, as a result of detailed field and petrologic studies and integration of previous studies, I herein define a stratigraphic framework for the Columbus Promontory that consists of four distinct mappable sequences that includes the Henderson Gneiss (Keith, 1907; Reed and Bryant, 1964), the Poor Mountain Formation (Sloan, 1907; Shufflebarger, 1961; Hatcher, 1969,1970) , the Sugarloaf gneiss, and the Mill Spring complex (Fig. 1–2; Plates I and III).

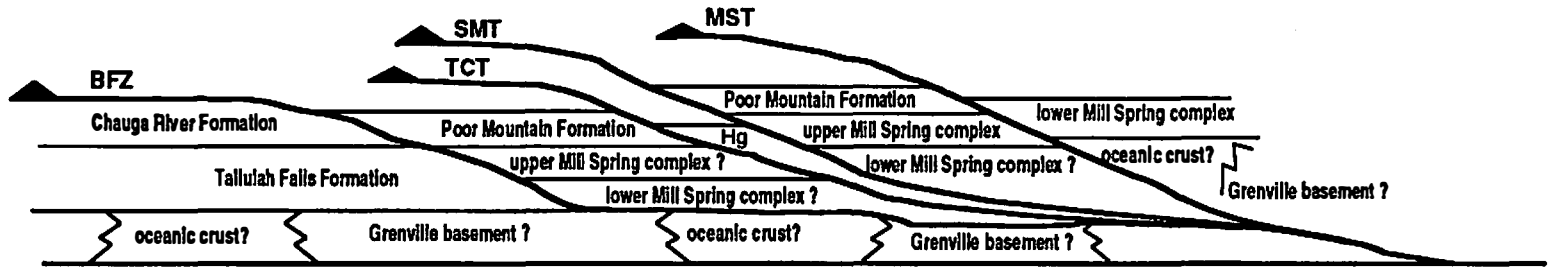
Structural Significance

The lithostratigraphic framework proposed above is partly consistent with the work of Lemmon (1973) and the unpublished work of Conley and Drummond (1975), but significant new discoveries and subsequent changes have had important bearing on the structural interpretation of the Columbus Promontory. Lithostratigraphic units discussed here define three crystalline thrust sheets within the Columbus Promontory herein called the Tumblebug Creek, Sugarloaf Mountain, and the Mill Spring thrust sheets (Fig. 1–2; Plates I and III). The structural and stratigraphic relationships between rock units of the Columbus Promontory are shown in Figures 1–2 and 2–1. The Tumblebug Creek thrust sheet contains only the Henderson Gneiss and is correlative with the Stumphouse Mountain thrust sheet defined by Liu (1991) to the southwest in South Carolina.

Figure 2–1. Conceptual stratigraphic and structural model (cross section) for rock units in the Columbus Promontory (Inner Piedmont) and the adjacent eastern Blue Ridge. MST–Mill Spring thrust; SMT–Sugarloaf Mountain thrust; TCT–Tumblebug Creek thrust; BFZ–Brevard fault zone; and Hg–Henderson Gneiss.

W – NW

E – SE


SMT
MST
BFZ
TCT
Poor Mountain Formation
lower Mill Spring complex
Chauga River Formation
Poor Mountain Formation
Hg
upper Mill Spring complex
oceanic crust?
upper Mill Spring complex ?
lower Mill Spring complex ?
Tallulah Falls Formation
Grenville basement ?
lower Mill Spring complex ?
oceanic crust?
Grenville basement ?
oceanic crust?
Grenville basement ?

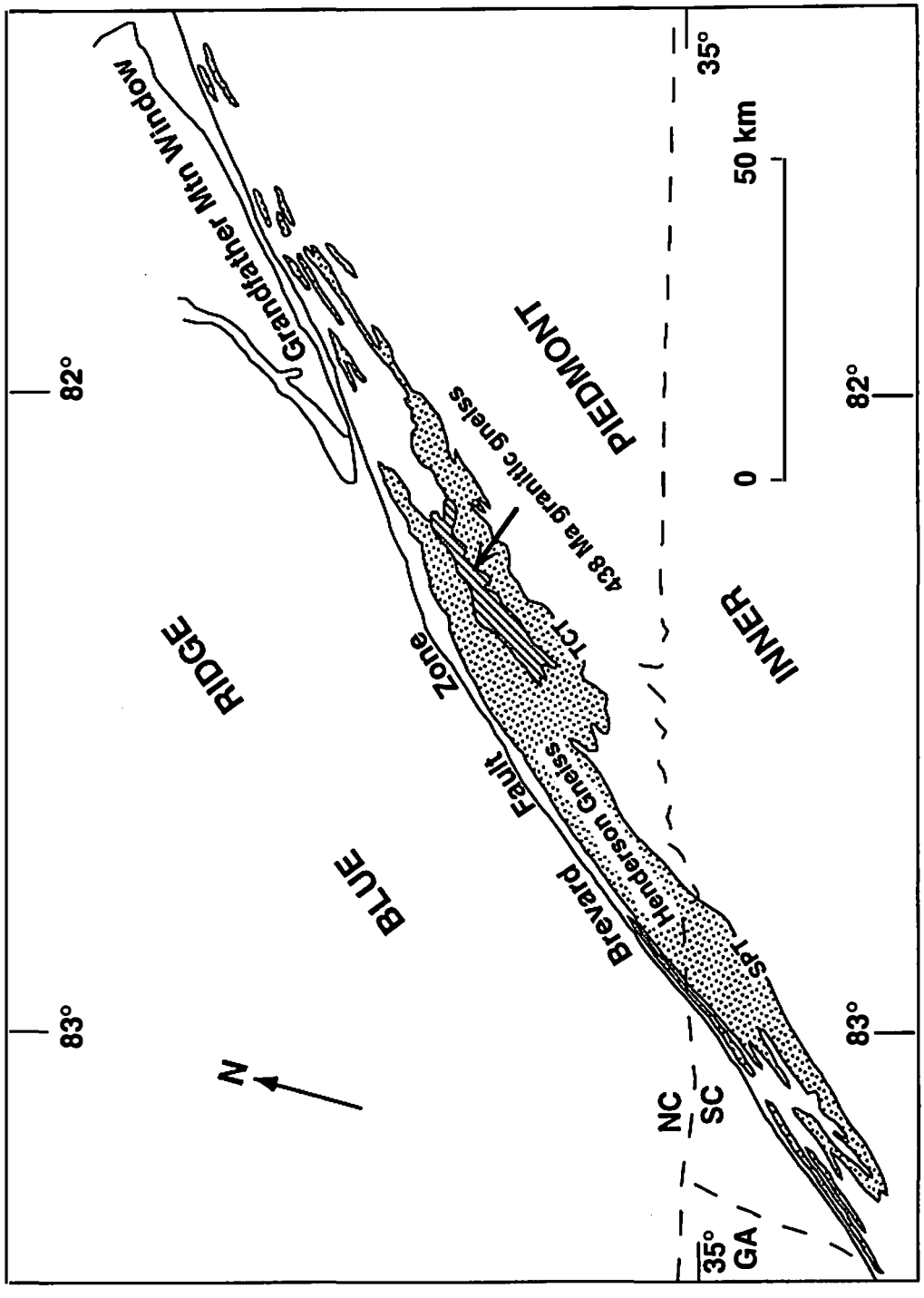
The Sugarloaf Mountain thrust sheet contains rocks of the Poor Mountain Formation and the upper Mill Spring complex. The Mill Spring thrust sheet contains rocks of the mafic–rich, lower Mill Spring complex. The Sugarloaf Mountain and Mill Spring thrust sheets maintain a similar structural position (Inner Piedmont rocks over Chauga belt rocks) as other thrust sheets observed elsewhere in the Inner Piedmont including the Smith River allochthon (Conley and Henika, 1973) in Virginia, the Alto allochthon (Hatcher, 1978b; Hopson and Hatcher, 1988) in NE Georgia, the Walhalla nappe (Griffin, 1971a, 1971b, 1974a, 1974b) or Cedar Creek thrust sheet (Liu, 1991) in South Carolina, and the Six Mile thrust sheet (Griffin, 1971a, 1971b 1974a, 1974b), also in South Carolina. Thrust sheets containing rock units similar to those of the Mill Spring complex in the Inner Piedmont of South Carolina were also discussed by Nelson and others (1987), and in the Inner Piedmont of North Carolina by Goldsmith and others (1988). The kinematics of emplacement and deformation of thrust sheets in the Columbus Promontory are discussed in Chapter IV.

FIELD AND PETROGRAPHIC CHARACTERISTICS OF LITHOSTRATIGRAPHIC UNITS

Henderson Gneiss

Keith (1905, 1907) defined and delineated the Henderson Granite, with the type section located in Henderson County, North Carolina (Plate III). Reed and Bryant (1964) redefined the Henderson Gneiss and restricted the outcrop unit to southeast of the Brevard fault zone. Thus, as defined by Reed and Bryant (1964), the Henderson Gneiss extends in the Piedmont from the South Carolina-Georgia border northeastward to the southeastern flank of the Grandfather Mountain window (Figs. 1–1 and 2–2). In the Columbus Promontory the most extensive exposures of the Henderson Gneiss occur in the

Figure 2–2. Outcrop belt of the Henderson Gneiss in the western Inner Piedmont of North and South Carolina. Structural analysis indicates Henderson Gneiss was thrust–emplaced along the Stumphouse Mountain thrust (SPT) in South Carolina and the Tumblebug Creek thrust (TCT) in North Carolina. Modified from Liu (1991).


Grandfather Mtn Window
PIEDMONT
438 Ma granitic gneiss
TCT
Zone
Fault
Brevard
Henderson Gneiss
ps
INNER
RIDGE
BLUE
N
NC
SC
GA
35°
82°
83°
0
50 km

Fruitland, Bat Cave, Hendersonville, Lake Lure and the NW corner of the Cliffield Mountain quadrangles (Figs. 1–2 and 1–4; Plates I and III). The Henderson Gneiss was also mapped in the Mill Spring quadrangle through either a window, or a reentrant in the Sugarloaf Mountain thrust sheet (Figs. 1–2 and Plate III).

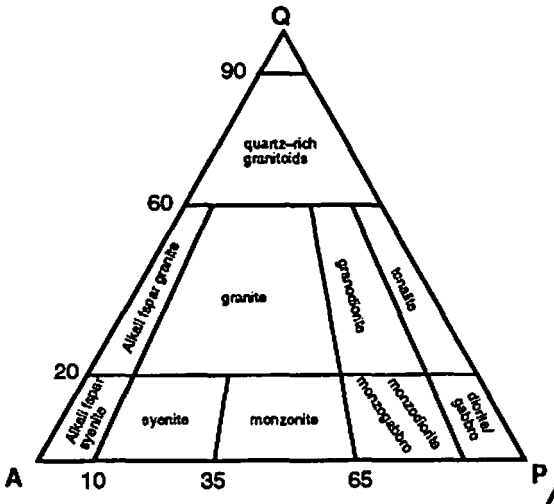
In the Columbus Promontory, the composition of the Henderson Gneiss varies from that of granite to quartz monzonite (Table 2–1 and Fig. 2–3) and is composed of microcline, oligoclase, quartz, and biotite with accessory muscovite, garnet, allanite, zircon, sphene, and opaque minerals (Lemmon 1973). One of the most distinctive characteristics of the Henderson Gneiss is the presence of distinct K–feldspar augen (Fig. 2–4). The augen are white microcline, ovoid to asymmetric in cross section and elongate within the foliation plane. The augen are commonly rimmed by quartz, plagioclase, and embayments of myrmekite (Fig. 2–4). The Henderson Gneiss in the Columbus Promontory and throughout much of the outcrop length, contains a pronounced NE–SW–trending mineral lineation defined by quartz ribbons, elongated K-feldspar porphyroclasts, and flakes of biotite, and occasional muscovite (Fig. 2–4), and in places is an L tectonite.

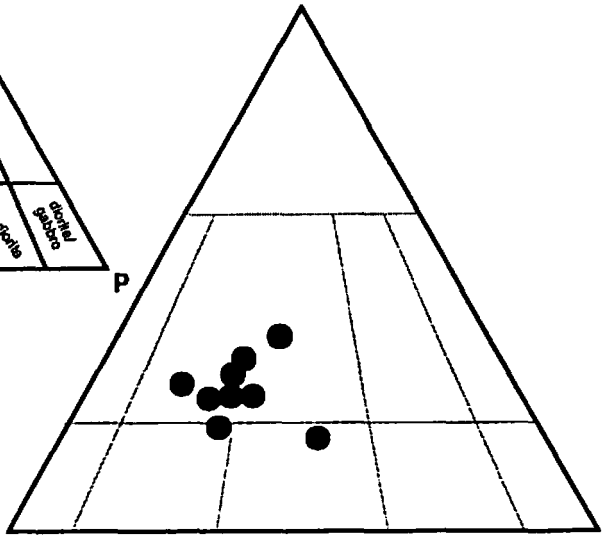
The Henderson Gneiss has been the focus of many geochronological studies, but, unfortunately, many discrepancies exist in the results. Odom and Fullagar (1973) reported a Rb–Sr whole–rock age of 535 Ma for the Henderson Gneiss with an initial Sr^{87}/Sr^{86} ratio of 0.70309 and a U–Pb age of 538 Ma. They interpreted these to represent crystallization ages and the low initial Sr^{87}/Sr^{86} ratio indicative of an igneous lower crustal origin. Odom and Fullagar (1973) also reported an age of 356 Ma for mylonitic Henderson Gneiss in the Brevard fault zone. Sinha and Glover (1978) reported an U–Pb age of about 600 Ma based on a different common lead constant. Sinha and others (1989) reported a Rb–Sr age of 509 Ma (recalculated from Odom and Fullagar, 1973), and Sinha and others (1988) obtained a Rb–Sr age of 273 Ma from Henderson Gneiss ultramylonite in the Brevard fault zone. They attributed this young age to mylonitization, related to movement on the Brevard fault zone

Table 2–1. Modal analyses of Henderson Gneiss from the Columbus Promontory. Data From Lemmon (1973).

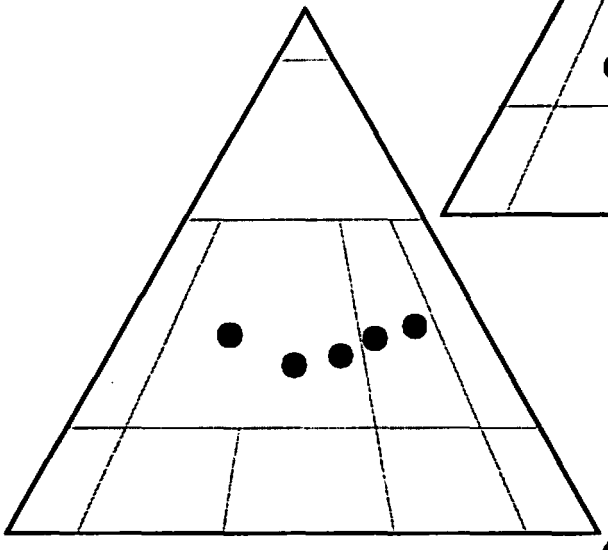
	L4–15	K8–11	E3–2	D4–1	D5–3	J1–4	J3–2	C8–6	F7–3
Plagioclase	32.5	32.8	29.2	27.6	30.1	34.5	41.5	35.5	33.3
x=An	16	18	16	18	18	12	17	12	19
Quartz	28.5	22.4	19.7	21.8	28.1	21.0	12.2	17.8	28.3
K-feldspar	14.4	32.3	23.5	21.3	38.7	23.5	15.6	32.2	22.8
Biotite	19.5	10.2	19.0	23.6	0.9	14.4	23.2	10.0	14.7
Muscovite	2.8	0.6	5.6	0.9	1.3	4.7	—	2.8	0.1
Garnet	—	tr	tr	—	—	—	—	—	—
Epidote	tr	tr	2.1	3.0	0.3	1.1	5.4	1.2	0.3
Sphene	2.0	1.1	0.8	1.4	tr	0.8	0.8	tr	tr
Opaques	tr	0.6	tr	tr	0.6	tr	0.2	0.4	0.4
Accessory	zir	zir	zir	zir	zir	zir	zir	zir	zir
	ap	ap	ap	ap	ap	ap	ap	ap	ap
	allan	chl	allan				allan	allan	allan

Figure 2–3. Classification of igneous rocks from the Columbus Promontory based on modal compositions. Nomenclature of Streckheisen (1976). Data is from Lemmon (1973).

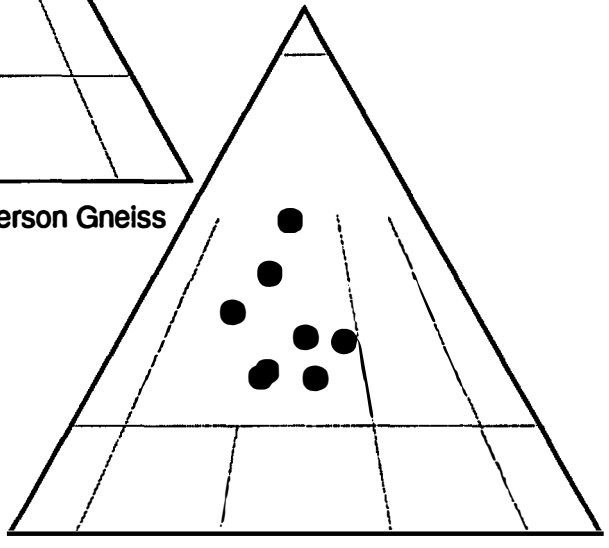




Henderson Gneiss



Granitic gneiss w/in Henderson Gneiss



Sugarloaf Gneiss

Figure 2–4. Mosaic of field photographs of the Henderson Gneiss and Sugarloaf gneiss, and a photomicrograph of the Henderson Gneiss. A) Augen (A) texture of Henderson Gneiss enhanced by weathering. Hammer in foreground is approximately 40 cm in length; B) Photomocrograph of Henderson Gneiss showing well developed K–feldspar ribbon(K). Section is cut perpendicular to S_2 foliation and parallel to the pervasive NE–SW oriented lineation (L) characteristic of the Henderson Gneiss. Field of view 12mm. C) Exposure of Henderson Gneiss showing strong linear fabric (L) and local shear zone characteristic of this unit; D) Hand sample of Sugarloaf gneiss from the top of Sugarloaf Mountain in the Bat Cave quadrangle. Note well developed NE–SW trending mineral lineation (L).

A
A
B
K
L
C
L
D
GSA
CM
IN
mm

during the late Paleozoic Alleghanian orogeny.

Mapping by Lemmon (1973) in the Columbus Promontory has shown that the Henderson Gneiss was intruded by a younger granite prior to the development of the metamorphic foliation (Fig. 1–2 and Plate III). The contact between the Henderson and the granitic gneiss is now concordant and parallel to the regional southeast–dipping foliation. This unit is distinguished from the Henderson Gneiss by the lack of K–feldspar augen, less biotite, and generally lighter color. The composition of this granitoid gneiss varies from granite to granodiorite (Table 2–2 and Fig. 2–3). Odom and Russell (1975) reported a Rb–Sr whole–rock age of 438 Ma, with an initial Sr^{87}/Sr^{86} of 0.7045 for the granitoid gneiss.

The Henderson Gneiss represents one of the most enigmatic bodies within the western Inner Piedmont and the southern Appalachian orogen. Several aspects of this body including the origin, age, shape, and emplacement history are not fully understood. In the Carolinas, the Henderson Gneiss occurs in a distinct thrust sheet(s) including the Tumblebug Creek thrust sheet (Figs. 1–2, 2–2, and 2–5; Plates I and III) in the Columbus Promontory (Davis and others, 1991a, 1991b) and the Stumphouse Mountain thrust sheet in South Carolina (Liu and others, 1991; Liu, 1991). Contact relationships along the fault strongly suggest that the Henderson Gneiss was emplaced as single, large, intact mass, and did not intrude other Chauga belt rocks (Figs. 2–2 and 2–5). Despite recognition of this structural relationship, its origin is still uncertain. Rast (in Hatcher, 1989) noted that the age of the Henderson Gneiss is similar to the age of plutonic bodies in the Carolina terrane (see Dennis, 1991) and speculated that the body may have originated there. More recently, Sinha and others (1989) and Sinha and Guy (in Drake and others, 1989) included the Henderson Gneiss as a member of a Late Cambrian–Early Ordovician (520–490 m.y.) plutonic belt that extends from Delaware to Alabama and interpreted this belt as the remnant of a continental margin magmatic arc. According to Sinha and others (1989) this belt is best exposed in the central Appalachians, where it includes the Port Deposit (U–Pb, 515 Ma) in

Table 2–2. Modal analyses of granitic gneiss within the Henderson Gneiss in the Columbus Promontory. Data From Lemmon (1973).

	K2–1	L4–8	K4–3	G7–4	J5–12
Plagioclase	37.2	38.5	39.9	19.4	29.1
x=An	17	17	13	—	17
Quartz	30.4	31.7	30.9	35.2	27.5
K-feldspar	21.9	14.7	7.4	38.7	28.1
Biotite	8.4	9.9	15.8	2.9	7.6
Muscovite	1.2	4.7	3.8	3.2	5.8
Garnet	tr	tr	—	tr	—
Epidote	tr	tr	1.3	o.4	1.3
Sphene	0.8	0.4	tr	tr	tr
Opaques	tr	tr	tr	tr	0.5
Accessory	—	zir	zir	allan	zir
		ap	ap		

Figure 2–5. Mosaic of field photographs of the Tumblebug creek thrust, hand sample of the Poor Mountain amphibolite, and photomicrograph of the Poor Mountain amphibolite. A) Exposure of Tumblebug Creek thrust in the Cliffield Mountain quadrangle. Note truncation of folds in the Poor Mountain Formation amphibolite (Pm) by the overlying Henderson Gneiss (Hg). Hammer in foreground is approximately 40 cm in length. B) Exposure of folded Tumblebug Creek fault approximately .25 km northwest of outcrop in A above. Outcrop also shows transposition of fault contact into the regional S_2 foliation of the Inner Piedmont. Hammer in foreground is approximately 40 cm in length. C) Tightly folded laminated (amphibole–quartzofeldspathic layers) Poor Mountain Formation amphibolite. D) Folded Poor Mountain amphibolite. Fold is defined by nematoblastic amphiboles. Field of view is 12 mm.

A
Hg
Pm
B
Hg
Pm
Hg
C
CM
IN
mm
D

Maryland, the Occaquan (Rb–Sr, 494 Ma), Melrose (U–Pb, 515 Ma), and Leatherwood (U–Pb, 516 Ma) granitoid plutons in Virginia, but they have extended this belt into the southern Appalachians to as far as Alabama through temporal and/or geochemical correlation with the Henderson Gneiss (Rb–Sr, 509 Ma) in the Carolinas, the Villa Rica gneiss in Georgia, and the Elkahatchee Quartz Diorite (U–Pb, 469±13 Ma and 509 Ma) in Alabama (Russell and others, 1992). Modally these plutons are predominantly tonalitic to granodioritic with rare granites, a characteristic Sinha and others (1989) and Sinha and Guy (in Drake and others, 1989) have suggested is an indication of subduction–related magmatism along a continental margin.

Sugarloaf Gneiss

The Sugarloaf gneiss is confined to the top of Sugarloaf Mountain in the Bat Cave quadrangle (Fig. 1–2; Plate III). It represents the structurally highest unit in the Columbus Promontory contained in the Sugarloaf Mountain thrust sheet (Fig. 1–2; Plate III). This unit was originally included as part of the Sugarloaf Mountain group of by Lemmon (1973) who, based on zircon morphology and scatter of Rb–Sr isotopic data, suggested that the Sugarloaf gneiss represents a recycled sedimentary rock. He was unable to definitively rule out an igneous protolith. New isotopic work in progress (P.D. Fullagar and S.A. Goldberg, University of North Carolina, Chapel Hill) should help elucidate the protolith history and age of this unit. As noted previously, because of the possibility of an igneous origin for this unit, I prefer to define it as a separate lithologic unit herein called the Sugarloaf gneiss. A nearly identical group of unnamed gneiss bodies present in the Chauga belt of South Carolina have a Rb–Sr age of 423 Ma (Harper and Fullagar, 1981). Both rock units maintain a similar structural (stratigraphic ?) position above the Poor Mountain Formation.

Modally, the Sugarloaf gneiss is granitic to granodioritic in composition (Table 2–3 and Fig. 2–3) and contains predominantly microcline, plagioclase, biotite, muscovite. (Lemmon, 1973). Accessory minerals include zircon, sphene, apatite, allanite, chlorite, epidote, and garnet. The rock is light–gray to white, massive to well–foliated, and contains a pronounced NE-SW mineral lineation defined by oriented micas, and elongated ribbons of quartz and feldspar (Fig. 2–4). The contact relationship with the underlying amphibolite is concordant and parallel to the southeast–dipping foliation. Locally, the contact is folded.

Poor Mountain Formation

Sloan (1907) named the Poor Mountain series from exposures on Poor Mountain, northwest of Walhalla, South Carolina. According to his original definition, the Poor Mountain sequence consists of low-rank amphibolite overlain by a marble-quartzite unit, succeeded by the Henderson Gneiss. Schufflebarger (1961) suggested that the "Poor Mountain Group" and the "Chauga River Group" represented an unbroken stratigraphic sequence, between the Poor Mountain area and the Chauga River, preserved in a synclinal fold in the upper plate of an overthrust. From the crest of Poor Mountain, Schufflebarger described a stratigraphic succession of chlorite schist, white siliceous marble, quartz feldspar-mica schist, and quartz sericite schist. The Poor Mountain sequence was redefined as a formation by Hatcher (1969, 1970) and noted that the amphibolite unit grades downward into a lithology that is almost identical to the Brevard phyllite, except more quartzofeldspathic and containing fewer muscovite augen. According to Hatcher, the Brevard-Poor Mountain Transitional member, represents the lowest exposed portion of the Poor Mountain Formation and the lithologic changes between the Chauga River and Poor Mountain Formations are the result of facies changes.

Table 2–3. Modal analyses of the Sugarloaf gneiss in the Columbus Promontory. Data from Lemmon (1973).

	N6–4	N7–1	N7–4	N7–6	N7–13	N7–14	M8–11	L8–6
Plagioclase	28.5	17.7	37.1	37.2	17.2	28.0	15.8	27.4
x=An	28	28	26	28	33	36	32	26
Quartz	29.8	53.0	28.7	34.6	38.4	31.9	35.9	28.3
K-feldspar	37.4	17.9	29.0	20.8	34.9	24.8	20.4	36.9
Biotite	2.8	11.4	2.0	4.1	0.9	1.1	24.0	3.7
Muscovite	1.6	tr	3.1	3.3	8.4	14.1	3.4	1.5
Gamet	—	tr	0.2	—	0.1	tr	0.4	0.3
Epidote	tr	tr	tr	tr	tr	tr	tr	tr
Sphene	tr	—	—	—	—	—	tr	—
Opaques	tr	tr	tr	tr	tr	tr	tr	2.0
Accessory	Zir	zir	zir	zir	chl		zir	zir
		chl					ap	chl
		ap					tour	allan
		tour						

In the Columbus Promontory, the Poor Mountain Formation (Figs. 1–2; Plates I and III) consists of three mappable units, equivalent to the Poor Mountain amphibolite, Brevard–Poor Mountain transitional member, and the quartzite member recognized in South Carolina by Shufflebarger (1961) and Hatcher (1969, 1970). In descending order these include: (1) laminated amphibolite and hornblende gneiss; (2) garnet–mica schist and quartzite; and (3) interlayered amphibolite and quartzite. Lemmon (1973) also noted discontinuous lenses of marble interlayered within the mica schist in the Bat Cave quadrangle.

In the Columbus Promontory, the Poor Mountain Formation crops out in two distinct thrust sheets structurally below and above the Henderson Gneiss (Fig. 1–2; Plates I and III). Structurally below the Henderson Gneiss, only Poor Mountain amphibolite has been observed in a window through the Henderson Gneiss along the Tumblebug Creek fault (Figs. 1–2, 2–5; Plates I, III). Along Tumblebug Creek, the contact between the Poor Mountain amphibolite and the Henderson Gneiss is clearly a faulted contact (Fig 2–5): Henderson Gneiss in the hanging wall truncates folded quartzofeldspathic layers of the Poor Mountain Formation of the footwall (Fig. 2–5). This fault contact is folded and has also been transposed into the regional S_2 foliation and interleaving of the Poor Mountain Formation and the Henderson Gneiss is quite evident in exposures along Tumblebug Creek (Figs. 2–5). Edelman and others (1987) and Liu (1991) have also recognized similar interleaving between the Poor Mountain Formation and the Henderson Gneiss in South Carolina. According to Lemmon (1973), Tennessee Valley Authority drill–core data from Cane Creek in the Bat Cave quadrangle indicate that other units of the Poor Mountain Formation and Chauga River Formation are also be present beneath the Henderson Gneiss in this area. Lemmon (1973) and Dabbagh (1975) also described rock units within the Brevard fault zone, northwest of the area discussed here identical to those of the Chauga River Formation recognized in South Carolina by Sloan (1907), Shufflebarger (1961), and Hatcher (1969,1970,1972).

Structurally above the Henderson Gneiss, all units of the Poor Mountain Formation have been observed in the Sugarloaf Mountain thrust sheet (Figs. 1–2 and 2–6; Plates I and III). Stratigraphic and petrologic characteristics of the Poor Mountain Formation of the Columbus Promontory contained within the Sugarloaf Mountain thrust sheet are described below.

Amphibolite–hornblende gneiss. The amphibolite unit crops out beneath the Sugarloaf Gneiss and is present in the Cliffield Mountain, Saluda, Mill Spring, and Lake Lure quadrangles (Fig. 1–2; Plates I and III). The map unit is fine to medium grained, dark gray to black, and is commonly laminated with well-defined quartzofeldspathic layers. Where folded, this laminated amphibolite produces some of the most spectacular mesoscopic folds in the Columbus Promontory (Fig. 2–5). Mineralogically, the unit contains 22–70 percent dark–green pleochroic hornblende, 7–61 percent plagioclase (An $_{25–37}$), 0–22 percent quartz, occasional diopside and small flakes of pleochroic biotite (Table 2–4). Other accessory minerals include garnet, sphene, tremolite, zircon, apatite, and opaque minerals. In hand-specimen, the amphiboles have a readily discernible nematoblastic shape and define a weak to strong linear fabric in the rock. Whole-rock geochemical data were gathered from a suite of 21 samples from this unit. A discussion of the results of these analyses is the focus of Chapter III.

Garnet-mica schist. The garnet–mica schist unit generally crops out below the amphibolite–hornblende gneiss unit (Fig. 1–2; Plates I and III), although in some areas these units are tightly folded together. In the northwestern part of the Columbus Promontory in the Bat Cave, Cliffield Mountain, and Lake Lure quadrangles, it rests directly on the Henderson Gneiss along the Sugarloaf Mountain thrust, forming one of the sharpest contacts in the entire study area (Figs. 1–2 and 2–6; Plates I and III). In many cases this unit

Figure 2–6. Mosaic of photographs showing field exposure and hand sample of the Sugarloaf Mountain thrust, photomicrograph of the Sugarloaf Mountian thrust, and photomicrograph of garnet–mica schist of the Poor Mountian Formation. A) Exposure of the Sugarloaf Mountain thrust (SMT) in the Cliffield Mountain quadrangle. Here the SMT placed sillimanite schist of the Poor Mountain Formation (Pm) over the Henderson Gneiss (Hg). Person in foreground is approximately 2 meters tall. B) Hand sample containing the SMT. Sample shows well developed mylonitic texture in both the Hg and Pm. Sense of shear is top–to–SW (left). C) Photomicrograph of the SMT. Section is cut perpendicular to S_2 and parallel to the NE–SW trending mineral lineation. Note grain size reduction of both Hg and Pm. Field of view is 4mm. D) Photomicrograph of garnet–mica schist in the Pm. Section is cut parallel to NE–SW mineral lineation and perpendicular to S_2 defined by biotite and muscovite. Note variation in garnet morphology from euhedral growing across S_2 and elongated within S_2. Field of view is 4mm.

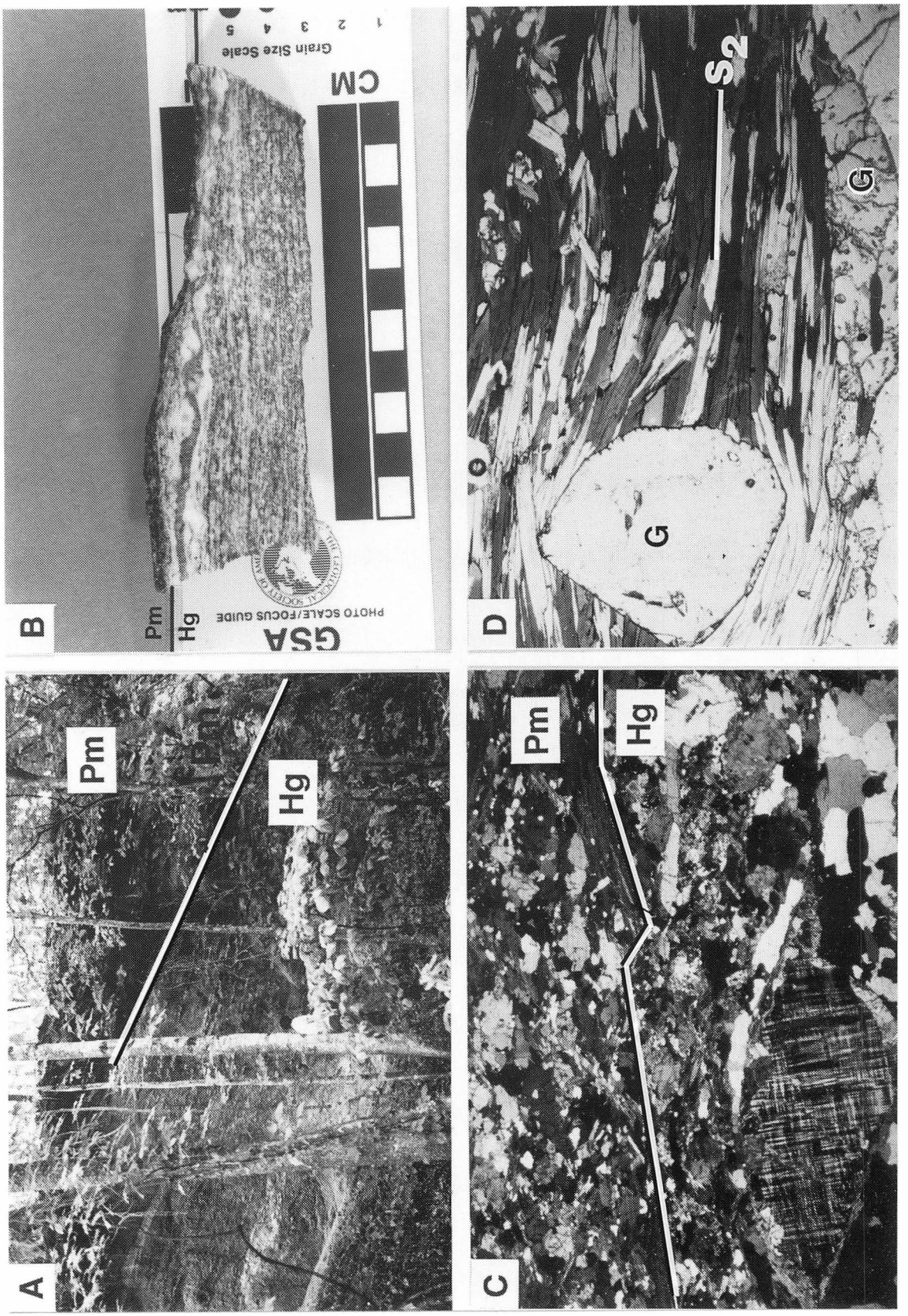

A
Pm
Hg
B
Pm
Hg
GSA
PHOTO SCALE/FOCUS GUIDE
CM
Grain Size Scale
1 2 3 4 5
C
Pm
Hg
D
S2
G
G

TABLE 2–4. Modal analyses of Poor Mountain schist from the Columbus Promontory. *Data from Lemmon (1973)

	*K9–12	*K8–2	*L7–4	*M5–11	*N6–14	I26A	CM677	CM81	CM551	CM501
Muscovite	30.2	27.5	29.1	24.3	27.7	1.9	30.8	24.1	37.7	27.3
Biotite	30.4	39.4	32.8	30.0	33.2	21.3	21.0	39.6	28.0	29.4
Quartz	25.7	22.0	29.5	30.9	32.5	49.6	38.7	33.2	29.2	27.0
Plagioclase	10.0	5.5	6.9	8.1	4.9	18.1	1.7	19.0	1.8	14.0
x=An	17	—	17	24	18	—	—	—	—	—
K–feldspar	1.5	2.2	0.7	0.7	tr	—	—	—	—	0.6
Chlorite	0.9	—	—	—	—	—	—	—	—	—
Garnet	tr	0.7	0.7	5.0	1.2	2.2	6.1	0.2	3.3	0.9
Opaques	1.3	2.5	0.3	0.6	0.4	tr	tr	tr	tr	0.6
Sillimanite	—	—	—	—	tr	13.1	1.7	tr	tr	0.2
Accessory	apatite sphene	zircon apatite	zircon apatite sphene	apatite sphene	zircon apatite	—	—	—	—	—

occurs on the topographically highest areas capping the ridge tops. This rock is purplish–red, to brown, to light gray, with the color being related to the amount of sillimanite, biotite, or muscovite in the rock and the degree of weathering. Modal analysis suggests that the protolith was probably a clay–rich sandstone (metagraywacke) or shale (Fig. 2–7). The schist consists of folia of strongly aligned grains of biotite (21–40 percent), muscovite (2–38 percent), fibrolitic sillimanite (0–13 percent) alternating with ribbons or layers of recrystallized quartz (22–50 percent), and minor amounts of K–feldspar. Accessory minerals include zircon, apatite, magnetite, ilmenite, and graphite (Table 2–5). Garnets have several morphologies: some are elongated parallel to the dominant foliation; others (up to 5mm) are anhedral to subhedral with inclusion–rich cores and clear rims, while others (1-2mm) have sub- to euhedral outlines and lack inclusions. Commonly, a second foliation can be observed that is defined by asymmetric muscovite grains and sillimanite bundles, asymmetric quartz–feldspar pods, or shear bands that disrupt the dominant foliation (see Chapters IV and V for more detailed discussion).

Lemmon (1973) also reported pods and discontinuous lenses of marble within the garnet-mica schist unit in the Columbus Promontory. A single chemical analysis of this marble (Lemmon, 1973) shows the rock to be a high–calcium marble similar to the chemistry of the marble reported from Poor Mountain, South Carolina by Hatcher and others (1973), further supporting the interpretation that these rocks in the Columbus Promontory are correlatives of the Poor Mountain Formation.

Quartzite–amphibolite. The lowest unit of the Poor Mountain Formation in the Columbus Promontory is a discontinuous sequence of interlayered impure quartzite and amphibolite (Fig. 1–2; Plates I and III). The quartzite varies from light yellow or white to dark brown or black. Mineralogically it contains predominantly quartz, although in some cases it does contain muscovite, sillimanite, amphibole, garnet, and other minor accessory minerals.

Figure 2–7. Quartz–feldspar–mica diagram comparing composition of metasedimentary rocks of the Columbus Promontory. Sandstone classification after Pettijohn (1948).

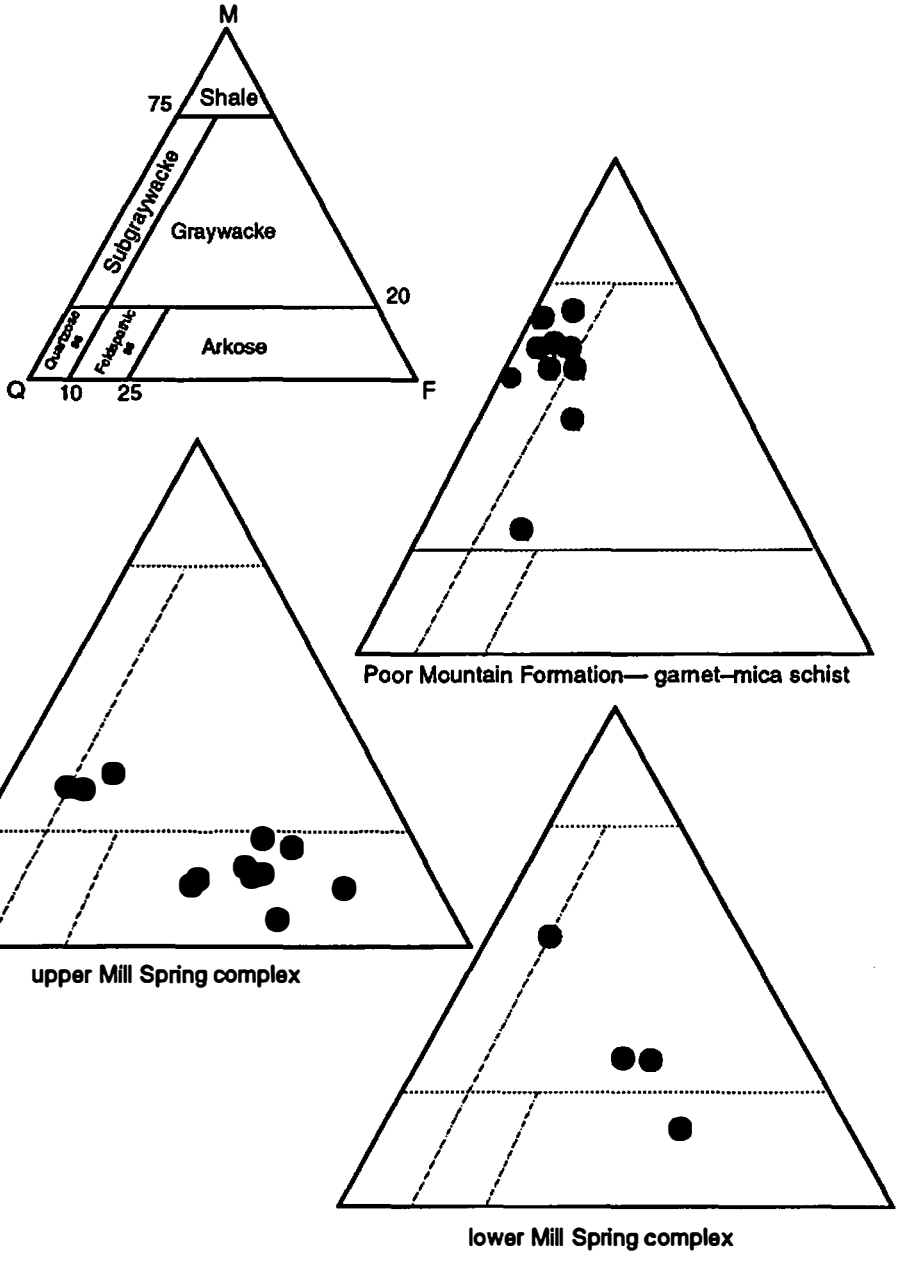

M
75
Shale
Subgraywacke
Graywacke
20
Quartzose
Feldspathic
Arkose
Q
10
25
F
Poor Mountain Formation— garnet–mica schist
upper Mill Spring complex
lower Mill Spring complex

TABLE 2–5. Modal analyses of Poor Mountain amphibolite from the Columbus Promontory. *Data from Bat Cave quadrangle (Lemmon 1973)

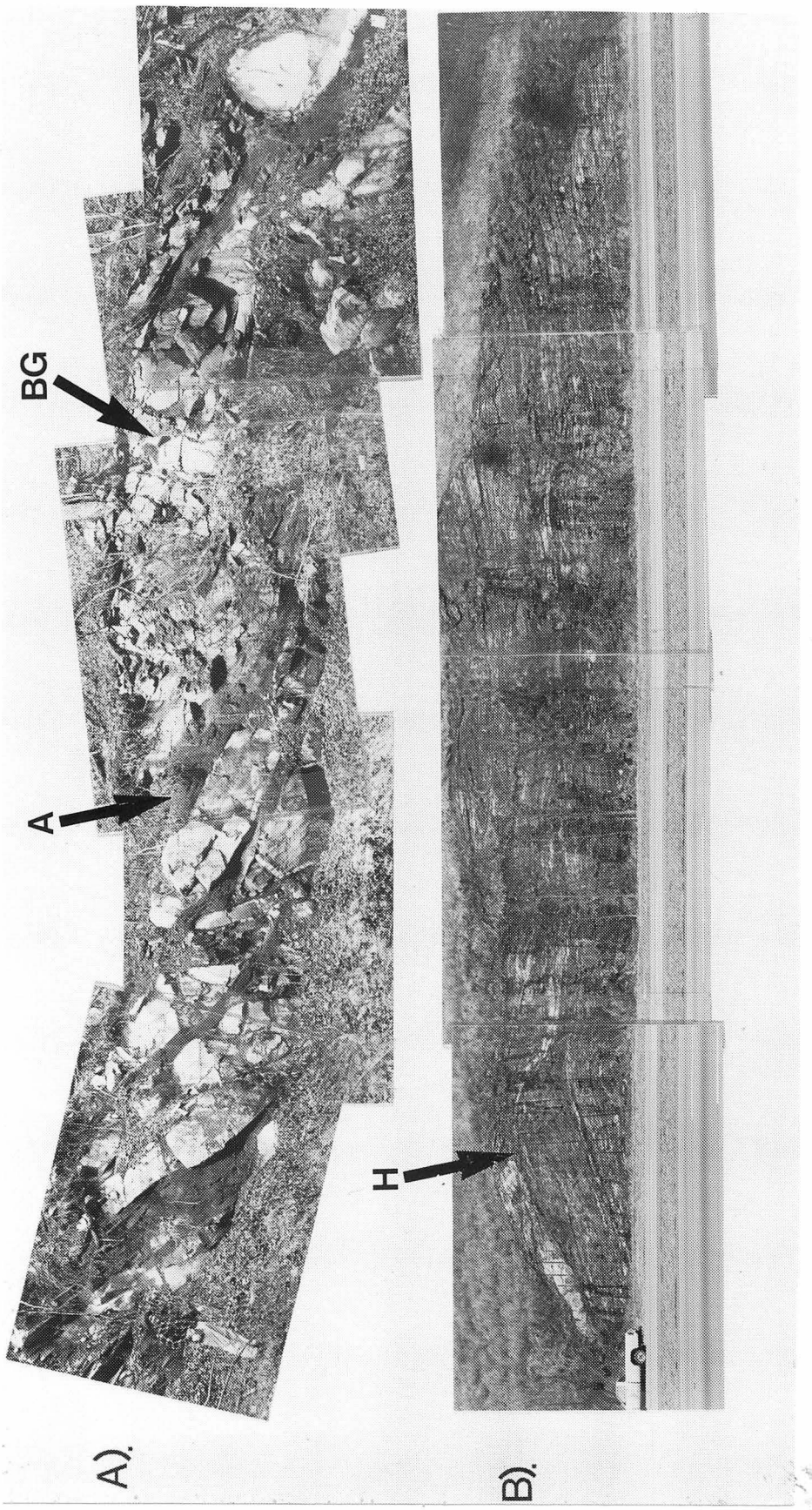
	*L8–1	*M5–15	*M8–4	*N7–26	*N6–6	TCF	CM499	CM361	CM255	BC1
Hornblende	48. 2	56.4	68.4	22.1	31.8	53.5	61.4	55.2	55.2	63.1
Plagioclase	28.2	40.4	30.5	60.6	24.9	21.3	7.5	39.6	28.2	19.4
x=An	34	32	26	25	37	34	27			32
Quartz	1.2	0.3	tr	9.3	tr	21.5	1.6	0.6	0.6	3.8
Diopside	14.2	—	—	—	11.9	—	—	—	—	—
Epidote	5.2	tr	tr	tr	31.4	tr	21.9	1.6	16.0	8.4
Tremolite	—	—	—	2.3	—	—	—	—	—	—
Sphene	—	0.4	—	tr	tr	tr	tr	—	—	—
Opaques	3.1	2.4	1.1	5.7	tr	3.7	2.0	2.4	—	0.6
Garnet	—	—	—	—	tr	—	tr	—	—	—
Chlorite	—	—	—	—	—	—	—	—	—	—
Biotite	tr	—	—	—	—	—	—	0.6	tr	0.4
Zircon	tr	tr	tr	—	tr	tr	5.6	—	—	4.3
Accessory	apatite	—	—	—	sericite	—	—	—	—	—

The amphibolite unit is mineralogically and texturally identical to the main body of Poor Mountain amphibolite described above. This unit is discontinuous and is commonly found at the contact between the Poor Mountain Formation and the underlying rocks of the upper Mill Spring complex (Plates I and III). At some localities both rock types are present, while at others only one of the rock units is visible. The contact between the Poor Mountain Formation and the underlying Mill Spring complex is interpreted to be primarily stratigraphic, although this is not entirely clear. The best exposures of this contact occurs on Long Ridge in the Cliffield Mountain quadrangle and at Melrose Mountain in the Saluda quadrangle (Plates I and III). At these localities, however, a stratigraphic versus fault contact is difficult to discern. On Long Ridge (Plates I and III) the contact is sharp and the lowermost quartzite–amphibolite unit of the Poor Mountain Formation has mylonitic characteristics and the amphibolite is occasionally intensely folded. On Melrose Mountain there is a stratigraphic interleaving of the biotite gneiss of the upper Mill Spring complex with the overlying Poor Formation, although the contact could represent either a transposed stratigraphic or early(?) premetamorphic fault contact.

Mill Spring Complex

The Mill Spring complex (Figs. 1–2, 2–1, and 2–8; Plates I and III) represents the areally most extensive rock unit in the Columbus Promontory. Detailed mapping suggests that the Mill Spring complex can be divided into upper and lower subunits based on the relative abundance of amphibolite. The upper Mill Spring complex is relatively amphibolite–poor whereas the lower Mill Spring complex contains abundant amphibolite. The upper Mill Spring complex is the lowest unit within the Sugarloaf Mountain thrust sheet; the lower Mill Spring complex comprises the Mill Spring thrust sheet ((Figs. 1–2 and 2–1; Plates I and III). Field and petrographic characteristics of the Mill Spring complex are outlined below.

Figure 2–8. Photomosaics of exposures of Mill Spring complex rocks along Interstate 26 between the Green River and Columbus, North Carolina. A) Interlayered biotite gneiss–metagraywacke (BG) and amphibolite (A) of the upper Mill Spring complex. Note the folding of the entire section, particularly in the interlayered amphibolite (dike?). Person in foreground is approximately 2 meters tall. Photo facing north. B) Migmatitic amphibole gneiss–amphibolite of the lower Mill Spring complex. Note large asymmetric lozenge (horse block (H)) on the east (left) side of the photo mosaic. Photo facing south.


A).
BG
A
B).
H

Upper Mill Spring Complex. The upper Mill Spring complex is dominantly a thick sequence of migmatitic biotite gneiss and metagraywacke (Fig. 1–2). It generally produces massive exposures (Fig. 2–8) and commonly forms the cliffs and balds in the study area. The mineralogy of the biotite gneiss–metagraywacke is quite variable, but on average contains 12-60 percent plagioclase (An_{20-35}), 12–56 percent quartz, 0-25 percent muscovite, 2-19 percent biotite, with minor amounts of sillimanite, garnet, and sphene (Fig. 2–9; Table 2–6). Accessory amounts of epidote, zircon, and opaque minerals are also present. Modal analysis indicates that the protolith of this unit included both arkosic sandstone to clay–rich sandstone (graywacke) (Fig. 2–7). The biotite gneiss–metagraywacke is light to medium gray, equigranular, fine- to medium–grained, massive to slightly banded. Locally the grain size of the mica is quite large and the unit resembles mica schist. Foliation is produced by parallel oriented biotite flakes and by parallel elongated grains of quartz and feldspar and trains of garnet (Fig. 2–9). In many areas this unit appears very migmatitic with marked segregations of the felsic, more micaceous, and mafic–rich layers (Fig. 2–8).

The biotite gneiss–metagraywacke contains pods and lenses of amphibolite parallel to the regional foliation (Fig. 2–8). These lenses commonly have a sill-like geometry and in most cases are parallel to the regional S_2 foliation (Fig. 2–8). This unit also contains pods and lenses of pegmatitic material parallel to the dominant foliation. In the western part of the study area, along the Green River (Plates I and III), the biotite gneiss of the upper Mill Spring Formation is a porphyroclastic biotite gneiss (Fig. 2–9). These rocks (e.g., samples CM 379, CM 750, CM 330, CM 306 in Table 2–6) generally contain higher contents of K–feldspar and less biotite and muscovite (Fig. 2–9). The porphyroclastic gneiss has a matrix identical to the biotite gneiss, but contains gray to pink, carlsbad–twinned microcline porphyroblasts.

Figure 2–9. Mosaic of photographs and photomicrographs of rocks of the Mill Spring complex. A) Biotite gneiss–metagraywacke of the upper Mill Spring complex. Sample composed primarily of quartz, biotite, plagioclase, fibrolitic and prismatic sillimanite, and accessory garnet. Section is cut perpendicular to S_2 and parallel to an E–W trending mineral lineation. Field of view is 4mm. B) Porphyroclastic gneiss of the upper Mill Spring complex from along the Green River in the Cliffield Mountain quadrangle. Porphyroclasts (arrow) are pink microcline (±1 cm). C) Photomicrograph of porphyroclastic gneiss from the top of White Oak Mountain in the Mill Spring quadrangle. Porphyroclasts are white microcline (K). Field of view is 4mm. D) Photomicrographs of amphibole–gneiss from the lower Mill Spring complex. Section cut parallel to E–W mineral lineation and perpendicular to S_2. Amphibole (A); quartz and plagioclase (Qf). Field of view is 4mm.

A
S2
B
GSA
IN
mm
C
K
D
Qf
A

Table 2–6. Modal analyses of biotite gneiss–metagraywacke of the upper Mill Spring complex. * Data from Lemmon (1973).

	*N8–19	*N9–21	*O9–1	*O9–2	CM152	CM183	CM427	CM54	CM379	CM750	CM330	CM306	CM723
Plagioclase	42.5	12.2	47.7	45.9	48.5	19.2	15.7	58.7	42.1	47.3	38.4	46.8	36.4
x=*An*	34	—	23	24	—	—	—	—	—	—	—	—	—
Quartz	43.0	56.5	30.5	32.7	26.7	46.5	52.6	21.5	30.2	32.3	31.3	16.9	39.6
K-feldspar	0.9	—	8.0	6.1	3.6	0.2	—	0.2	13.0	7.3	22.8	25.4	6.0
Biotite	11.3	10.1	11.2	12.4	15.3	7.5	18.5	18.9	10.8	8.6	2.7	8.2	8.6
Muscovite	—	20.0	2.4	2.5	5.9	25.0	10.8	0.4	3.2	4.5	1.7	2.7	2.7
Garnet	1.1	tr	—	—	tr	0.3	2.4	tr	—	—	tr	—	—
Epidote	1.1	—	tr	0.3	tr	tr	—	tr	—	tr	0.7	tr	2.1
Sphene	tr	—	—	—	—	—	—	—	—	—	0.5	tr	—
Chlorite	—	—	tr	tr			tr			tr	1.9	—	4.7
Opaques	tr	1.1	0.2	tr	tr	1.3	tr	0.3	0.7	tr	tr	—	tr
Accessory	zir	ap	zir	zir ap	—		sill		ser		ser	ser	ser

Lower Mill Spring Complex. The lower Mill Spring Formation (Figs. 1–2 and 2–1; Plate I and III) consists of a migmatitic sequence of biotite–granitic gneiss–metagraywacke, coarse amphibolite gneiss, and fine- to medium–grained amphibolite (Fig. 2–8). The complex interlayering of these rocks types makes it very to difficult to subdivide the individual units. Like the biotite gneiss–metagraywacke of the upper Mill Spring complex, the mineral composition of the biotite gneiss–metagraywacke in the lower Mill Spring complex is also quite variable. On average it consists of 10–45 percent plagioclase, 28–35 percent quartz, 0-29 percent K–feldspar, 11–27 percent biotite, and 6–26 percent muscovite (Table 2–7). Zircon, apatite, sphene and opaque minerals are generally present in accessory amounts. Epidote occurs in veins and as fillings in late brittle fractures. This unit is generally a mesocratic, light–gray, segregation banded, inequigranular, biotite gneiss–metagraywacke. It is permeated by migmatites and concordant pegmatitic layers (Fig. 2–8). The protolith of biotite gneiss–metagraywacke of the lower Mill Spring complex was probably also an arkosic sandstone or graywacke (Fig. 2–7). This rock is part of the unit mapped as migmatite by Hadley and Nelson (1971).

On the top of White Oak Mountain (Plates I and III) the migmatitic granitic gneiss and amphibolite of the lower Mill Spring complex grades into a porphyroclastic biotite gneiss (e.g., see samples 12–2–4 in Table 2–7). The porphyroclasts are composed of white microcline (Fig. 2–9). This unit commonly contains abundant mica and in many cases is very schistose. Thin amphibolite stringers are rare but do occur in this unit. Towards the western boundary of the lower Mill Spring Formation in the Saluda quadrangle, migmatitic amphibolite and granitic gneiss grade into a more amphibolite poor biotite-gneiss similar to that in the upper Mill Spring Formation (Fig. 1–2; Plates I and III). Here the lower Mill Spring complex can be seen overlying the garnet-mica schist of the Poor Mountain Formation and the biotite gneiss – metagraywacke of the upper Mill Spring complex along the Mill Spring thrust.

Table 2–7. Modal analyses of porphyroclastic biotite gneiss–metagraywacke of the lower Mill Spring complex.

	12–2–4	1–19–3	1–8–2	WO
Plagioclase	10.8	25.3	45.6	14.1
x=An	—	—	—	—
Quartz	33.4	32.4	29.2	28.0
K-feldspar	0.2	12.1	8.2	28.6
Biotite	26.7	22.4	11.3	21.0
Muscovite	25.9	6.9	3.5	8.2
Garnet	3.0	0.9	—	tr
Epidote	—	—	2.0	0.1
Sphene	—	—	—	—
Chlorite	tr	—	tr	—
Opaques	—	tr	0.2	tr
Accessory	—	ser	ser	

Amphibolite and amphibole gneiss in the lower Mill Spring complex occur as both large pods and tabular or sill–like stringers (Fig. 2–8). The large pods are commonly permeated with leucogranite or pegmatitic layers as in the biotite gneiss–metagraywacke units (Fig. 2–8). The foliation in the amphibolite and amphibole gneiss is defined by alternating mafic and felsic layers. The mineralogic makeup of the amphibolite in the lower Mill Spring complex is also variable (Table 2–8), but on average includes 35–60 percent dark–green pleochroic hornblende, 25–50 percent plagioclase (An_{20-30}), 2–20 percent quartz, 0–30 percent biotite, with minor amounts of epidote, garnet, and opaque minerals (Fig. 2–9). Zircon, sphene, and chlorite occur as accessory minerals. Amphibolite of the lower Mill Spring complex is generally more massive and coarser grained than the amphibolite of the Poor Mountain Formation, although this is not always the case. Individual amphibole minerals also have a readily observable nematoblastic shape and define a weak to strong linear fabric in the rocks. Twenty–eight amphibolite samples from the lower Mill Spring complex were selected for geochemical analysis and the data and results are also discussed in Chapter III.

REGIONAL RELATIONSHIPS

Correlation of Stratigraphic Units

Regional lithostratigraphic correlations in the crystalline southern Appalachians have been made based on the similarities of physical stratigraphy, structural positions, compositional (modal), and geochemical similarities. This approach has resulted in important contributions toward the understanding of the regional lithostratigraphic correlations in the crystalline southern Appalachians and include the studies of Shufflebarger (1961), Hatcher

Table 2–8. Modal analyses of amphibolite of the lower Mill Spring complex.

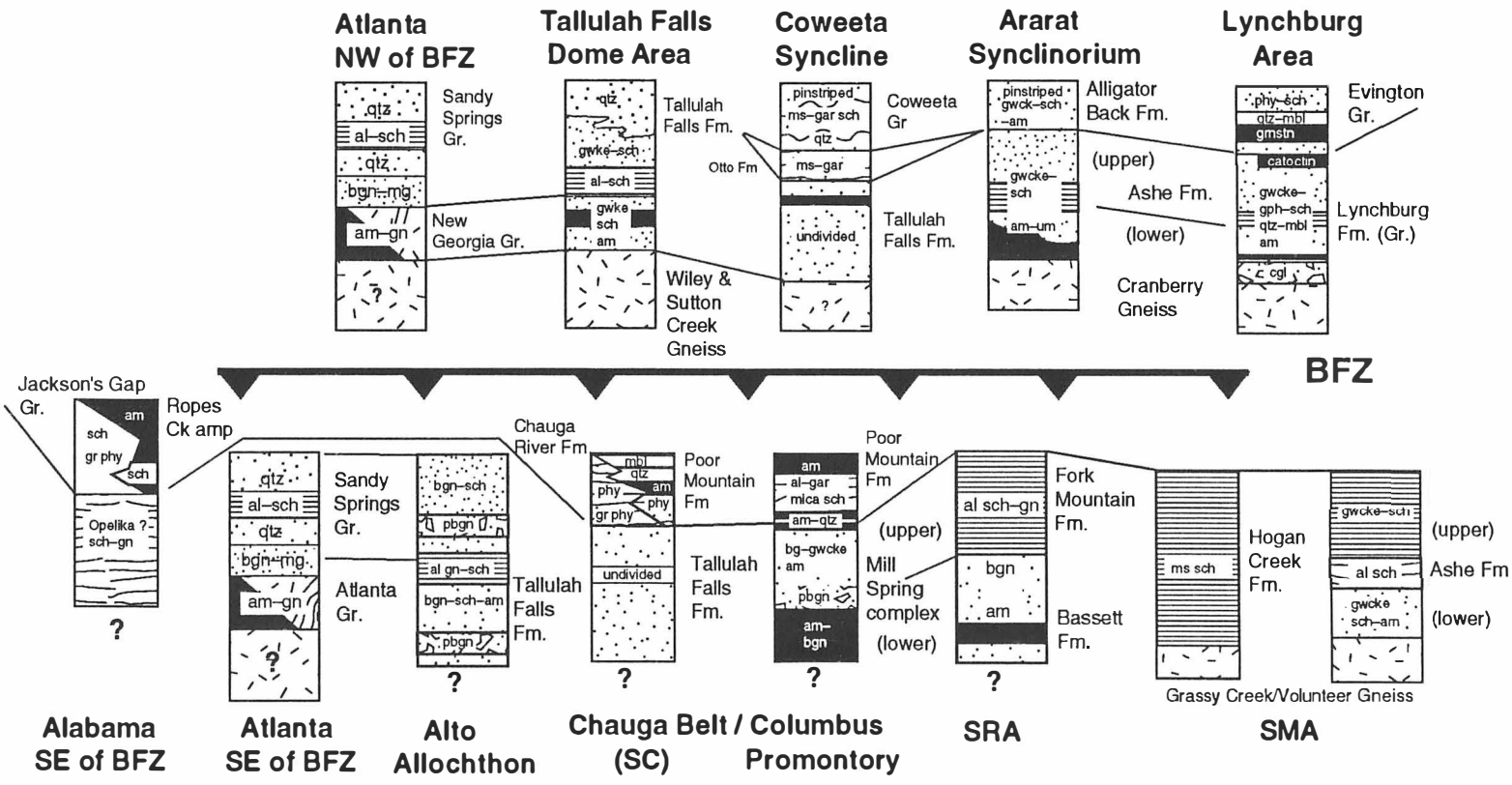
	3–16–12	1–14–3	11-16–1	1–19–1	3–16–11	1–17–2
Hornblende	44.4	37.5	47.2	60.5	34.7	53.6
Plagioclase	24.8	50.0	21.2	36.1	28.2	39.6
x=An	—	—	—	—	—	—
Quartz	19.6	2.8	31.6	1.8	3.2	4.8
Diopside	—	—	—	—	—	—
Epidote	2.6	5.5	tr	tr	—	—
Tremolite	—	—	—	—	—	—
Sphene	—	—	—	—	—	—
Opaques	4.4	4.0	tr	1.6	—	—
Garnet	2.4	—	—	—	—	—
Chlorite	—	—	tr	—	3.4	—
Biotite	1.8	0.2	—	—	30.5	2.0
Zircon	tr	tr	tr	—	—	—
Accessory	—	—	—	—	—	—

(1973,1978a), Rankin (1970, 1975), Rankin and others (1973), Hurst and Jones (1973), McConnell and Abrams (1984), Wehr and Glover (1985), Hatcher and Goldberg (1990). The studies have shown that the eastern flank and central part of the Blue Ridge contains a major metasedimentary and metavolcanic unit that extends discontinuously from Virginia to Alabama (Hatcher and Goldberg, 1990). Locally this unit is known by several different names including the Lynchburg Formation in Virginia (Espenshade, 1954; Brown, 1958; Wehr and Glover, 1985), the Ashe Formation in NW North Carolina (Rankin, 1970, 1975), the Tallulah Falls Formation in NE Georgia and adjacent South Carolina (Hatcher, 1971a, 1978, 1989), and the Sandy Springs/New Georgia Groups near Atlanta, Georgia (McConnell and Abrams, 1984) (Fig. 2–10). The details of the correlation of these units was most recently discussed by Hatcher and Goldberg (1990).

A characteristic of the Lynchburg–Ashe–Tallulah Falls–Sandy Springs/New Georgia Group sequence of rocks is the general separation of these units into a mafic and felsic sections. In several areas within the eastern Blue Ridge in the Carolinas and Georgia this unit displays a transition from a basal(?) section consisting of a thick sequence of biotite gneiss, metagraywacke, and schist with abundant mafic and ultramafic rocks that grade upward (?) into a similar sequence of gneiss, metagraywacke, and schist, but with fewer mafic and ultramafic rocks. These characteristics have been described in the eastern Blue Ridge by Rankin (1970, 1975) for the Ashe Formation in North Carolina, Hatcher (1971a, 1978a) for the Tallulah Falls Formation in NE Georgia, and McConnell and Abrams (1984) for rocks of the Sandy Springs Group/ New Georgia Group near Atlanta, Georgia. Wehr and Glover (1985) similarly discussed a mafic rich versus mafic poor stratigraphic subdivision in the Lynchburg Group, however, noted a reversed succession with the mafic rich units overlying the relatively mafic poor units that they suggested may be the result structural complexities (e.g., thrust faults) within the Lynchburg Group. Despite this, they also interpreted the Lynchburg Group to be stratigraphically correlative with the Ashe Formation of Rankin (1970, 1975).

Figure 2–10. Proposed regional stratigraphic correlation of metasedimentary rocks of the eastern Blue Ridge and Inner Piedmont, including rocks of the Poor Mountain Formation and Mill Spring complex of the Columbus Promontory. Diagram is modified from Hopson and Hatcher (1988) and Hatcher and Goldberg (1990).

Eastern Blue Ridge



Inner Piedmont

This lithostratigraphic pattern (mafic rich vs. mafic poor section) has also been recognized in the Inner Piedmont rocks of South Carolina by Griffin (1969, 1971a, 1974a) , in the Sauratown Mountains (Heyn, 1984; Hatcher, 1988; McConnell, 1990) and in the Alto allochthon by Hopson and Hatcher (1988). In both the Alto allochthon and Sauratown Mountains window, detailed mapping has delineated a lithostratigraphic succession nearly identical to that of the Tallulah Falls Formation originally defined in eastern Blue Ridge of NE Georgia by Hatcher (1971b) in which he noted the presence of more mafic rocks near the base of the formation. Rock units described by Conley and Henika (1973) in the Smith River allochthon (Basset Formation overlain by Fork Mountain Formation) in the Inner Piedmont of NW North Carolina and adjacent Virginia also contain this stratigraphic succession. Conley (1978) has correlated rocks of the Smith River allochthon to the Lynchburg Group in the eastern Blue Ridge of SW Virginia. The geologic map of the Winston Salem 1° x 2° sheet of Goldsmith and others (1988) contains rock units that also display a similar stratigraphic pattern. The detailed mapping and petrographic analysis of this study supports the conclusion that this stratigraphic pattern is also recorded by rocks of the Mill Spring complex. Consequently, it is interpreted that the Mill Spring complex is equivalent to the Lynchburg –Ashe–Tallulah Falls Formation and correlative rock units recognized in both the eastern Blue Ridge and other areas in the Inner Piedmont.

Throughout much of the eastern Blue Ridge and adjacent Inner Piedmont, rocks of the lower sequence described above (Lynchburg–Ashe–Tallulah Falls Formation and equivalents) are overlain by a sequence of rocks including the Evington Group in Virginia, the Alligator Back Formation in NW North Carolina , the Chauga River and Poor Mountain Formations in the Carolinas and Georgia (Fig. 2–10). Stratigraphically (and structurally), rocks of this sequence maintain a similar position above the Lynchburg–Ashe–Tallulah Falls Formation rocks and their equivalents throughout the eastern Blue Ridge and Inner Piedmont, and are commonly preserved in regional synclinoria. These include the James

River synclinorium in Virginia, the Ararat River synclinorium in North Carolina, and the Chauga belt in the Carolinas and Georgia. Contact relationships between the upper and lower sequences are generally considered conformable (Hatcher, 1973; Rankin and others, 1973; Rankin, 1975; Wehr and Glover, 1985; Hatcher and Goldberg, 1990). Field observations indicate that this lithostratigraphic succession also is present in the Columbus Promontory between rocks of the Mill Spring complex and the overlying Poor Mountain Formation, consistent with regional lithostratigraphic patterns.

In the Ararat River synclinorium in the North Carolina Blue Ridge, Rankin and others (1973) recognized a stratigraphic sequence distinctly different from the typical layered gneiss and schist of the Ashe Formation that forms a mappable unit consisting of gneiss, pelite, and amphibolite with minor amounts of quartzite and marble they designated the Alligator Back Formation. Rankin and others (1973) suggested that the most obvious correlation of the Alligator Back Formation is with the Evington Group (Espenshade, 1954; Brown, 1958; Patterson, 1989) of central Virginia because both are in synclinoria and overlie formations (Ashe and Lynchburg) considered to be correlative. Although a matter of considerable debate (e.g., Brown, 1958; Patterson, 1989) the stratigraphy of the Evington Group consists of a varied sequence of pelitic schist, some graphitic schist, considerable marble and quartzite, and metabasalt. This correlation was also suggested by the studies of Wehr and Glover (1985) and more recently by Patterson (1989), both of which also suggested that the Evington Group may be the deep–water equivalent of the Chilhowee Group exposed in the western Blue Ridge of Virginia.

Shufflebarger (1961) was the first to suggest the possibility that rocks of the Poor Mountain Formation (series) in South Carolina were correlative with rocks of the Evington Group to the NE. The similarity of reoccurring rock sequences in the Brevard belt (Chauga River and Poor Mountain Formations) and Evington Group indicated to Shufflebarger (1961) that they are at least partly correlative. Stirewalt and Dunn (1973) also proposed that this region in South Carolina

is part of a regionally gently northeast–plunging synclinorium similar to the James River synclinorium in Virginia that contains rocks of the Evington Group that are at a higher structural level than the adjacent Blue Ridge and Inner Piedmont. The Chauga River Formation and Poor Mountain Formation extend from type localities in South Carolina (Sloan 1908, Shufflebarger 1961, Hatcher 1969,1970,1971b) to the southwest as far as Gainesville, Georgia (Hurst 1973), and they extend from the type locality (in South Carolina) to the northeast into the present study area. Recent work by Yanagihara and others (1992) indicates that Poor Mountain Formation rocks are also present immediately northeast of the area discussed in this paper, and probably continue as least as far NE as Morganton, North Carolina. These correlations indicate that the Chauga River and Poor Mountain Formation rocks extend for a considerable distance within the western Piedmont of the Carolinas and Georgia.

Similarities in physical stratigraphy indicate that upper sequence rocks are also present adjacent to the Brevard fault zone in the Inner Piedmont of Alabama. Rocks from this area include the Jackson's Gap Group and the Ropes Creek amphibolite. Rocks of the Jackson's Gap Group, which include sericite–quartz phyllite, graphitic schist and phyllite, metaquartzite, and local pebble conglomerate are similar to those described by Hatcher (1969, 1970) from the Chauga River Formation in South Carolina. Likewise, the Ropes Creek amphibolite is remarkably similar, both in hand sample and geochemically, to amphibolite of the Poor Mountain Formation. Bentley and Neathery (1970) speculated on the stratigraphic and structural correlation between the Jackson Gap Formation and the Ropes Creek amphibolite with the Chauga River and Poor Mountain Formations. This correlation is again proposed here based on similarities in physical stratigraphy and structural positions.

Thus based on the similarities in physical stratigraphy and structural positions, it is suggested that the Poor Mountain Formation and the Mill Spring complex of the Columbus Promontory, are correlative with other lithostratigraphic units in the eastern Blue Ridge and Inner Piedmont.(Fig. 2–10). Here it proposed that the Poor Mountain Formation and the Mill Spring

Formation are representatives of two regionally (VA to AL) persistent lithostratigraphic (structural?) successions present in the crystalline southern Appalachians. These include 1) a lower sequence consisting of Lynchburg–Ashe–Tallulah Falls–Mill Spring–Sandy Springs/New Georgia–type rocks, and 2) an upper sequence consisting of Evington–Alligator Back–Chauga River/Poor Mountain–Jackson's Gap/Ropes Creek type rocks (Fig. 2–10). Rocks of the lower sequence are generally considered to be Late Proterozoic to Early Cambrian, whereas those of the upper sequence younger Late Proterozoic or Early Cambrian (Rankin, 1970, 1975; Rankin and others, 1973; Hatcher, 1972, 1973, 1987, 1989). This suggests, based on the above correlations, that the Poor Mountain Formation and Mill Spring complex are also Late Proterozoic to Early Cambrian.

Depositional Environment and Tectonic Implications

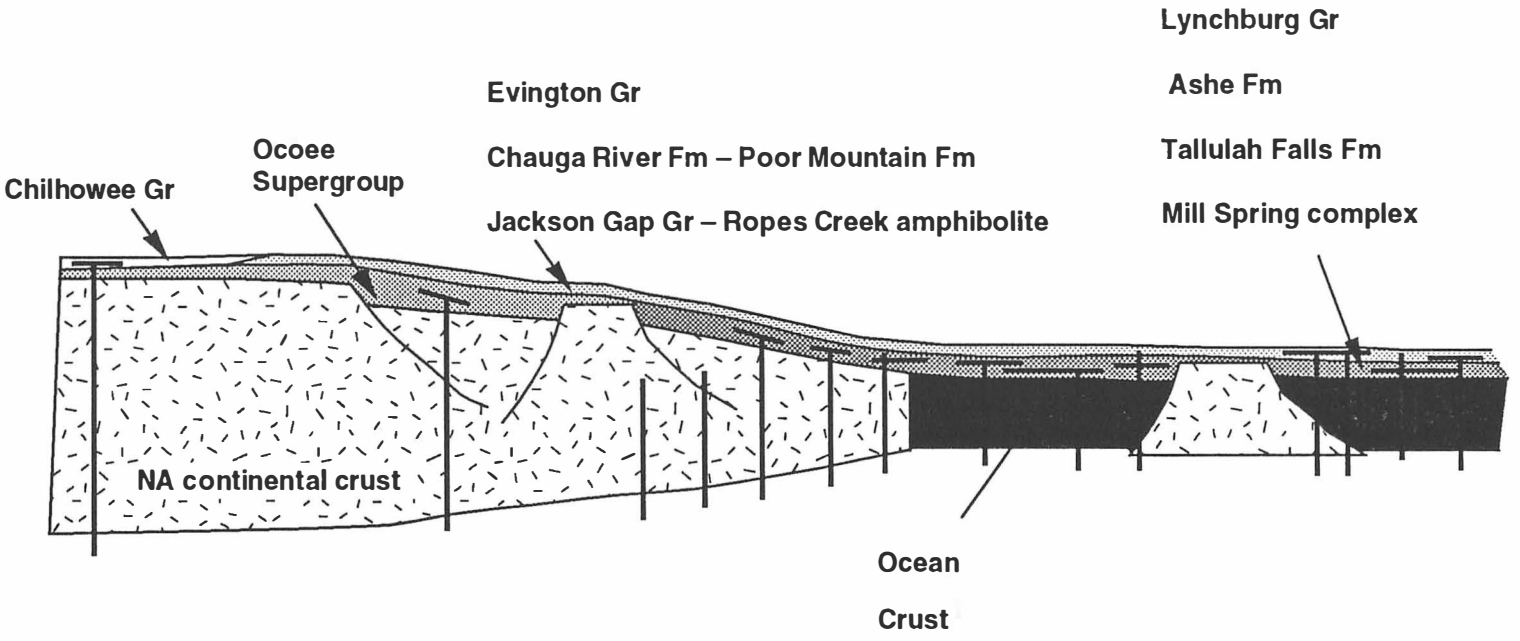
It has been proposed by many southern Appalachian researchers (Thomas, 1976, 1977, 1983, 1991; Rankin, 1975, 1976; Hatcher, 1978a, 1987, 1989; Hatcher and Odom, 1980; Rast and Kohles, 1986; Wehr and Glover, 1985) that the opening of the Iapetus and Theic–Rheic Oceans in the Late Proterozoic–Early Cambrian resulted in an irregular, Atlantic–type rifted North American margin. This irregular margin was outlined by promontories and embayments of continental crust along which depositional basins of various depths developed. The accumulation of Late Proterozoic–Early Cambrian sedimentary and volcanic rocks, discussed above and including the Poor Mountain Formation and the Mill Spring complex, is generally considered to have occurred within these fault–bounded basins along this irregular margin (Thomas, 1991). These rocks have been interpreted by Rankin (1970, 1975), Rankin and others (1989), Hatcher (1978a, 1987, 1988), Wehr and Glover (1985), Hatcher and others (1989), Thomas (1991) as a sequence of North American deep– to shallow–water, rift–facies sandstone, shale, and mafic volcanic lava flows deposited along the Laurentian margin. By analogy (based

on physical similarities), lithostratigraphic units in the Columbus Promontory (Poor Mountain Formation and Mill Spring complex) are also interpreted to represent part of the deep–water rift facies rocks deposited along the Laurentian margin (Fig. 2–11).

Rankin (1970, 1975), Hatcher (1973), Wehr and Glover (1985), McConnell (1988), and Stieve (1989) have shown that in the eastern Blue Ridge this assemblage locally rests on Grenville basement (Fig. 2–11). Hatcher (1978a) and McConnell and Abrams (1984) have also suggested that this sequence was also deposited, in part, on oceanic crust. As will be discussed in greater detail in Chapter III, the geochemistry of mafic rocks within the Poor Mountain Formation and the Mill Spring complex, suggest that these rocks were most likely deposited in an oceanic setting, possibly on oceanic crust, and therefore represent the offshore equivalents of those rocks (e.g., parts of the Tallulah Falls–Ashe Formation) that were deposited on continental crust (Fig. 2–11).

An important consequence of this proposed correlation relates to the tectonic relationship between the eastern Blue Ridge and the Inner Piedmont. As previously noted, Hatcher (1978a,1987, 1989) and Hatcher and others (1990) suggested that stratigraphic sequences within the Inner Piedmont are equivalent to those in the eastern Blue Ridge. Alternatively, Horton and others (1989), and Rankin and others (1989) suggested that the Inner Piedmont represents a separate tectonic entity from their Jefferson terrane (eastern Blue Ridge), with one or both terranes possibly exotic to the North America Laurentian margin sequence (e.g., western Blue Ridge). Higgins and others (1984 and 1988) visualized the entire crystalline terrane of Georgia and Alabama as consisting of a huge stack of crystalline thrust sheets with rocks of both North American and African affinity juxtaposed during a continuum of Paleozoic orogenesis. More recently, Dennis (1991) speculated that the Inner Piedmont may represent the basement upon which the Carolina arc was built and subsequently exposed by a southeast–dipping, low–angle detachment fault similar to those in the western U.S. Cordillera (see Snoke and others, 1984).

Figure 2–11. Schematic cross section of the Laurentian margin showing the proposed depositional setting and regional relationship of stratigraphic units discussed in this chapter.


Lynchburg Gr
Ashe Fm
Tallulah Falls Fm
Mill Spring complex
Evington Gr
Chauga River Fm – Poor Mountain Fm
Jackson Gap Gr – Ropes Creek amphibolite
Ocoee
Supergroup
Chilhowee Gr
NA continental crust
Ocean
Crust

Based on the correlation of rocks in the Columbus Promontory with rocks of the eastern Blue and elsewhere in the Inner Piedmont presented here, this study further supports the interpretation of Hatcher (1978, 1987, 1989) and Hatcher and others (1990) that lithostratigraphic units in the eastern Blue Ridge and the Inner Piedmont are equivalent and record deposition along the ancient Laurentian margin during the Late Proterozoic or Early Cambrian. An important corollary of this interpretation is that the Brevard fault zone, although recognized as a significant structural discontinuity, does not separate terranes of different tectonic affinity. This interpretation is also consistent with the previous interpretation of Hatcher (1978a, 1987, 1989) and Hatcher and others (1990).

CHAPTER III

GEOCHEMISTRY OF AMPHIBOLITE FROM THE COLUMBUS PROMONTORY, WESTERN INNER PIEDMONT, NORTH CAROLINA

INTRODUCTION

Metamorphosed mafic and ultramafic rocks represent a significant component of the stratigraphy of the crystalline terrane of the southern Appalachian orogen internides east of the Hayesville–Gossan Lead fault (Hatcher and others, 1990). General characteristics of numerous bodies within the southern Appalachian orogen were most recently reviewed by Misra and Keller (1978) and Misra and McSween (1984). Most detailed mafic rock geochemical studies in the southern Appalachians have concentrated on those bodies in the Blue Ridge (e.g., Bland, 1978; Hatcher and others, 1984; McConnell and Abrams, 1984; Badger, 1989; Gillon, 1989, Hopson, 1989; and Misra and Conte, 1991), whereas few mafic rock geochemical studies have been undertaken in the southern Appalachian Inner Piedmont; a fact consistent with the general lack of detailed study for many aspects of the geology in the Inner Piedmont terrane. Mafic rock geochemical studies in the Inner Piedmont include those of Conley (1978) in the Inner Piedmont of southwestern Virginia, Achaibar (1983) and Achaibar and Misra (1984) in the Smith River allochthon, Stow and others (1984), and Neilson and Stow (1986) in the Alabama Piedmont. The purpose of this chapter is to discuss the geochemistry of amphibolite within the Poor Mountain Formation and the Mill Spring complex in the Inner Piedmont of North Carolina.

Sampling and Analytical Techniques

Amphibolites in the Columbus Promontory occur in two distinct stratigraphic sequences, the Poor Mountain Formation and the Mill Spring complex. The field and petrologic characteristics of these amphibolites were previously outlined in Chapter II. Based on field relationships and petrographic criteria, 45 amphibolite samples from the Columbus Promontory were selected for geochemical analysis (Fig. 3–1). Samples were chosen based on their geographic distribution and lack of secondary alteration. As a result, 19 samples from the Poor Mountain Formation and 26 samples from the Mill Spring complex were selected for whole-rock XRF analysis (Fig. 3–1). Whole-rock XRF analysis was performed on an EG&G Ortec automated energy dispersive X-ray fluorescence spectrometer. Values for 10 major and 8 minor and trace elements were obtained using an igneous rock protocol appropriate for amphibolites and metamorphic rocks with an igneous protolith. The spectrometer run conditions were as follows: 1) Rh anode with no filter for Na, Mg, Al, Si, P, K, Ca, and Mn; 2) W anode with Cu filter for Ti, V, Cr, Fe, and Ni; and 3) W anode with In filter for Rb, Sr, Y, Zr, and Nb. The counting time for all analyses was 300 seconds. Results of these analyses are shown in Tables 3–1 and 3–2.

Whole–Rock Approach and Limitations

Because metamorphism, penetrative deformation, and transposition have obliterated any relict igneous textures and megascopic field criteria for determining the protolith history of the Columbus Promontory amphibolites, this study relies heavily on whole-rock geochemistry. This approach has been successful in many studies in the crystalline southern Appalachians (Hatcher and others, 1984; Stow and others, 1984; Goldberg and others, 1986; Misra and Conte, 1991) and in other orogenic regions (Pearce

Figure 3–1. Location of Columbus Promontory amphibolite samples selected for whole–rock XRF analysis. Corresponding whole–rock geochemical data shown in Tables 3–1 and 3–2.

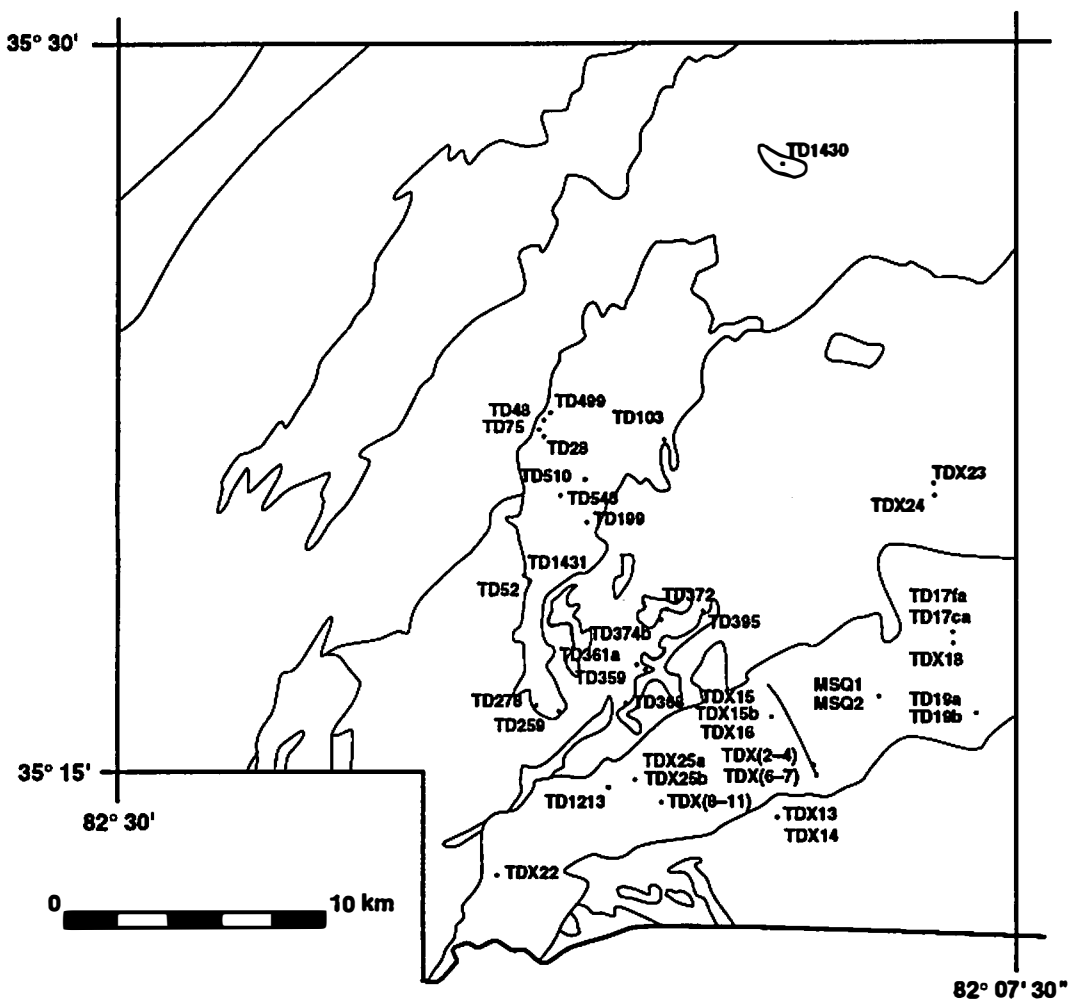

35° 30'
35° 15'
82° 30'
82° 07' 30"
0
10 km
TD1430
TD48
TD75
TD499
TD103
TD28
TD510
TD545
TD199
TD1431
TD52
TD372
TD395
TD374b
TD361a
TD359
TD278
TD259
TD388
TDX15
TDX15b
TDX16
MSQ1
MSQ2
TDX23
TDX24
TD17fa
TD17ca
TDX18
TD19a
TD19b
TDX25a
TDX25b
TDX(2–4)
TDX(6–7)
TDX(8–11)
TD1213
TDX13
TDX14
TDX22

Table 3–1. XRF analyses of Poor Mountain Formation amphibolite from the Columbus Promontory.

wt% oxide	TD1431	TD1430	TD361A	TD374B	TD395	TD359F	TD48	TD103	TD259	TD276	TD372	TD52	TD366	TD543	TD28	TD75	TD499	TD199	TD510
SiO_2	50.54	50.05	49.61	48.62	55.07	50.10	54.99	49.41	47.55	51.26	48.58	52.01	49.96	45.76	48.40	49.90	48.22	50.67	65.37
TiO_2	1.65	1.12	1.24	0.67	1.33	1.76	1.12	1.43	0.51	0.40	1.05	1.84	1.74	1.13	1.16	0.68	1.95	1.08	0.46
Al_2O_3	13.76	14.39	15.70	16.47	15.23	15.13	16.83	15.82	11.69	14.59	15.21	13.56	13.61	15.11	17.76	16.66	14.72	16.60	13.12
$^1Fe_2O_3$	13.38	11.79	13.38	12.15	10.11	8.94	8.65	11.25	12.74	10.15	11.98	13.10	15.96	12.76	10.19	11.62	13.00	13.13	4.99
MnO	0.21	0.20	0.29	0.62	0.20	0.20	0.27	0.19	0.24	0.45	0.26	0.22	0.31	0.23	0.15	0.26	0.21	0.24	0.24
MgO	5.90	7.23	5.77	5.83	4.40	7.92	2.91	6.30	12.08	6.90	6.16	5.72	5.07	11.99	6.35	6.73	7.94	3.47	4.17
CaO	9.68	10.54	8.25	8.76	6.26	5.44	7.12	6.80	11.93	8.26	10.12	8.46	8.44	10.51	11.34	9.44	14.43	8.02	7.17
Na_2O	2.93	3.98	3.60	4.61	1.61	5.61	3.67	1.59	3.77	3.11	3.65	2.22	1.89	2.95	3.41	2.02	3.49	2.55	4.46
K_2O	0.32	0.44	0.12	1.05	0.01	6.06	0.54	0.12	0.73	0.23	0.70	0.36	0.76	0.26	0.22	0.12	0.67	0.46	0.38
P_2O_5	0.23	0.19	0.03	0.07	0.14	0.00	0.16	0.24	0.11	0.07	0.13	0.22	0.08	0.14	0.13	0.11	0.42	0.03	0.31
TOTAL	99.27	99.87	98.35	98.03	97.57	97.40	98.40	99.23	99.38	98.10	99.34	99.13	98.17	99.83	100.65	98.97	101.59	97.37	98.76
trace elements (ppm)																			
Cr	114.0	201.2	122.1	209.5	16.2	327.1	25.0	263.2	354.6	511.5	314.4	97.6	143.2	460.1	295.7	304.3	216.3	90.7	1.0
Nb	5.2	2.5	2.3	0.5	4.6	26.0	13.7	6.3	0.5	3.1	2.6	7.6	7.7	2.1	2.2	2.3	3.2	2.2	22.4
Ni	41.2	50.6	54.6	64.4	12.1	149.7	0.0	126.6	84.1	99.9	135.5	27.5	41.4	245.6	158.2	100.2	65.4	23.6	11.2
Rb	5.3	6.0	3.0	26.6	3.8	306.4	10.6	6.3	11.2	7.7	16.1	7.6	14.1	9.8	7.4	5.2	20.7	6.2	9.0
Sr	206.0	204.1	168.0	277.6	234.4	1007.6	225.9	561.6	96.6	112.2	151.4	215.1	133.2	131.6	174.4	220.7	204.6	147.1	97.1
V	272.0	257.5	207.6	163.6	135.6	175.2	163.9	213.5	262.9	139.7	236.3	238.0	252.6	251.3	270.5	200.4	465.9	216.0	66.5
Y	47.6	26.5	23.0	15.6	40.6	16.4	92.1	23.3	11.7	25.0	24.9	50.7	41.6	23.4	27.3	19.1	31.6	28.5	63.2
Zr	125.2	61.7	62.2	59.9	91.4	387.6	144.6	148.2	49.7	62.5	67.1	148.5	73.5	67.6	74.7	64.9	96.2	66.9	222.3
** normative mineralogy*																			
[1] Total Fe																			
* Calculated assuming $Fe^{+3}/Fe^{2+} = 0.1$																			
Q	0.00	0.00	0.00	0.00	3.97	0.00	0.00	0.00	0.00	0.00	0.00	0.42	2.61	0.00	0.00	0.00	0.00	0.63	27.66
C	0.00	0.00	0.00	0.00	0.00	0.00	0.00	0.00	0.00	0.00	0.00	0.00	0.00	0.00	0.00	0.00	0.00	0.00	0.00
Or	1.93	2.66	0.73	0.73	0.06	37.19	3.27	0.72	4.39	1.70	4.21	2.17	4.77	1.68	1.30	0.72	3.94	2.63	2.26
Ab	29.26	25.35	34.67	34.66	42.12	10.56	46.64	31.62	13.70	32.60	25.21	31.54	19.42	16.20	23.90	29.47	10.09	30.70	21.95
An	21.61	25.37	25.34	25.34	20.63	15.74	19.62	26.82	23.57	22.68	25.93	19.97	25.71	32.34	34.65	30.48	29.00	29.96	23.63
Ne	0.00	0.00	0.00	0.00	0.00	2.67	0.00	0.00	0.00	0.00	0.65	0.00	0.00	0.00	0.61	0.00	3.75	0.00	0.00
Di	21.43	22.19	13.64	13.64	8.61	9.69	13.02	13.24	29.32	15.54	20.03	17.93	14.38	15.93	17.09	13.76	32.73	9.51	8.74
Hy	15.47	12.01	7.02	7.02	20.21	0.00	9.39	8.17	3.49	10.42	0.00	22.30	27.32	3.12	0.00	10.49	0.00	22.52	13.33
Ol	4.36	6.35	14.25	14.24	0.00	19.10	2.41	16.72	22.70	14.61	19.95	0.00	0.00	26.62	16.65	12.03	14.30	0.00	0.00
Mt	1.63	1.44	1.65	1.65	1.25	1.11	1.09	1.37	1.55	1.25	1.46	1.60	1.98	1.55	1.22	1.42	1.55	1.63	0.61
IL	3.58	2.17	2.42	2.42	2.61	3.50	2.16	2.76	0.99	0.78	2.03	3.57	3.42	2.17	2.25	1.32	3.69	2.13	0.89
Cm	0.02	0.03	0.02	0.03	0.00	0.05	0.00	0.04	0.06	0.08	0.04	0.02	0.02	0.07	0.04	0.05	0.03	0.02	0.00
Ap	0.56	0.46	0.07	0.07	0.37	0.00	0.44	0.58	0.27	0.17	0.31	0.53	0.20	0.34	0.31	0.27	0.99	0.07	0.75

Table 3–2. XRF analyses of lower Mill Spring complex amphibolite from the Columbus Promontory.

wt% oxide

	TDX9	TDX19	TDX24	TDX4	TDX26A	TDX26B	TDX8	TDX3	TDX23	TD17CA	TDX14	TDX22	TDX11	TDX15	TDX13	TDX10	TDX16	TDX15	TDX2	TD17FA	TD15B	TDX19A	MSO1	MSO2	TDX5	TD1213
SiO_2	45 51	48 80	50 36	48 24	50 08	50 34	48 67	53 80	53 78	55 37	49 10	53 60	49 31	52 44	51 80	49 41	50 11	49 42	50 68	45 66	49 27	50 06	48 92	50 38	51 91	48 75
TiO_2	2 64	1 87	2 04	0 56	0 48	0 69	2 56	1 98	1 68	0 63	0 71	1 43	2 52	0 71	0 61	2 49	0 45	0 55	1 81	1 22	0 98	1 67	0 98	0 46	0 49	0 89
Al_2O_3	10 78	12 64	12 54	13 09	15 09	15 11	10 97	12 29	14 14	13 84	14 69	14 70	11 31	15 31	15 84	11 70	13 73	12 71	13 07	13 62	14 74	12 75	13 58	15 49	18 38	15 72
$^tFe_2O_3$	20 02	15 63	14 75	12 70	10 91	7 15	18 55	15 29	13 85	9 45	11 87	12 03	18 75	10 26	11 15	18 25	10 33	10 60	14 79	13 65	11 15	15 74	11 08	7 39	10 78	12 11
MnO	0 46	0 27	0 20	0 33	0 27	0 11	0 35	0 28	0 21	0 25	0 43	0 25	0 33	0 39	0 24	0 33	0 48	0 22	0 31	0 32	0 20	0 25	0 35	0 18	0 08	0 45
MgO	5 83	6 72	7 40	10 76	7 88	4 87	4 80	4 51	4 45	6 05	7 48	4 92	5 31	5 87	5 70	6 53	10 37	10 87	6 78	9 75	9 17	6 86	9 99	4 32	3 19	6 38
CaO	12 14	9 57	9 44	7 75	9 88	7 49	8 25	6 47	8 59	8 75	10 04	7 60	8 07	9 95	9 17	8 05	10 07	11 25	7 18	14 74	11 08	9 53	12 15	7 71	7 37	11 09
Na_2O	1 25	1 59	1 54	1 85	2 04	3 43	2 54	2 72	2 01	2 42	2 83	3 96	2 84	3 32	2 77	2 52	2 49	2 50	2 76	1 20	2 27	1 33	2 19	2 94	3 74	2 77
K_2O	1 06	0 67	0 41	2 09	1 03	0 97	1 07	0 71	0 62	0 86	0 67	1 39	0 71	0 76	0 72	0 76	0 68	0 77	1 04	0 82	0 77	0 62	0 68	0 66	1 48	0 80
P_2O_5	0 24	0 12	0 12	0 05	0 09	0 18	0 22	0 27	0 13	0 13	0 05	0 35	0 15	0 07	0 05	0 18	0 08	0 13	0 13	0 22	0 15	0 09	0 13	0 15	0 00	0 10
TOTAL	99 93	98 87	98 78	97 41	98 97	98 44	98 88	98 23	99 45	97 73	98 05	99 11	99 32	98 19	98 04	99 22	99 08	99 03	97 63	101 07	99 78	98 80	100 05	97 88	97 41	100 03
trace elements (ppm)																										
Cr	169 9	189 9	119 8	613 7	264 2	58 4	209 5	117 8	78 3	98 2	76 5	89 4	205 6	45 3	129 6	193 0	296 8	606 4	143 6	174 7	335 1	199 4	230 6	19 8	18 7	209 4
Nb	5 3	4 5	4 4	1 7	2 4	0 1	8 8	16 8	3 4	7 7	3 2	5 1	6 8	7 4	3 7	11 7	1 4	4 0	8 7	0 6	2 2	3 7	1 4	5 8	1 0	1 5
Ni	49 6	62 5	40 9	155 1	83 6	24 3	77 6	39 3	48 6	42 8	45 0	18 6	70 7	39 2	76 4	65 2	69 5	231 8	51 7	67 6	100 9	68 0	112 4	30 8	16 0	88 1
Rb	7 8	11 2	5 0	58 0	20 6	26 2	15 2	15 3	9 2	16 4	9 4	36 1	9 5	9 6	14 3	11 1	24 1	11 4	24 6	13 7	21 4	5 8	9 3	22 2	37 2	8 1
Sr	185 6	79 2	144 9	84 4	244 4	247 3	113 6	220 2	204 6	266 6	90 0	185 4	141 9	107 5	236 9	142 9	51 8	105 1	102 0	236 1	84 0	84 9	204 7	332 3	168 7	162 1
V	7 8	11 2	5 0	58 0	20 6	26 2	15 2	15 3	9 2	16 4	9 4	36 1	9 5	9 6	14 3	11 1	24 1	11 4	24 6	13 7	21 4	5 8	9 3	22 2	37 2	8 1
Y	44 9	43 8	45 3	18 1	19 7	37 2	69 5	117 5	32 1	35 6	26 0	47 5	54 8	41 5	22 5	81 7	19 4	15 6	54 8	22 2	26 7	36 0	19 9	25 4	13 7	23 0
Zr	88 0	77 2	97 5	40 6	67 6	161 4	168 4	295 4	72 8	53 5	53 8	123 5	107 7	60 0	88 6	162 2	49 1	52 2	158 7	70 1	61 3	72 8	88 4	72 6	60 0	63 7
normative mineralogy																										
[1] Total Fe																										
[2] Calculated assuming $Fe^{3+}/Fe^{2+} = 0.1$																										
Q	0 00	1 64	4 97	0 00	0 00	11 09	0 00	9 31	10 24	8 85	0 00	4 62	0 00	0 43	1 42	0 82	0 00	0 00	1 62	0 00	0 00	4 92	0 00	19 44	0 00	9 88
C	0 00	0 00	0 00	0 00	0 00	0 00	0 00	0 00	0 00	0 00	0 00	0 00	0 00	0 00	0 00	0 00	0 00	0 00	0 00	0 00	0 00	0 00	0 00	0 00	0 00	7 97
Or	6 39	4 07	2 49	12 77	6 22	5 26	6 61	4 33	3 73	5 18	5 30	7 72	4 30	4 63	4 39	4 60	6 90	4 84	8 39	4 95	4 61	5 18	4 06	5 23	8 95	6 32
Ab	10 78	13 82	13 37	16 26	25 42	29 68	22 13	23 77	17 24	21 14	24 88	25 58	24 62	28 05	24 18	21 88	21 47	22 07	24 26	4 81	19 45	11 56	19 71	25 60	32 83	26 36
An	31 07	24 06	26 78	22 09	25 48	23 79	15 83	19 88	26 29	25 18	25 58	23 49	16 41	25 82	29 54	16 83	23 83	21 13	31 00	29 40	26 10	28 02	25 46	27 29	30 14	9 84
Ne	0 00	0 00	0 00	0 00	0 00	0 00	0 00	0 00	0 00	0 00	0 00	0 00	0 00	0 00	0 00	0 00	0 00	0 19	0 00	2 90	0 00	0 00	0 00	0 00	0 00	0 00
Di	32 78	18 39	17 01	14 32	20 16	10 76	21 18	8 82	12 06	16 62	20 88	10 75	20 00	16 09	14 20	17 88	21 62	28 37	12 76	34 87	21 75	16 84	28 10	9 21	6 88	0 00
Hy	11 06	30 06	29 32	10 62	3 78	16 41	24 88	28 63	23 21	21 45	4 73	22 84	25 59	22 18	23 63	26 88	8 06	0 00	26 33	0 00	8 87	30 29	2 59	17 09	15 61	36 80
Cl	9 82	0 00	0 00	21 16	16 44	0 00	1 82	0 00	0 00	0 00	16 72	0 00	1 51	0 00	0 00	0 00	16 77	20 85	0 00	18 70	13 62	0 00	17 47	0 00	3 59	0 00
Mt	2 44	2 04	1 81	1 58	1 33	0 88	2 41	1 88	1 88	1 17	1 47	1 47	2 30	1 26	1 38	2 24	1 26	1 84	1 84	1 35	1 93	1 34	0 91	1 34	1 63
IL	5 11	3 65	3 88	1 10	0 93	1 73	5 01	3 88	3 26	1 24	1 39	2 77	4 90	1 39	1 19	4 85	0 87	1 09	3 67	2 32	1 88	3 26	1 88	0 90	0 97	1 90
Or	0 03	0 03	0 02	0 09	0 06	0 02	0 09	0 02	0 01	0 02	0 02	0 02	0 03	0 00	0 02	0 02	0 06	0 09	0 03	0 03	0 04	0 03	0 03	0 00	0 00	0 09
Ap	0 58	0 27	0 29	0 12	0 22	0 44	0 84	0 86	0 31	0 32	0 15	0 85	0 36	0 17	0 10	0 44	0 19	0 31	0 32	0 52	0 38	0 22	0 31	0 37	0 00	0 61

and Cann, 1973; Miyashiro and Shido, 1975; Wood and others, 1979; Shervais, 1982, and Wilson, 1989). When attempting to use amphibolite compositions to indicate the nature of the protolith, partial melting and fractionation trends, and paleotectonic settings, the question of element mobility during post-crystallization modification must be addressed. The effects of subaerial weathering can generally be eliminated by selection of samples with no petrographic evidence for such alteration. Assessing the amount of element mobility associated with submarine alteration and regional metamorphism, however, is more difficult. There is general agreement by many workers (Pearce and Cann, 1973; Shervais, 1982; Pearce, 1975,1980; Pearce and Flower, 1977; Pearce and Norry, 1979; Wilson 1989) that cations least mobile during alteration tend to be those cations that have small ionic radii and a high charge radius ratio or high field strength (e.g., Ti, Zr, P, Nb, Y). Because of this, these elements are not usually transported in aqueous fluids and tend to remain unaffected in rocks which have experienced alteration. This property, together with systematic variations of concentrations in unaltered lavas, allows these elements to be used to study metamorphosed and weathered basalts in which mineralogy has otherwise been too greatly altered for meaningful interpretation (Pearce and Norry, 1979). Several studies (e.g., Pearce and Cann, 1973; Wood and others, 1979; Meschede, 1986) have shown the utility of covariation and discriminant diagrams using these high field-strength elements or element ratios for elucidating the genesis of fresh basaltic magmas and subsequently as analogs for examining ancient mafic volcanic suites. Therefore, this study follows these approaches to determine the petrogenesis of the Columbus Promontory amphibolites.

PROTOLITH — PARA VERSUS ORTHOAMPHIBOLITE

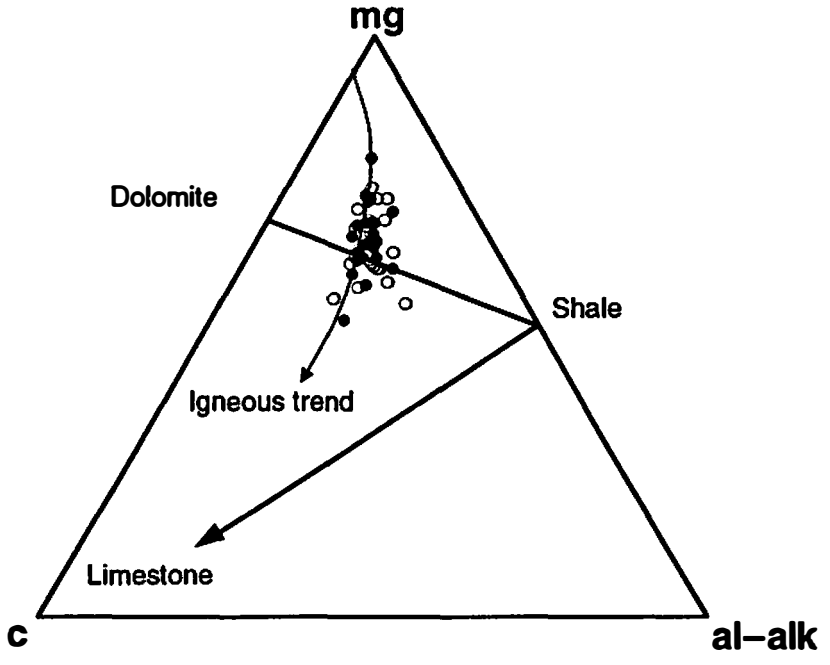
In both Poor Mountain Formation and Mill Spring complex amphibolites, relict igneous textures are absent because of thorough recrystallization, and intrusive or

sedimentary contacts have been obliterated by penetrative deformation and transposition. Consequently, any interpretation based solely on petrographic or field criteria is tenuous, and therefore additional information from geochemical characteristics is needed. Leake (1964) suggested that a ternary plot of Niggli values mg–c– (al-alk) provides a method for discriminating para–and orthoamphibolites by the nature of variation in trends in the concentrations of the elements, and their relation to known igneous and sedimentary trends. Leake's diagram (Fig. 3–2) shows that the line joining dolomite and typical pelite is at right angles to the trend of variation by a typical mafic igneous series (Fig. 3–2). Although he admitted that unusual combinations of dolomite and pelite could produce a similar trend, he suggested that it is difficult to see how any sedimentary rock could plot appreciably above the dolomite-pelite join, whereas many basic igneous rocks and amphibolites do plot above this line. The Niggli mg–c–(al-alk) diagram (Fig. 3–2) for amphibolite of the Poor Mountain Formation and the Mill Spring complex clearly reveals a trend of the data points at a high angle to the dolomite-pelite join, thus indicating an igneous parentage for both amphibolite suites.

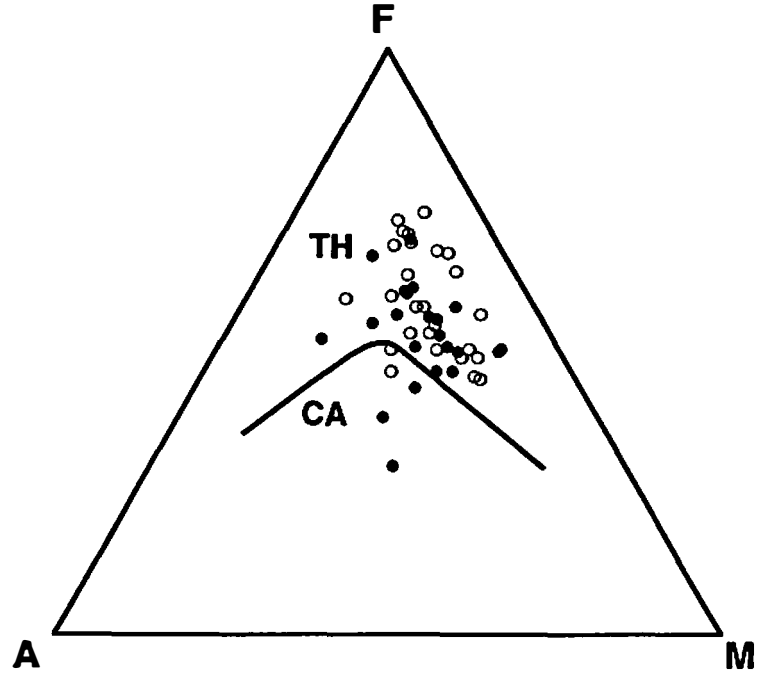
Other geochemical characteristics of the Columbus Promontory samples also suggest that they were derived from an igneous protolith(s). AFM relationships (Fig. 3–2) show that both suites show iron enrichment characteristic of tholeiitic basalts (Wilson, 1989). Most samples from the from both suites are hypersthene normative, also a common characteristic observed in tholeiitic basalts (Tables 3–1 and 3–2). The tholeiitic nature of the Columbus Promontory amphibolites is further substantiated by the Y/Nb ratios (Pearce and Cann, 1973: Floyd and Winchester, 1975). As shown in Tables 3–1 and 3–2, the Columbus Promontory amphibolites all have Y/Nb ratios greater than 1, indicating a tholeiitic source. Thus, the data presented above strongly suggest that the Columbus Promontory amphibolites had an igneous origin and were probably tholeiitic basalts.

Figure 3–2. Niggli mg–c–(al–alk) and AFM plots for amphibolites of the Columbus Promontory. a) Niggli diagram clearly shows trend of data at high angle to sedimentary trend indicating an igneous protolith. b) AFM diagram displays iron– enrichment characteristics of tholeiitic basalts. Boundary between the tholeiitic (TH) and calc–alkaline (CA) fields from Irvine and Baragar (1971). Niggli diagram modified after Leake (1964). On both diagrams, open circles – Mill Spring complex; filled circles–Poor Mountain Formation.

a)



b)



FRACTIONATION TRENDS

The compositional range of volcanic rocks is a consequence of at least two fundamental processes, partial melting and fractional crystallization. Although these are not the only processes, they are the dominant ones (Wilson, 1989). The AFM diagram shown in Figure 3–2 indicates fractionation processes were important in the petrogenesis of the Columbus Promontory amphibolites. To further examine the degree of fractional crystallization and/or partial melting that has occurred, several covariation (Harker type) diagrams have been used (Figs. 3–3, 3–4, and 3–5) . The standard Harker diagram plots a fractionation index as the abscissa versus various elements or oxides on the ordinate to demonstrate igneous variations as fractionation proceeds. SiO_2 is most commonly used as the fractionation index, but, because the range of silica contents in basaltic rocks is so restricted, SiO_2 is not a useful as index of fractionation (Wilson, 1989). Furthermore , in metamorphosed basalts, SiO_2 is considered to be highly mobile. Because of these restrictions, the incompatible trace element Zr has been used as the fractionation index in this study. Additional multi-element covariation diagrams using Ti, Mg* (100 (Mg/Mg + Fe^{2+})) and P_2O_5 have also been used to help reveal fractionation trends.

One of the most striking features shown in the covariation diagrams (Figs. 3–3, 3–4, and 3–5) is the similarity in the chemistry and chemical trends shown by the Poor Mountain and Mill Spring complex amphibolites. Figure 3–3 shows Mg*, Ni, and P_2O_5 plotted against TiO_2. TiO_2, considered to be relatively immobile and incompatible elements show a decrease with fractionation against Mg*, while the highly incompatible P_2O_5 shows an increase with fractionation versus TiO_2. Ni, however, does not show a readily discernible trend. Misra and Conte (1991) used this sequence of diagrams to subdivide amphibolites from the Ashe and Alligator Back Formations of the North Carolina Blue Ridge into three (low, intermediate, and high Ti) amphibolite groups unrelated to a single fractionation trend.

Figure 3–3. Harker–type covariation diagrams using TiO_2 as index of fractionation. a) TiO_2 vs. Mg# (100 (mg + Fe^{2+} /mg)), b) TiO_2 vs. Ni, and c) TiO_2 vs. P_2O_5. Note the geochemical similarity between the Poor Mountain amphibolite and amphibolite of the Mill Spring complex. Open boxes–Mill Spring complex; filled circles–Poor Mountain Formation. Arrows indicate increasing fractionation.

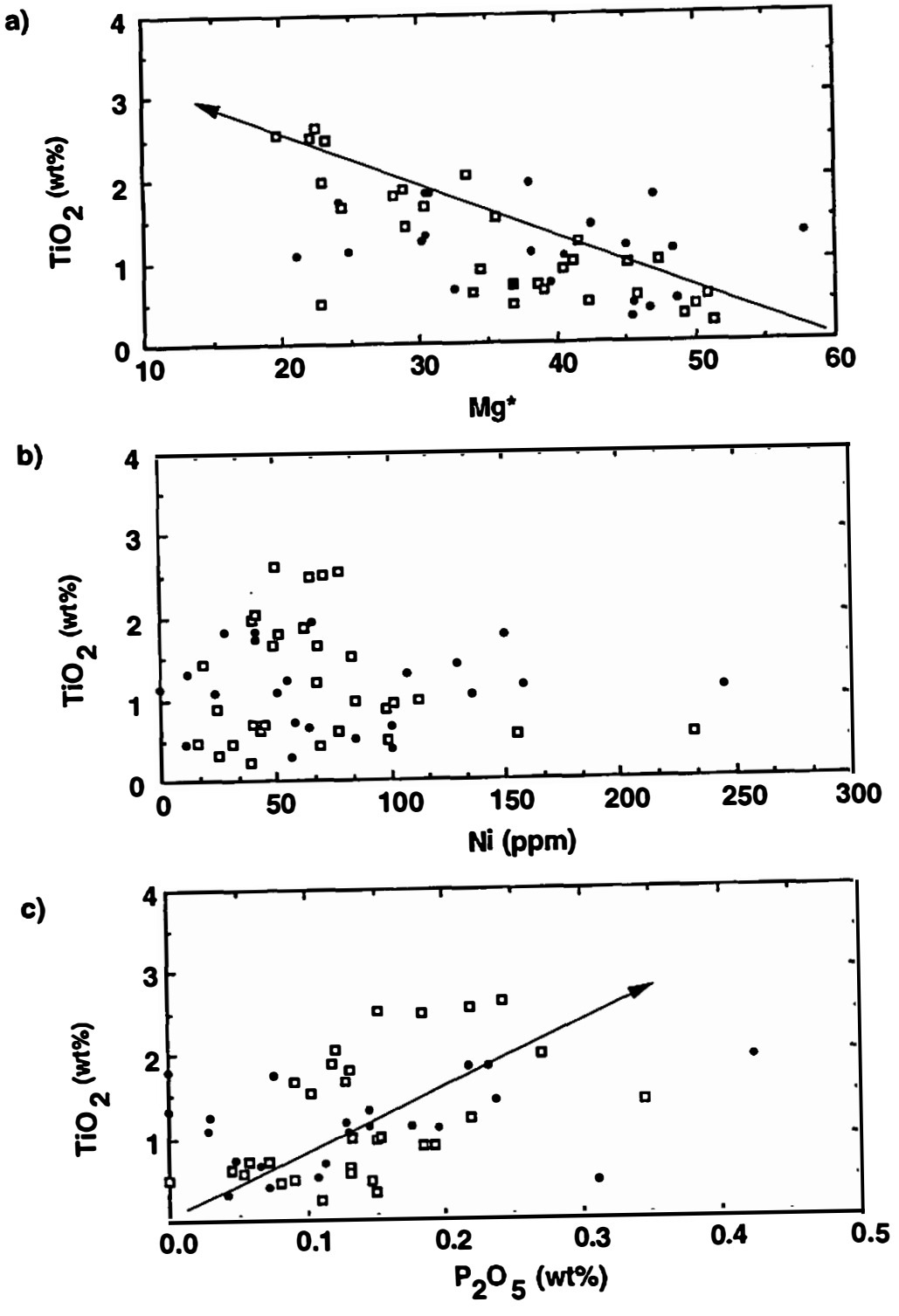
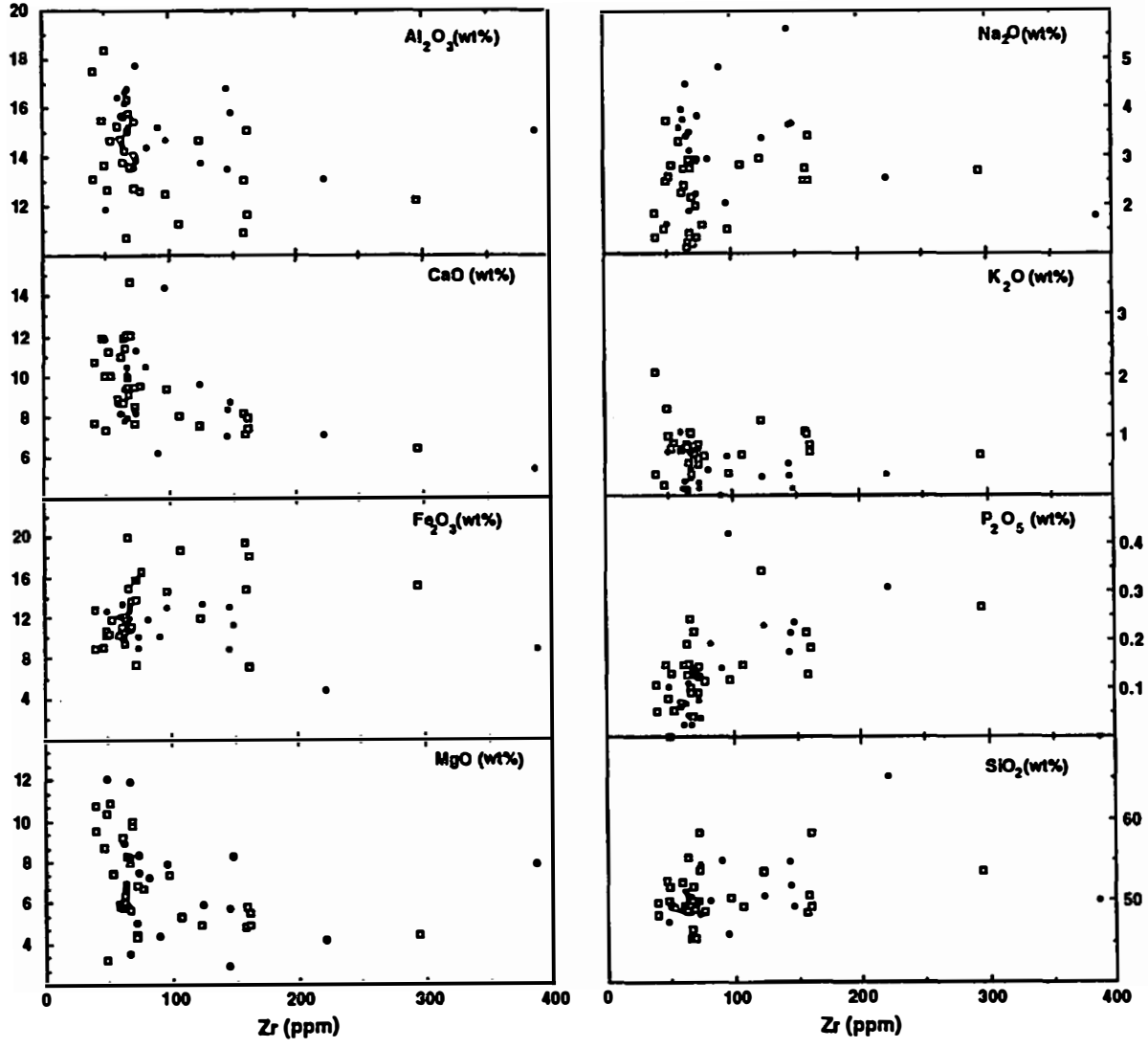
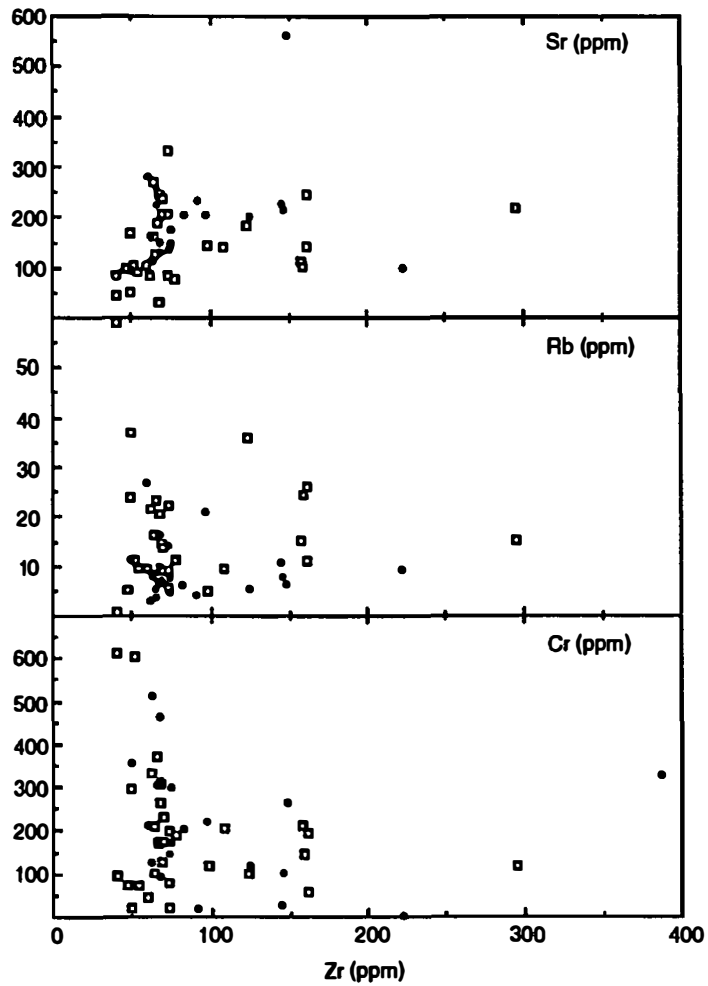

a)
TiO2 (wt%)
Mg*
b)
TiO2 (wt%)
Ni (ppm)
c)
TiO2 (wt%)
P2O5 (wt%)

Figure 3–4. Harker–type diagrams using Zr as fractionation index. a) Covariation diagram of Zr versus major and minor elements. b) Covariation diagram of Zr versus trace elements. Note the geochemical similarity between the Poor Mountain amphibolite and Mill Spring complex amphibolite. Open boxes –Mill Spring complex; filled circles – Poor Mountain Formation.

a)


Al2O3(wt%)
CaO (wt%)
Fe2O3(wt%)
MgO (wt%)
Na2O(wt%)
K2O (wt%)
P2O5 (wt%)
SiO2(wt%)
Zr (ppm)
Zr (ppm)

b).



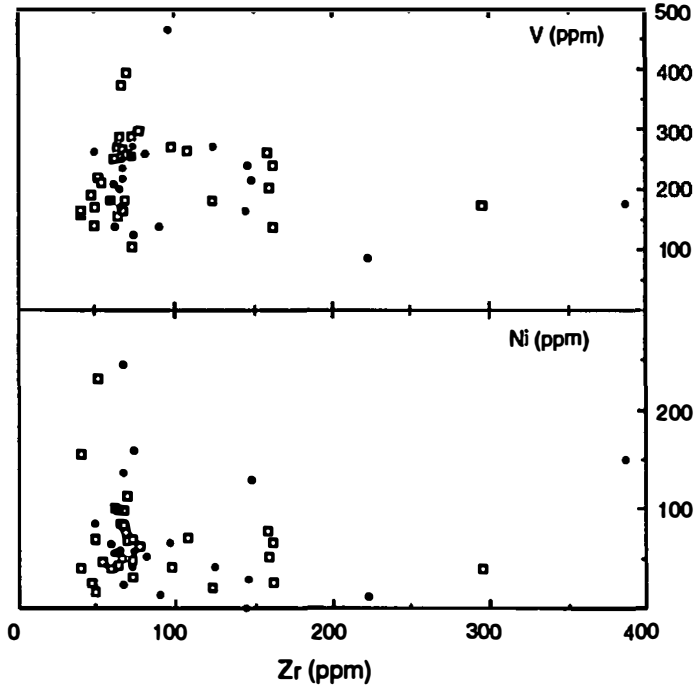
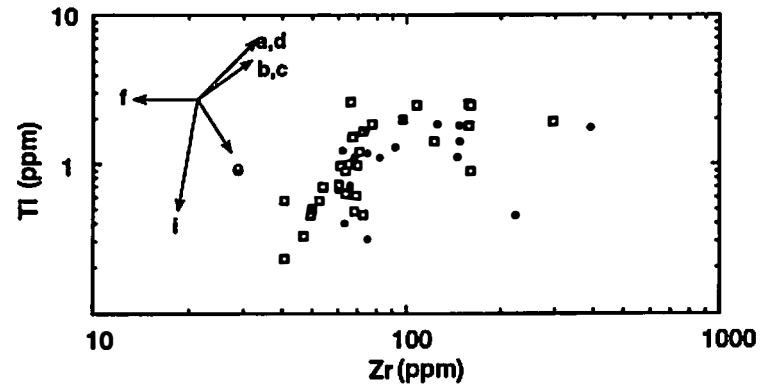
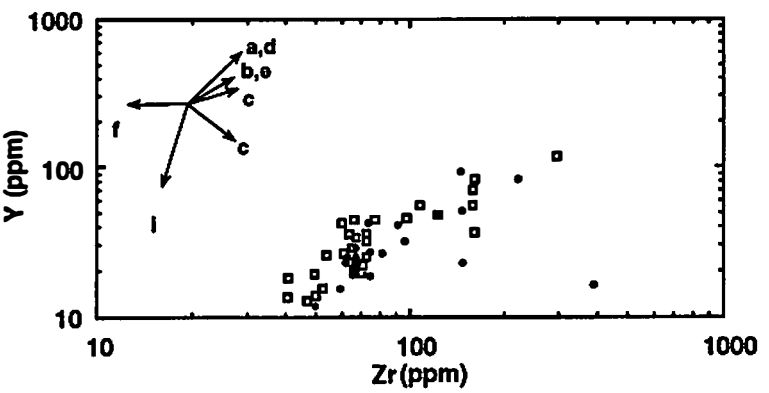
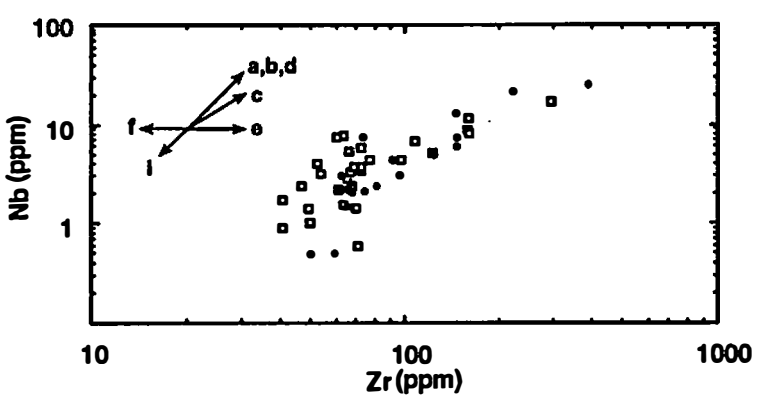
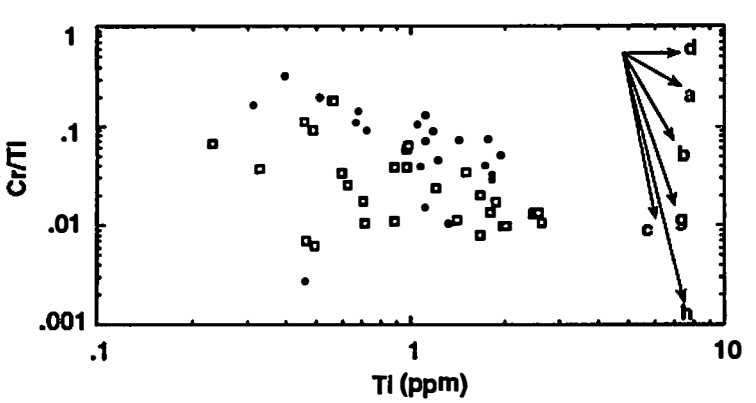


Figure 3–5. Covariation diagram using immobile trace elements (Nb, Y, Zr, and Ti) and minor element Cr. Included on the diagram are the experimentally determined fractionation vectors of Pearce and Flowers (1977) and Pearce and Norry (1979). Vectors correspond to specific fractionally crystallized phases: a) olivine, b) orthopyroxene, c) clinopyroxene, d) plagioclase, e) magnetite, f) zircon, g) garnet, h) olivine + 1.2 spinel, and i) amphibole. Open boxes –Mill Spring complex; filled circles–Poor Mountain Formation.


10
1
Tl (ppm)
10
100
1000
Zr (ppm)
a,d
b,c
f
e
i


1000
100
10
Y (ppm)
10
100
1000
Zr (ppm)
a,d
b,e
c
f
c
i


100
10
1
Nb (ppm)
10
100
1000
Zr (ppm)
a,b,d
c
f
e
i


1
.1
.01
.001
Cr/Tl
.1
1
10
Tl (ppm)
d
a
b
g
c
h

Unlike their results, data (Tables 3–1 and 3–2; Fig. 3–3) gathered in this study suggest that the Columbus Promontory amphibolites compose a single compositional group with trends related to fractionation of a similar parental source.

Examination of the Zr fractionation diagrams (Figs. 3–4 and 3–5) further attests to the compositional similarities of the Poor Mountain and Mill Spring complex amphibolites. These diagrams display weak to strong trends for many of the constituents versus Zr, further supporting the importance of fractional crystallization or partial melting during the genesis of these amphibolites. Against Zr, the high field-strength cations (Ti, Y, P, and Nb) have the most well-defined trends, all increasing with fractionation (Figs. 3–4 and 3–5). Of the major oxides CaO and MgO show the most discernible trends, decreasing with fractionation. The other major oxides Al_2O_3, K_2O, SiO_2, and the incompatible element Rb, all show considerable scatter versus Zr; probably a reflection of their post-crystallization mobility (Fig. 3–4). Somewhat surprising, the incompatible element Sr displays a relatively well-defined trend that increases with fractionation, whereas the compatible elements Cr and Ni have weak to uninterpretable trends versus Zr (Fig. 3–4)

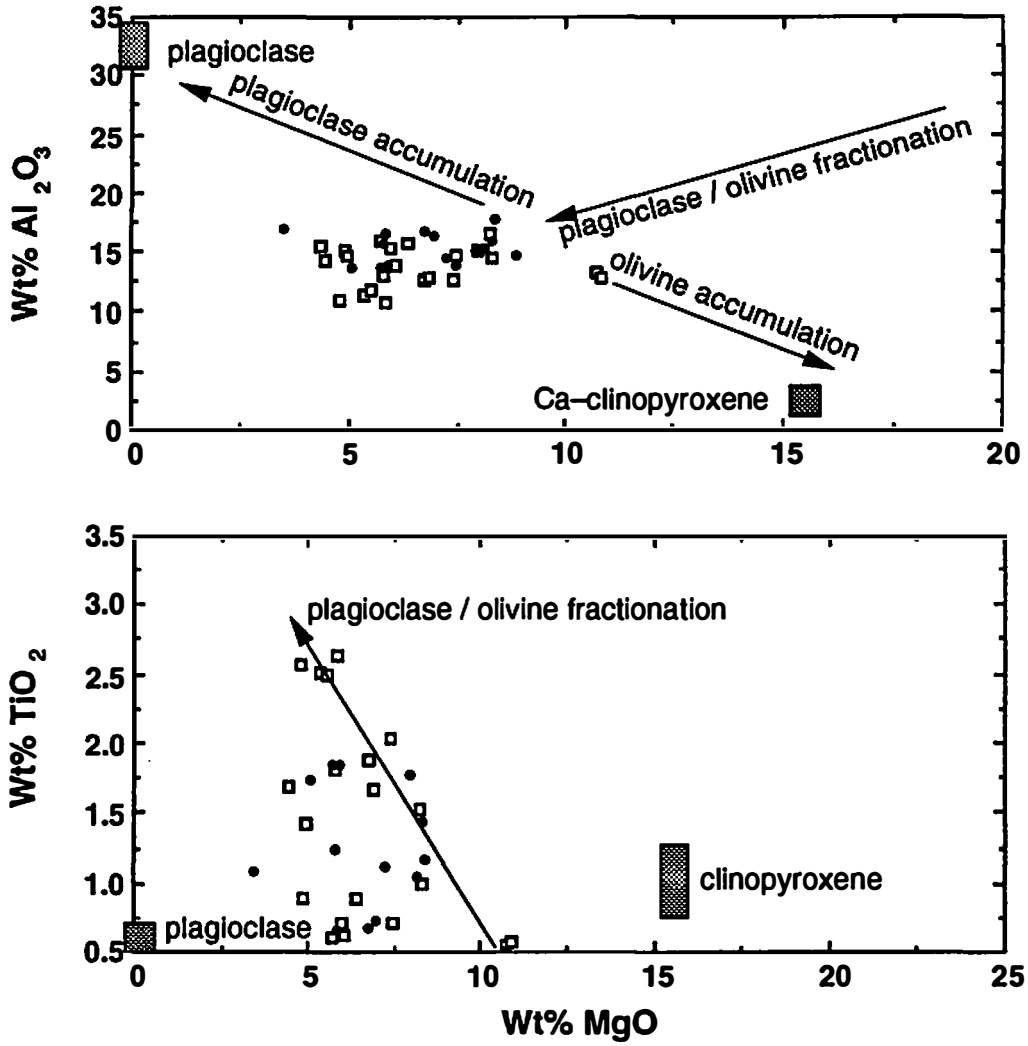
Studies by Pearce and Norry (1979), Bryan and others (1976) and Schilling and others (1983), from experimental modeling and natural examples, have shown that genetic relationships between the element or oxide chemistry of volcanic suites and fractional crystallization of specific mineral phases can be established. Pearce and Norry (1979) and Pearce and Flower (1978) have experimentally established mineral-liquid distribution coefficients for the high field-strength elements Ti, Nb, Y, and Zr. They suggested that the variations in the Ti, Nb, Y and Zr content on magma, as it evolves from basic to acidic compositions, can be interpreted in terms of the nature and proportion of the crystallizing phases. Using these distribution coefficients, they have determined fractional crystallization vectors whose geometry and magnitudes are specific to the constituent elements (Ti, Nb, Zr and Cr/Ti) and directly related to crystallization of various mineral phases during fractional

crystallization processes. Figure 3–5 shows the Zr versus Ti, Y, Nb and Cr/Ti covariation diagrams, and for comparative purposes, it also contains the experimentally determined closed-system fractionation vectors of Pearce and Norry (1979) and Pearce and Flower (1978). Bryan and others (1976) discussed the importance of cotectic crystallization of olivine and plagioclase at low pressures in controlling the bulk rocks chemistry of mid–ocean ridge basalts (MORB). This was also discussed by Schilling and others (1983) who indicated that trends of variation of Al_2O_3 and TiO_2 versus MgO for basalts from 29°N to 73°N along the mid-Atlantic Ridge can be explained in terms of olivine and plagioclase fractionation.

The purpose of Figures 3–5 and 3–6 is to qualitatively assess what fractionally crystallized mineral phases may have contributed to the observed elemental variations observed in the Columbus Promontory amphibolites. On the Zr versus Ti, Nb, and Y diagrams (Fig. 3–5), the trend of the Columbus Promontory data is consistent with crystallization of olivine, clinopyroxene, plagioclase, magnetite, and garnet during fractional crystallization. The decrease in Ti with increasing Zr may also indicate crystallization of Fe - Ti oxides such as ilmenite. The Cr/Ti versus Ti diagram also suggests that garnet may have also been an important crystallizing phase. Comparison of Columbus Promontory data (Fig. 3–6) with the MgO versus Al_2O_3 and TiO_2 trends of Schilling and others (1983), also supports the interpretation that olivine and plagioclase are important crystallizing phases controlling the fractionation trends observed in the Columbus Promontory samples, but that clinopyroxene was not an important crystallizing phase.

This qualitative assessment suggests that the observed variations in the contents of Ti, Y, MgO, Cr, Al_2O_3, CaO, Zr, and the Cr/Ti ratio can be explained by the fractionation of olivine, clinopyroxene, plagioclase, magnetite, and garnet. Overall the information presented by the AFM relationships (Fig. 3–2), the covariation diagrams (Figs 3–4, 3–5, and 3–6) and the qualitative use of the fractionation vectors of Pearce and Norry (1979), Pearce and Flower (1978), and the Al_2O_3 and TiO_2 versus MgO trends support the interpretation

Figure 3–6. Covariation diagram of Al_2O_3 and TiO_2 vs. MgO. Included are fractionation trends from Schilling and others (1983) from 29° to 73° along the Mid–Atlantic Ridge. Diagram suggests trend of Columbus Promontory data can be explained by the fractionation of olivine and plagioclase. Open boxes –Mill Spring complex; filled circles–Poor Mountain Formation.


plagioclase
plagioclase accumulation
plagioclase / olivine fractionation
olivine accumulation
Ca–clinopyroxene
Wt% Al 2O3
plagioclase / olivine fractionation
clinopyroxene
plagioclase
Wt% TiO 2
Wt% MgO

that Columbus Promontory amphibolites were derived from a strongly fractionated magma. It could alternatively be argued that the fractionation trends observed in the amphibolites could be the result of mixing between metasedimentary and volcanic rocks, or due to mixing of multiple basaltic flows. Such an interpretation must be considered, particularly in terranes like the Inner Piedmont where there has been extensive transposition and recrystallization during deformation and metamorphism. It is, however, argued that the total data set, including the trends shown on the AFM diagram and Niggli diagrams, and the similarity between fractionation trends of amphibolite from the Columbus Promontory and those of modern environments (e.g., Schilling and others (1983); Basaltic Volcanism Project (1981)), is consistent with an interpretation that Columbus Promontory amphibolites were derived from a similar fractionated magma source.

PALEOTECTONIC SETTING

Constraints

The chemical composition of basaltic rocks from different tectonic settings has been shown to vary significantly. During the past 15 to 20 years, several papers have appeared in which major, minor and trace element compositions of young basalts have been related to the tectonic environment in which the basalts were generated (e.g., Pearce and Cann, 1973; Miyashiro and Shido, 1975; Sun and Nesbitt; Shervais, 1982; and Meschede, 1986). Importantly, this has led to the development of tectonomagmatic discrimination diagrams (Wilson, 1989), which can be used as analogs to elucidate the tectonic affinity of ancient mafic volcanic suites. Generally, these tectonomagmatic discriminant diagrams have been devised to distinguish between volcanic rocks from the major tectonic regimes related to plate tectonic motions including diverging plate margins (ocean floor basalts), converging

plate margins (volcanic arcs basalts), oceanic island basalts (within-plate oceanic basalts), and continental basalts (within-plate continental basalts). Because the majority of ancient basalts have undergone post crystallization alteration, these diagrams rely on the use of relatively immobile, high field-strength cations. To make some qualitative interpretations about the tectonic affinity of the Columbus Promontory amphibolites, a series of several tectonomagmatic discrimination diagrams using those elements considered to be immobile have been employed.

In order to use tectonomagmatic discriminant diagrams, it is necessary to know the degree of fractionation that has occurred in the volcanic rocks being classified, as they are only strictly applicable to basic volcanic rocks (Wilson, 1989). The previous section of this chapter demonstrated that the amphibolite samples from the Columbus Promontory are from a strongly fractionated basaltic suite. Most of the tectonomagmatic discriminant diagrams are designed for use with non–cumulative mafic lavas, therefore, screening for possible cumulative phases must be employed. Pearce and Cann (1973) indicated that a compositional limit of 12% < CaO + MgO < 20% can be used as an index of fractionation to eliminate mafic volcanic samples containing a significant proportion of cumulate phases. All of the Columbus Promontory samples were screened following the guidelines of Pearce and Cann (1973). From this process, four samples from the Mill Spring complex and five samples from the Poor Mountain Formation were eliminated from further study, thus reducing the number of samples from each suite to 15 and 21, respectively.

Possible Paleotectonic Settings

The fractionation sequence of olivine, clinopyroxene, plagioclase, magnetite, and garnet presented earlier in this chapter, is consistent with a low–pressure fractionation sequence characteristic of spreading–ridge basalts (Basaltic Volcanism Studies Project, 1981)

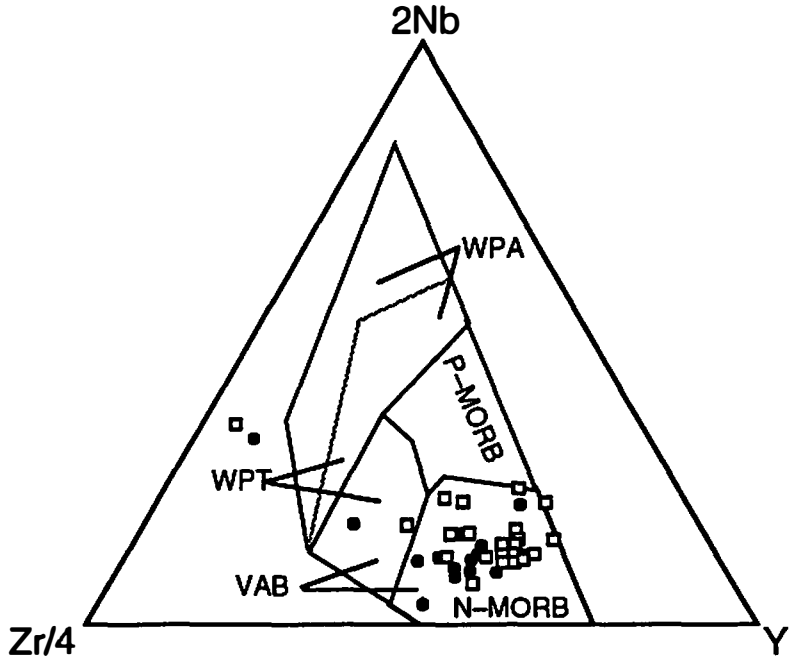
and supports an interpretation that the Columbus Promontory amphibolites were generated at an oceanic spreading center. Furthermore, the similarities between the Al_2O_3 and TiO_2 versus MgO trends from the Columbus Promontory amphibolites, and those reported by Bryan and others (1976) and Schilling and others (1983), indicate these amphibolites have mid–ocean ridge basalt (MORB) characteristics, similar to those reported from the Mid–Atlantic Ridge (MAR).

Schilling (1975) and Sun and others (1979) have shown that various segments of mid–ocean ridges have distinctive trace element geochemistry, and classified them into three types including normal (N–type), depleted in incompatible elements, plume (P–type), enriched in incompatible elements, and transitional (T–type), transitional between the depleted and enriched types. Erlank and Kable (1976), and Meschede (1986) have noted that variations in the Nb content of MORB cannot be ascribed to seawater interaction or to fractional crystallization processes, but are indicative of mantle differentiation processes and source heterogeneity. Consequently, Nb is potentially useful in discriminating different MORB types. Based on this fact, Meschede (1986), devised a tectonomagmatic discriminant diagram using Nb, Y, and Zr, which he has shown effectively discriminates different MORB types, and between N–type MORB and continental tholeiite. This diagram was employed in this study (Fig. 3–7) and the results strongly suggest that the Columbus Promontory amphibolite suite is an N–type MORB. This diagram displays a pronounced consistency for nearly all samples in the N–type MORB field with little scatter into other fields (Fig. 3–7).

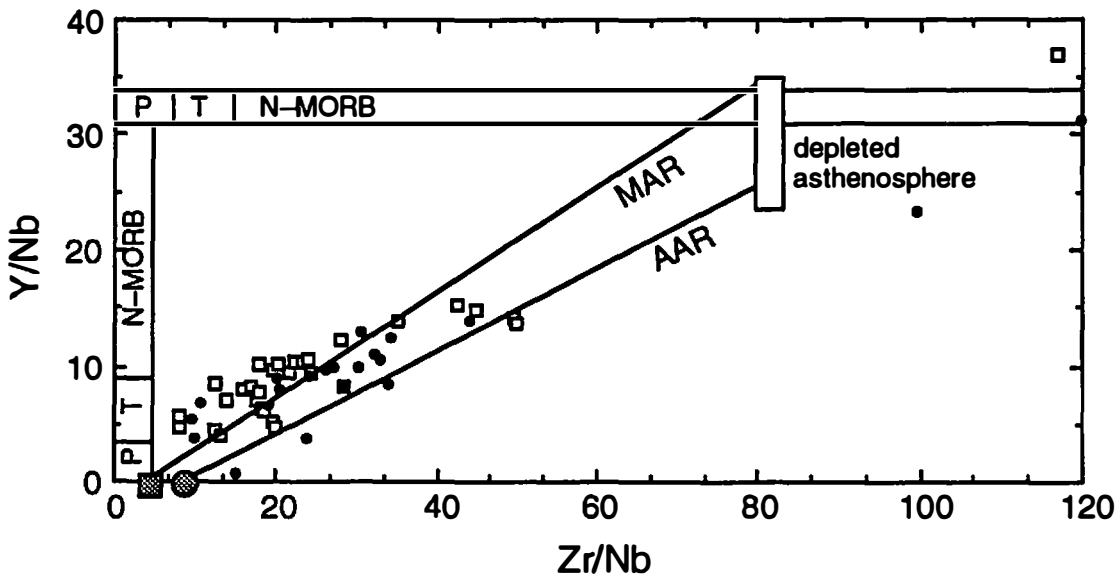
Humphris and others (1985) and Wilson (1989) indicated that Zr/Nb and Y/Nb ratios can also be used to demonstrate qualitatively the mixing of mantle sources. Humphris and others (1985) and Wilson (1989), suggested that the high–valence cations (e.g., Zr, Nb, and Ti) behave incompatibly and tend to be concentrated in oceanic–island basalts relative to MORB. Consequently, the Zr/Nb ratio is characteristically low (<10) in oceanic–island basalts (P–type MORB) and higher in N–type MORB (>30). A covariation diagram of these ratios,

Figure 3–7. Tectonomagmatic discriminant diagrams showing MORB character of the Columbus Promontory amphibolites. a) Nb–Zr–Y ternary tectonomagmatic discriminant diagram (Meschede, 1986). Open circles represent samples from the Mill Spring complex; filled circles from the Poor Mountain Formation. WPA–within–plate alkalic basalts; WPT– within–plate tholeiitic basalts; VAB–volcanic arc basalts. b) Y/Nb vs. Zr/Nb ratios for the Columbus Promontory samples. Diagram also includes the average values for the Tristan da Cuhna mantle plume basalt (filled box) and the Bouvet mantle plume basalt (filled circle). Also included are the trends of data from MORB erupted along the Mid–Atlantic Ridge in the vicinity of Tristan da Cuhna (MAR) and Bouvet (AAR). Compositional ranges of P(plume)–, T (transitional)–, and N normal depleted)– type MORB are indicated by bars along axes of the diagram. (Modified from Wilson, 1989). Open boxes–Mill Spring complex; filled circles –Poor Mountain Formation. On both diagrams, only samples in the range of $12 < MgO + CaO < 20$ were used.

a)


2Nb
WPA
P-MORB
WPT
VAB
N-MORB
Zr/4
Y

b)


40
30
20
10
0
P
T
N-MORB
depleted
asthenosphere
MAR
AAR
Y/Nb
0
20
40
60
80
100
120
Zr/Nb

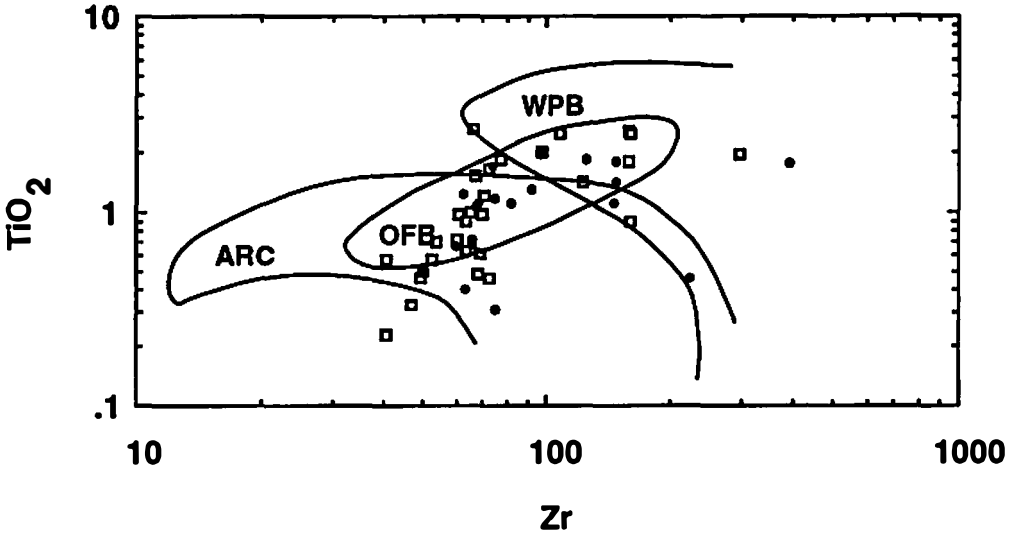
adapted from Wilson (1989) is shown in Figure 3–7. Wilson (1989) suggested that the scatter of these data (represented by the lines) can be explained by the mixing of depleted N–type MORB and enriched (P–type) MORB components. The Columbus Promontory data set, also shown on this diagram, has a similar trend as MAR and suggests that the Poor Mountain amphibolite and amphibolite from the Mill Spring complex could also record a similar mixing of depleted (N–type MORB) and more enriched (P–type) components. This possibility was also suggested for the amphibolites in the Ashe Formation and Alligator Back Formations in the eastern Blue Ridge of North Carolina by Misra and Conte (1991).

Tectonomagmatic discriminant diagrams, employing other trace elements (Ti, V, Cr, Zr, and Y), reveal a consistent pattern of ocean–floor and volcanic arc characteristics for the Columbus Promontory samples. The TiO_2–Zr relationship (Pearce, 1980) for the suite imply a strong correlation for all Columbus Promontory amphibolites with ocean floor basalts (OFB), although there is some scatter of the data into the arc field (Fig. 3–8). This pattern is also present in the Zr vs Zr/Y discriminant diagram (Fig. 3–8) of Pearce and Norry (1979). The Cr versus Ti plot of Pearce (1975) for distinguishing OFB from low-K tholeiites of island arcs (Fig. 3–9) and the Cr versus V of Miyashiro and Shido (1975) also show that most of the Columbus Promontory data plot in the OFB field with some scatter into the volcanic arc fields (Fig. 3–9).

Shervais (1982) discussed the utility of Ti and V ratios in resolving the tectonic setting of modern ophiolites. Shervais (1982) indicated that modern island arcs have Ti / V ratios < 20, MORB and continental tholeiites Ti / V ratios of 20 to 50, and calc–alkaline rocks > 50. Shervais also suggested that back–arc basins have either MORB–like or arc ratios. The Ti/1000 versus V plot of Shervais (1982) using the Columbus Promontory samples (Fig. 3–10), shows the majority of the data has Ti /V ratios of 20 to 30 and fall in the field of MORB and back–arc basin basalts with some scatter in the arc and oceanic islands fields similar to the patterns shown by the other tectonomagmatic discriminant diagrams used. The presence

Figure 3–8. Tectonomagmatic discriminant diagrams showing ocean–floor basalt characteristics of the Columbus Promontory suite. a) Zr vs. TiO_2 tectonomagmatic discriminant diagram after (Pearce, 1980), and b) Zr vs. Zr/Y tectonomagmatic discriminant diagram after (Pearce and Norry, 1979). ARC, island arc tholeiites; OFB, ocean floor basalts; WPB, within–plate basalts. Open boxes–Mill Spring complex; filled circles –Poor Mountain Formation. On both diagrams, only samples in the range of $12 < MgO + CaO < 20$ were used.

a)


10
1
.1
TiO2
WPB
OFB
ARC
10
100
1000
Zr

b)

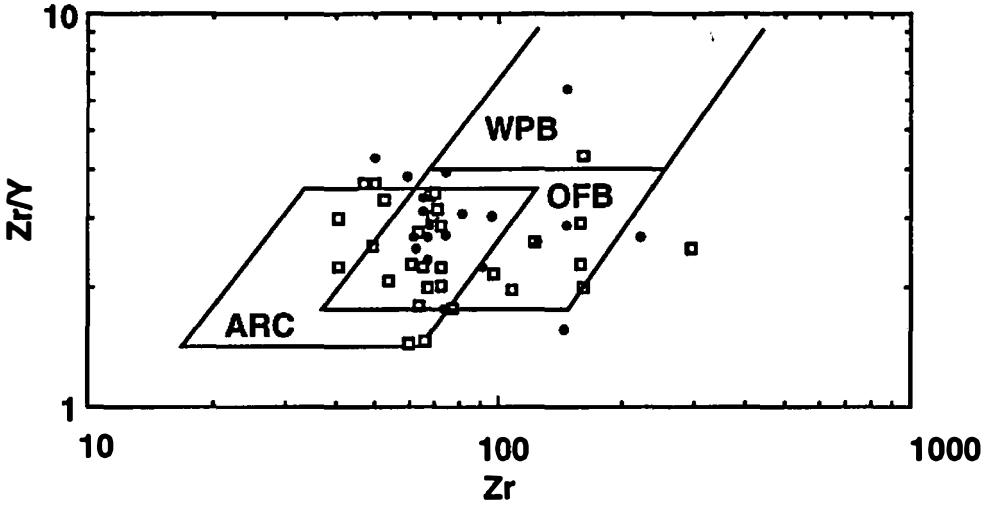
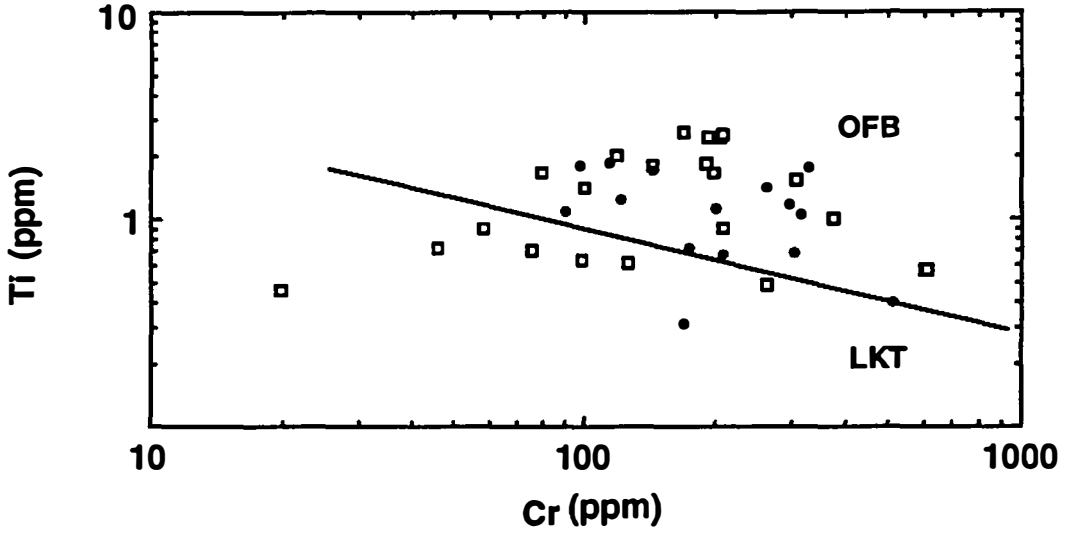

10
1
Zr/Y
WPB
OFB
ARC
10
100
1000
Zr

Figure 3–9. Cr vs. Ti and Cr vs. V tectonomagmatic discriminant diagrams. Diagrams are used to distinguish ocean floor basalts (OFB) from low K–tholeiites (LKT) of island arcs. Cr vs. Ti after (Pearce, 1975); Cr vs. V after Miyashiro and Shido (1975). Diagrams suggest primarily ocean–floor characteristics for the Columbus Promontory suite, but with some volcanic arc component. CA, calc–alkaline series; TH, tholeiitic series; OFB, ocean island basalts. Only samples in the range of 12< MgO + CaO < 20 were used. In both diagrams, open boxes represent samples from the Mill Spring complex; filled circles from the Poor Mountain Formation. On both diagrams, only samples in the range of 12< MgO + CaO < 20 were used.

a)


10
1
Ti (ppm)
OFB
LKT
10
100
1000
Cr (ppm)

b)

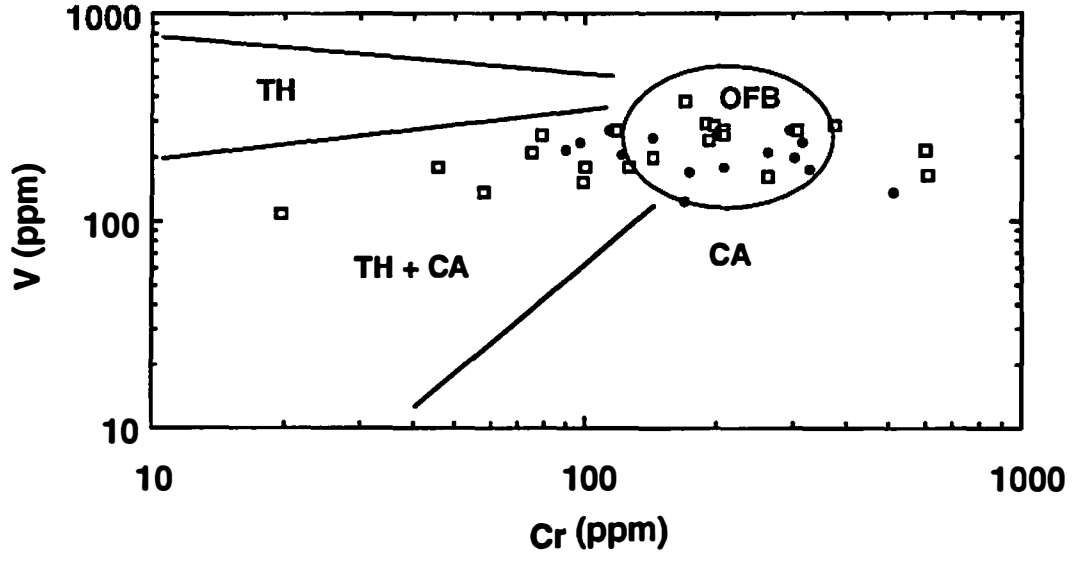
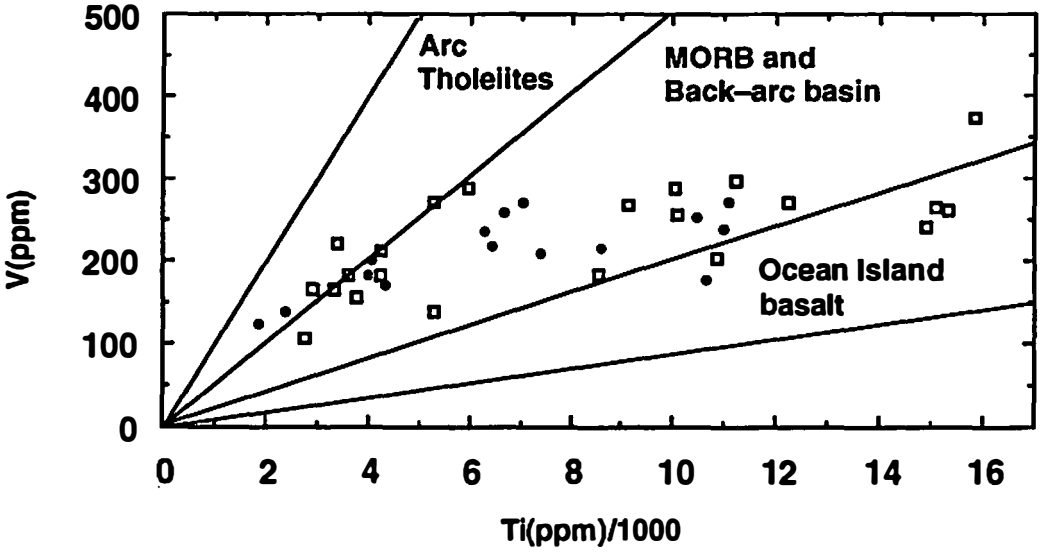

1000
100
10
V (ppm)
TH
OFB
TH + CA
CA
10
100
1000
Cr (ppm)

Figure 3–10. Ti vs. V tectonomagmatic discriminant diagram. for the Columbus Promontory samples. This diagram suggests possibility of back–arc basin setting for the Columbus Promontory suite and may explain combination of ocean–floor and volcanic arc characteristics observed in previous diagrams. Only samples in the range of 12< MgO + CaO < 20 were used. Open boxes–Mill Spring complex; filled circles –Poor Mountain Formation. Diagram from (Shervais, 1982)


500
400
300
200
100
0
V(ppm)
0
2
4
6
8
10
12
14
16
Ti(ppm)/1000
Arc
Tholeiites
MORB and
Back–arc basin
Ocean Island
basalt

of both mafic rocks with MORB and volcanic–arc characteristics is common in many back–arc basins (e.g., Lau Basin in the western Pacific, Leg 135 Scientific Party, 1992). Saunders and Tarney (1984) also concluded that many back–arc basins are floored by basalts transitional between N–type MORB and island–arc or calc–alkaline basalts; a characteristic also displayed by the Columbus Promontory suite. The possibility of a back–arc basin setting for the mafic rocks in other areas of the eastern Blue Ridge and Inner Piedmont was suggested by McConnell and Abrams (1984), Gillon (1989), and Misra and Conte (1991) in the eastern Blue Ridge and by Stow and others (1984) and Neilson and Stow (1986) in the Inner Piedmont of Alabama. These areas also contain a stratigraphic sequence and a structural history similar to that preserved in the Columbus Promontory, discussed previously in Chapter II. Therefore a similar tectonic affinity of the Columbus Promontory amphibolites is consistent with regional geologic patterns.

Misra and Conte (1991) interpreted the Ashe and Alligator Back amphibolites to represent metamorphosed oceanic crust generated at a spreading center. They suggested that the juxtaposition of depleted, low–Ti basalts and MORB–like basalts may record a back–arc basin setting, as has been postulated for many ophiolites. Alternatively, they also proposed that this trend may be indicative of multistage melting of an upper–mantle source adjacent to a mantle plume in a mid–oceanic ridge environment. Gillon (1989) noted that the amphibolites in the eastern Blue Ridge of NE Georgia have back–arc basin or island–arc geochemical signatures. Gillon (1989) similarly interpreted these mafic units to have been generated in a marginal back–arc spreading center within the tectonic influence of an island arc system. McConnell and Abrams (1984) also showed that the mafic rocks of the Pumpkinvine Creek Formation of the New Georgia Group to be chemically similar to abyssal tholeiites and chemically dissimilar to basalts found in intracratonic rifts. They suggested that these mafic rocks were derived in either an ocean–ridge or back–arc basin environment. Stow and others (1984), and Neilson and Stow (1986), indicated that amphibolites in the Alabama

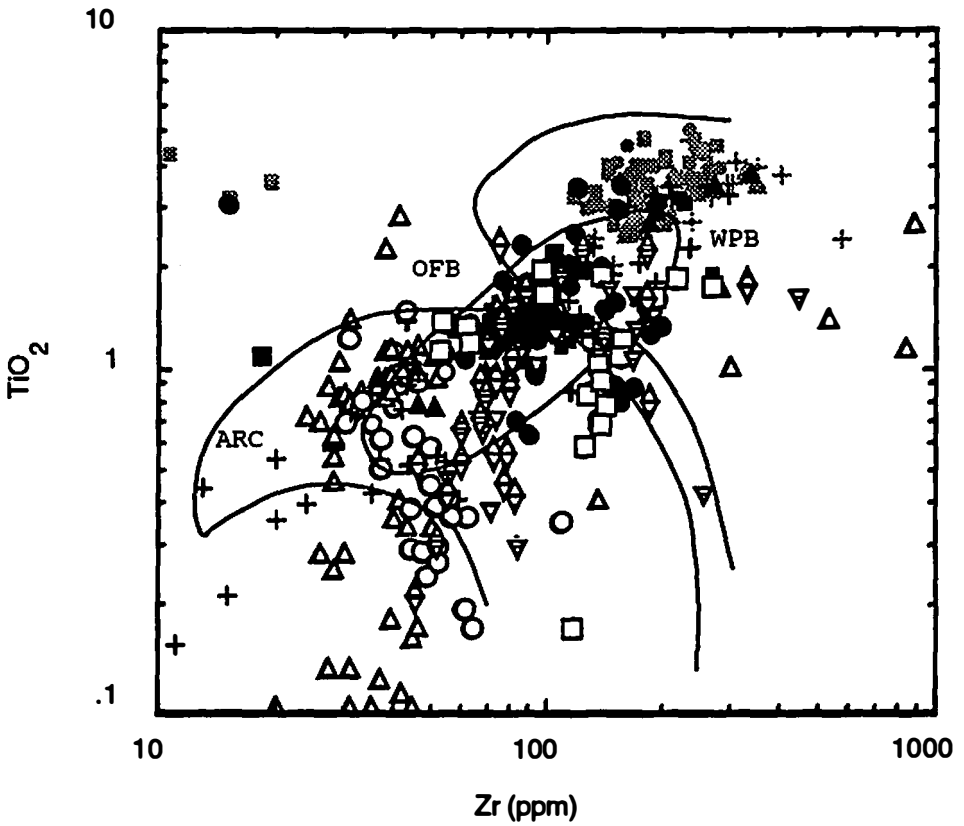
Piedmont including the Ropes Creek, Mitchell Dam, Ketchepedrakee, Beaver Dam , and Hudson Rapids amphibolites are geochemically similar. They also concluded that the parental basalts of these amphibolites have an E–MORB (enriched) character and were generated in an oceanic rifting environment, possibly a back–arc basin.

Although I cannot clearly define the tectonic environment from which the Columbus Promontory amphibolites were generated, I feel the most plausible interpretation that can be drawn from the entire data set is one involving mid–oceanic spreading. Fractionation trends strongly support MORB characteristics and along with the Y/Nb and Zr/Nb suggest the a mixing of a N–type and P–type MORB components. Alternatively, the combination of MORB and a volcanic–arc characteristics suggest the possibility of a back–arc basin setting. Thus, the back–arc basin pattern suggested by the Ti / V ratios (Fig. 3–10) may be the most diagnostic in terms of the paleotectonic setting of the Columbus Promontory suite. In either case, I interpret these to be tholeiitic basalts generated in an oceanic rifting environment. None of the diagrams suggests any similarity of either of these two suites with continentally derived within-plate basalts. The geochemical trends of amphibolites from the Poor Mountain and Mill Spring complex are very similar, suggesting that they may have been generated from a similar parental source that was active during the deposition of both stratigraphic sequences (Poor Mountain Formation and Mill Spring complex) in which these amphibolites are intercalated.

Regional Considerations

Excluding the later Mesozoic dikes (see Ragland and others, 1983), the majority of the mafic–ultramafic rocks in the eastern Blue Ridge and the Inner Piedmont are part of the Late Proterozoic to early Paleozoic stratigraphy related to the development of the Laurentian margin, the Iapetus ocean, and related marginal basins. Chemically these rocks are very diverse and record different tectonomagmatic settings (Fig. 3–11). Mafic rocks with a continental affinity have

Figure 3–11. Regional variations of geochemical composition (Ti vs. Zr) and tectonic setting of amphibolites in the eastern Blue Ridge and Inner Piedmont.



- Chunky Gal / Kimsey Bald
- Carroll Knob
- Lake Burton
- Unicoi Formation
- Bakersville dikes
- Montezuma basalt
- Catoctin Formation
- Ropes Creek Amphibolite
- Tallulah Falls Formation (GA)
- Tallulah Falls / Otto Formations (NC)
- Ashe Formation
- Alligator Back
- Poor Mountain Formation
- Mill Spring complex

been reported by Bland (1978) from the Evington Group, Achaibar (1983) from amphibolites in the Smith River allochthon, and Badger (1989 and 1992), Badger and Sinha (1988, 1991), and Aleinikoff and others (1991) from the Catoctin Formation. Mafic rocks with an oceanic affinity, many of which are considered to be ophiolitic fragments, have been reported by Hatcher and others (1984), Shaw and Wasserburg (1984), McSween and Hatcher (1985), Gillon (1989), and Quinn (1990) from Tallulah Falls Formation rocks in the central Blue Ridge of North Carolina and Georgia, McConnell and Abrams (1984) from the New Georgia Group, Misra and Conte (1991) from the Ashe and Alligator Back Formations in eastern the Blue Ridge of North Carolina, and Stow and others (1984) from the Ropes Creek Amphibolite in the Alabama Inner Piedmont. Mafic rocks with volcanic arc characteristics include the Hillabee greenstone in Alabama (Tull and others (1978) and Tull and Stow (1979)), the Kimsey Bald and Carroll Knob complexes in the central Blue Ridge of North Carolina (Eggers, 1983; Walters, 1990), the Doss Mountain and Slaughters suites from the Dadeville complex in the Alabama Inner Piedmont (Stow and others, 1984 and Neilson and Stow 1986) , and the Lake Burton mafic–ultramafic complex in the eastern Blue Ridge of Georgia (Hopson, 1989) (Fig. 3–11).

The distribution and geochemical characteristics of the mafic rocks outlined above within the crystalline southern Appalachians provides important information towards our understanding of the development and destruction of the Laurentian margin. These rocks represent a diverse assemblage that records the developmental stages of continental rifting along the Laurentian margin, ocean or marginal basin development, and arc volcanism related to the destruction of the Laurentian margin (e.g., Fig. 2–11). The spatial and temporal diversity of these mafic units is consistent with an evolving continental margin and with the interpretation of Rodgers (1970), Hatcher (1972, 1978a, 1987, 1989), Rankin (1975 and 1976), and Thomas (1976, 1977, 1983, and 1991) for a diachronous history of rifting, deposition and destruction of the Laurentian margin. In the case of the Columbus Promontory, amphibolite of the Poor Mountain Formation and Mill Spring complex appear to reflect a period of ocean or marginal basin development. In

Chapter II, it was suggested that the Poor Mountain Formation and Mill Spring complex were members of the regionally extensive deep–water facies assemblage deposited along the ancient Laurentian margin. The geochemical characteristics of the intercalated mafic units in the Poor Mountain Formation and the Mill Spring complex, which suggest extrusion in an oceanic environment, further supports previous interpretations (e.g., Hatcher, 1978a,1987, 1989) that the some members of the upper (Ashe–Tallulah Falls–Mill Spring–Sandy Springs/New Georgia) and lower (Evington–Alligator Back–Chauga River/Poor Mountain–Jackson's Gap/Ropes Creek) deep-to shallow water facies rocks, discussed in Chapter II, were deposited in an oceanic environment possibly, in part, on oceanic crust.

CHAPTER IV

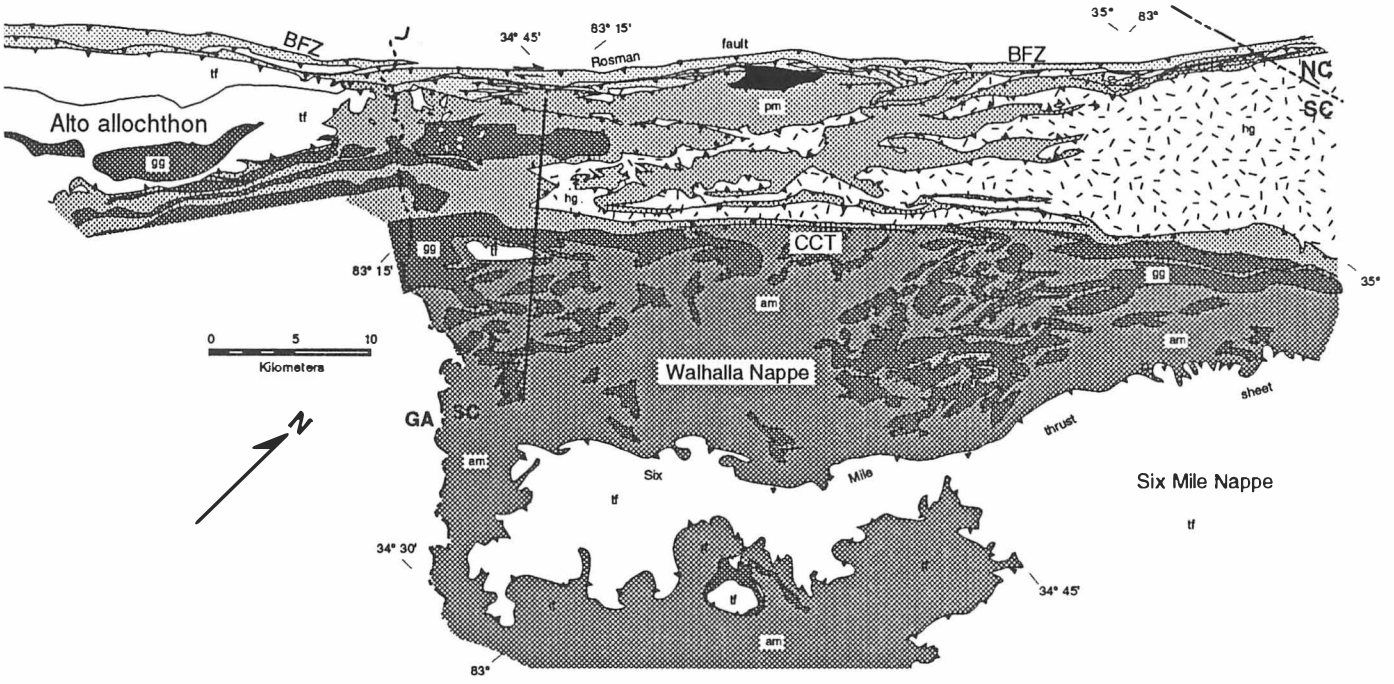
DEFORMATION HISTORY, KINEMATICS AND PARTITIONING OF COEVAL OROGEN–OBLIQUE (E–W) AND OROGEN PARALLEL (NE–SW) DUCTILE DEFORMATION, WESTERN INNER PIEDMONT, CAROLINAS AND NE GEORGIA

INTRODUCTION

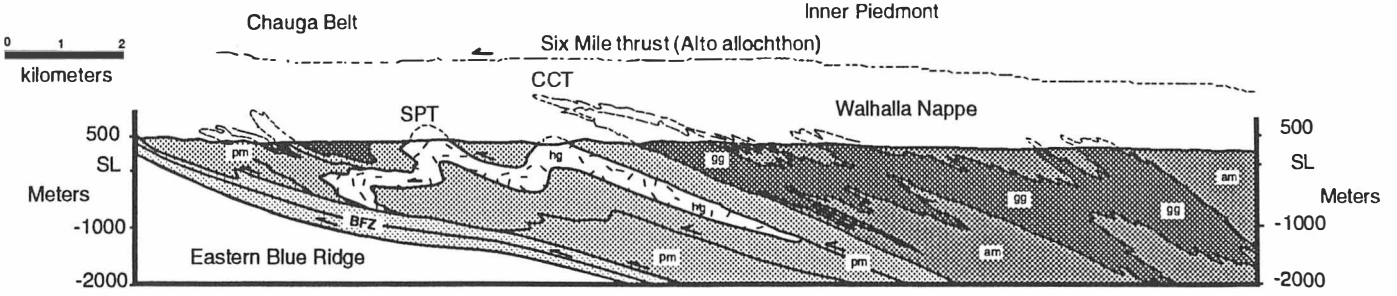
The southern Appalachian Inner Piedmont (Fig. 1–1) is well known for its complex and protracted history of penetrative ductile deformation and metamorphism, and represents part of the internides of an orogen where distinct changes in structural orientation and displacement direction occur. Both orogen–oblique to orogen–normal (W–to NW– directed) and orogen–parallel (SW–directed) structures in the Inner Piedmont have long been recognized (e.g., Reed and Bryant, 1964; Bryant and Reed, 1970; Hatcher, 1972; Roper and Dunn ,1973; Stirewalt and Dunn, 1973; Griffin, 1974a; Bobyarchik and others, 1988), but have been treated separately in the overall deformational history of the Inner Piedmont because some were clearly formed during the late Paleozoic Alleghanian events. The orogen–oblique (to–normal) structures, represented by west–northwest–vergent folds, thrusts, and thrust nappes such as the Six Mile thrust sheet and Walhalla nappe (Fig. 4–1) (Griffin, 1967, 1971a, 1974a, and 1974b) are generally considered products of early–to middle Paleozoic (Taconian or Acadian) tectonothermal events synchronous with peak middle–to upper–amphibolite facies metamorphism. Some orogen–parallel structures, like the Brevard fault zone and central Piedmont suture (Figs. 1–1, 1–2, and 4–1), formed and were reactivated during several orogenies under both high and low P–T conditions (Hatcher, 1972; Stirewalt and Dunn , 1973; Horton, 1974; Sinha and Glover, 1978; Bobyarchik and others, 1988; Hatcher and Hooper,

Figure 4–1. Geologic map (a) and cross section (b) of the western Inner Piedmont in the Tamassee area. am – amphibolite, hornblende gneiss, and biotite gneiss. tf – Tallulah Falls Formation. ggn (dark screen)–Paleozoic granitoid (423 Ma, Harper and Fullagar 1981). hg (light screen) – Henderson Gneiss. (medium screen)– Poor Mountain Formation. (lightest screen) – Chauga River Formation. (black) mylonite gneiss Six Mile thrust sheet and Alto allochthon are unpatterned. Teethed lines are thrust faults (teeth on hanging wall). BFZ – Brevard fault zone. CCT – Cedar Creek thrust. SPT – Stumphouse Mountain thrust. Map compiled from Griffin (1967, 1969, 1971a, 1974b), Hatcher 1971b, Hatcher and Acker (1984), and unpublished data of Hatcher and Liu. Cross section from Hatcher and Hooper (1991).

a)


BFZ
34° 45'
83° 15'
Rosman
fault
BFZ
35°
83°
NC
SC
Alto allochthon
tf
pm
hg
gg
CCT
83° 15'
35°
0 5 10
Kilometers
am
Walhalla Nappe
sheet
thrust
GA
SC
N
Six
Mile
Six Mile Nappe
34° 30'
34° 45'
83°

b)


Chauga Belt
Inner Piedmont
0 1 2
kilometers
Six Mile thrust (Alto allochthon)
CCT
SPT
Walhalla Nappe
500
SL
Meters
-1000
-2000
pm
hg
gg
am
BFZ
Eastern Blue Ridge

1988), and much of the recent work has concentrated on the retrograde movement history of the Brevard fault zone (Horton, 1974; Edelman and others, 1987; Bobyarchik and others, 1988; Hatcher and others, 1989).

In this chapter a hypothesis is presented suggesting that early (early– to middle Paleozoic) west–northwest directed displacement of thrust sheets in the Inner Piedmont were kinematically linked to early southwest– directed orogen–parallel displacement in the Chauga belt and Brevard fault zone. The basis for this hypothesis is the recent work of Davis and others (1989a, 1989b, 1990a, 1990b, 1991a, 1991b), Tabor and others (1990), and Liu and others (1991), in the western Inner Piedmont of the Carolinas and northeastern Georgia, which have documented that the linear fabric and kinematic indicators within the Chauga belt (principally Henderson Gneiss) are also pervasive in overlying Inner Piedmont thrust sheets where they formed in equilibrium with the upper amphibolite facies mineral assemblage in these rocks. Furthermore, this fabric occurs in distinct orientations: northeast–southwest in the western Inner Piedmont (mostly Chauga belt) and east–west in the more internal parts of the Inner Piedmont. It is suggested that this structural pattern is the result of a thrust–wrench partitioned deformation developed during $D_2 - D_3$ deformational episodes in this polydeformed (D_1 to D_5) terrane between a primordial (?) Brevard fault zone and thrust sheets in the high–grade Inner Piedmont and manifestation of an early (middle Paleozoic) oblique convergence or transpressional deformation regime within the crystalline southern Appalachians. In addition, it is argued that the internal partitioning of deformation and development of related D_2 and D_3 structures within this thrust–wrench complex was controlled by a pervasive S_2 mylonitic foliation interpreted to represent a regionally extensive shear surface (C surface, Berthé and others, 1979). Consequently, the western Inner Piedmont may represent a crustal–scale shear zone.

This chapter focuses on the relevant structures in two areas in the western Inner Piedmont: (1) the Tamassee area in northwestern South Carolina and northeastern Georgia (Figs. 1–1 and 4–1); and (2) the Columbus Promontory area in western North Carolina (Figs. 1–1

and 1–2; Plates I, II, and III). The Tamassee area is located in the western Inner Piedmont of northwestern South Carolina and northeastern Georgia. It includes the Chauga belt (Hatcher, 1970 and 1972) and parts of the higher–grade Inner Piedmont. As previously discussed in Chapter I, the Columbus Promontory (Figs. 1–1 and 1–2) is located in the western Inner Piedmont in North Carolina. This area extends from the Brevard fault zone 40 km to the southeast into the Inner Piedmont and sits astride the boundary between the Inner Piedmont and Chauga belt.

The lithostratigraphy of the Tamassee area and Columbus Promontory area is nearly identical, consisting of the Tallulah Falls Formation overlain by rocks of the Chauga belt (Fig. 4–1). The Tallulah Falls Formation (Hatcher 1971a, Hatcher 1973) here consists of biotite gneiss–metagraywacke, pelitic schist, quartzite, and amphibolite, is commonly migmatitic, and locally unconformably overlies North American Grenville basement in the Blue Ridge (Hatcher 1977; Stieve, 1989). In the Columbus Promontory, Tallulah Falls Formation equivalents are termed the Mill Spring complex (Fig. 1–2). Rocks of the Chauga belt include the Chauga River Formation, Poor Mountain Formation, and the Henderson Gneiss (Figs. 1–1, 1–2, 4–1). The Chauga River Formation, occurring mostly in the Brevard fault zone, consists of graphitic phyllite, muscovite–chlorite phyllite, impure carbonate, and quartzite. The Poor Mountain Formation (Sloan, 1908; Shufflebarger, 1961; Hatcher, 1969 1970) consists of micaceous metasiltstone, laminated amphibolite, quartzite, and marble. Chauga River and Poor Mountain Formations occur both structurally beneath and above the by the 509 Ma Henderson Gneiss (Sinha and others, 1989). The Henderson Gneiss is mostly coarse augen gneiss, and varies compositionally from granite to quartz monzonite to granodiorite (Lemmon 1973).

Within the Columbus Promontory, Brevard fault zone rocks display a retrograde overprint (Lemmon, 1973; Dabbagh, 1975) while rocks southeast of the Brevard fault zone, including Chauga belt and Inner Piedmont, are in the upper amphibolite–facies sillimanite–muscovite zone. In the Tamassee area, Chauga belt rocks are in the lower to middle amphibolite facies,

garnet and staurolite zones (Hopson and Hatcher, 1988; Liu 1991) whereas the deeper Inner Piedmont is at the upper amphibolite facies; the Walhalla nappe contains kyanite and or sillimanite, and the Alto allochthon and Six Mile thrust sheets contain abundant sillimanite.

DEFORMATION HISTORY

The detailed structural analysis of two sizable areas (~3000 km^2 in the Tamassee area and 1500 km^2 in the Columbus Promontory) and those of the several previous studies within the western Inner Piedmont (e.g., Griffin, 1974a, Horton and McConnell ,1990) strongly indicate a consistent regional pattern of temporally and spatially related structural features within the western Inner Piedmont of the Carolinas and NE Georgia. Both study areas contain evidence for a polyphase deformation history bracketed by the relationship to the last middle–to upper amphibolite facies metamorphism (M_1) that has affected these areas. This pattern is represented by pre–peak D_1 deformation, pre– to syn- to late– peak D_2 and D_3 deformations, and post–peak D_4 and D_5 deformations. D_2 and D_3 structures are the most pervasive and important to the hypothesis concerning the kinematics and partitioning of deformation between orogen–oblique and orogen–parallel deformation in the western Inner Piedmont. Although chronologically separated, these episodes probably represent a continuum of deformation. The age of $D_2 - D_3$ deformation is, at present time, bracketed by a 423 Ma granitoid (Harper and Fullagar 1981) in the Tamassee area (Fig. 4–1) and a 438 Ma granitoid (Odom and Russell 1975) in the Columbus Promontory (Fig. 1–2). Both of these bodies were deformed by D_2 and D_3. Dallmeyer (1988) indicates that hornblende closure within the Alto allochthon, a major D_3 structure, occurred between 335 and 360 Ma and suggested this age closely approximates uplift and emplacement of the thrust sheet. These ages strongly suggest that $D_2 - D_3$ is a lower– to middle Paleozoic tectonothermal event. Although this discussion is concerned with the development of D_2 and D_3 structures, included below is a brief summary of the attributes of

the other deformational events in the study areas to enable the D_2 and D_3 structures to be related to the regional tectonic framework.

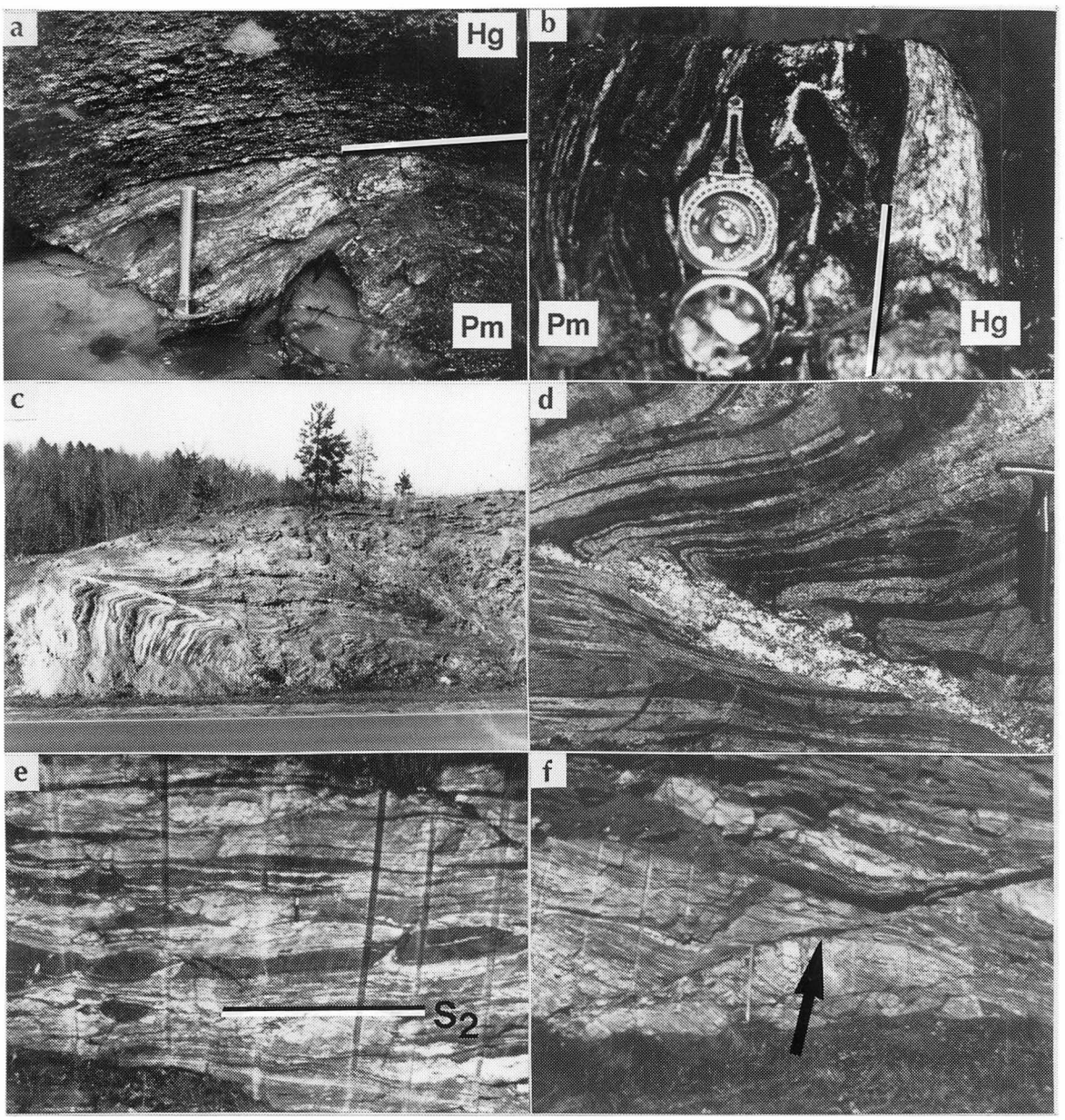
D_1 Deformation

The earliest recognized deformation, here designated D_1, occurred prior to the main phase of recrystallization affecting the western Inner Piedmont and is not widespread. The oldest structures observed in both areas and are F_1 folds. This generation of folding was also observed within the adjacent eastern Blue Ridge by Roper and Dunn (1973), Stirewalt and Dunn (1973), Hatcher (1977), Hatcher and Butler (1979), and Hopson and Hatcher (1988). F_1 folds are preserved primarily as small rootless intrafolial folds and truncated folds within boudins. Hopson and Hatcher (1988) indicated F_1 was accompanied by formation of a penetrative S_1 foliation axial planar to F_1 folds, and defined by alternating micaceous and quartzofeldspathic layers. In the Columbus Promontory early F_1 folds that compositional layering have been observed in Poor Mountain Formation rocks exposed in a small window through the Tumblebug Creek thrust sheet (TCT) (Figs. 1–2 and 4–2).

D_2 Deformation

D_2 represents the most pervasive deformation in the study areas and is divided into two phases. D_{2a} deformation includes a major episode of pre– (M_1) peak thrusting event that emplaced the Henderson Gneiss in both study areas. Thrust sheets containing the Henderson Gneiss are the Stumphouse Mountain thrust sheet (SPT) in the Tamassee area and the TCT in the Columbus Promontory (Figs. 1–2, 4–1, and 4–2). D_{2b} deformation was the most pervasive deformation within both study areas and throughout the entire western Inner Piedmont.

Figure 4–2. Outcrop photographs of D_2–D_3 structures from the Columbus Promontory (a,b,e,and f) and Tamassee area (c and d). a) Exposure of TCT showing truncation of F_1 folds in Poor Mountain amphibolite (Pm) by Henderson Gneiss (Hg). View looking NW. Hammer is 40 cm. b) folded TCT with thrust contact transposed into S_2 foliation. Compass is 20 cm. c) Reclined F_3 folds in weathered amphibolite (dark layers) and granitoid gneiss in the Walhalla nappe along U.S. 76 at Chauga River in NW South Carolina. View looking N. Hammer is 40 cm. d) closeup of (c) showing small thrust, drag folds, and pegmatite along limb of westernmost fold in (d). Note discontinuous (dark) layers of amphibolite interpreted as sections of hinges of SW–vergent sheath (?) folds. Hammer is 40 cm. e) outcrop photo showing composite makeup of regional S_2 foliation including compositional layering, boudinaged amphibolite layers, elongated quartzofeldspathic pods. View looking S. Hammer is 40 cm. f) Large–scale shear band (Berthé et al., 1979) or extensional crenulation cleavage (Platt and Vissers 1980) marked by arrow. Shear sense is top–to–W (right). Hammer is 1 m.


a
Hg
Pm
b
Pm
Hg
c
d
e
S_2
f

Metamorphic textures indicate that D_{2b} was coeval with upper amphibolite facies metamorphism (Fig. 4–3) in the western Piedmont. D_{2b} deformation is characterized by extensive tight to isoclinal F_2 folding (recumbent to reclined) and development of the regional foliation S_2. A penetrative mineral lineation (L_2) occurs within the S_2 foliation. D_{2b} deformation includes emplacement of large thrust sheets in both study areas and includes the Walhalla nappe and Cedar Creek (CCT) thrust sheet in the Tamassee area (Fig. 4–1), and the Sugarloaf Mountain (SMT) and Mill Spring (MST) thrust sheets in the Columbus Promontory (Fig. 1–2). Because of the importance of D_2 structures to the thesis of this chapter, they are discussed in greater detail below.

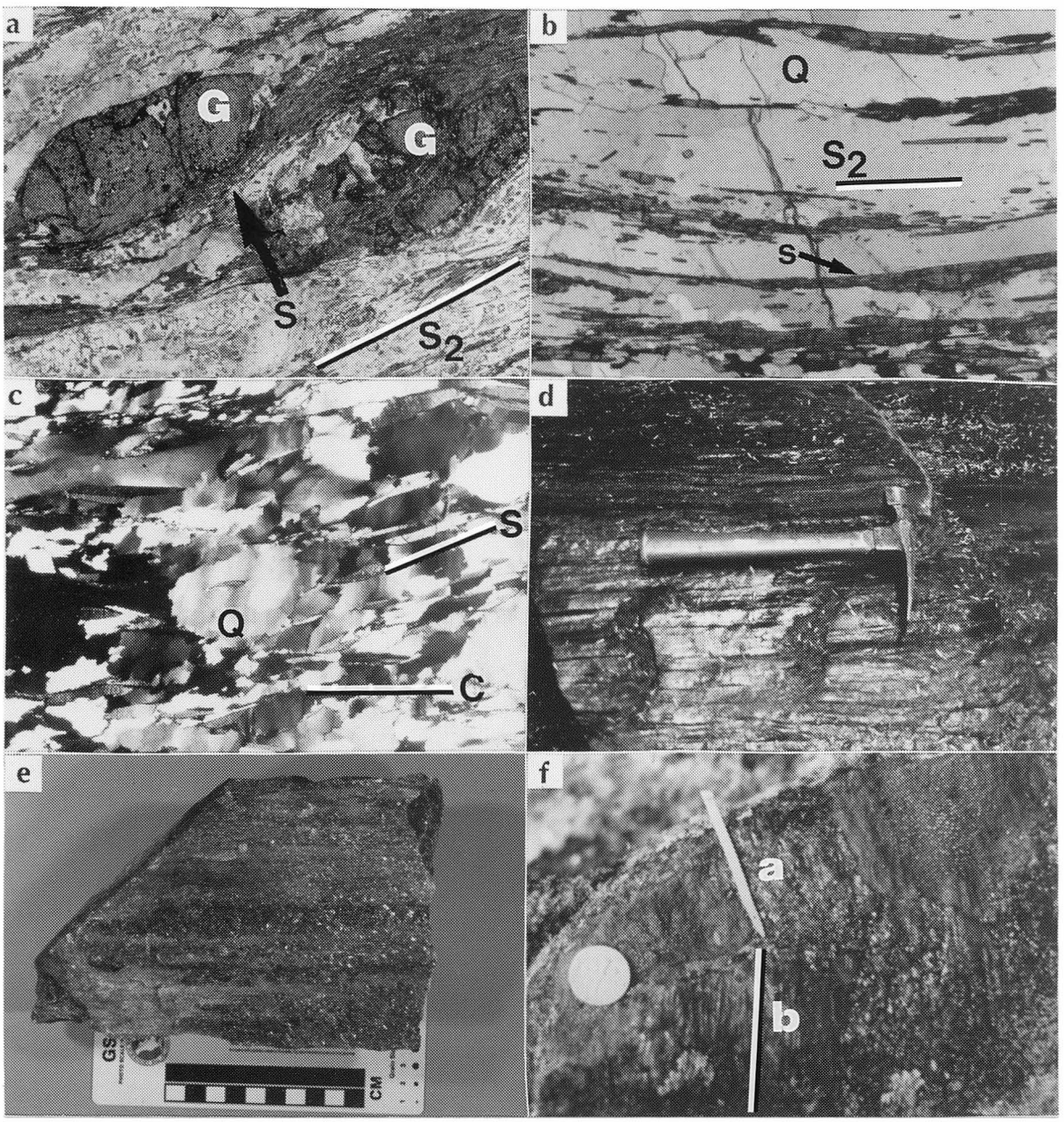
D_3 Deformation

D_3 deformation included late syn- to post metamorphic deformation that are common in both study areas, but not penetrative. D_3 structures are considered to be post peak, but formed prior to complete cooling of the rocks (Hopson and Hatcher, 1988). Importantly, D_3 appears to generally represent late– to postpeak final emplacement of thrust sheets as coherent masses. In the Tamassee area this includes the emplacement of the Alto allochthon (AA) and Six Mile thrust sheet. More specific details about D_3 folds and faults are also outlined below.

$D_4 - D_5$ Deformation

This deformation produced postmetamorphic, nonpenetrative folds in both study areas. In the Tamassee area, D_4–D_5 deformation produced several map–scale folds and dome–and–basin interference patterns. F_4 folds are broad, open structures that refold earlier F_1–F_3 folds. Similar upright, open folds with steep axial planes that warp S_2 are also present in the Columbus Promontory. Thrust sheets (MST and AA) within both the areas are preserved within broad F_4

Figure 4–3. Mosaic of photographs and photomicrographs of D_2 lineations and microstructures from the Columbus Promontory. a) Sheared garnets (G) within S_2 showing top–to–SW (right) shear sense. Note sillimanite (S) growth paralleling garnet boundaries suggesting synkinematic sillimanite growth during shearing. Field of view is 4 mm. Plane light. b) Quartz ribbons defining S_2. Also note sillimanite parallel to quartz ribbon. Quartz c–axis pattern for this sample (cp12–2–5) is shown in Figure 4–8. Field of view is 4 mm. Plane light. c) Type II S–C mylonite (S and C in photo) defined by highly strained quartz (Q) microfabric and asymmetric white–mica fish. Shear sense is top–to–W (right). Quartz c–axis pattern for this sample (cp593) is shown in Figure 4–8. Field of view is 4 mm. Plane light. d) NE–SW oriented mineral lineation (parallel to hammer) in interleaved Poor Mountain amphibolite and Henderson Gneiss. Hammer is 40 cm. e) E–W oriented lineation from metagraywacke of Mill Spring complex in the MST. f) Sample containing two mineral stretching lineations, (a) oriented 18°/243°; (b) oriented 22°/272°.


a
G
G
S
S2
b
Q
S2
S
c
S
Q
C
d
e
GS
CM
f
a
b

synforms. In the Tamassee area F_5 folds occur as upright, NW–trending open folds that refold the F_4 folds, producing broad dome–and–basin interference patterns.

D_2 AND D_3 STRUCTURES

D_2 Structures

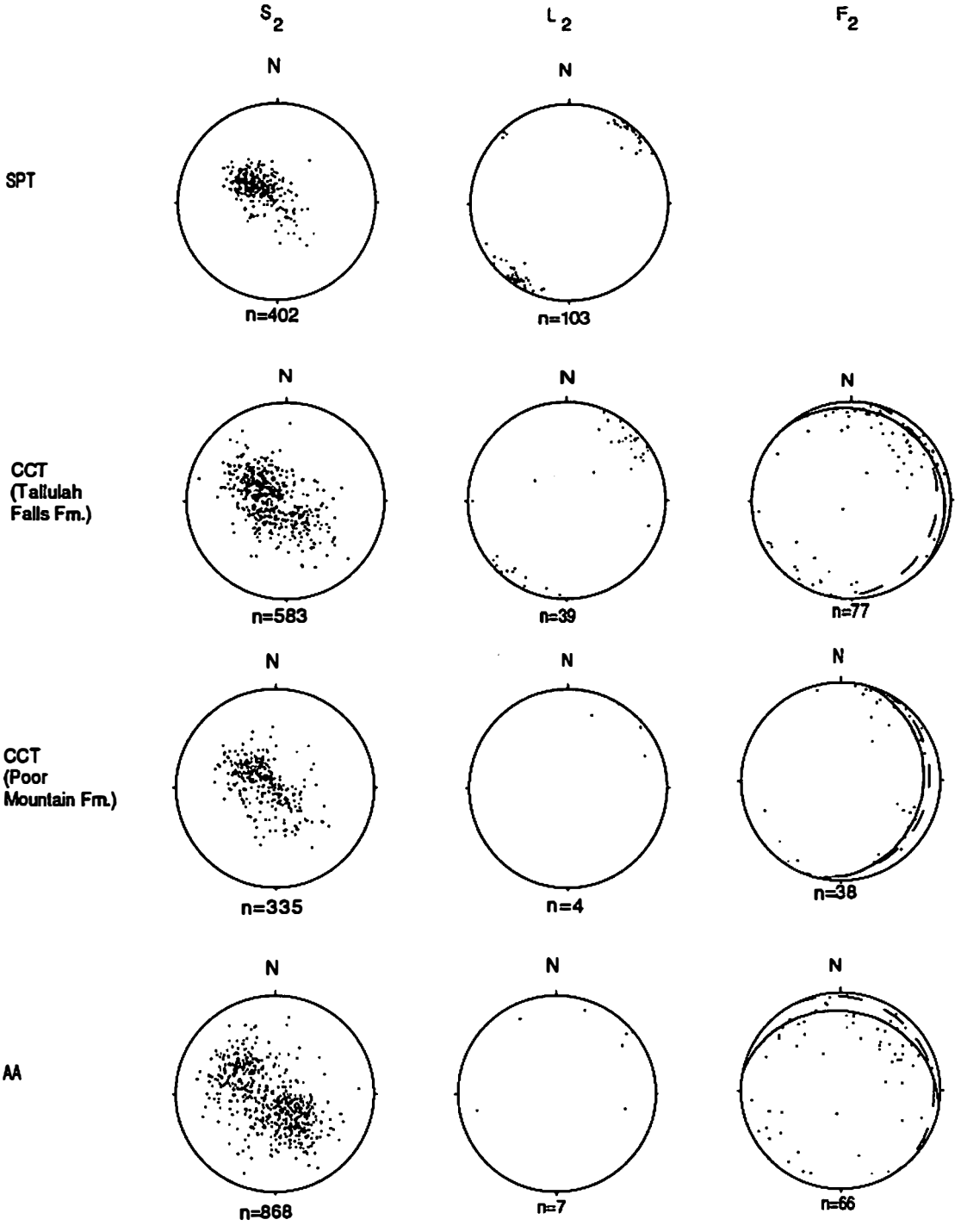
Foliation. S_2 generally strikes slightly oblique (N–NE) to the orogen and has a shallow (< 30°) southeast dip, although variations exist (Fig. 4–4). Near the Brevard fault zone, the strike of foliation parallels the fault zone and dips gently to moderately southeast. Within the Brevard fault zone, S_2 foliation dips moderately (~40°), with steepening related to later Alleghanian deformation. The shallow dip of foliation in the Inner Piedmont and Chauga belt, but with steepening along the Brevard fault zone, has also been clearly imaged in seismic reflection profiles (Cook and others, 1979; Costain and others, 1989).

Components of the S_2 foliation (Fig. 4–2), including compositional layering, schistosity, and gneissic banding, as well as intrafolial folds and boudinage, indicate that S_2 is composite, in the usage of Tobisch and Paterson (1988), and represents an end–product stage of a strongly transposed, evolved fabric. In most cases, compositional layering does not represent bedding (S_0) because the overall parallelism between the foliation, stratigraphic contacts, and major faults indicates that all earlier foliations were transposed into the S_2 foliation (Fig. 4–2). This fabric is discussed in more detail in Chapter VI.

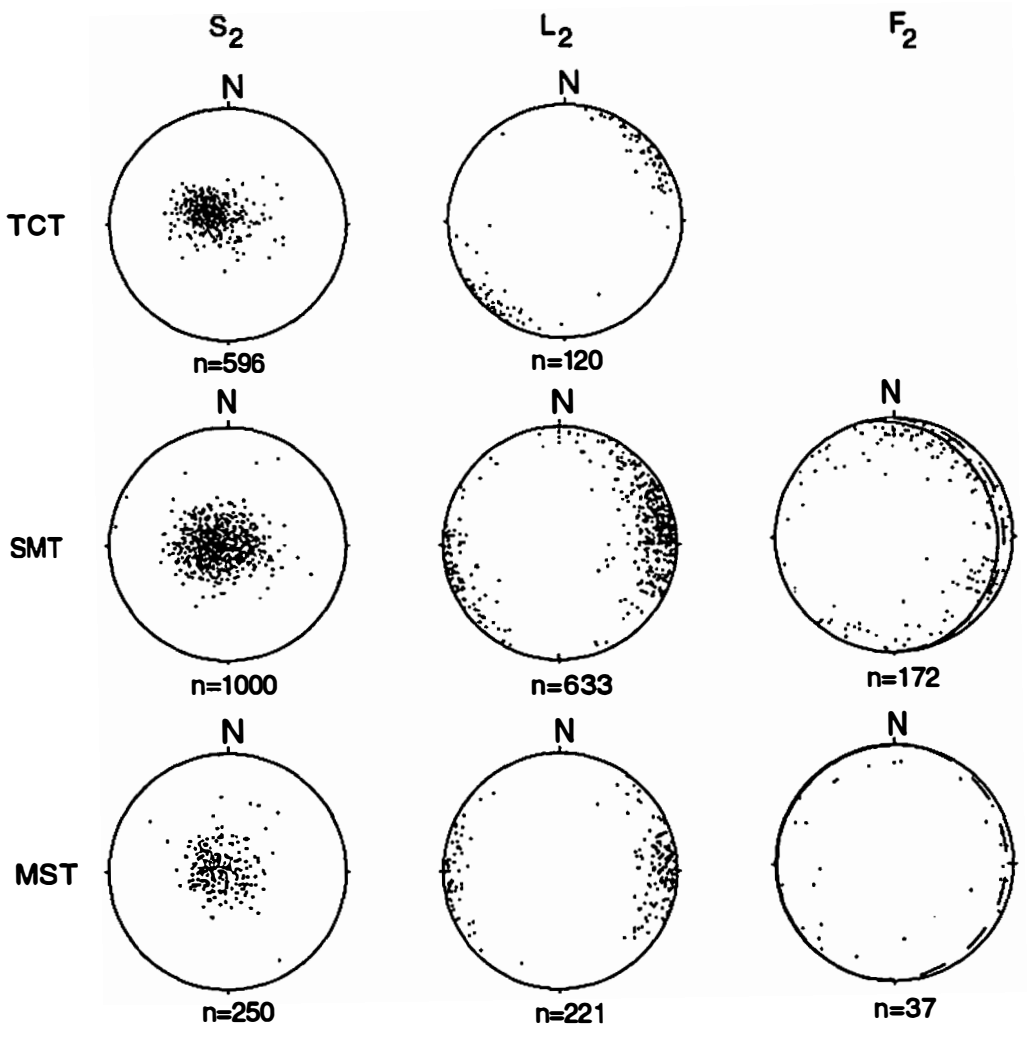
Careful examination of both mesoscopic and microscopic attributes of the S_2 fabric indicates this foliation is mylonitic (commonly annealed), or is an S–type banded structure of Cobbold (1977). This fact is manifested by the strong planarity of the foliation, the presence of mineral stretching lineations on nearly all foliation surfaces, and the widespread occurrence of structures indicative of noncoaxial deformation, such as composite–planar fabrics, asymmetric

Figure 4–4. Lower–hemisphere equal–area projections of structural data a) Tamassee area, and b) Columbus Promontory. In (a) SPT–Stumphouse Mountain thrust; CCT–Cedar Creek thrust; AA–Alto allochthon. In (b) TCT–Tumblebug Creek thrust; SMT–Sugarloaf Mountain thrust; MST–Mill Spring thrust. Dashed great circles on equal–area projections of F_2 folds represent plane normal to mean vector of poles to S_2 mylonitic foliation; solid great circles are the best fit plane to F_2 hinges. (fold–hinge girdle). This shows the low angular discordance between S_2 and the F_2 fold–hinge girdle common in contemporaneous mylonitic foliation and folds formed in ductile shear zone. Tamassee area data compiled from Hopson and Hatcher (1988) Hatcher 1971b, Hatcher and Acker (1984), and unpublished data of Hatcher and Liu (1987–1991). Columbus Promontory data compiled from Lemmon 1973, and unpublished data of Davis (1987–1990), and Tabor (1988–1990).

a)


S_2
L_2
F_2
N
SPT
n=402
n=103
CCT
(Tallulah
Falls Fm.)
n=583
n=39
n=77
CCT
(Poor
Mountain Fm.)
n=335
n=4
n=38
AA
n=868
n=7
n=66

b)



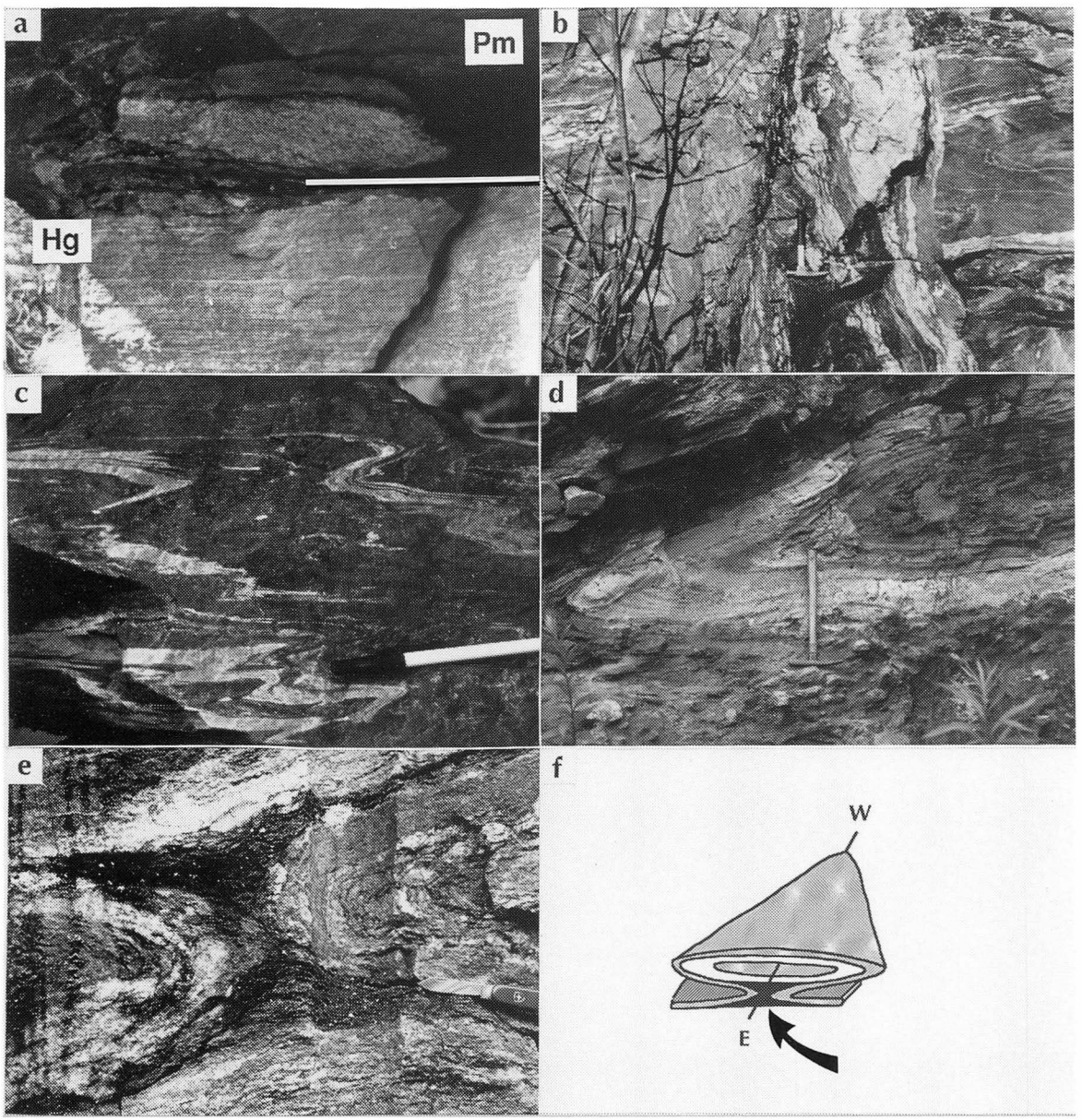
intrafolial folds, and σ-type tails (Simpson, 1986; Simpson and Schmid, 1983) on porphyroclasts and porphyroblasts (Figs. 4–3). In both areas middle–to upper amphibolite facies mineral assemblages help define S_2 (Figs. 4–3). Depending on rock type, the foliation is defined by alignment of micas, quartz ribbons, sillimanite, amphiboles, and elongate garnets (Figs. 4–3).

The extreme planar nature of S_2 and the kinematic indicators within S_2 (Figs. 4–2 and 4–3) permit the interpretation that this foliation developed as a C surface (Berthé and others, 1979; Lister and Snoke, 1984). The more schistose rocks commonly contain an oblique foliation defined by mica–fish (buttons) characteristic of Type II S–C mylonite (Fig. 4–3), defined by Lister and Snoke (1984), and micro– and mesoscale shear bands or extensional crenulation cleavage dipping in the direction of flow (Fig. 4–2), defined by Platt and Vissers (1980). The preservation of asymmetric S–C fabrics within S_2 suggests that it may record a deformation path characterized by a boundary parallel noncoaxial laminar flow (Lister and Snoke, 1984). If this interpretation is correct, the areal extent of S_2 implies that it represents a regionally extensive shear surface.

Folds. Recumbent F_2 folds, with variably oriented hinges, are the dominant folds preserved throughout the western Inner Piedmont (Figs. 4–4 and 4–5). These folds are typically isoclinal, reclined to recumbent with thickened hinges and attenuated limbs (Fig. 4–5). F_2 fold hinges commonly have long straight hinge lines with well–developed cylindricity parallel to L_2 mineral lineations (Fig. 4–4). In most cases axial planes are defined by the S_2 foliation, except in the hinges of the F_2 folds.

In the Tamassee area, F_2 folds are northwest–vergent, northeast–trending reclined to recumbent isoclinal folds (Fig. 4–4). The trend of F_2 folds dominates the outcrop pattern in this area (Hatcher, 1978b; Hatcher and Butler, 1979). In the Columbus Promontory, F_2 fold hinges exhibit a wide variation in orientation and most verge W, although several exposures indicate NW and SW vergence. F_2 also includes sheath folds observed in the SMT and the MST (Fig.

Figure 4–5. Outcrop photographs of D_2 faults and folds from the Columbus Promontory. a) Contact of SMT showing Poor Mountain schist overlying Henderson Gneiss. Knife is 10 cm. b) NW–trending strike–slip in the MST. Note truncation of fold in on the east side (right) of the photograph. View is toward the SE. Hammer is 40 cm. c) F_2 folds in Poor Mountain amphibolite. Pen is 15 cm. d) F_2 folds in Mill Spring complex. Hammer is 60 cm. e) part of W–vergent sheath fold from SMT. View is facing E parallel to E–W trending L_2 mineral stretching lineation. Knife is 10 cm. f) reconstruction of sheath fold in (e). Arrow shows section of folds shown in (e)


a
Pm
Hg
b
c
d
e
f
W
E

4–5). These are recognized in outcrop by the characteristic eye, anvil, and arrowhead shapes, and small–scale folds with highly curvilinear hinges. Definitive sheath folds have been observed in the Columbus Promontory in areas where the east–west deformation is intense (Figs. 4–5). Folds with highly curvilinear hinges are also present in strongly layered rocks in the Tamassee area (Fig. 4–5) and may be sheath folds. Outcrop patterns in the Chauga belt (Figs. 1–2 and 4–1) yield complex fold geometries and are also interpreted as large–scale sheath folds.

Faults. In both study areas, major D_2 thrust faults dip gently southeast, parallel to the S_2 mylonitic foliation and strike northeast roughly parallel to the orogen, although some local discordance is present (Figs. 1–2 and 4–1). D_{2a} faulting involved emplacement of the SPT in the Tamassee area and the TCT in the Columbus Promontory; both thrust sheets contain only Henderson Gneiss (Figs. 1–2, 4–1, 4–2, and 4–3). The along–strike continuity and contact relationships with underlying rock, suggest that the entire Henderson Gneiss body was emplaced as a coherent mass and not intruded into the Chauga belt. Several fundamental structural relationships have been observed along the SPT and the TCT: (1) footwall rocks and earlier F_1 isoclinal folds in the Poor Mountain Formation are sharply truncated by these faults (Fig. 4–2); (2) emplacement of the SPT and TCT occurred before the development of pervasive S_2; and (3) the fault contact has been transposed into S_2 (Fig. 4–2).

Two distinct D_{2b} thrust sheets (Fig. 4–1) have been recognized in the western part of the Tamassee area and include the Walhalla nappe and the Cedar Creek thrust sheet (CCT). The CCT is part of the larger–scale Walhalla nappe of Griffin (1969, 1971a, and 1974a) and straddles the boundary between the Chauga belt and Inner Piedmont. This boundary, between the Chauga belt and Inner Piedmont, has been interpreted as tectonic (Griffin, 1969, 1971a, and 1974a; Hatcher, 1969; Nelson and others, 1987; Liu 1991), a metamorphic gradient (Hatcher and Butler, 1979), or a metamorphic boundary locally faulted (Hatcher and Acker, 1984; Nelson and others, 1987). The CCT placed Poor Mountain amphibolite and amphibolite–

granitoid gneiss of the Inner Piedmont over Henderson Gneiss and other Chauga belt rocks. Liu (1991) suggested that the frontal portion of the CCT may be the overturned limb of the Walhalla nappe. Liu (1991) also indicated that the CCT is a major thrust fault (tectonic slide of Fleuty (1964)) related to F_2 folding (Fig. 4 –1). Hatcher and Hooper (1991) interpreted this feature as a Type F thrust sheet related to fold–nappe style F_2 folding and thrusting. The nature of this boundary in this area is still unresolved.

Two D_{2b} thrust sheets have been identified in the Columbus Promontory by Lemmon (1973) and Davis and others (1989, 1990a): the SMT and the MST (Fig. 3). The SMT, originally identified by Lemmon (1973), Lemmon and Dunn (1973a), represents one of the most abrupt structural contacts in the Columbus Promontory (Figs. 1–2 and 4–5). This thrust emplaced sillimanite–bearing pelitic schist, quartzite, and amphibolite of the Poor Mountain Formation and biotite gneiss of the upper Mill Spring complex over the Henderson Gneiss (Fig. 1–2). Extreme grain–size reduction of the augen in the Henderson Gneiss occurs along this contact (Fig. 4–5). Everywhere this fault has been observed, the contact is knife sharp, subhorizontal, and does not appear to have been appreciably folded after emplacement. Abundant kinematic indicators within this thrust sheet indicate both top–to–SW and top–to–W shear sense; this transition occurs from NW to SE (respectively) within the thrust sheet. The SMT has stratigraphic and structural similarities to the AA and Six mile thrust sheet, but shear sense indicators defined by sillimanite indicates sillimanite growth was synkinematic with ductile thrusting and emplacement of the SMT, whereas sillimanite growth occurred before emplacement of AA and Six mile thrust sheet. The structurally highest MST (Fig. 1–2) placed migmatitic biotite–granitic, amphibole gneiss, and amphibolite of the lower Mill Spring complex over rocks of the upper Mill Spring complex and Poor Mountain Formation. Shear–sense indicators and associated mineral lineations within this thrust sheet indicate a top–to–W displacement. Synkinematic sillimanite growth is also present in the MST.

Lineation. Penetrative subhorizontal mineral lineations (L_2) lying in the plane of the S_2 mylonitic foliation are also widespread structural features in both study areas (Figs. 4–3, 4–4, 4–6, and 4–7). In both study areas, L_2 mineral lineations are commonly parallel to F_2 fold hinges (Fig. 4–4). In the Tamassee area, Chauga belt lineations define a tightly restricted NE–SW concentration (Fig. 4–4). In the Henderson Gneiss, mineral lineations are defined by elongate and rodded quartz, micas, and feldspar; in schist by elongate micas and quartz rods; and in amphibolite by elongate amphiboles (Fig 4–3). This orientation is persistent into the Brevard fault zone. It is important to emphasize that this linear fabric formed under distinctly different P–T conditions from the coaxial linear fabric related to late Paleozoic retrograde greenschist facies mylonitization in the Brevard fault zone discussed by Reed and Bryant (1964) Bryant and Reed (1970), Hatcher (1969), Griffin (1974), Bobyarchik and others (1988), and Vauchez and Brunel, 1988). Southeast of the Chauga belt, this northeast–southwest concentration is more scattered and east–west orientations become apparent in the highest–preserved Six Mile thrust sheet (Figs. 4–4 and 4–6). Here L_2 lineations are defined by elongate micas, quartz rods, and sillimanite needles. Hatcher (1970), Roper and Dunn (1973), and Griffin (1974a), related the northeast–southwest trending lineations to early isoclinal folding. Griffin (1974a) proposed that the lineations developed by preferential elongation growth synchronous with primary isoclinal folding and formed mimetic to the fold hinges. Roper and Dunn (1973) interpreted the northeast–southwest trending mineral lineation in the Brevard fault zone to be associated with folding of the mylonitic rocks parallel to the direction of maximum extension within the plane of the mylonitic foliation, and that no fabric elements observed required southwest–directed transport along the fault. Kinematic indicators in the Chauga belt rocks, particularly in the Henderson Gneiss, clearly indicate that this is a stretching lineation related to southwest–directed shear along the flat–lying foliation (Fig 4–2).

Across the Columbus Promontory from northwest to southeast is a distinct change in the trend of mineral lineations from northeast–southwest to east–west, respectively (Figs. 4–4 and

Figure 4–6. Distribution and orientation of mineral stretching lineations from the Tamassee area. Each arrow represents one measurement. Geology is the same as shown in Fig. 4–1. Data compiled from Griffin (1967, 1969, 1971a, 1974b), Hatcher and Acker (1984), and unpublished data of Hatcher.

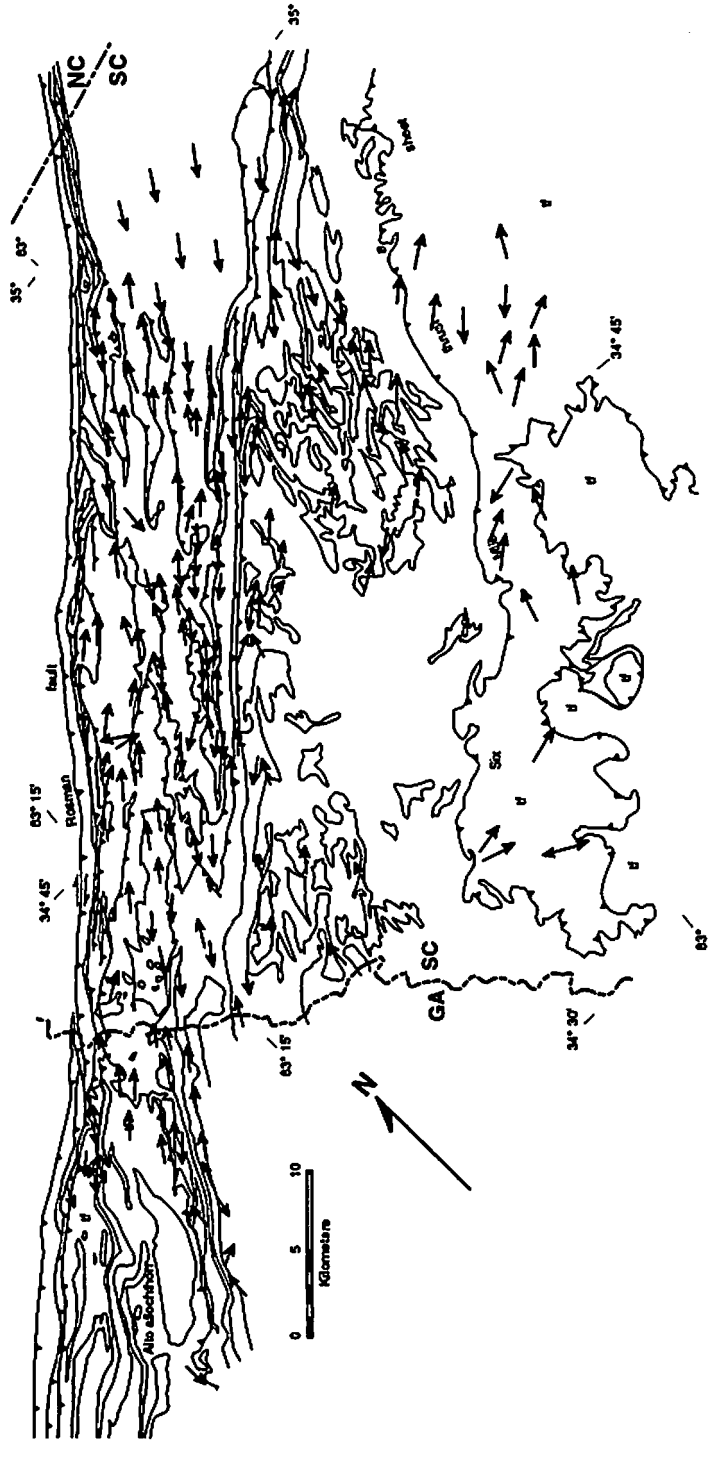
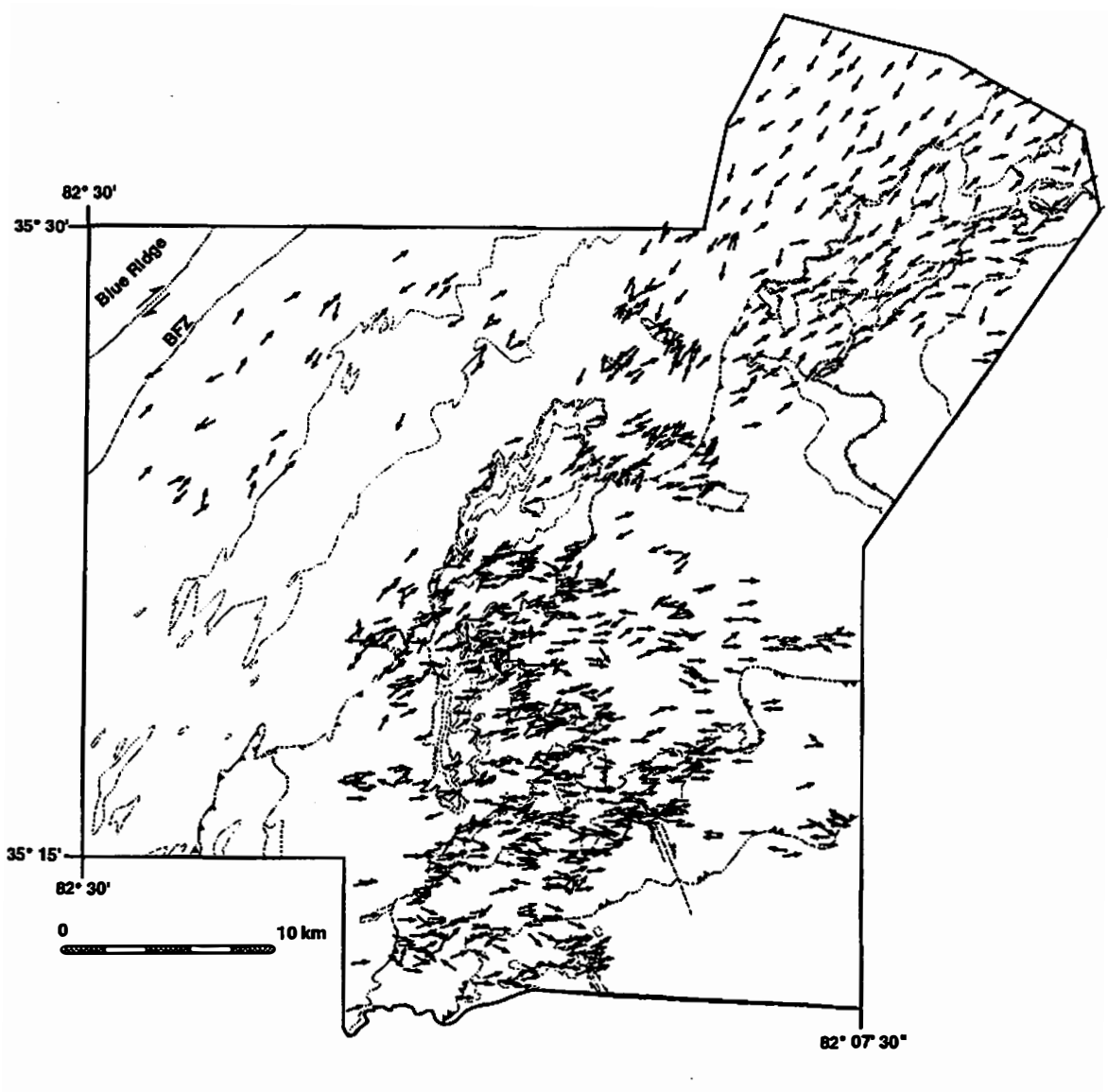

NC
SC
GA
SC
35°
34° 45'
34° 30'
83° 15'
83°
Ridgeland
Bluffton
Hilton Head Island
Port Royal Sound
Broad River
Skull Creek
Calibogue Sound
Daufuskie Island
Savannah River
Tybee Island
Wilmington Island
Tybee Roads
Fort Pulaski
Cockspur Island
Elba Island
Fort Screven
Tybee Light
Tybee Pier
Tybee Beach
Tybee Creek
Lazaretto Creek
Lazaretto Point
Six
N
0
5
10
Kilometers

Figure 4–7. Distribution and orientation of mineral stretching lineations from the Columbus Promontory. Each arrow represents one measurement. Geology is the same as shown in Fig. 1–2. Data compiled from Lemmon 1973, and unpublished data of Davis (1987–1990), and Tabor (1988–1990) and Yanagihara (1991–1993).

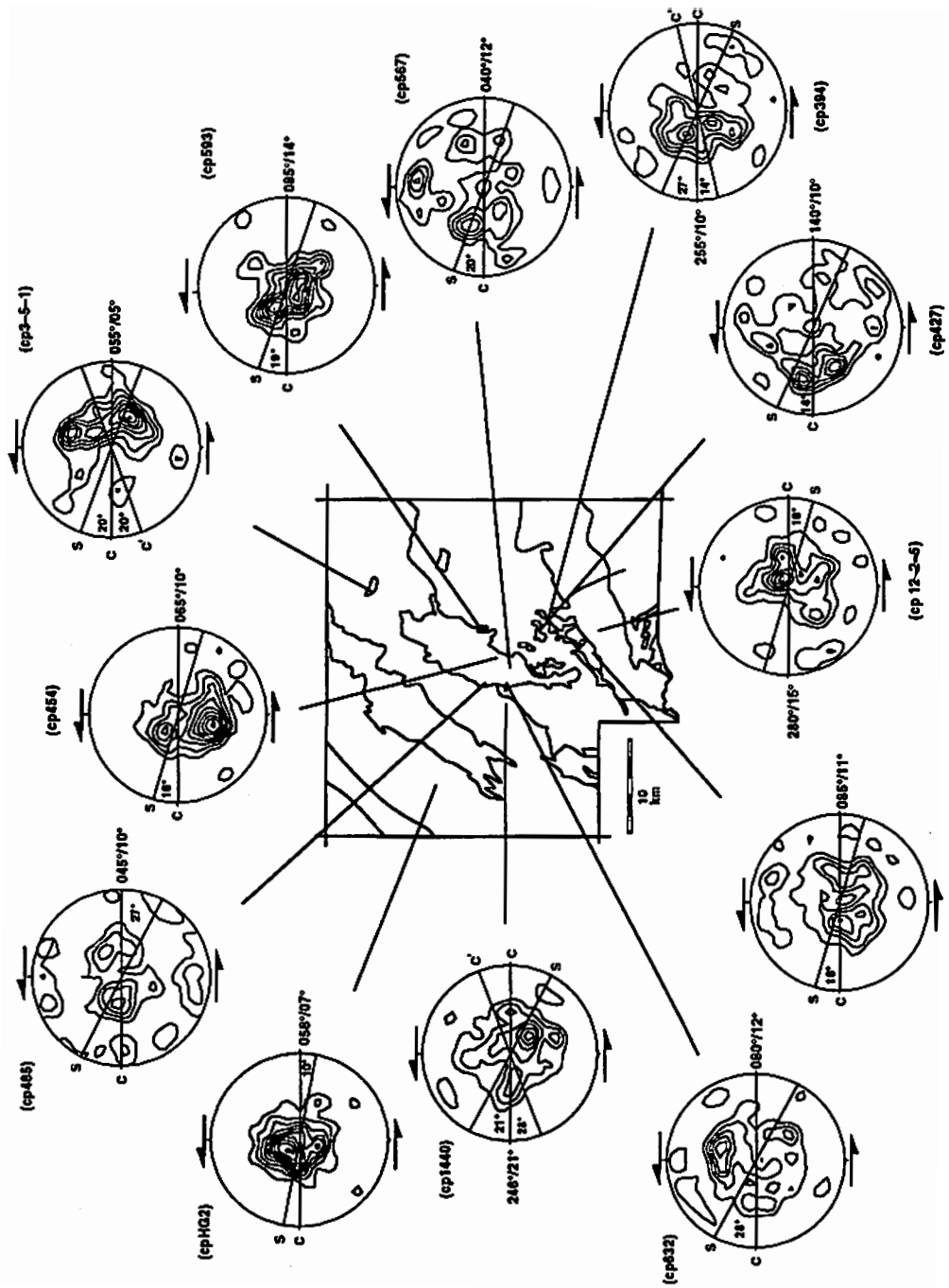

82° 30'
35° 30'
Blue Ridge
BFZ
35° 15'
82° 30'
0
10 km
82° 07' 30"

4–7). Along the western margin of the Columbus Promontory (Chauga belt), mineral lineations also have a ubiquitous northeast–southwest orientation (Figs. 4–3, 4–4, and 4–7). In fact, this northeast–southwest linear fabric is so well developed in the Henderson Gneiss that it is commonly an L–tectonite. This lineation is defined by elongate K–feldspar porphyroclasts, commonly with recrystallized tails, quartz ribbons, and preferentially oriented biotite and muscovite. Asymmetric porphyroclasts, boudinaged feldspar grains, and S–C fabrics indicate a stretching origin related to southwest–directed shear (Fig. 4–2).

Southwest–directed mineral lineations are also present in the western part of the SMT (Figs. 4–4 and 4–7). Here the lineation, depending on rock type, is defined by recrystallized quartz ribbons, elongate amphibole and micas, and preferentially oriented sillimanite. Farther east in the SMT, however, a distinct change occurs in the orientation of the lineation to east–west trends (Figs 4–3, 4–4, and 4–7). Shear sense indicators suggest both top–to–southwest and top–to–west displacement, respectively. Both lineation orientations have been observed in a few localities; here the curvilinear geometry of the lineations indicate a progressive change in orientation (Fig. 4–3). In the structurally highest MST, nearly all lineations are oriented east–west (Figs. 4–4 and 4–7). The east–west lineations, depending on rock type, are defined by quartz rods, elongate amphibole and micas, and preferentially oriented sillimanite. Abundant kinematic indicators including micro– and mesoscale shear bands, S–C fabrics, sheath folds, and boudinaged amphibolite layers indicate intense east–west stretching.

Quartz c–axis fabrics. Quartz c–axes were measured in 12 samples from the Columbus Promontory by standard universal stage techniques (e.g., Turner and Weiss, 1963) from twelve polymineralic, quartz–rich (>75%) samples in thin sections cut perpendicular to the mylonitic foliation and parallel to the mineral stretching lineation. The purpose here was to determine if a change in the quartz c–axis patterns occurs from the southeast corner of the study area, where mineral lineations (L_2) trend east–west and other kinematic indicators suggest top–to–west

Figure 4–8. Contoured lower–hemisphere equal–area projections of quartz c–axis measurements from quartz–rich metagraywacke, quartz–rich pelitic schist, and quartzite in the Columbus Promontory. Arrows indicate shear sense determined by other independent kinematic criteria. N=200 for each sample. Orientations adjacent to diagrams are trend and plunge of mineral stretching lineation.


(cp3–5–1)
055°/05°
20°
20°
S
C
C'
(cp593)
085°/14°
18°
(cp567)
040°/12°
20°
(cp384)
255°/10°
27°
14°
(cp454)
065°/10°
18°
(cp427)
140°/10°
14°
(cp 12–3–5)
280°/15°
18°
(cp 1–14–2)
085°/11°
18°
(cp485)
045°/10°
27°
(cpHG2)
055°/07°
15°
(cp1440)
245°/21°
21°
28°
(cp632)
080°/12°
28°
10 km

surface orientation. Y–maxima patterns are frequently observed in quartz–rich tectonics and have generally been attributed to the activity of prismatic {m} slip planes along the < a > slip direction during high temperature (>400° C). Models by Jessell and Lister (1990) have shown, however, that Y maxima can be produced during shear accompanied by high strain and high temperature by the concomitant activity of multiple slip systems and dynamic recrystallization. Therefore, Y maxima patterns cannot be uniquely assigned to the activity of a single slip system, but do appear to be indicative of shearing at high strain and temperature conditions.

D_3 Structures

Folds. F_3 folds that deform S_2 are common in the Tamassee area, but are not penetrative (Fig. 4–2). These generally contain a weakly developed S_3 axial planar foliation. Axial surfaces of F_3 folds vary from near vertical to gently inclined (Hopson and Hatcher, 1988; Liu 1991). F_3 folds within the Columbus Promontory include outcrop–scale undulations to cm–scale crenulations that locally produce a crenulation cleavage (S_3) in the rocks. In both study areas many F_3 folds have a common limb, parallel to S_2, that is sheared or faulted in a sense indicative of general westerly displacement parallel to the ductile thrusts. Hopson and Hatcher (1988) suggested that this shearing occurred at the time of emplacement of the AA and the Six Mile thrust sheet.

Faults. The AA (Figs. 1–1 and 4–1) is a late– to postmetamorphic peak D_3 crystalline thrust sheet recognized by Hatcher (1978a), and described in detail by Hopson and Hatcher (1988). The Toccoa Falls–Shorts Mill thrust fault bounds the allochthon and separates overlying migmatitic sillimanite–bearing Tallulah Falls Formation rocks of the AA from the garnet–bearing nonmigmatitic Chauga River and Poor Mountain Formation rocks of the Chauga belt.

Earlier F_1 and F_2 folds are truncated by the Toccoa Falls–Shorts Mill fault, along with juxtaposition of high– and medium–grade rocks, indicating postmetamorphic emplacement of

the allochthon. Two distinct episodes of mylonitization are recorded within the AA: (1) early high–temperature mylonitization along the Toccoa–Shorts Mill fault, and (2) later retrograde mylonitization along the northwestern margin of the AA, associated with deformation in the Brevard fault zone (Hopson and Hatcher 1988). Nelson (1985) and Hopson and Hatcher (1988), on the basis of stratigraphic, metamorphic, and deformational similarities, suggested that the AA may be a dismembered remnant of the Six Mile thrust sheet (Fig. 4–1). The Six Mile thrust (Griffin 1967, 1971a, and 1974a) separates sillimanite–grade pelitic schist, gneiss, and deformed granitic plutons from underlying amphibolite and granitic gneiss of the northwestern flank of the Walhalla nappe (Fig. 4–1).

D_3 faulting in the Columbus Promontory includes a northwest–trending, ductile strike–slip fault (Figs. 1–2 and 4–5) that cuts the MST. This fault is nearly vertical with a NW–SE horizontal mineral lineation, and deflection of wall–rock units into the fault indicates a sinistral displacement sense (Fig. 4–5). The areal extent of this structure has not been determined, despite detailed map coverage. Metamorphic textures indicate this feature also developed near the peak of M_1 metamorphism, but after emplacement of the MST and development of S_2 mylonitic foliation and the F_2 folds.

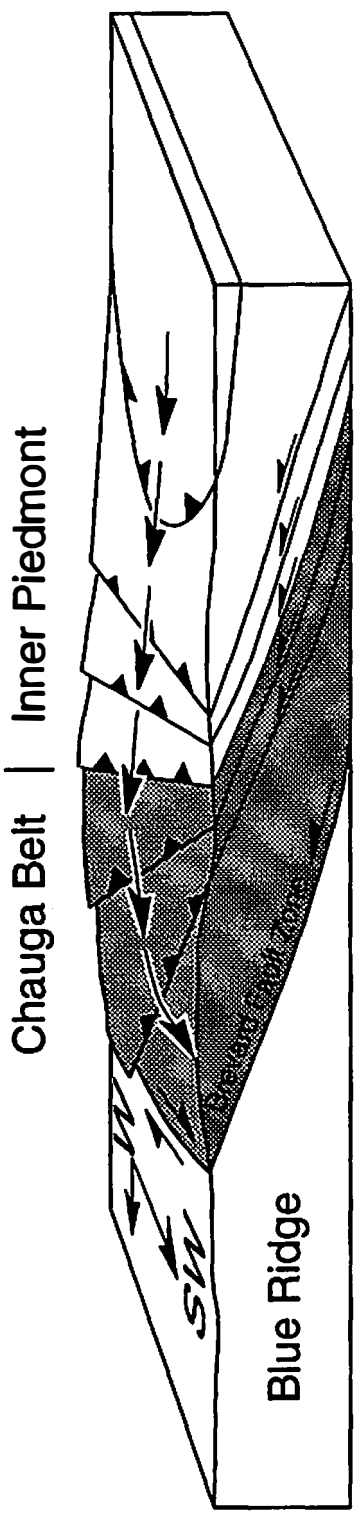
DISCUSSION

Kinematics of Orogen–Parallel and Orogen–Oblique Deformation

An important observation from this investigation is the recognition of a change in orientation in the displacement direction within the western Inner Piedmont from east to west in the deeper Inner Piedmont to northeast to southwest in the Chauga belt and Brevard fault zone (Figs. 4–6 and 4–7) during D_2 and D_3. Variation in trend of macro– and mesoscopic structural elements is a common attribute of many orogenic belts (Ramsay, 1958 and 1967; Tobisch and

others, 1970; Reed and Bryant, 1964; Bell , 1978; Coward and Potts, 1983; Ridley, 1986; Ellis and Watkinson, 1987; Oldow, 1990). These variations can result from noncoaxial polyphase deformation, partitioning of deformation during a single event (Lister and Williams, 1983; Williams, 1970 and 1985), or combinations of different deformation paths. At one time, it was argued (Tabor and others, 1990) that these patterns in the Columbus Promontory represented two distinct episodes of movement. The consistent and progressive change in orientation of lineations and kinematic indicators across both study areas, and similarities in metamorphic conditions for both kinematic directions, suggested by metamorphic assemblages and textures (Figs. 4–3), however, indicates these structures formed coevally at upper amphibolite facies metamorphic conditions. Because of these observations, it is argued that NE–SW and E–W structures resulted from partitioned southwest–directed, orogen–parallel displacement in the Brevard fault zone and Chauga belt, and orogen–oblique to orogen–normal, west–northwest–directed ductile deformation in Inner Piedmont thrust sheets during $D_2 - D_3$ (Fig. 4–9). The implication of this interpretation is that early (synchronous with upper amphibolite facies metamorphism vs. retrograde) movement on a primordial (?) Brevard fault zone was kinematically linked to the emplacement crystalline thrust sheets in the Inner Piedmont. This possibility was, perhaps implied, by the earlier studies of Clarke (1952), Bentley and Neathery (1970), Griffin (1971b, 1974a), Hatcher (1969, 1972, and 1978a), Stirewalt and Dunn (1973), and Edelman and others (1987), but lacked supporting kinematic data. The new data presented in this chapter appear to provide strong kinematic evidence for such a movement history. The interpretation shown in Figure 4–9 explains the juxtaposition of those Inner Piedmont thrust sheets farthest east, dominated by structures indicative of east–west displacements, to structures farther west, where there is a progressively greater amount of southwest–directed displacement. This configuration also suggests a linked décollement system between the Inner Piedmont thrust sheets and the Brevard fault zone (Fig. 4–9). The

Figure 4–9. Schematic configuration of the thrust stacking and deformational sequence envisioned for the western Inner Piedmont. Configuration shows dominance of W–directed (orogen–oblique) displacement in the deeper Inner Piedmont and stronger component of SW–directed displacement (orogen–parallel) and stretching within the Chauga belt and Brevard fault zone. Configuration also shows linkage of the Brevard fault zone and western Inner Piedmont thrust sheets along common décollement system.


Chauga Belt
Inner Piedmont
Blue Ridge
Brevard Fault Zone
MS
SW

northeast–southwest ductile deformation affecting the pre– (SPT and TCT), syn– (SMT), and late– to post metamorphic peak (AA) thrust sheets indicates this system was linked and active throughout the last upper amphibolite facies metamorphic event that affected this part of the western Inner Piedmont.

Structural patterns similar to those observed in the Tamassee area and the Columbus Promontory have been described by Brun and Burg (1982), Coward and Potts (1983), Lisle (1984), and LaGarde and Michard (1986). Studies of finite strain in ductile thrust zones in the Scandinavian and British Caledonides (Lisle, 1984; Coward and Potts, 1983), and in the Variscan belt (Brun and Burg, 1982), reveal large areas with longitudinal mineral stretching lineations subparallel thrust fronts and normal to the regional thrust transport directions. Coward and Potts (1983), using the Moine thrust as an example, proposed that longitudinal strain may be explained by differential movement and are related to complex strain patterns developed at the frontal tips of thrust zones. LaGarde and Michard (1986) interpreted similar longitudinal strain patterns, along frontal tip of the Central Meseta thrust in the Rehamna massif in the southwest Moroccan Meseta, to be the product of thrust–wrench shearing, combining ductile thrusting and wrenching during progressive synmetamorphic shortening.

Oldow (1990) has shown displacement compatibility for coeval transcurrent and contractional faults requires that these faults share a common décollement system. Such a linked décollement system can produce a complex array of transport directions within a single orogen that include dip–slip and strike–slip motion despite being spatially separated in parts of the same displacement field. This model seems particularly significant to the observations in the western Inner Piedmont discussed in this chapter. Oldow (1990) also pointed out that oblique convergence is, in many cases (e.g., North American Cordillera), the driving force for synchronous development of contractional and strike–slip systems. By analogy, it is suggested that oblique convergence or a transpressional regime, between one of several terranes (e.g., Blue Ridge, Inner Piedmont, and Carolina terrane in Fig. 1–1) during amalgamation of the

southern Appalachian orogen, may have been the large–scale tectonic mechanism that oriented the dominant flow paths (W and SW directed) in the foreshortening crust in the western Inner Piedmont.

Transpressional models to explain the Alleghanian (retrograde) transcurrent displacement along the Brevard fault zone, the Brookneal shear zone, and faults of the eastern Piedmont fault system (Hatcher and others, 1977) have been proposed by LeFort (1984), Gates and others (1986, 1988), and Vauchez and others (1987). These models generally discuss only the retrograde movement on the Brevard fault zone, and thus do not discuss the possible relationship between the Brevard fault zone and Inner Piedmont thrust sheets. The transpressional or oblique convergent model presented in this chapter is significantly different in that it suggests a kinematic connection between earlier deformation along the Brevard fault and the emplacement of thrust sheets in the western Inner Piedmont during the last (?) high grade tectonothermal event in the western Inner Piedmont.

Vauchez (1987) and Vauchez and Brunel (1988) suggested that development of the linear fabric in the Henderson Gneiss discussed in this chapter formed during an earlier (Alleghanian) phase of dextral strike slip along the Brevard fault. In their interpretation, this fabric was produced during low amphibolite facies P–T conditions and forms a restricted domain near the Brevard fault zone. Vauchez and others (1987, 1989), furthermore suggested southwestward extrusion of the Inner Piedmont as a rigid block between the Brevard fault zone, the Kings Mountain shear zone, and related faults during the Carboniferous–Permian continent–continent collision between North America and Africa originally proposed more generally by LeFort (1984). It is alternatively argued here, based on considerable amount of new structural and metamorphic data that, during development of this linear fabric in the Henderson Gneiss and in the overlying thrust sheets (SMT, AA, MST), the Inner Piedmont did not behave as an nondeforming rigid block, but was undergoing internal ductile deformation at middle– to upper amphibolite facies conditions. The fabric elements of ductile thrust sheets in

the western Inner Piedmont record changes in rheological behavior related to their emplacement history related to the peak metamorphic event that affected the western Inner Piedmont. The Inner Piedmont thrust sheets had to have cooled enough to have sufficient strength to remain coherent during transport, but were sufficiently ductile to become penetratively deformed. Penetrative ductile deformation occurred early accompanying formation of D_2 structures that are pervasive throughout the western Inner Piedmont. This was followed by some cooling accompanying transport at which time individual thrust sheets crossed a rheological threshold that provided greater internal strength permitting them to move tens of kilometers westward as thin (<< 5km) coherent sheets during late D_2 or D_3 (e.g., Alto allochthon). It is possible that the conclusion of this deformation episode is represented by the early retrograde shearing along the Brevard fault zone which overprints rocks on the northwest end of the Alto allochthon observed by Hopson and Hatcher (1988).

Development and Kinematic Importance of the S_2 Mylonitic Foliation

Ductile thrusting, that formed relatively thin crystalline thrust sheets has been recognized as the dominant map–scale deformation that affected the western Inner Piedmont by Griffin (1967 1969, 1971a, 1974a), Hatcher (1969, 1972, 1978b, 1987, 1989), Goldsmith and others, 1988) Nelson and others (1987), Higgins and others (1988), Hopson and Hatcher (1988), Horton and McConnell (1990) and recent work in the study areas discussed in this chapter. The flat–lying S_2 foliation, however, is the most pervasive structural element in the southern Appalachian Inner Piedmont. It is suggested here that the S_2 mylonitic foliation strongly controlled the internal development of $D_2 - D_3$ structures in this thrust–wrench deformational environment within the western Inner Piedmont. Such an interpretation is consistent with observations in both study areas in the western Inner Piedmont that indicate a genetic relationship between the S_2 mylonitic foliation and the orientation, geometry, and

kinematics of other $D_2 - D_3$ structures, especially D_2 structures. As previously discussed, L_2 and associated kinematic indicators occur within S_2, F_2 folds are generally defined by the S_2 mylonitic foliation, D_2 thrust faults dip gently southeast, parallel to the S_2 mylonitic foliation, and many overturned F_3 folds have a sheared or faulted common limb parallel to S_2.

The suggestion that S_2 is a regionally extensive shear surface contrasts markedly with previous interpretations of this structural feature, including Griffin (1971a, 1974a), Hatcher (1978b), Hopson and Hatcher (1988), and Horton and McConnell (1990), who resolved the relative timing of development of this structure, but related it only to large–scale isoclinal, recumbent folding and formation by a flattening mechanism (parallel to XY plane of finite strain) (e.g., Ramsay, 1967; Ramsay and Graham, 1970), an argument supported by the axial planar relationship between the S_2 foliation and F_2 folds. Although such an interpretation may be in part correct, it is alternatively argued here that these folds, defined by the S_2 mylonitic foliation, developed as passive features and represent an artifact of high strains within the S_2 mylonitic foliation. This interpretation is supported by the orientation and geometry of F_2 folds and their relationship to the S_2 mylonitic foliation within the western Inner Piedmont. A distinct characteristic of the F_2 folds in both study areas is the planar distribution of F_2 hinge lines and the development of fold–hinge girdles (Fig. 4–4). This pattern is particularly well developed in the Columbus Promontory area (Fig. 4–4). Fold–hinge girdle patterns are commonly recognized in ductile shear zones, and folds that display such girdle patterns are defined by the mylonitic foliation, are shear related, and are considered to be contemporary with the mylonitic foliation (Mies, 1991). Figure 4–4 shows the low angular discordance between the girdle of F_2 hinges and the best–fit plane to the mean vector of S_2 poles, which Mies (1991) has shown to be consistent with folds formed within a mylonitic foliation. The fact that F_2 folds within the western Inner Piedmont are defined by the S_2 mylonitic foliation, and produce a fold–hinge girdle pattern, strongly suggests that these structures (S_2 and F_2) formed contemporaneously. This phenomenon has also been observed in the Moine thrust (Christie, 1963), the Cap de

Creus shear zone (Carreras and others, 1977), and shear zones at the base of the Blue Ridge thrust complex in northwestern North Carolina by Mies (1991), and by analogy, suggests that F_2 folds in western Inner Piedmont formed in a similar manner during regional–scale ductile shearing within S_2.

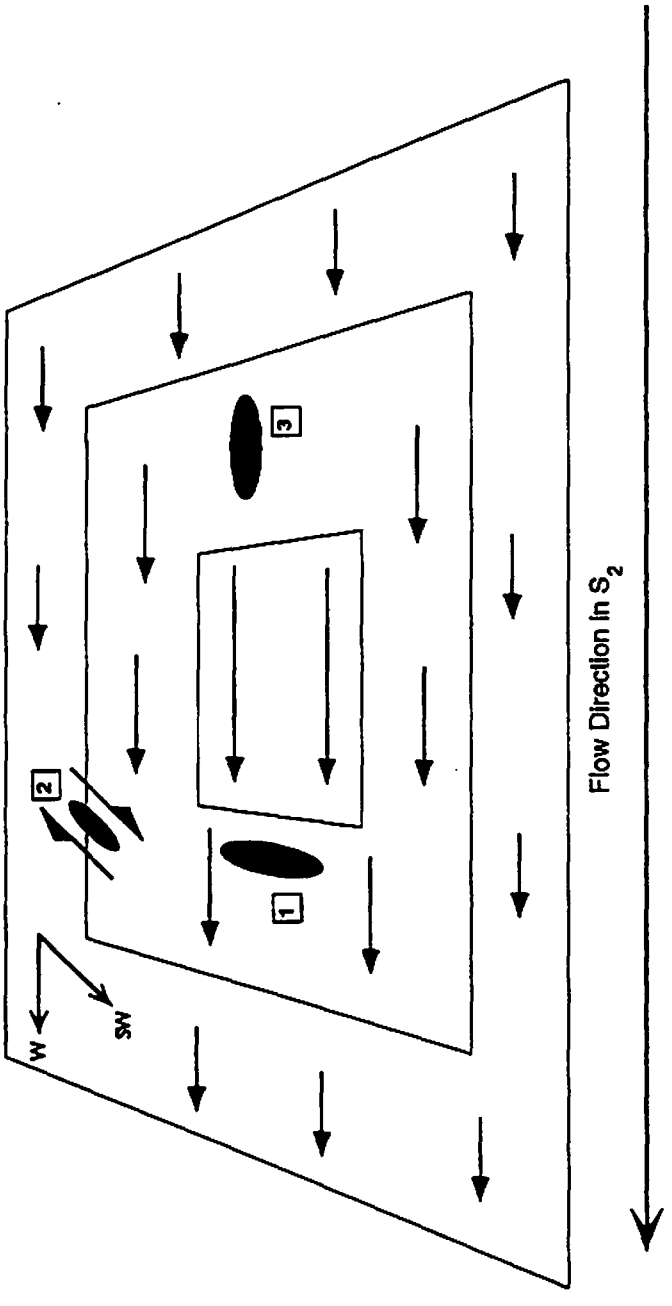
This possibility of contemporaneous S_2 and F_2 is further supported by the observation in both study areas of the parallelism between L_2 mineral stretching lineations and F_2 fold hinges (Fig. 4–4). One possible interpretation for this, suggested by others for similarly deformed areas (Reed and Bryant, 1964; Bell, 1978; Evans and White, 1984; Mies, 1991), is that the folds formed initially at high angles to the shear direction defined by the stretching lineation and where shear strains were large, the folds were progressively rotated into parallelism with the lineation. This study has not found evidence to support such an interpretation and alternatively it is argued that this phenomenon is better explained by variations in strain patterns within the S_2 mylonitic foliation. Watkinson (1975) has shown that, where the maximum stretch is within the layering and the intermediate stretch is perpendicular, folds have a well–developed cylindricity parallel to maximum extension. These conclusions are consistent with observations made in both study areas and explains the parallelism of F_2 fold hinges, L_2 lineations, and the geometry of F_2 folds in the western Inner Piedmont. This interpretation also explains the presence of sheath folds in both study areas. Studies by Hudleston (1983), and Cobbold and Quinquis (1980) have also shown that in areas of high strain where the finite stretch is at a low angle to the layering, folds will have relatively long straight hinge lines parallel to the stretching lineation and become accentuated in the high noncoaxial strain fields (e.g., ductile shear zones) in which sheath folds are generated.

The quartz c–axis patterns, recorded by samples (Fig. 4–8) from the Columbus Promontory, do not appear to provide additional kinematic evidence related to displacement patterns within the Columbus Promontory. Similar Y–maxima distributions, however, have been recognized in quartzites from natural shear zones and reproduced in experimental and

theoretical studies (Eisbacher, 1970; Starkey, 1979; Burg and others, 1981; Schmid and Casey, 1986; Manktelow, 1987; Law, 1987; Jessell, 1988b; Dell' Angelo and Tullis, 1989; Jessell and Lister, 1990). Computer simulations by Jessell (1988a and 1988b) and Jessell and Lister (1990) indicate that, with increasing strain and increasing temperature, c-axis distributions contract to strongly developed Y-maxima. Thus the Y maxima patterns (Fig. 48) within S_2, further suggest that D_2 in the Columbus Promontory (and throughout much of the western Piedmont) involved regionally extensive high-temperature shearing along S_2.

Ridley (1986) and Holdsworth (1990) have proposed models whereby structures indicative of a partitioned thrust-wrench deformation can be explained by flow perturbations within the mylonitic foliation. Such perturbations lead to the development of velocity gradients, either perpendicular or parallel to the slip direction, within the mylonitic foliation surface and result in a heterogeneous strain field. Structural analysis in both the Tamassee area and the Columbus Promontory suggest that the orientations of finite strain ellipsoids within the regional S_2 in the western Piedmont may be schematically represented (Fig. 4-10) in a manner analogous to those developed in the models of Ridley (1986) and Holdsworth (1990) and can explain the resulting structures observed in the western Inner Piedmont. Figure 4-10 attempts to show how perturbations normal to the flow direction could produce southwest-directed , orogen-parallel structures within the Brevard fault zone and Chauga belt. Alternatively, perturbations parallel to the flow direction result in compression and produced west-directed structures including overturned F_2 and sheath folds, E-W mineral stretching lineations,and ductile thrusts and shear-parallel extension that produced the meso- and microscale C' (Berthé and others, 1979) or extensional crenulation cleavage (Platt and Vissers, 1980) observed in this study. Likewise, perturbations either normal or parallel to flow in S_2 could account for the variation in the orientation of F_2 hinges, sense of vergence, and geometry of folds (e.g., see hinge-girdle patterns in Fig. 4-4) observed in both study areas analogous to the development of the folds discussed by Ridley (1986).

Figure 4–10. Diagrammatic sketch of S_2 mylonitic foliation plane modified after Ridley (1986) and Holdsworth (1990). The arrows represent flow velocity within the plane of S_2 and illustrate how gradients in flow could account for the orientation, and kinematics of D_2 structures observed in the western Inner Piedmont. 1) shear parallel shortening resulting in west–vergent folds, sheath folds; foliation – parallel thrust faults, and E–W mineral stretching lineations; 2) dextral wrench shear along the Brevard fault zone resulting in a NE–SW mineral stretching lineation, and NW and SE–vergent asymmetric folds with NE–SW hinges (locally sheaths); and 3) shear parallel extension resulting in micro– and mesoscale shear bands or extensional crenulation cleavages dipping in direction of shear.


Flow Direction In S_2
1
2
3
W
SW

Throughout this section of this chapter an attempt has been to document the important role of the S_2 mylonitic foliation on the development of D_2 and D_3 structures in the western Inner Piedmont and as a regional shear surface along which $D_2 - D_3$ displacement occurred. Geometric relationships between various structural features including microscale kinematic indicators, lineations within the S_2 foliation plane, parallelism between ductile thrust fault surfaces and S_2, the orientation of fold hinges, and quartz c–axis, Y–maxima patterns within S_2, strongly indicate participation in and control by S_2 of the development of D_2 and D_3 structures throughout the western Inner Piedmont. Although the overall kinematics of deformation in this area were probably controlled by the large–scale oblique convergence or transpressional mechanism, the observations discussed in this section suggest that local changes in displacement direction and development of associated kinematic indicators in the western Inner Piedmont were also controlled partly by flow perturbations within regional shear planes represented by the S_2 mylonitic foliation. The regionally pervasive nature of S_2 and its control on other $D_2 - D_3$ structures throughout the western Inner Piedmont suggest the western Inner Piedmont is part of a region of extensive shear of crustal dimension, and possibly represents a remnant of a crustal–scale shear zone. In addition, it is suggested that the S_2 mylonitic foliation was the common décollement that linked SW–directed transcurrent movement along the primordial Brevard fault zone with E–W contractional movement of Inner Piedmont thrust sheets.

CHAPTER V

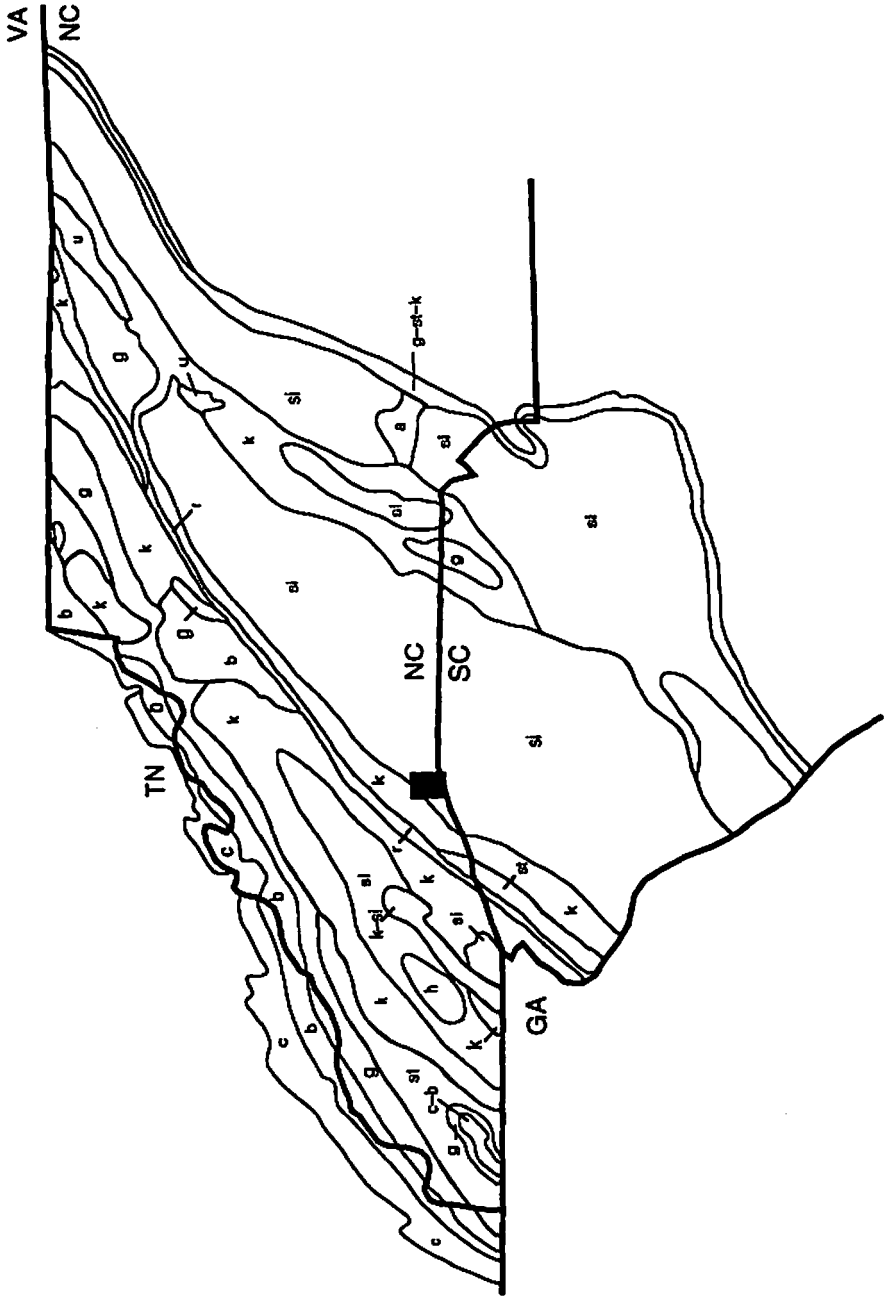
METAMORPHIC AND MICROSTRUCTURAL DEVELOPMENT OF SILLIMANITE–BEARING PELITIC SCHIST IN THE SUGARLOAF MOUNTAIN THRUST SHEET, COLUMBUS PROMONTORY, WESTERN INNER PIEDMONT, NORTH CAROLINA

INTRODUCTION

The Inner Piedmont represents the metamorphic crystalline core of the southern Appalachians (Figs. 1–1 and 5-1). In the Carolinas, the early to middle Paleozoic metamorphic pattern of the Inner Piedmont, as recorded by pelitic units, is characterized by an extensive high–grade (sillimanite–muscovite) core, bounded on the NW by lower–grade (garnet to kyanite) rocks of the Chauga belt and the Brevard fault zone (Fig. 5–1). This pattern of decreasing metamorphic grade, from the deeper Inner Piedmont westward towards the Chauga belt, is considered to be the result of retrograde emplacement of higher–grade thrust sheets (e.g., Six Mile thrust sheet and Alto allochthons) and fold nappes (e.g. Walhalla and Anderson nappes) of the Inner Piedmont, over the lower–grade rocks of the Chauga belt and Brevard fault zone (Griffin, 1969, 1971a, 1971b, 1974a, 1974b; Hatcher, 1972, 1978a, 1987, 1989; Lemmon, 1973, 1982; Lemmon and Dunn, 1975; Roper and Dunn, 1973; Nelson and others, 1987; Hopson and Hatcher, 1988; and Horton and McConnell, 1990).

The geology of the Columbus Promontory is characterized by the presence of three distinct ductile crystalline thrust sheets that include the Tumblebug Creek, Sugarloaf Mountain, and Mill Spring thrust sheets, each of which contain a distinct stratigraphy (Fig. 2, Plates I and II). Of these three, the Sugarloaf Mountain thrust sheet (SMT) is the only one that contains an appreciable

Figure 5–1. Distribution of Paleozoic metamorphic isograds in the southern Appalachian orogen. Study area is shown by black box. Modified after Butler (1990). k–kyanite; si–sillimanite; a–andalusite; st–staurolite; g–garnet; b–biotite; c–chlorite; u–unmetamorphosed; h–hypersthene; and r–retrograde.


VA
NC
TN
NC
SC
GA

amount of pelitic rock and allows the relationship between metamorphism, penetrative deformation, and thrust sheet emplacement to be investigated. Similar to the thrust sheets cited above, the Sugarloaf Mountain thrust sheet emplaced sillimanite and muscovite–bearing pelites over rocks of the westernmost Inner Piedmont (Chauga belt).

The focus of this chapter is on the petrogenetic development of this first–sillimanite zone assemblage and its relationship to the deformation and emplacement of the SMT. Metamorphic textures and mineral zoning indicate that sillimanite growth occurred as a result of continuous reactions. These continuous reactions include both garnet–consuming and garnet–producing reactions that operated following the metamorphic peak. These observations support the interpretation that the sillimanite–muscovite zone assemblage, in the pelites of the SMT, represents a post thermal–peak rather than a prograde metamorphic assemblage as interpreted for other thrust sheets in the western Piedmont. Microstructural analysis indicates that this first–sillimanite assemblage defines a pervasive S_2 mylonitic foliation, L_2 lineation, and associated shear–sense indicators in the pelites which are related to penetrative deformation and emplacement of the SMT. These relationships strongly suggest that penetrative deformation and emplacement of the SMT occurred synchronously with development of the observed metamorphic assemblage along the retrograde portion of the P–T path followed by these rocks.

GENERAL CHARACTERISTICS OF METAMORPHISM

Mineral Assemblage

Pelitic units represent a significant part of the stratigraphy of the SMT and occur within the Poor Mountain Formation and the upper part of the Mill Spring complex. Pelitic schist of the Poor Mountain Formation define a distinct mappable stratigraphic unit, whereas pelitic rocks of the upper Mill Spring complex occur throughout the thick sequence of biotite gneiss–metagraywacke that

crops out over a significant part of the study area (Fig. 1–2, Plates I and II). Pelitic rocks in both the Poor Mountain Formation and the upper Mill Spring complex, invariably contain a metamorphic assemblage consisting of the mineral phases

$$gar + bio + mus + si + plag\ (An_{13-38}) + qtz \pm il \qquad (A_1)$$

This assemblage is characteristic of the first–sillimanite zone of regional metamorphism (Winkler, 1978; Yardley, 1989) and is present in thrust sheets throughout much of the southern Appalachian Inner Piedmont (Conley and Henika, 1973; Nelson and others, 1987; Goldsmith and others, 1988; Hopson and Hatcher, 1988; Butler, 1990). A significant part of this chapter is devoted to the petrogenetic development of this assemblage in the SMT and will be discussed in greater detail below.

Metamorphic Zones and Isograds

Detailed field and petrologic data obtained during this study indicate that this first–sillimanite zone assemblage remains constant across the SMT, consequently no other isograds have been mapped. Hadley and Nelson (1971) broadly included the Columbus Promontory area within the sillimanite zone and placed the sillimanite isograd at the boundary between the Henderson Gneiss and paragneiss and schist of the Inner Piedmont, coincident with the westernmost boundary of the SMT. Lemmon (1973) also placed the sillimanite isograd at the contact between the SMT and the Henderson Gneiss. These interpretations are shown on the recent isograd map of Butler (1990) (Fig. 5–1). Field and petrographic observations from the present study indicate that the position of the sillimanite isograd along this boundary is a function of rock type changes, pelites to granitoid, and does not represent a metamorphic break. Meso– and microstructural features (L_2 and S_2) in the SMT, which developed synchronous with mineral growth in assemblage A_1, can also be traced

across the thrust boundary into the Henderson Gneiss where they are defined by biotite, K–feldspar, quartz, and occasional muscovite.

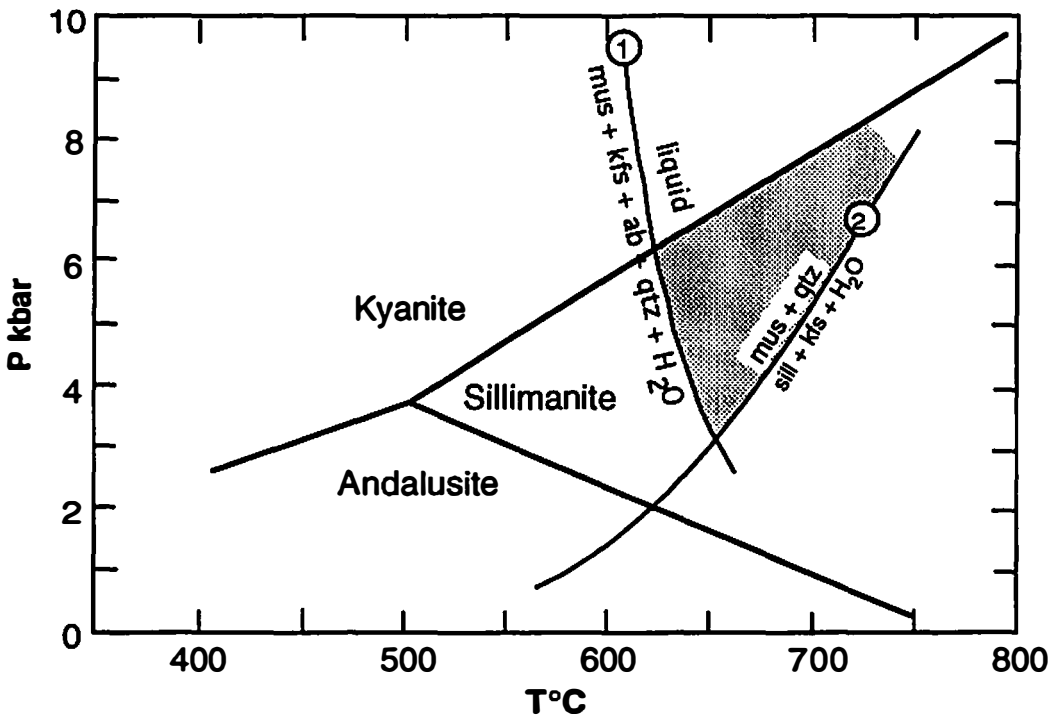
The areal extent of the sillimanite–muscovite zone across the area is consistent with the nature of regional metamorphism recognized throughout the western Inner Piedmont. Butler (1990) noted that isogradic surfaces in the central Inner Piedmont of the Carolinas must be nearly horizontal, because over and area of more than 60 kilometers the metamorphic grade is constantly first sillimanite zone (sillimanite–muscovite) and does not increase to second sillimanite zone (sillimanite + K–feldspar) or drop to kyanite grade. In Chapter IV, it was noted that in the Columbus Promontory, stratigraphic contacts (transposed), foliation, and thrust surfaces are subhorizontal and parallel. The persistence of the sillimanite–muscovite assemblage across the Sugarloaf Mountain thrust sheet, suggests that isotherms also maintain a similar subhorizontal orientation, consistent with the interpretation of Butler (1990) for other areas in the Inner Piedmont.

Metamorphic Conditions

The general metamorphic conditions attained by pelites of the SMT are constrained by several field and petrographic observations (Fig. 5–2). In all hand samples and thin–sections examined,sillimanite is the only aluminum silicate polymorph observed in the Poor Mountain Formation and upper Mill Spring complex pelitic rocks. Although recognized in many thrust sheets elsewhere in the western Piedmont, no kyanite was observed in any of the thin sections examined or during field mapping, thus qualitatively restricting the P–T conditions to occur below the kyanite–sillimanite boundary (Fig. 5–2). Although a few samples examined contained minor amonts of K–feldspar (Table 2–3), reaction textures indicative of second–sillimanite zone metamorphic conditions, generally characterized by the reaction

$$mus + qtz = Kfs + si + H_2O \qquad (1)$$

Figure 5–2. P–T grid showing inferred maximum metamorphic conditions for SMT pelites. P–T conditions shown in shaded area is based on field observations and petrographic analysis. Reaction (1) after Thompson and Algor (1978); Reaction (2) after Chatterjee and Johannsen (1974). Al_2SiO_5 triple point after Holdaway (1971).


10
8
6
4
2
0
P kbar
400
500
600
700
800
T°C
Kyanite
Sillimanite
Andalusite
mus + kfs + ab + qtz + H2O
pinhil
mus + qtz
sill + ks + H2O
1
2

of (Chatterjee and Johannes, 1974), were not observed. This suggests that peak metamorphic conditions occurred on the lower P–T side of this reaction (Fig. 5–2). Finally, in many areas within the Sugarloaf Mountain thrust sheet, rocks of the upper Mill Spring complex are migmatitic suggesting metamorphic conditions were, at least locally, higher than the minimum granite melting curve. Migmatitic textures are much more commonly observed in the interlayered biotite gneiss–metagraywacke and schist of the upper Mill Spring complex than in the Poor Mountain Formation. This suggests that, at least locally, the minimum melting reaction for pelitic rocks (Thompson and Algor, 1977)

$$mus + Kfs + ab + qtz + H_2O = liquid \qquad (2)$$

may have been operative. These observations qualitatively suggest metamorphic conditions for these pelites are within the sillimanite stability field with near peak conditions possibly within the shaded area shown in Figure 5–2.

MICROSTRUCTURE DEFINED BY ASSEMBLAGE A_1

Composite–Planar Fabric

The dominant microstructure present in pelites in the SMT is a pervasive S_2 mylonitic foliation. In Chapter IV, it was noted that S_2 is mesoscopically composite. S_2 is also composite on the microscopic scale, and can be subdivided into three component parts, designated S_{2c}, S_{2s}, and S_{2e}, based on their geometric and kinematic significance . These S_2 foliation components are defined by parallel orientation of the minerals of assemblage A_1 which impart an anastomosing microscopic texture to the pelites. Associated with the S_2 foliation components is a well-developed mineral lineation (L_2) also defined by biotite, muscovite, quartz ribbons, and fibrolitic sillimanite of

assemblage (A_1).

The S_2 foliation components outline a series of microscopic–scale shear zones within the pelites (Figs 5–3, 5–4). S_{2c} is the best developed foliation component in the pelites and defines the shear zone boundaries. S_{2c} parallels the direction of shear and is analogous to C–surfaces of Berthe' and others (1979). S_{2c} is defined by quartz ribbons, muscovite, biotite, fibrolitic sillimanite, and elongate garnets (Figs. 5–3 and 5–4).

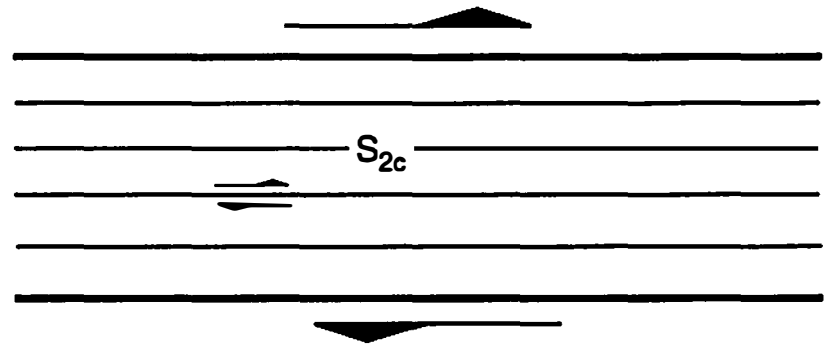
S_{2s} dips at angles between approximately 10° and 45° from S_{2c} in a direction opposite to the overall direction of shear. S_{2s} is most commonly defined by sigmoidal–shaped mica (buttons) or mica fish of Lister and Snoke (1984), fibrolitic sillimanite, asymmetric garnets, and quartz pods (Figs. 5–3 and 5–4). S_{2s} is interpreted to represent a component of pure shear or flattening across the microscopic scale shear zones formed similar to that defined by Lister and Snoke (1984). The combination of S_{2c} and S_{2s} define an S–C fabric (Berthe' and others, 1979; Simpson and Schmid, 1983; Lister and Snoke, 1984) in the pelites of the SMT (Figs. 5–3 and 5–4).

S_{2e} also dips at angles between approximately 10° and 45° from S_{2c}, but in the direction of overall shear (Figs. 5–3 and 5–4). S_{2e} disrupts S_{2c} and defines a set of extensional shear surfaces in the pelites. S_{2e} is analogous to C' surfaces of Berthe' and others (1979), extensional crenulation cleavage (Platt and Vissers, 1980), shear bands (White and others (1980 and Dell' Angelo and Tullis (1989) and normal–slip crenulations (Dennis and Secor, 1988). S_{2e} is defined primarily by parallel alignment of biotite and muscovite and also fibrolitic sillimanite and quartz ribbons.

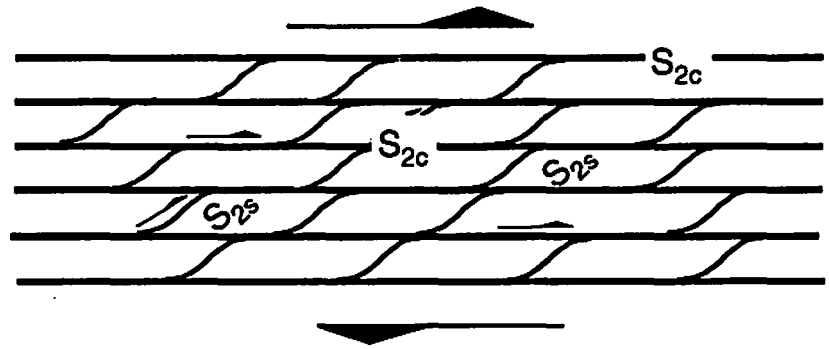
Geometric and kinematic relationships indicate that S_2 represents a composite foliation produced primarily by progressive simple shear, with both simple shear and flattening (pure shear) components. Thus it is suggested that the microstructure of Poor Mountain and Mill Spring complex pelites are analogous to the Type II S–C mylonites of Lister and Snoke (1984). The S_2 foliation components, L_2, and the larger–scale structural features discussed in Chapter IV, record two coeval directions of displacement (W–NW and SW) within the SMT and other thrust sheets in the Columbus Promontory and western Inner Piedmont. The fact that S_2 foliation components and

Figure 5–3. Schematic representation of the geometric and kinematic relationships between S_2 foliation components: a) S_{2c}; b) S_{2s}, and; c) S_{2e}.

A)



B)



C)

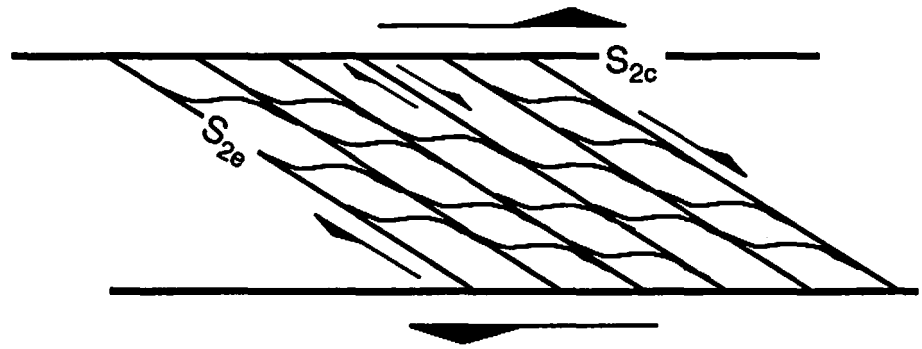
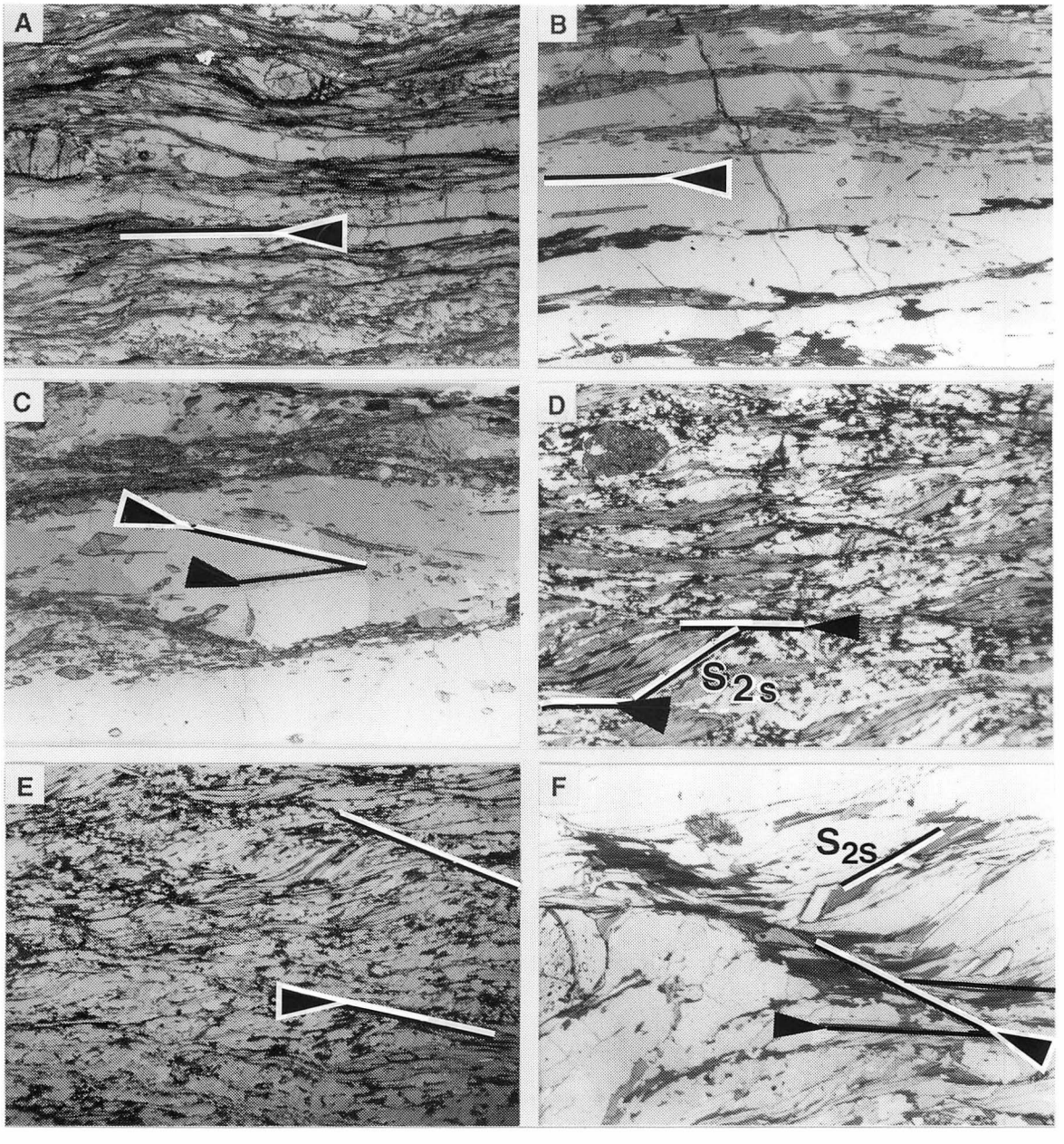


Figure 5–4. Photomicrographs of S_2 foliation components. A and B) S_{2c} component defined by quartz ribbons (arrow and line); C) S_{2c} defined by quartz ribbons and fibrolitic sillimanite (white outlined arrow and line). S_{2s} defined by fibrolitic sillimanite (black arrow and line); D) S_{2s} mica–fish defined by biotite and muscovite (labled) and S_{2c} (black arrow and line) ; E) S_{2e} component defined primarily by biotite and muscovite (arrow and lines); F) All three foliation components, S_{2c} (black arrrows and line); S_{2s} (labled); S_{2e} (white arrow and line). Field of view for A, B, C, D, and is 4mm; E is 12 mm.


A
B
C
D
S_{2s}
E
F
S_{2s}

L_2 are defined by the A_1 mineral assemblage indicates that mineral growth was nearly synkinematic with deformation that produced these microstructural features.

Garnet Porphyroblasts

Garnet porphyroblasts represent another kinematically important microstructure in the pelitic rocks of the SMT. Garnets are morphologically very diverse (Fig. 5–5), with the diversity related to intense shearing of these rocks. Variations in garnet morphology include elongated garnets parallel to S_{2c}, asymmetric garnets whose boundaries help define S_{2c} and S_{2s}, and garnets stacked in an en echelon pattern that help define the S_{2s} fabric (Fig. 5–5). Many garnet porphyroblasts have tails (Fig. 5–5), streaming in the direction of shear, defined by muscovite, biotite, fibrolitic sillimanite, and quartz ribbons.

PETROGRAPHY AND CHEMISTRY OF MINERAL PHASES IN ASSEMBLAGE A_1

Sampling and Analytical Techniques

During the course of detailed field study, 50 samples of pelitic rocks of the Poor Mountain Formation and the Mill Spring complex were selected for detailed petrologic, chemical, and microstructural analysis. From this suite, 7 pelitic samples from across the SMT were selected for detailed electron microprobe analysis. The locations of samples analyzed are shown in Figure 5–6. The mineral phases garnet, biotite, muscovite, and plagioclase were analyzed in polished thin sections for mineral composition and intragranular and intergranular compositional variations. A minimum of two grains for each phase were analyzed. Mineral compositions were measured on the four spectrometer Cameca SX50 electron microprobe at The University of Tennessee. Analyses

Figure 5-5. Photomicrographs showing the morphology, optical zoning patterns, and shear textures of garnets. A and C) examples of well–defined optical zoning in garnets. Inclusions in core and intermediate locations consists of very fine, biotite, and ilmenite. B). Elongated garnet parallel to the S_{2c} foliation component. D) Porphyroblast with internal foliation defined primarily by ilmenite. Shear sense is top–to–SW (right) consistent with that defined by other matrix minerals. E and F) Sheared garnets. Sense of shear is top–to–W (right) consistent with the S_2 composite–planar fabric. Field of view for A, B, D, E, and F is 4mm; C is 1.5 mm.

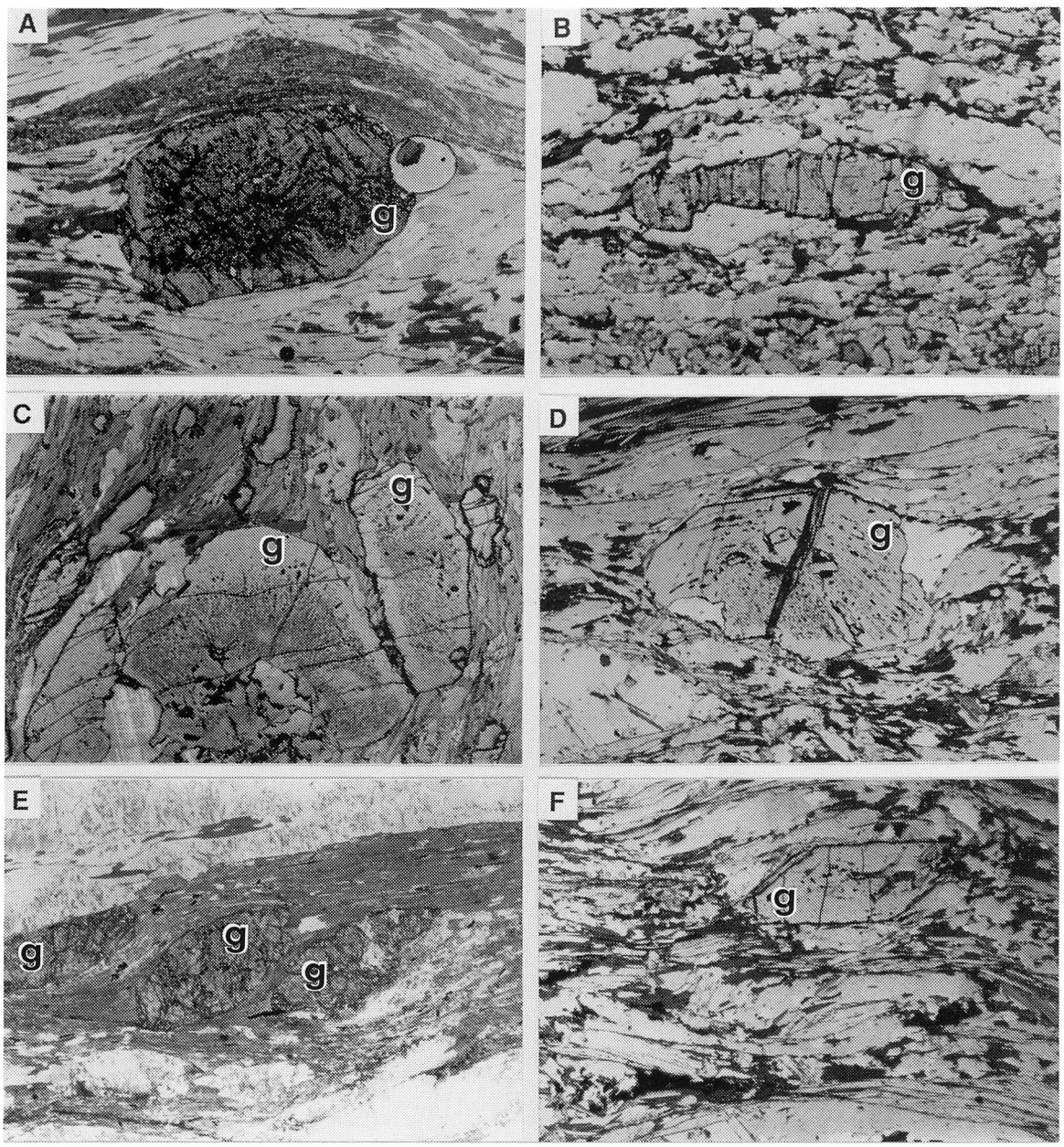
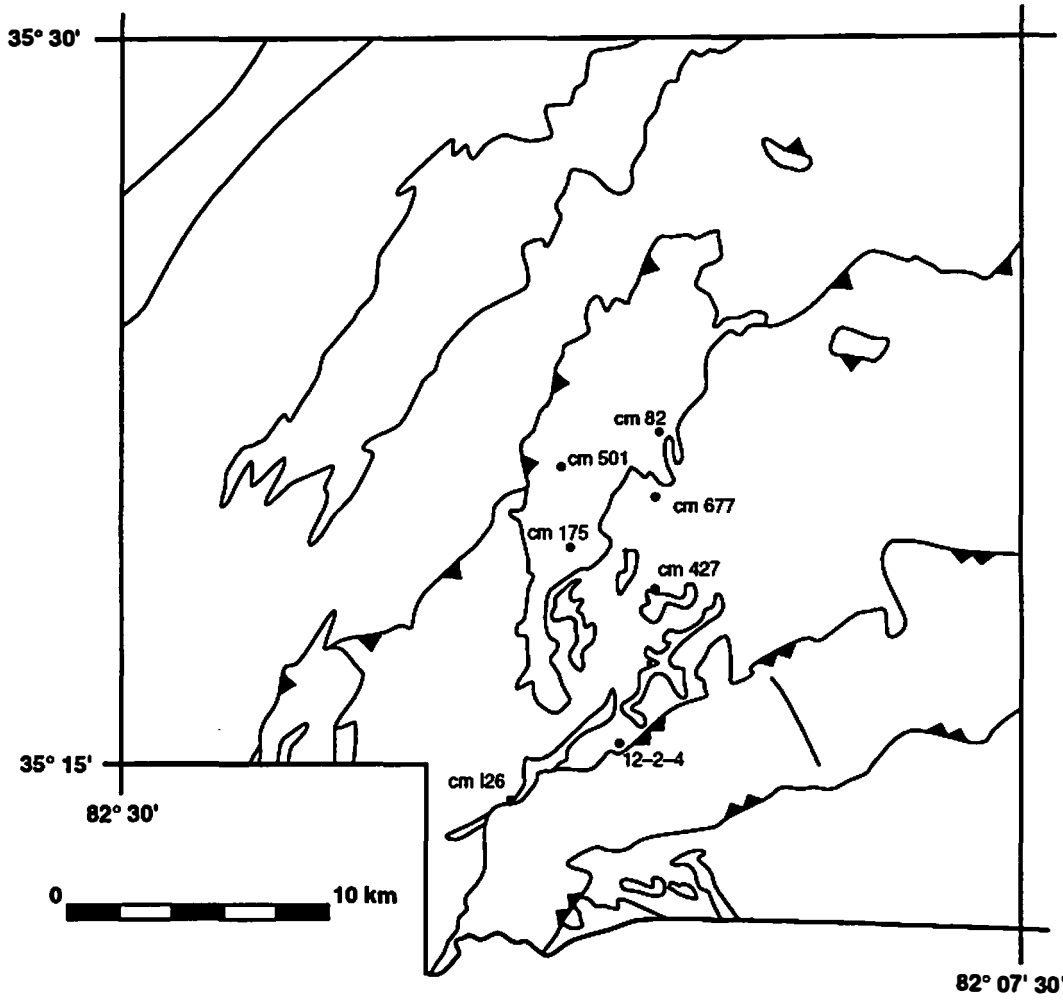

A
g
B
g
C
g
g
D
g
E
g
g
g
F
g

Figure 5–6. Location of pelitic schist samples analyzed by electron microprobe techniques.


35° 30'
cm 82
cm 501
cm 677
cm 175
cm 427
12-2-4
35° 15'
cm 126
82° 30'
0
10 km
82° 07' 30"

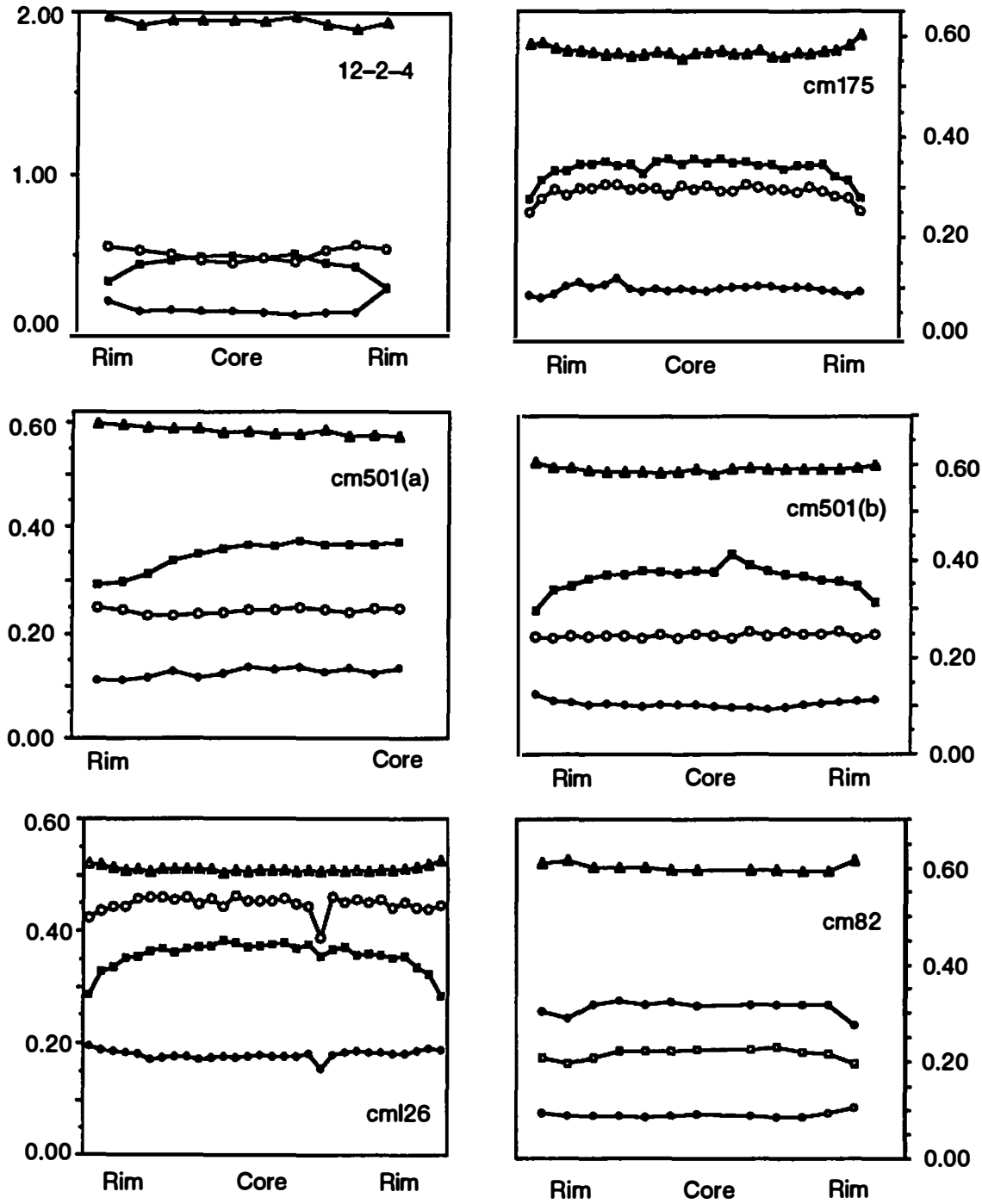
were performed using natural and synthetic standards, ZAF corrections, and an operating voltage of 15 KeV. For individual phases operating conditions were: for garnet, a beam current of 30 nA, and beam size of 5mm; for biotite, muscovite, and plagioclase, a beam current of 20 nA, and a defocused beam size of 10 mm. Microprobe data for the silicate phases were normalized following the recommendations of Papike (1987, 1988). A complete listing of mineral analyses is contained in Appendix B.

Mineral Phases

Garnet. Garnet occurs as subidioblastic to idioblastic porphyroblasts ranging in size from 0.1 mm to 5 mm in diameter. Garnet porphyroblasts tend to have well–developed crystal faces, except where embayed by mats of fibrolitic sillimanite and quartz. Where adjacent to biotite and muscovite, the interfaces are generally sharp (Fig. 5–5). Garnet porphyroblasts possess several morphologies (Fig. 5–5) and, as previously noted, are commonly aligned or elongated within the S_2 foliation. Many garnet porphyroblasts have poikilitic cores and inclusion–free rims (Fig. 5–5). Inclusions within garnet are dominantly quartz and ilmenite, with minor plagioclase and biotite. The composition and zoning profiles of the garnet analyzed are discussed in greater detail below.

Garnet Zoning. Garnet zoning was analyzed in five samples across the study area, producing profiles for almandine, pyrope, spessartine, and grossular components (Fig. 5–7). In general, for all porphyroblasts examined, cores have flat profiles for all components, whereas rims display strong compositional zoning for all components. Rim zoning profiles are generally symmetrical, although there are exceptions. In all garnet porphyroblasts analyzed, core–to–rim traverses display increases in almandine and Fe/(Fe + Mg) values, and decreases in the pyrope component (Fig. 5–7). Spessartine and grossular contents, although generally dilute (X_{Mn} 0.018 to 0.074 and X_{Ca} 0.027 to 0.187, respectively), show varying zoning patterns at the garnet rim. Sample cm175

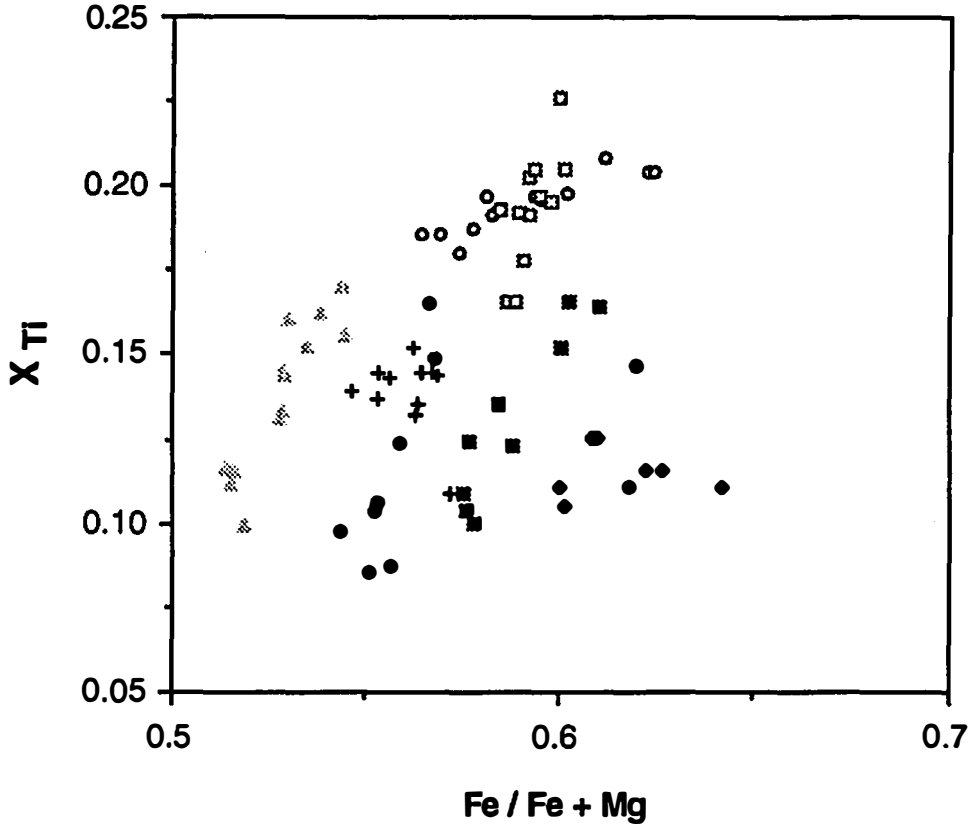
Figure 5–7. Compositional zoning profiles from garnets in pelitic schist of the Sugarloaf Mountain thrust sheet. Patterns are interpreted to be result of intracrystalline diffusion during garnet consumption. Note that all samples show core to rim increase in almandine content and decreases in pyrope content from core to rim. Also note the slight increases in grossular content near the rims in samples cm501, 12–2-4, cml26, and cm 82 suggesting late–stage garnet growth. Filled triangles–almandine; open circles–magnesium; filled squares–manganese; filled circles–grossular. See text for more detailed discussion of the zoning patterns.


2.00
1.00
0.00
12-2-4
Rim
Core
Rim
0.60
0.40
0.20
0.00
cm175
Rim
Core
Rim
0.60
0.40
0.20
0.00
cm501(a)
Rim
Core
0.60
0.40
0.20
0.00
cm501(b)
Rim
Core
Rim
0.60
0.40
0.20
0.00
cml26
Rim
Core
Rim
0.60
0.40
0.20
0.00
cm82
Rim
Core
Rim

(~1 mm in diameter) displays a spessartine profile that is relatively flat in the core and decreases at the rim. Similarly, the grossular profile is relatively flat in the core and intermediate locations, with some undulations, but displays a decrease at the rim. In sample cm501, core–to–rim traverses were done on two garnet porphyroblasts. Traverse cm501a (~1.3 mm in diameter), displays a spessartine profile that is flat in the core, decreases slightly at intermediate locations, then increases at the rim. The grossular profile in this porphyroblast is also relatively flat in the core, but shows a slight decrease at the garnet rim. Traverse cm501b (~0.7 mm in diameter) has a flat (~1.3 mm in diameter), the spessartine profile is relatively flat in the core, increases at intermediate locations, then decreases at the garnet rim. Similarly, the grossular profile is relatively flat in the core, but also increases sharply at the garnet rim. Porphyroblast cml26a (~0.6 mm) displays an asymmetric spessartine profile that is flat in the core, decreasing at one rim, and increasing at the other rim. The grossular profile is symmetric with a flat profile in the core and an increase at the rim. Sample cm82 (~0.5 mm) also shows an asymmetric zoning profile. The grossular profile shows an increase from the core to rim on both ends of the traverse. Spessartine displays an increase on one rim relative to the core, and a decrease at the rim relative to the core at the other rim along the traverse.

Biotite. Biotite, along with muscovite, is the predominant matrix phase that defines the pervasive S_2 foliation in the Poor Mountain Formation and upper Mill Spring complex pelites (Fig. 5–4). Biotite occurs as idioblastic, dark brown to red brown pleochroic crystals. The size of the biotite idioblasts ranges from ± 1 cm to very fine (< 0.2mm). Biotite composition for the entire sample suite exhibits a restricted compositional range (Fig. 5–8; Appendix B). For all grains analyzed, Fe/(Fe + Mg) values range from 0.5 to 0.65, and Ti contents (per 11 oxygens) range from 0.07 to 0.23 mole percent (Fig. 5–8). Individual samples show a much more restricted range of Fe/(Fe + Mg) values and Ti contents, and indicate there is no significant compositional zoning present in the biotite grains analyzed (Fig. 5–8; Appendix B).

Figure 5–8. X_{Ti} versus Fe/Fe + Mg in biotite analyzed for pelitic schists. Plot shows the restricted compositional range of biotite compositions in the pelitic schists of the Sugarloaf Mountain thrust sheet. Open squares–cml26; open circles–cm501; triangles–cm175; crosses–cm427; filled squares– cm677; diamonds– 3–16–15.


0.25
0.20
0.15
0.10
0.05
X Ti
0.5
0.6
0.7
Fe / Fe + Mg

Plagioclase. Plagioclase occurs primarily as xenoblastic crystals varying in size up to 0.5 mm in diameter. Plagioclase occurs most commonly as a matrix phase and rarely as inclusions in garnet. Microprobe analyses indicate that plagioclase in the Poor Mountain and Mill Spring complex is primarily composed of anorthite and albite components (Appendix B), but with a minor orthoclase component. Albite and anorthite contents vary, with anorthite contents for the entire suite ranging from An_{13} to An_{38}. Individual samples exhibit changes in An content from rim to core between 0.01 to 0.06 mole percent, and show general trends of decreasing An content from core to rim (Fig. 5–9).

Muscovite. Muscovite occurs in three distinct habits in the pelitic samples. The most dominant habit is subidioblastic laths (~ 2 mm) or asymmetric mica fish that helps define the S_2 foliation and shear textures within the samples (Figs. 5–3 and 5–4). This mode is commonly intergrown with or contains inclusions of fibrolitic sillimanite (Fig. 5–10). The second most dominant habit is fine–grained flakes replacing fibrolitic sillimanite and plagioclase grains. The third mode is less common and occurs as large (~5 mm) idioblasts that are truncated by the S_2 foliation and commonly replaced by sillimanite and quartz (Fig. 5–10). The composition of the dominant mode of muscovite is very restricted (Appendix B), with large K contents (~0.9 mole percent), low values of Na (< 0.1 mole percent), and no Ca component (Table 5–1 and Appendix B).

Sillimanite. The majority of sillimanite growth appears to have nucleated at the expense of other phases within the pelites (Figs 5–5, 5–10 and 5–11). Sillimanite occurs in two distinct habits. The first habit, present in only a few samples (e.g., cml26a and 12–2–4), occurs as well–developed prismatic crystals. In cross section, prisms are as large as 0.2 mm in diameter, whereas in the long dimension grains are up to ~ 0.7 mm. The second habit, much more commonly observed in thin section, occurs as acicular fibrolitic needles. Fibrolitic sillimanite most commonly occurs intertwined with matrix biotite and helps define the S_2 foliation (Figs. 5–5, 5–10 and 5–11). Fibrolitic sillimanite also occurs in reaction rims around garnet porphyroblasts and muscovite idioblasts, and as an

Figure 5–9. Plot of plagioclase compositions. Values enclosed in square represent highest An contents from plagioclase cores, those in circles the lowest An values from plagioclase rims. Diagram shows the general trend of decreasing An content from core to rim in plagioclase grains analyzed. Scatter of points off the trend of the line reflect the orthoclase component in the samples.

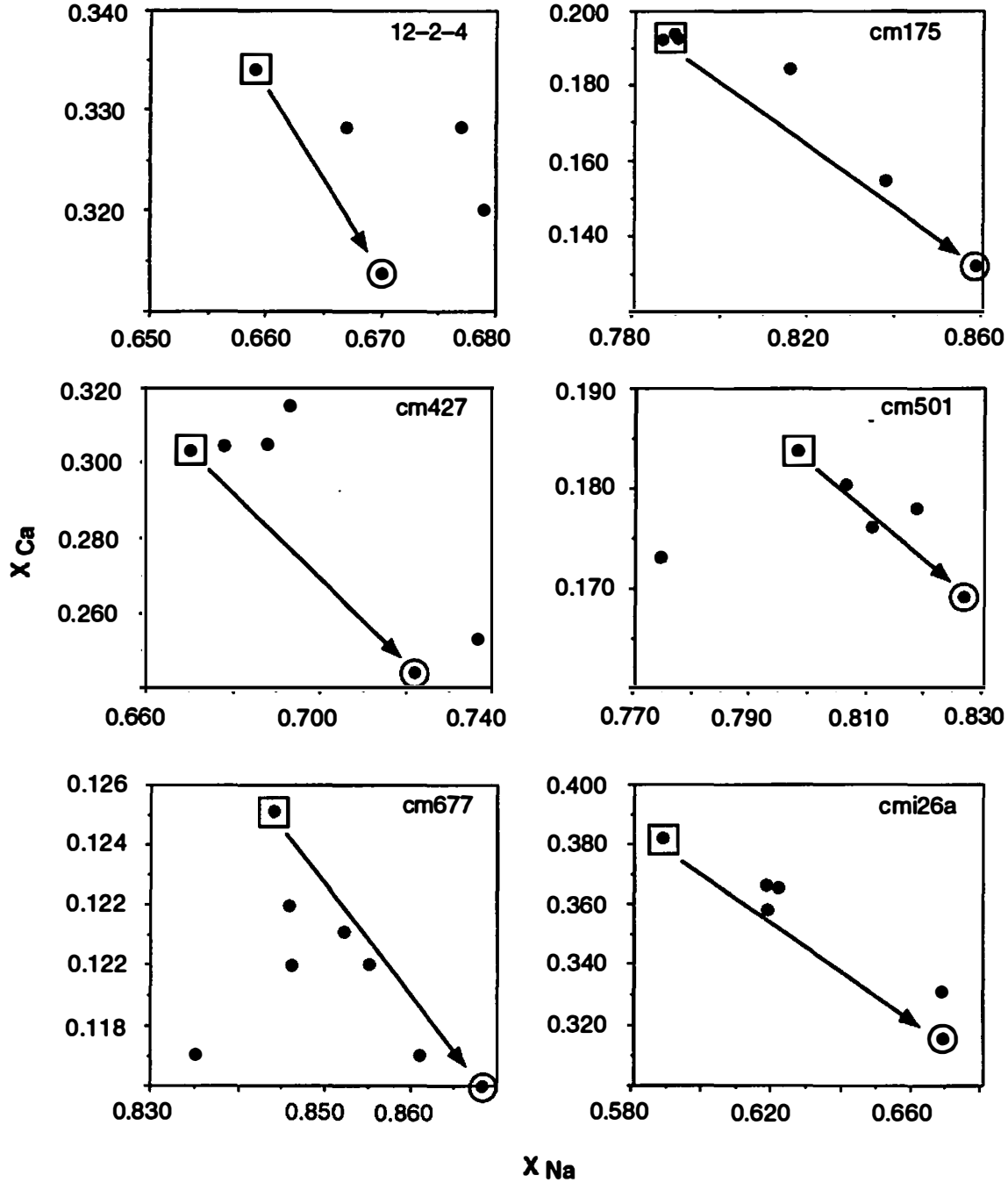

12-2-4
cm175
cm427
cm501
cm677
cmi26a
X Ca
X Na
0.340
0.330
0.320
0.650
0.660
0.670
0.680
0.200
0.180
0.160
0.140
0.780
0.820
0.860
0.320
0.300
0.280
0.260
0.660
0.700
0.740
0.190
0.180
0.170
0.770
0.790
0.810
0.830
0.126
0.124
0.122
0.122
0.118
0.830
0.850
0.860
0.400
0.380
0.360
0.340
0.320
0.580
0.620
0.660

Figure 5–10. Photomicrographs of textural relationships between sillimanite and muscovite. A and B) muscovite (M) idioblasts truncated and replaced by fibrolitic sillimanite and biotite (S&B) that defines S_{2C} foliation component. C) Muscovite idioblast (M) with abundant fibrolitic sillimanite (S) inclusions; D) Close–up of muscovite (M) idioblast in C. In both D and C note the small fold that is defined by fibrolitic sillimanite (S) within the muscovite idioblasts. Field of view for A, B is 4mm; C is 12 mm; D is 1.5 mm.

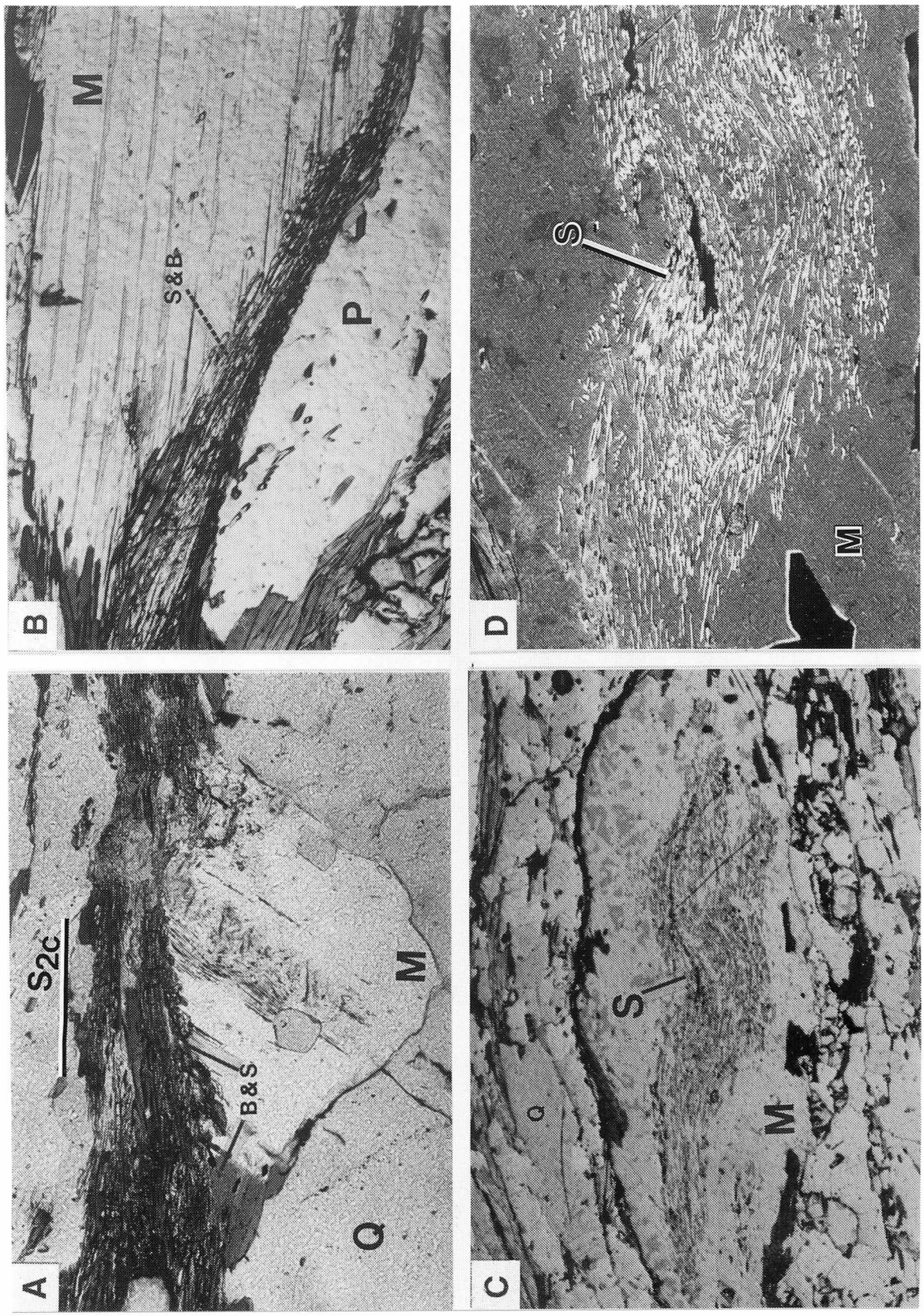
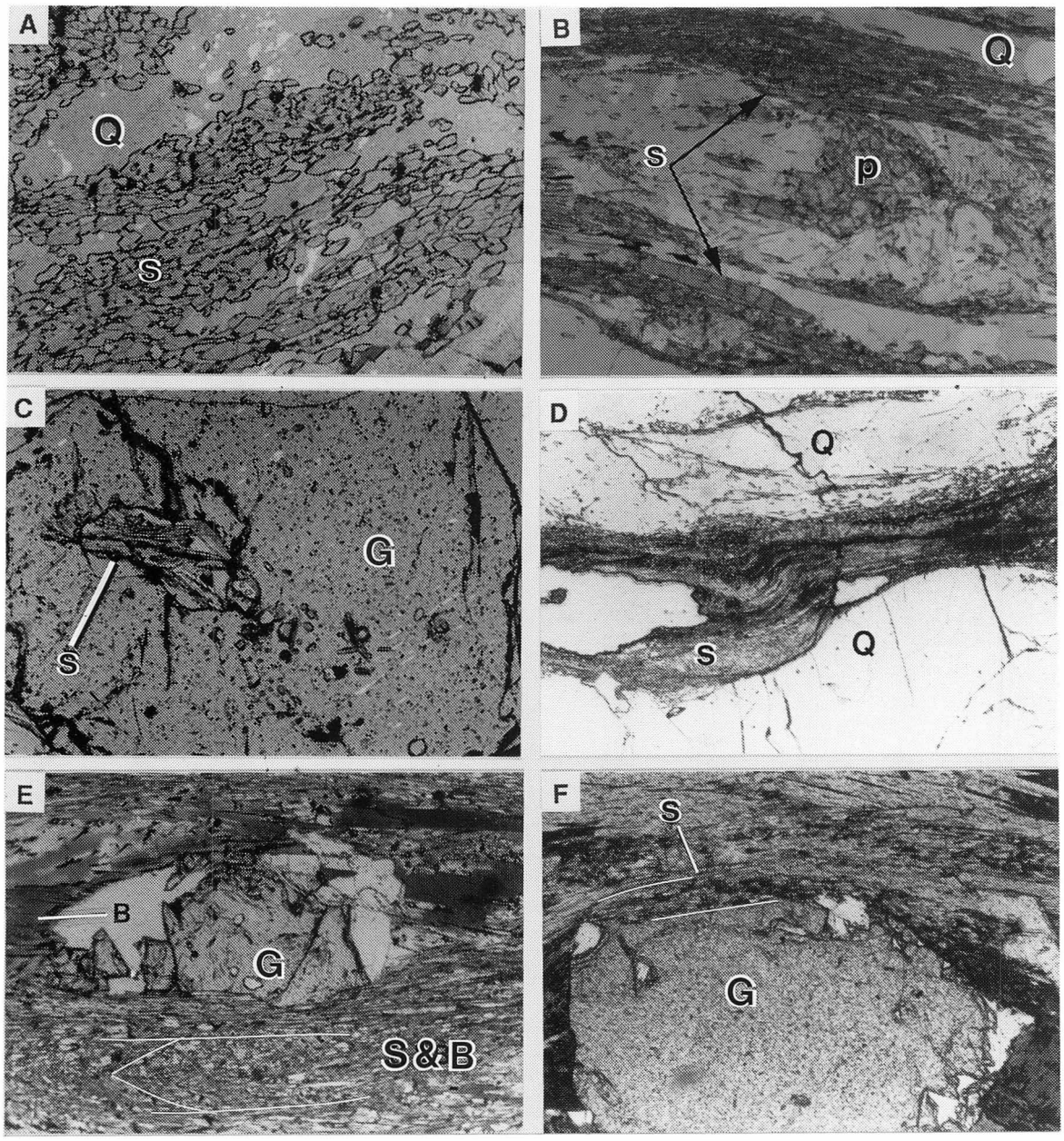

A
S2c
B&S
Q
M
B
M
S&B
P
C
S
Q
M
D
S1
M

Figure 5–11. Photomicrographs showing sillimanite morphology and textural relationship between fibrolitic sillimanite and garnet porphyroblasts. A) prismatic sillimanite (S) in sample cml26. Sillimanite defines S_2 foliation. Q –quartz . B) Fibrolitic sillimanite (S) defining S_2 foliation in sample 12–2–4. C) Fibrolitic sillimanite inclusion (S) in garnet (G) from sample cm 501. D) Microscale fold defined by fibrolitic sillimanite (S) in sample 12–2–4. Q–quartz; E) Garnet (G) truncated by fibrolitic sillimanite and biotite (S & B) that define S_2 foliation in sample 12–2–4. Also note the microscale shear zone defined by fibrolitic sillimanite at the bottom of the photomicrograph. F) Garnet (G) rim showing replacement by fibrolitic sillimanite (S) in sample cm175. Field of view for A, B, C, D, E is 4mm; F is 1.5 mm.


A
Q
S
B
Q
S
P
C
G
S
D
Q
S
Q
E
B
G
S&B
F
S
G

inclusion phase within muscovite and garnet (Figs. 5–5, 5–10 and 5–11). Textural information suggest that sillimanite was preferentially nucleated in these phases and was not included during garnet or muscovite growth (Figs. 5–5, 5–10 and 5–11). Sillimanite was not analyzed for chemical composition.

Quartz. Pelitic rocks of the Poor Mountain Formation and Mill Spring complex are very quartz rich (± 50 percent). Quartz occurs as varying habits from very fine (<0.1 mm) to large (>5 mm) xenoblastic matrix grains, to ribbons that traverse entire thin sections and help define the S_2 foliation (Fig. 5–4). Quartz grains commonly contain subgrains and undulose extinction indicative of unrecovered strain, although samples with completely annealed grains are present. Quartz is the dominant inclusion phase within garnet porphyroblasts. Quartz also was not analyzed for chemical composition.

Ilmenite. Ilmenite is present as a very minor accessory phase in most pelitic samples. Ilmenite occurs as very small (< 0.1 mm) ellipsoidal shaped grains commonly observed within the matrix parallel to the S_2 foliation, and as an inclusions within garnet. In a few cases, ilmenite defines an internal foliation within garnet porphyroblasts (Fig. 5–5). This phase was only analyzed by energy dispersive techniques for identification purposes in the samples.

PETROGENESIS OF ASSEMBLAGE A_1

Reactions Relationships

In a general sense, assemblage A_1 can be portrayed on an AFM diagram that models reactions in the KFMASH system . Using the method of Thompson (1957) and rim compositions of the ferromagnesian silicates, garnet and biotite analyzed from several samples in

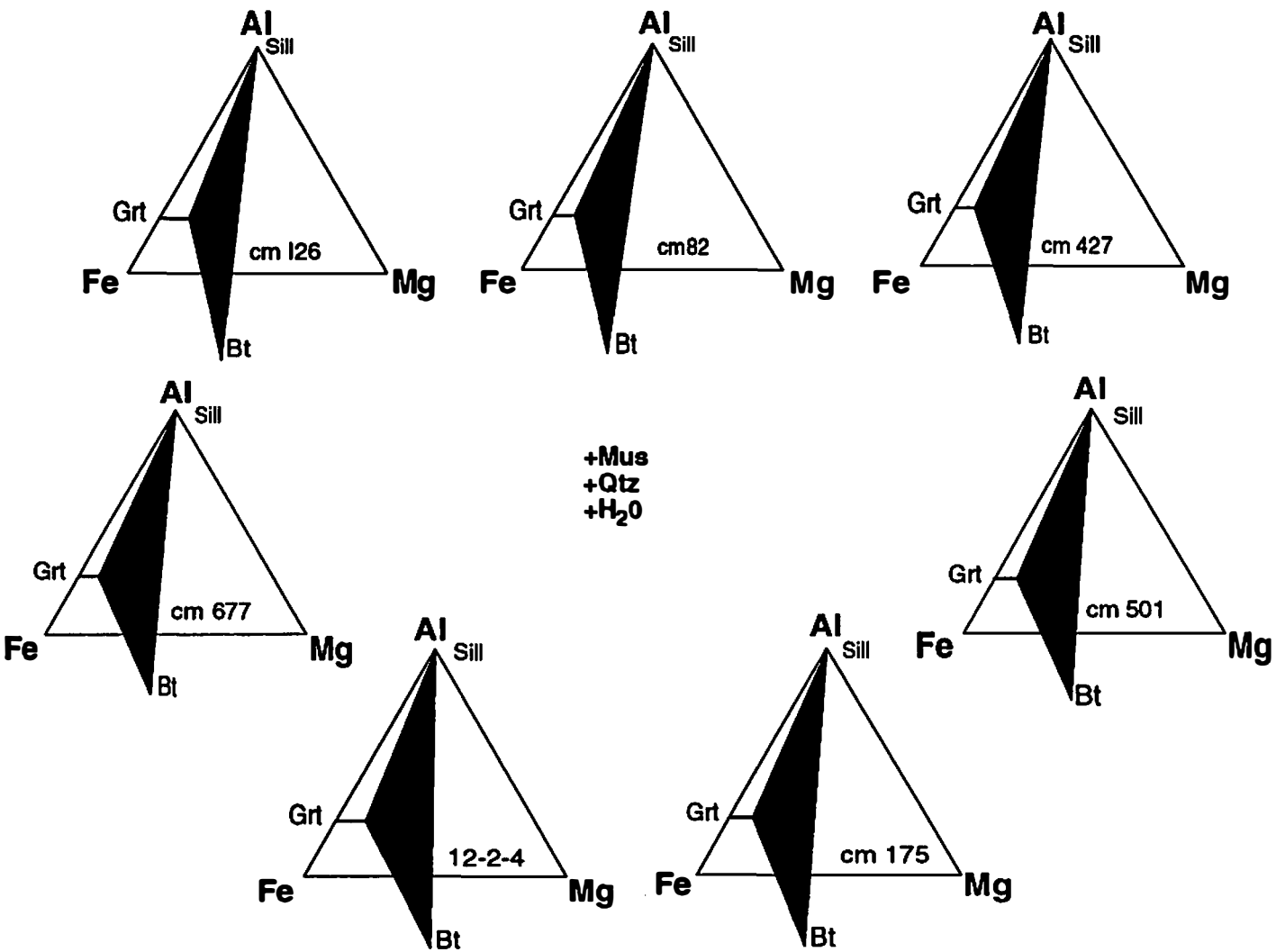
in this study, assemblage A_1 is projected onto the Al_2O_3–FeO–MgO (AFM) plane through the composition of end–member muscovite and quartz (Fig. 5–12). Abundant inclusions of quartz and ilmenite, together with sparse inclusions of biotite, plagioclase, and muscovite in garnet, and the presence of these same mineral phases in the matrix, indicate that these phases were present throughout garnet growth, and probably throughout a significant part of the metamorphic history of these pelites. Textural evidence (Figs. 5–5, 5–10, and 5–11) and mineral zoning (Figs. 5–7 and 5–9), discussed below, however, clearly shows that sillimanite growth and development of assemblage A_1 occurred as a result of continuous reactions that involved both the consumption of garnet and late–stage growth of garnet. This also resulted in additional growth of biotite, and quartz. No evidence for any discontinuous reactions were observed in any of the pelite samples examined and supported by the absence of crossing tie–lines on the AFM diagrams in Figure 5–12.

The determination of metamorphic reactions responsible for development of sillimanite in assemblage A_1 is based on textural criteria (Figs. 5–5, 5–10 and 5–11) and chemical zonation patterns present in plagioclase and garnet porphyroblasts (Figs 5–8 and 5–9). Pelitic schists containing garnets embayed by intergrown fibrolitic sillimanite, biotite and quartz, and replacement of muscovite, also by fibrolitic sillimanite, biotite, and quartz (Figs. 5–5, 5–10 and 5–11) provide strong textural evidence that the general garnet consuming reaction

$$gar + mus = 2\,si + bio + qtz \qquad (3)$$

was operative during the metamorphic development of these pelites. The compositional zoning observed in garnets analyzed in this study, and discussed previously, provide additional evidence that reaction (3) was operative in pelites of the SMT. The compositional zoning profiles in the garnets analyzed in this study are interpreted to be primarily the result of intracrystalline diffusion during garnet consumption. Blackburn (1969), Woodsworth (1977), Tracy (1982), and Spear (1989), have shown that intracrystalline diffusion may affect garnets (and other zoned minerals) in

Figure 5-12. AFM diagrams plotted using the method of Thompson (1957) and the rim compositions of garnet–biotite pairs. Note the narrow compositional range of garnet–biotite pairs suggesting possible reequilibration of the entire sample suite to similar garnet–biotite compositions during cooling.


Al
Sill
Grt
Fe
Mg
Bt
cm 126
cm82
cm 427
cm 677
cm 501
12-2-4
cm 175
+Mus
+Qtz
+H_2O

two ways. The first way is for intracrystalline diffusion to modify preexisting growth zoning in the garnet. This occurs in cases where temperatures are sufficiently high such that the growth profile relaxes with time, resulting in a compositionally homogeneous garnet crystal. The second way is for the equilibrium rim composition of the garnet to change in the absence of garnet growth or during garnet consumption. In this case, the rim is out of equilibrium with the interior resulting in a diffusion zoning profile at the garnet rim. The latter appears to be the case in most of the garnets analyzed in this study.

That the garnet rim zoning in this study is the result of intracrystalline diffusion during garnet consumption is supported by the textural criteria discussed above, and by observed zoning profiles in garnet. Since biotite and garnet are the only significant (+ rare ilmenite) ferromagnesian phases in the pelitic samples, all closed system garnet consuming reactions result in biotite formation. Furthermore, because biotite is lower in Mn and Fe/(Fe + Mg) than garnet, and $X_{Mg}^{bio} >> X_{Mg}^{gar}$, consumption of garnet results in the depletion of Mg at the garnet rim, and increases of Fe, Fe/(Fe + Mg), and Mn at the garnet rim (Hollister 1966, Tracy 1982; Helms, 1990). The presence of these compositional patterns in the garnets analyzed in this study are consistent with selective resorption of garnet as indicated by reaction 3.

The textural features (e.g., garnet embayed by sillimanite) and compositional zoning profiles at garnet rims (e.g., increasing almandine and Fe/Fe + Mg, decreasing pyrope) described above are consistent with garnet having reacted with the decreasing temperature from the peak metamorphic conditions. Reaction 3 has been observed in pelitic schist from several other orogenic belts and were recently discussed by Mohan and others (1989) from pelites in the Himalaya, Spear and others (1990) from pelites in the high–grade terrane of western New Hampshire, and by Helms (1990) from pelitic units in the Black Hills of South Dakota. In these studies, the garnet–consuming and sillimanite–producing reaction (reaction 3) is interpreted to be the result of continuous reactions during retrograde metamorphic conditions. Tracy (1982) discussed a similar garnet–consuming reaction from pelitic rocks of New England, but with K–feldspar and H_2O in place of muscovite.

Similarly, Tracy (1982) indicated that this reaction also occurs during the initial stages of cooling following the metamorphic peak. These relationships suggests that assemblage A_1 in the SMT also represents a retrograde metamorphic mineral assemblage.

Zoning patterns of garnets (e.g., 501, 12–2–4 in Fig. 5–7) showing increases in the grossular component and decreases in the spessartine component at the rim indicate a later stage period of garnet growth in the SMT pelites. A late stage of garnet growth is also supported by the euhedral shape of many of the porphyroblasts in the samples analyzed. Lemmon (1973) suggested two periods of garnet growth in the pelitic rocks from this study area based on the occurrence of garnet porphyroblasts with poikilitic cores and clear rims. Lemmon interpreted the first stage to be recorded by the included garnet cores and the second stage by the inclusion–free garnet rims. Similar optical patterns were also observed in the suite of rocks examined in this study (Fig. 5–5). In some cases (e.g., 501, 12–2–4 in Fig. 5–7), this increase in grossular appears to correspond to the demarcation between the poikilitic cores and clear rims of garnet porphyroblasts. The increase in the grossular component is interpreted to be concomitant with the general decrease in An from core to rim in plagioclase xenoblasts analyzed (Fig. 5–9). Because grossular and anorthite are the only Ca–bearing phases in the pelites, garnet growth must be accompanied by a anorthite consumption (Spear and Peacock, 1989; Spear and others 1990), consistent with the Ca variations in observed in several of the samples analyzed (Figs. 5–7 and 5–9). Such textural and compositional relationships suggest that some sillimanite growth in assemblage A_1 was related to a late stage of garnet growth involving the reaction

$$3\,an = gross + 2\,si + qtz \qquad (4)$$

This reaction also accounts for the presence of sillimanite, along with quartz and plagioclase, in the matrix of several pelite samples (e.g. cm l26a), which displays no textural relationship to garnet, biotite, and muscovite as suggested by reaction 3.

Lemmon (1973) argued that these optical zoning patterns observed in garnets were the result of two periods of prograde metamorphism. It is alternatively argued here, based on the synkinematic relationship between microstructural features and assemblage A_1, that this late–stage garnet growth also occurred during post–peak metamorphic conditions contemporaneously with reactions 3 and does not represent a second prograde metamorphic event. Furthermore, the pelites in the Sugarloaf Mountain thrust sheet contain no other evidence, either in the form of other mineral growth or overprinting microstructures, to suggest an additional prograde episode. In a few samples (e.g. cm 501 and cm 175, cml26a) there is evidence for both garnet consumption and growth reaction relationships. For example, in sample cml26a there is textural evidence for garnet consumption, whereas zoning trends in grossular and anorthite suggest garnet growth (Figs. 5–7 and 5–10). Spear (1989) and Spear and others (1990) discussed a similar pattern of concomitant garnet consumption (reaction 3) and garnet growth (reaction 4) from high–grade rocks in western New Hampshire and interpreted this to reflect changes in equilibrium conditions at the thin section scale. Spear (1989) and Spear and others (1990) also recognized this to be part of the post peak (retrograde) P–T path followed by these rocks. Based on the interpretation that the mineral assemblage and reaction relationships in the pelites of the SMT formed as part of the same metamorphic episode, a similar argument is made that the observed reaction relationships also record changes in equilibrium conditions at a similar scale of observation as those discussed by Spear (1989) and Spear and others (1990). Interpreting this late–stage garnet growth as the result of changes in equilibrium conditions during retrogression is a more simple explanation consistent with the majority of petrographic, chemical, and microstructural features observed in these rocks and does not require a second prograde metamorphic event. These observations further support an interpretation that development of assemblage A_1 is the result of a post thermal peak (retrograde) reaction history.

Geothermobarometry

The use of geothermobarometric techniques to determine absolute peak temperature–pressure conditions attained by the Poor Mountain Formation and upper Mill Spring complex pelites is problematic. Textural evidence and compositional zoning patterns in garnet suggest that phases in assemblage A_1 were involved in a series of continuous reactions following the peak of metamorphism, therefore it is unlikely that rim and matrix mineral compositions reflect peak metamorphic compositions. In addition it is difficult to assess what the mineral assemblage may have been during peak metamorphic conditions. The garnets in the samples analyzed may have grown in the presence of a variety of mineral assemblages (e.g., kyanite versus sillimanite), therefore it is uncertain what equilibrium relationships to use. Furthermore, garnets generally lack inclusion pairs (e.g., biotite, plagioclase, muscovite) that could possibly allow peak temperature–pressures to be estimated. Alternatively, textural criteria, and compositional data (garnet zoning) indicate that the pressure–temperature information, preserved in the Poor Mountain Formation and upper Mill Spring complex pelites, is related to the retrograde portion of the P–T path followed by these rocks. Therefore, this section of the paper is focused on estimation of absolute pressure–temperature conditions during the retrograde portion of the metamorphic history of these pelites.

Techniques. Based on the above observations, post peak temperature–pressure values were estimated using rim compositions of garnet and the compositions of matrix biotite, plagioclase, and muscovite (Table 5–1). Temperatures were estimated from the Fe–Mg exchange reaction between garnet and biotite based on the relationship

$$Mg_3Al_2Si_3O_{12} + KFe_3AlSi_3O_{10} =$$

$$Fe_3Al_2Si_3O_{12} + KMg_3AlSi_3O_{10}(OH)_2 \qquad (5)$$

Table 5–1. Mineral compositions and estimated temperature and pressures for pelitic schist of the Sugarloaf Mountain thrust sheet.

	cm 175	cm 501	cm l26	cm 677	cm 427	12–2–4
Garnet						
X_{Alm}	0.771	0.778	0.673	0.853	0.721	0.642
X_{Pyr}	0.105	0.104	0.119	0.100	0.084	0.110
X_{Sps}	0.094	0.080	0.150	0.026	0.142	0.179
X_{Gro}	0.030	0.039	0.060	0.020	0.052	0.069
Biotite						
X_{Ann}	0.567	0.563	0.601	0.576	0.595	0.514
XPhl	0.433	0.437	0.399	0.424	0.404	0.486
Plagioclase						
X_{An}	0.185	0.178	0.331	0.117	0.303	0.320
Muscovite						
X_K	0.798	0.850	0.838	0.759	0.854	0.902
X_{Na}	0.109	0.136	0.069	0.117	0.068	0.080
$X_{Al^{IV}}$	0.938	0.930	0.917	0.948	0.927	0.923
Temperature (°C)						
F & S (1978)	565	555	640	535	545	580
G & S (1984)	580	560	670	545	590	610
H & S (1982)	590	570	665	545	565	610
Pressure (kbs)						
GASP–N & H (1981)	4.1	4.9	5.5	4.0	4.0	5.2
GASP–H & S (1982)	3.8	4.5	5.2	3.5	4.0	5.1
GPMB–G & S (1981)	3.5	4.1	4.1	3.6	4.1	4.0
GPMB–H & C (1985)	4.5	5.0	7.2	4.2	4.2	5.2
GRAIL – Bohlen and others (1983)*	6.2	6.2	5.5	7.0	5.0	4.1

Representative mineral compositions; X_{Alm} = (Fe/Fe+Mg+Mn+Ca), X_{Pyr} = (Mg/Fe+Mg+Mn+Ca), X_{Sps} = (Mn/Fe+Mg+Mn+Ca), X_{Gros} = (Ca/Fe+Mg+Mn+Ca); X_{Ann} = (Fe/Fe+Mg) X_{Phl} = (Mg/Fe+Mg); X_{An} =Ca; X_K= K, X_{Na}=Na, $X_{Al^{IV}}$= Al^{IV}; all Fe is assumed Fe^{2+}; * Ilmenite assumed pure.

The experimental calibration of Ferry and Spear (1978) and the empirical calibrations of Hodges and Spear (1982) and Ganguly and Saxena (1984) were used to estimate temperatures. The refinement of Hodges and Spear (1982), based on the experimental data of Ferry and Spear (1978), corrects for non–ideal mixing of Ca in garnets. The Ganguly and Saxena (1984) model corrects for the effects of both Mn and Ca on Fe–Mg mixing in garnet. Both of these calibrations generally result in higher estimated temperatures than the Ferry and Spear calibration (Spear and Peacock, 1989).

Pressures were estimated using equilibrium relationships that involve net exchange reactions between the grossular component in garnet and the anorthite component in plagioclase. The techniques used include the garnet–plagioclase–sillimanite–quartz (GASP) barometer of Ghent and Stout (1981) which is based on the reaction

$$3CaAl_2Si_2O_8 = 2\,Al_2SiO_5 + Ca_3Al_2Si_3O_{12} + SiO_2 \qquad (6)$$

For this barometer, the calibrations of Newton and Haselton (1981) and Hodges and Spear (1982) were used. For comparative purposes, pressures were also estimated using the garnet–plagioclase–muscovite–biotite (GPMB) barometer which is based on the reaction

$$Fe_3Al_2Si_3O_{12} + Ca_3Al_2Si_3O_{12} + KAl_3Si_3O_{10}(OH)_2 =$$
$$3CaAl_2Si_2O_8 + KFe_3AlSi_3O_{10}(OH)_2 \qquad (7)$$

For this relationship the calibrations of Ghent and Stout (1981) and Hodges and Crowley (1985) were used. Reactions 8 and 9 are potentially powerful barometers because of the large volume changes that accompany the net exchange of Ca between garnet and plagioclase, with grossular being favored at higher pressure and anorthite at lower pressure. Furthermore, reactions based on this relationship between the Ca component in garnet and plagioclase are relatively insensitive to

temperature (Essene, 1989).

Although no rutile was observed in any of the pelite samples examined, the GRAIL barometer of Bohlen and others (1983) was used in an attempt to obtain an upper limit of pressures attained by pelites of the SMT. This barometer is based on the reaction

$$Fe_3Al_2Si_3O_{12} + 3TiO_2 = 3FeTiO_3 + Al_2SiO_5 + 2SiO_5 \quad (8)$$

In using this barometer, ilmenite composition was assumed to be pure because this phase was analyzed by EDS techniques during electron microprobe analysis.

Results. The results of geothermobarometric estimates suggest post peak temperatures in the range of 535 to 690 °C and pressures in the range of 3 to 6 kbs (Table 5–1). These P–T estimates fall within the sillimanite stability field, consistent with the observation of sillimanite being the only Al_2SiO_5 polymorph present in any of the samples analyzed. Synkinematic relationships observed in these samples suggests that these values record minimum P–T conditions for emplacement of the SMT.

For individual samples, temperatures estimated by the different calibrations of the Fe–Mg exchange display differences of less than 35°C. The Ferry and Spear (1978) calibration consistently yielded the lowest temperatures. Temperatures estimated using the Hodges and Spear (1982) and Ganguly and Saxena (1984) calibrations yielded temperatures generally between 20° to 30° C higher than the Ferry and Spear (1978) calibration.

The clustering of temperature values, (with the exception of sample cm l26) in the temperature range of 535–565° C (Table 5–1), suggests that these values may reflect terminal temperatures (closure) of the garnet–biotite exchange reaction. Spear and Peacock (1989) noted that rim analysis of garnet–biotite pairs, even from high–grade terranes where reequilibration occurs during cooling, commonly record temperatures in the range of 525–600°C and reflect termination

of the garnet–biotite exchange reaction. The possibility that these temperatures obtained here may reflect closure temperatures is also suggested by the limited compositional range of the garnet–biotite pairs shown in the AFM diagram in Figure 5–12.

The highest temperatures are recorded by sample cml26a, consistent with other petrologic and compositional evidence indicating that this sample may have attained the highest temperature of the sample suite. Sample cml26a contains the best–developed prismatic sillimanite. In a review of the Al_2SiO_5 polymorphs, Kerrick (1986), suggested that the presence of fibrolitic versus prismatic sillimanite in pelitic rocks may be a function of P–T conditions: prismatic sillimanite being favored at higher temperatures and pressures. Furthermore, biotite in cml26 contained the highest Ti contents (Fig. 5–8) of all samples analyzed. Studies by Guidotti (1984) and Spear and others (1990) have suggested that Ti content in minerals such as biotite and amphibole increases with increasing metamorphic grade. Sample cml26a was collected from a locality immediately adjacent to the contact between the Sugarloaf Mountain thrust sheet and the overlying Mill Spring thrust sheet (Figs 1–2; Plates I and III). Therefore the consistently higher pressure–temperature values for this sample may reflect a response to the emplacement of the Mill Spring thrust sheet.

Pressures calculated using the GASP barometer indicate values for the entire sample suite ranging from 3 to 5 kbs (Table 5–1). Pressures estimated using the calibration of Newton and Haselton (1981) are generally 0.5 to 1 kb higher than those calculated using the calibrations of Hodges and Spear (1982). Pressures estimated by the empirically derived GPMB barometer using the calibrations of Ghent and Stout (1981) and Hodges and Crowley (1985) yielded values generally consistent with pressures determined by GASP. Values determined by the Ghent and Stout (1981) calibration range from 3 to 4 kbs, those using the Hodges and Crowley (1985) are about a kilobar higher ranging from 4 to 5 kbs. As with the temperature values, sample cml26a recorded the highest pressure values, again interpreted to reflect a response to the overlying Mill Spring thrust sheet.

Results obtained using the GRAIL barometer of Bohlen and others (1983) indicate an

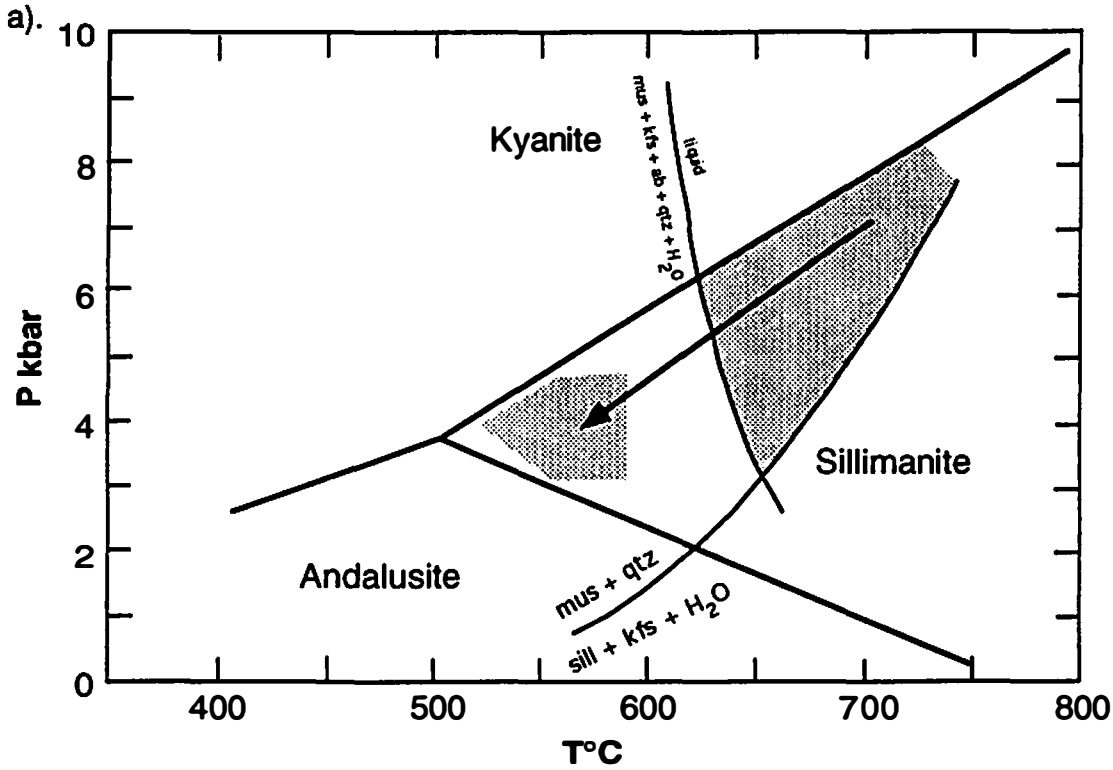
upper pressure limit of approximately 5.5 to 6 kbs for the pelite samples analyzed. Estimated pressure values for samples cm427, cml26a, and cm12–2–4 are 5.0, 5.5, and 4.1 kbs respectively. These values fall within the sillimanite stability field. Alternatively, samples cm175, cm 501, and cm677 recorded pressures of 6.2, 6.2, and 7 kbs which were out of the sillimanite stability field.

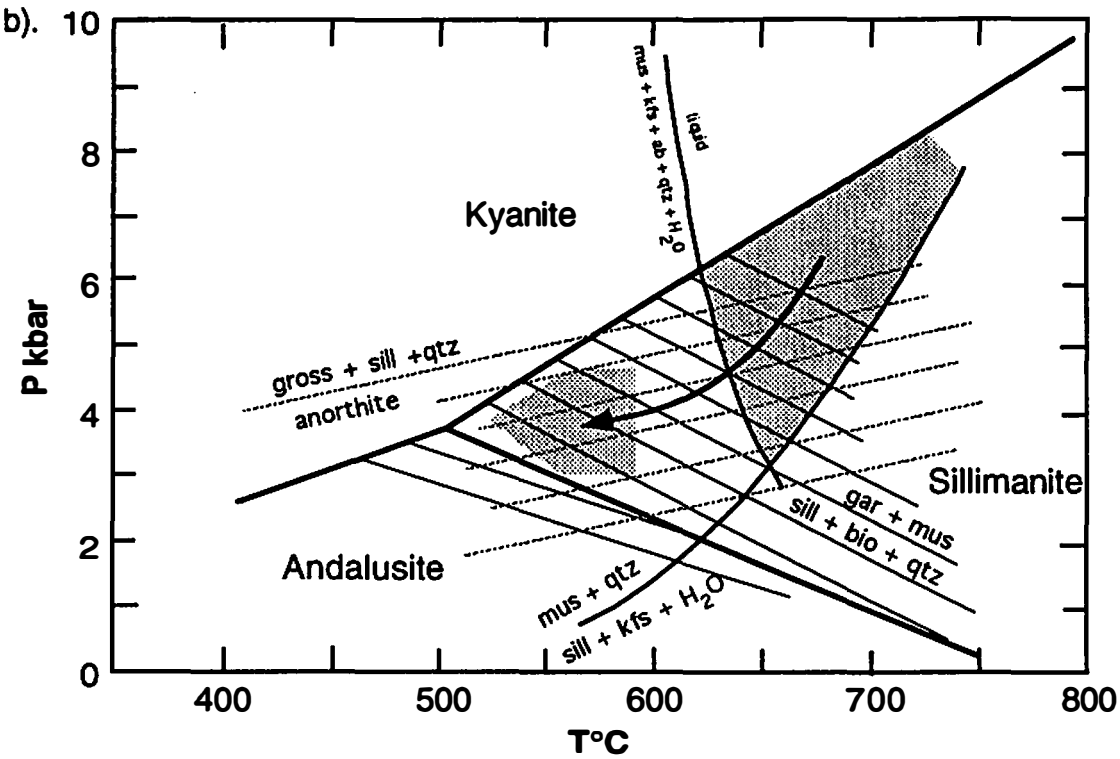
QUALITATIVE CONSTRAINTS ON THE P–T PATH DURING EMPLACEMENT OF THE SUGARLOAF MOUNTAIN THRUST SHEET

Unfortunately, neither the absolute peak pressure–temperature conditions, nor the prograde part of the P–T path followed by pelites of the SMT can be determined at this time. It is likely that these relationships will never be uniquely defined because of the restricted mineral assemblage, lack of appropriate inclusions and prograde mineral zoning in the garnets, and because post metamorphic peak continuous reactions have been operative thus resulting in mineral compositions that are not indicative of peak or prograde metamorphic conditions. The field and petrographic observations, reaction textures, mineral zoning, and the geothermobarometric estimates discussed in this chapter do, however, permit the retrograde portion of the P–T path to be qualitatively assessed. Importantly, based on the metamorphic and structural relationships discussed herein and in Chapter IV, this portion of the P–T path is, perhaps, the most important to the understanding of the metamorphic conditions during emplacement of the SMT.

Field and petrographic observations indicate that the highest P–T conditions recorded by the pelitic rocks of the SMT are at least qualitatively constrained within the shaded area shown on the petrogenetic grid in Figure 5–2. In the most simple scenario, the use of the P–T values in this shaded area (highest P–T conditions) and the results of the geothermobarometric estimates (Table 5–1), suggests the general retrograde P–T path as shown in Figure 5–13 for pelites in the Sugarloaf Mountain thrust sheet. Although such a path may be generally valid, additional constraints are provided by the metamorphic textures and zoning profiles discussed in this chapter.

Figure 5-13. Petrogenetic grids showing possible retrograde P–T paths for pelites in the SMT. a) General retrograde P–T path for pelites in the Sugarloaf Mountain thrust sheet determined using the results of geothermobarometric estimates (Table 5–1) and the conditions of metamorphism, determined from field and petrographic observations and shown in Figure 5–2. b). P–T grid showing a proposed retrograde P–T path for the Sugarloaf Mountain thrust sheet based on the metamorphic textures, and mineral composition of garnet and plagioclase. Diagram also contains garnet–biotite isopleths (after Helms, 1990), and grossular isopleths (after Spear and others, 1989) for the KFMASH assemblage of garnet + biotite + sillimanite + muscovite + quartz. Al_2SiO_5 triple point after Holdaway (1971).


a).
P kbar
T°C
Kyanite
Sillimanite
Andalusite
mus + qtz
sill + kfs + H2O
pa + qtz + H2O
10
8
6
4
2
0
400
500
600
700
800


b).
P kbar
T°C
Kyanite
Sillimanite
Andalusite
gross + sill +qtz
anorthite
gar + mus
sill + bio + qtz
mus + qtz
sill + kfs + H2O
pa + qtz + H2O
10
8
6
4
2
0
400
500
600
700
800

Reaction relationships, based on these textural criteria and mineral zoning, require that any proposed path must account for periods of both garnet consumption (reactions 3) and garnet growth (reaction 4) in these pelitic rocks.

Helms (1990) has shown that isopleths of garnet and biotite composition (reaction 3) in the KFMASH assemblage garnet + biotite + sillimanite + muscovite + quartz have a negative slope in P–T space (Fig. 5–13). According to Helms (1990) because garnet is on the high P–T side of the isopleths, the greatest amount of garnet consumption occurs with decompression and cooling. Alternatively, Spear (1989) and Spear and others (1989) indicate that garnet growth by reaction 4 in the KFMASH assemblage garnet + biotite + sillimanite + muscovite + quartz precludes a path that involves significant decompression and cooling because grossular isopleths (reaction 4) have a positive slope in P–T space (Fig. 5–13).

Using these constraints, it is proposed that the retrograde portion of the P–T path followed by pelites in the SMT varied between a path of decompression and cooling parallel to the grossular isopleths, and a path that may have approached isobaric cooling (Fig. 5–13). Samples that contain evidence for garnet consumption, but lack Ca enrichment at the garnet rim suggest a path of decompression and cooling that paralleled the grossular isopleths. Alternatively, samples containing both textural evidence for garnet consumption by reaction 3 and Ca enrichment at garnet rims consistent with garnet growth by reaction 4, indicate a P–T path less steep than the grossular isopleths that could approach conditions of isobaric cooling. Spear and others (1989) and Spear (1990) indicated that garnet growth by reaction 6 is common in metamorphic terranes that have experienced isobaric cooling. Such a path is consistent with the interpretation that the textural and compositional variations observed in the SMT pelites record changes in equilibrium conditions (e.g., garnet growth versus garnet consumption) along the retrograde portion of the P–T path discussed earlier. In addition, this proposed path suggests that the textural (e.g., variations in garnet morphology) and mineral composition variations observed in these pelites can be explained by a single metamorphic episode and does not require two prograde metamorphic episodes as

suggested by Lemmon (1973).

The Sugarloaf Mountain thrust sheet maintains a similar structural position (e.g., Inner Piedmont rocks over Chauga belt rocks), and contains a sillimanite–muscovite assemblage similar to thrust sheets elsewhere in the western Piedmont including the Six Mile thrust sheet in South Carolina (Griffin, 1974a), the Alto allochthon in southwestern South Carolina and northeast Georgia (Hopson and Hatcher, 1988), and the Smith River allochthon in southwestern Virginia (Conley and Henika, 1973). Like the Sugarloaf Mountain thrust sheet, pelites in these thrust sheets also contain a sillimanite–muscovite metamorphic assemblage, but which has generally been interpreted to represent a prograde or peak metamorphic assemblage. Emplacement of these thrust sheets is interpreted to have occurred subsequent to development of this peak metamorphic assemblage. Comparison of the Sugarloaf Mountain thrust sheet with the structurally and metamorphically similar thrust sheets, mentioned above, indicates that the relationship between the development of the sillimanite–muscovite assemblage and crystalline ductile thrusting in the western Inner Piedmont may have been diachronous (e.g., retrograde and synkinematic in the SMT; prograde and prekinematic in the Alto allochthon). These observations may also suggest that previous interpretations indicating that the sillimanite–muscovite assemblage in these thrust sheets is a peak or prograde assemblage may need to be reassessed.

The timing of this tectonothermal activity in the Columbus Promontory is best constrained by the observations of Lemmon (1973, and 1982). An important contribution was the recognition that the 535 Ma Henderson Gneiss and the 438 Ma granitic intrusion within the Henderson Gneiss are strongly foliated, isoclinally folded, and metamorphosed, leading him to suggest that an Acadian tectonothermal event (post 438 Ma) is recorded in this part of the southern Appalachian Inner Piedmont. Pending the results of ongoing geochronological work, it is also concluded that the emplacement of the SMT sheet along the retrograde P–T path proposed here occurred during an Acadian tectonothermal episode in the western Inner Piedmont.

CHAPTER VI

CONCLUSIONS

The Columbus Promontory, as defined in this study, represents a unique area along the Blue Ridge physiographic front in North Carolina where geologic features characteristic of the southern Appalachian Inner Piedmont are very well preserved and exposed. Because of the outstanding exposure of rock units, atypical of most of the Inner Piedmont, this area has provided an outstanding opportunity to examine the geologic history of the western Inner Piedmont. This investigation represents a multidisciplinary study that has attempted to integrate the stratigraphic, structural and metamorphic to gain a complete understanding of the geologic development of this terrane. It was also the intent of this study to place the geologic feature features observed in the Columbus Promontory into the regional framework of the southern Appalachian orogen. As a result of the approach taken, this investigation has resulted in the generation of a significant amount of new data and several new hypotheses about the stratigraphy, internal deformation, and emplacement conditions of crystalline thrust sheets the western Inner Piedmont. Important results and conclusions from this multidisciplinary examination of the western Inner Piedmont from the area defined as the Columbus Promontory are summarized below.

The lithostratigraphy of the Columbus Promontory consists of four mappable units that include the Henderson Gneiss, the Sugarloaf gneiss, the Poor Mountain Formation, and the Mill Spring Complex. These units are contained within three distinct thrust sheets that characterize the map–scale geology of the crystalline thrust terrane exposed in the Columbus Promontory

and include the Tumblebug Creek thrust sheet, Sugarloaf Mountain, and Mill Spring thrust sheets. The Tumblebug Creek contains only the Henderson Gneiss; the Sugarloaf Mountain thrust sheet contains rocks of the Poor Mountain Formation, the Sugarloaf gneiss, and amphibolite–poor upper Mill Spring complex; the Mill Spring thrust sheet contains rocks of the amphibolite–rich lower Mill Spring complex.

Lithostratigraphic units defined in the Columbus Promontory are similar to stratigraphic units recognized elsewhere in the eastern Blue Ridge and Inner Piedmont. Similarities in physical stratigraphy between the Mill Spring complex and Poor Mountain Formation and other rock units in the eastern Blue Ridge and Inner Piedmont further supports the interpretation that the crystalline southern Appalachians contains two distinct lithostratigraphic suites that include: 1) a lower sequence consisting of Lynchburg–Ashe–Tallulah Falls–Mill Spring–Sandy Springs/New Georgia –type rocks, and 2) an upper sequence consisting of Evington–Alligator Back–Chauga River/Poor Mountain–Jackson's Gap/Ropes Creek –type rocks. As with these correlative units , rocks of the Mill Spring complex and the Poor Mountain Formation are interpreted to be part of the deep–water facies rocks deposited along the Laurentian margin in Late Proterozoic to early Paleozoic time. The addition of the rocks of the Columbus Promontory to this regional stratigraphy further supports the argument that stratigraphic sequences in the eastern Blue Ridge and Inner Piedmont are equivalent. Furthermore, this correlation indicates that the Brevard fault zone, although recognized as a major structural discontinuity between the eastern Blue Ridge and Inner Piedmont, does not separate terranes of different tectonic affinity.

Amphibolite represents a significant rock unit within the Poor Mountain Formation and the upper Mill Spring complex and was the subject of geochemical analysis. Geochemical trends shown on AFM and Niggli diagrams, and fractionation trends observed in several covariation diagrams support an interpretation that protoliths of amphibolite in the Poor Mountain Formation

and Mill Spring complex were tholeiitic basalts. The covariation diagrams used in this study also indicate the Columbus Promontory suite was fractionated with trends explained by fractionation of olivine, plagioclase, clinopyroxene, garnet, and magnetite. This assemblage is similar to the low–pressure fractionation sequence observed in mid–ocean ridges and indicated a MORB character for the Columbus Promontory suite. Zr/Nb, and Y/Nb ratios further define the MORB character to be N–type MORB, but also suggest some P–type component.

Tectonomagmatic discriminant diagrams also suggest an ocean– floor setting, but also indicate a volcanic–arc component. These observations suggest two possible paleotectonic interpretations for the origin of the amphibolite of the Poor Mountain Formation and the Mill Spring complex that include: 1) a mid-oceanic ridge setting adjacent to a mantle plume, and 2) a back–arc basin setting. Regardless of the interpretation, the total data set supports an oceanic origin for the Columbus Promontory suite. The oceanic character of these amphibolites also supports the interpretation that the Poor Mountain Formation and the Mill Spring complex, and correlative units in the eastern Blue Ridge and Inner Piedmont, were deposited, at least partly, on oceanic crust.

The internal deformation and emplacement history of ductile crystalline thrust sheets in the western Inner Piedmont of the Carolinas and NE Georgia was investigated by detailed mapping and meso– and microstructural analysis of rocks in the Columbus Promontory and the Tamassee area in NE Georgia and adjacent South Carolina. The large–scale structure of the western Inner Piedmont in these areas consists of a stack of thin penetratively deformed ductile crystalline thrust sheets. Although this part of the western Inner Piedmont is polydeformed (D_1 to D_5), the D_2 and D_3 episodes were the most important and represent a deformation continuum. D_2 was the most penetrative and synchronous with the latest upper amphibolite facies (Taconian–Acadian?) metamorphism in the western Inner Piedmont. D_3 generally represents late– to

postpeak final emplacement of thrust sheets as coherent masses prior to complete cooling of the thrust stack. The emplacement history and internal deformation of thrust sheets in the Tamassee area and the Columbus Promontory is complex and involves coeval W and SW orogen oblique–to–normal and orogen–parallel displacements The NE–SW and E–W structures developed coevally and are not the result of discrete deformation or metamorphic events. The major implication of this observation is that a primordial (?) Brevard fault zone and the Inner Piedmont thrust sheets were part of a linked décollement system. It is proposed that this deformation was the result of an early (pre–Alleghanian orogeny) oblique convergent or transpressional tectonic event in the crystalline southern Appalachians.

The most characteristic structural element of the Inner Piedmont is the regional mylonitic (S_2) foliation. Meso– and microscopic scale kinematic criteria indicate that S_2 is dominated by C surfaces and, suggests that much of the Inner Piedmont can be considered a regional of crustal–scale shear. S_2 was also a major controlling factor in the development of other micro– and mesoscale D_2–D_3 structures within the western Inner Piedmont. A hypothesis is presented suggesting that internal deformation within the thrust sheets was the result of flow perturbations within the S_2 mylonitic foliation caused by the transpressional or oblique convergence event. This resulted in enhanced partitioning of deformation into thrust and wrench components recognized as orogen–oblique–to–normal displacement of crystalline thrust sheets in the deeper Inner Piedmont and orogen–parallel movement within the Brevard fault zone and Chauga belt. The recognition of the linked displacement between the primordial Brevard fault zone and the thrust sheets in the Inner Piedmont, and recognition of S_2 as a regional C surface are important aspects that distinguish this work from previous studies

The metamorphic history of the Columbus Promontory was examined in pelitic schist contained in the Sugarloaf Mountain thrust sheet. Pelitic schist in the Sugarloaf Mountain thrust

sheet contain a sillimanite –muscovite metamorphic assemblage (A_1) consisting of the mineral phases

$$gar + bio + sill + plag\ (An_{13-38}) + qtz \pm il$$

Textural relationships and compositional zoning in garnet and plagioclase indicate that A_1 was produced by a series of continuous reactions involving both garnet consumption and garnet growth. These reactions are interpreted to have operated subsequent to the metamorphic peak, and therefore A_1 is interpreted to represent a post metamorphic peak assemblage. The textural observations strongly suggest that development of the sillimanite–muscovite zone assemblage (A_1) was synkinematic with development of microstructural features related to emplacement of the Sugarloaf Mountain thrust sheet.

The interpretation that the sillimanite–muscovite assemblage (A_1) represents a post–peak assemblage, and the synkinematic relationships support an interpretation that the SMT was emplaced along the retrograde portion of the P–T path followed by these rocks. Textural relationships and mineral zoning patterns in garnet and plagioclase suggest a retrograde P–T path characterized by general decompression and cooling, but with periods of isobaric cooling. Geothermobarometric estimates, using rim compositions of mineral phases in A_1, were made using the garnet–biotite thermometer and GASP and GPMB barometers. Results indicate temperatures of 535° C to 670° C and pressures of 3 to 5 kbs for final equilibration of mineral phases in A_1. Synkinematic relationships indicate that these values approximate minimum P–T conditions during emplacement of the Sugarloaf Mountain thrust sheet. This path is interpreted to represent an Acadian (post 438 Ma) tectonothermal event.

The interpretation that the sillimanite–muscovite assemblage in the SMT is post thermal peak assemblage contrasts with previous interpretations for the same assemblage in structurally similar thrust sheets elsewhere in the western Inner Piedmont (e.g., Alto allochthon, Smith River allochthon). This suggests that the relationship between development of this regionally extensive sillimanite–muscovite assemblage and ductile thrusting was diachronous in the western Inner Piedmont. Alternatively, this could also indicate that previous interpretations of this metamorphic assemblage may need to be reevaluated.

REFERENCES CITED

FOLIATION (S2)

Station	Strike	Dip	Dir
3	53	26	N
4	80	25	S
5	23	20	S
6	86	38	N
7	325	18	N
8	27	27	S
11	354	10	N
12	339	10	N
13	344	26	N
14	323	3	N
15	297	23	N
17	350	38	N
18	355	19	N
19	346	24	N
20	346	15	N
21	40	11	S
22	290	24	S
23	331	13	S
24	284	10	S
26	11	22	S
27	350	36	S
28	275	3	N
29	16	22	S
30	49	29	S
31	320	1	N
32	306	6	S
33	321	3	N
34	347	6	S
35	331	5	S
36	340	12	N
37	357	37	N
38	354	21	N
39	11	23	S
39	66	28	S
40	6	16	S
44	358	20	S
45	61	14	N
46	20	20	N
47	286	14	S
47	90	16	S
48	337	27	N
49	90	6	N
50	318	21	N
50	327	21	N
51	42	8	S
51	12	21	S
52	348	31	N
53	20	34	S
54	25	31	S
55	332	15	N
56	23	26	S
57	10	32	S
58	32	18	S
59	324	23	N
60	313	18	N
61	32	10	S
62	319	11	N
63	301	15	N
64	287	19	N
65	326	13	N
68	10	17	S
70	22	28	S
72	66	22	S
73	20	22	S
74	50	24	S
75	310	31	N
76	20	34	S
77	50	42	S
78	292	9	N
78	336	14	S
79	20	25	S
80	35	25	S
81	320	15	S
81	275	36	N
82	326	16	N
83	64	17	N
84	340	10	N
85	21	31	S
85	50	14	S
86	306	11	N
87	344	19	N
88	83	17	N
89	50	15	S
90	315	27	N
91	10	6	S
92	15	39	S
93	280	59	S
94	310	12	N
95	85	24	N
96	40	12	S
97	14	14	S
98	325	7	N
99	355	3	N
100	320	25	N
101	16	21	N
102	345	26	N
103	290	13	S
104	355	16	N
105	330	28	N
106	23	7	S
107	263	13	N
108	55	14	N
109	355	18	N
110	342	29	N
111	40	15	N
112	356	29	N
113	310	24	S
114	330	11	N
115	300	24	N
116	305	10	N
117	315	27	N
118	30	18	S
119	55	10	N
120	310	16	N
121	20	26	S
122	55	25	S
124	35	18	S
126	325	19	N
127	340	11	N
128	310	23	N
129	310	21	N
130	50	35	S
131	40	36	S
132	60	31	S
133	50	11	S
134	19	32	S
135	350	45	N
136	38	21	S
137	350	14	N
138	40	32	S
139	18	31	N
140	10	46	S

LINEATION (L2)

Station	Trend	Plunge
11	55	14
14	70	9
21	86	9
21	74	13
23	300	7
24	322	14
30	46	10
48	160	10
49	84	6
52	118	25
55	73	16
66	82	14
69	87	14
83	40	7
101	272	15
102	68	17
104	310	12
109	107	7
116	80	16
118	130	8
141	72	5
143	65	25
147	275	11
153	38	19
188	210	0
227	0	14
343	88	4
344	81	39
345	65	10
345	89	10
346	80	30
347	81	10
348	80	10
349	80	10
350	42	9
351	80	10
351	88	32
351	300	6
351	349	9
352	284	12
354	85	13
355	110	20
356	105	20
357	80	10
358	114	14
358	78	2
358	85	13
359	115	18
360	105	4
361	87	4
361	80	14
362	83	13
363	80	16
364	63	15
365	55	18
366	104	4
368	110	4
369	180	2
371	80	11
372	85	8
373	86	4
374	0	10
374	109	10
374	81	2
375	75	8
376	278	10
376	254	10
378	107	18
379	107	8
380	80	8
382	87	6
384	107	6
386	115	11
387	40	14
388	250	10
390	115	10
392	74	10
394	80	8
394	75	10
396	60	10
398	74	10
401	115	23
404	114	6
408	80	6
409	120	10
410	107	5
412	55	5
413	70	10
414	80	20
416	70	11
418	80	18
418	274	4
418	60	9
419	258	8
420	30	3
421	65	9
422	115	23
423	80	12
424	88	7
424	35	5
427	140	10
429	82	18
430	85	4
431	85	2
432	275	8
433	65	10
434	260	3
435	260	6
436	110	10
437	80	5
438	60	5
439	260	2
440	75	5
443	14	8
444	10	13
446	23	5
447	110	20
448	107	20
449	50	11
450	50	8
450	50	7
451	65	11
452	75	8
453	76	5
454	70	5
454	65	10
455	85	11
456	88	4
457	65	7
458	65	5
459	87	10
460	60	7

FOLDS (F2)

Station	Trend	Plunge
9	345	16
15	80	32
16	125	16
20	165	20
23	20	17
27	357	15
28	352	18
32	179	11
43	8	11
45	195	15
58	125	22
64	300	10
75	51	16
81	290	19
83	125	4
86	55	16
89	29	24
94	84	21
94	30	7
95	15	11
96	22	18
98	10	15
101	310	14
102	55	18
103	74	7
103	300	0
123	201	19
123	203	15
123	200	15
164	160	10
171	320	24
181	145	15
188	68	11
190	50	18
194	30	20
197	172	22
199	155	8
234	70	16
253	116	4
258	40	24
269	118	10
277	25	10
278	352	45
278	26	26
281	115	29
298	172	42
303	220	22
313	40	18
315	105	15
323	60	21
323	148	21
323	20	21
345	340	26
348	325	28
349	0	15
358	30	10
369	22	14
377	30	16
386	110	13
404	110	9
407	104	23
413	115	25
433	30	10
438	70	17
474	255	5
486	55	15
490	355	13
495	320	0
510	40	19
511	190	14
522	340	4
522	240	4
528	325	5
528	85	5
528	350	20
528	125	14
528	355	15
565	150	2
568	35	14
568	30	43
578	80	2
578	350	6
584	10	5
593	104	11
601	72	14
607	120	20
607	85	8
620	205	5
622	75	8
634	150	16
662	120	28
670	120	24
679	140	36
692	220	0
692	220	2
692	220	0
709	50	5
718	109	22
734	32	3
734	0	10
752	15	10
823	213	4
824	216	7
877	50	14
899	118	15
900	280	10
985	35	3
987	340	0
1016	323	8
1106	309	19
1106	155	12
1106	157	3
1106	309	2
1107	157	8
1107	147	4
1107	155	16
1108	15	7
1116	342	32
1126	110	37
1132	51	21
1132	13	13
1132	33	12
1133	185	3
1136	319	7
1136	305	4
1136	179	10
1136	359	24
1190	122	4
1195	6	11
1213	92	9
1251	115	7
1254	85	21

JOINTS

Station	Strike	Dip	Dir
26	330	79	S
68	24	58	N
76	314	76	S
85	272	66	S
85	307	53	N
88	83	17	N
92	82	68	S
93	280	59	S
94	40	86	S
95	44	54	S
96	80	74	S
101	300	59	N
103	286	74	S
121	53	87	N
121	301	84	N
121	284	78	S
124	35	18	S
124	53	82	N
124	292	71	S
124	318	86	N
124	75	82	N
126	325	19	N
126	310	82	S
126	32	81	S
126	16	83	N
126	47	80	N
126	327	64	N
137	88	90	
152	280	72	S
152	30	77	N
158	25	60	S
159	300	89	S
161	35	48	S
161	310	82	N
162	300	77	N
164	312	86	N
166	320	75	S
171	280	86	N
186	310	68	N
188	285	76	S
188	31	75	N
191	280	78	S
191	40	66	S
192	290	87	N
192	15	90	
194	5	72	N
209	70	84	N
212	35	90	
212	284	74	N
213	278	42	S
214	90	56	S
214	30	76	S
220	30	90	
220	275	70	S
221	65	85	S
222	50	65	S
223	40	79	S
223	332	87	N
224	78	83	S
224	290	90	
225	290	86	S
225	30	76	N
226	285	87	N
226	37	90	
227	290	85	N
227	60	76	S
228	30	80	S
228	275	82	S
230	275	87	S
231	290	87	S
231	35	88	S
232	287	90	
232	310	84	N
232	55	87	S
233	355	84	N
235	15	90	
235	285	90	
236	60	90	
236	290	88	S
237	72	90	
238	285	85	S
244	285	86	S
244	43	75	N
245	270	78	S
245		90	
246	15	80	N
246	80	85	S
247	275	76	N
247	80	85	S
248	288	90	
248	5	90	
250	288	85	N
250	50	83	S
254	50	86	N
254	340	83	S
256	318	54	S
256	62	82	S
257	310	55	S
257	40	75	S
257	275	90	
258	295	74	N
258	70	90	
262	280	90	
265	280	75	N
265	350	53	N
268	290	75	S
270	80	90	
270	296	74	S
273	278	65	N
273	314	90	
277	335	90	
277	65	35	S
283	10	76	S
284	43	85	N
301	330	70	N
301	26	60	N
302	40	69	N
302	329	44	S
302	42	90	
303	295	63	N
303	330	90	
303	40	64	N
304	30	74	N
304	55	72	N
304	292	71	N
305	35	77	S
305	327	77	S
306	325	90	
307	55	70	S
307	335	72	N
307	35	90	
307	285	80	N

FOLIATION (S2)

Station	Strike	Dip	Dir
143	2	30	S
144	358	30	N
145	355	32	N
146	340	23	N
147	40	24	N
148	330	22	N
149	300	11	N
150	300	24	N
151	38	25	S
152	350	7	N
153	352	26	N
154	20	33	N
155	35	15	N
156	20	31	N
157	342	36	N
158	12	17	S
159	20	33	S
160	10	22	S
161	10	21	S
162	27	17	S
163	355	36	N
164	20	23	S
165	355	40	N
166	350	16	N
167	3	5	S
168	30	14	S
169	355	46	N
170	45	37	S
171	320	27	N
172	330	15	N
173	355	15	N
174	30	32	S
175	10	17	N
176	310	15	N
177	340	7	S
178	320	10	N
179	10	16	S
180	30	24	S
181	0	30	E
182	55	17	N
183	55	6	N
184	43	17	S
185	25	9	N
186	10	8	N
187	15	16	N
188	15	6	N
189	40	15	N
190	20	16	S
191	10	2	N
192	20	14	S
193	320	15	S
194	305	11	N
195	38	10	S
196	295	2	N
197	30	25	N
198	30	15	S
199	352	25	S
200	320	10	N
201	50	35	N
202	35	9	S
203	325	30	N
204	320	9	N
205	300	12	N
206	20	28	S
207	10	10	S
208	30	16	S
209	30	10	N
210	10	20	S
211	25	13	N
212	325	2	N
213	50	31	S
214	30	16	S
215	30	20	S
216	30	20	N
217	40	12	S
218	40	30	S
219	45	15	N
220	337	7	S
221	310	6	S
222	305	6	S
223	340	13	N
224	334	11	N
225	340	20	N
226	325	11	N
227	340	21	N
228	320	15	N
229	333	12	N
230	345	14	N
231	330	15	N
232	320	14	N
233	40	4	N
234	317	6	N
235	330	24	N
236	330	20	N
237	307	14	N
238	320	11	N
239	319	30	N
240	320	25	N
241	310	15	N
242	345	15	S
243	35	4	N
244	315	15	N
245	335	15	N
246	70	20	N
247	80	10	N
248	314	11	N
249	315	15	N
250	325	10	N
251	330	20	N
252	325	15	N
253	350	15	N
254	0	20	E
255	45	10	N
256	305	42	N
257	320	30	N
258	345	20	S
259	305	13	N
260	55	15	N
261	58	7	N
262	10	19	S
263	330	25	N
264	330	30	N
265	26	14	S
266	305	26	N
267	295	20	N
268	325	29	N
269	290	15	S
270	5	15	N
271	20	3	S
272	350	21	N

LINEATION (L2)

Station	Trend	Plunge
465	88	10
466	55	5
467	65	10
468	40	0
469	87	10
470	75	5
471	255	3
472	110	15
473	245	10
474	265	15
475	82	7
476	80	12
477	295	8
480	350	5
482	18	5
483	55	15
485	45	10
486	55	20
490	50	14
492	75	2
493	45	10
494	105	15
494	135	17
497	105	17
499	55	5
501	50	6
506	210	4
509	70	10
511	245	10
513	30	25
514	75	3
515	350	16
517	245	0
517	90	0
518	115	7
520	58	5
522	55	4
523	83	2
524	360	3
525	300	2
526	115	12
526	60	11
527	255	2
529	110	5
530	77	10
532	30	12
533	240	5
534	269	2
537	155	30
538	255	8
539	10	7
539	85	26
542	120	18
543	250	12
543	180	5
544	120	15
544	65	25
544	360	15
546	5	7
547	60	20
548	87	2
549	114	14
550	55	30
551	55	25
552	55	10
553	70	2
554	60	10
554	80	6
556	75	10
557	140	16
561	30	10
562	60	13
563	108	5
564	75	25
564	70	30
565	320	0
567	40	12
568	75	23
568	35	14
568	70	29
569	85	3
571	14	20
573	235	23
577	55	10
578	245	10
578	65	25
578	75	10
578	75	14
579	247	5
580	88	7
581	75	6
581	210	15
582	76	15
583	226	9
584	160	7
586	82	12
587	80	15
588	50	9
589	15	20
590	90	25
591	105	50
593	80	20
595	80	15
596	70	15
596	105	15
598	105	10
599	115	15
600	80	10
605	115	2
606	272	5
607	120	20
607	85	10
608	65	8
611	80	2
614	82	15
615	85	2
616	65	14
617	66	1
618	61	4
619	200	6
620	85	10
623	225	10
624	86	10
625	80	18
626	75	10
627	275	10
629	76	0
632	80	12
634	50	20
642	90	23

FOLDS (F2)

Station	Trend	Plunge
1330	110	32
1365	90	2
1411	88	13
1437	0	16
1437	4	15
1437	220	5
1443	10	18
1448	22	9
1472	64	4
1473	140	11
1560	220	6
1560	242	6
1569	216	11

JOINTS

Station	Strike	Dip	Dir
309	297	90	
310	280	52	S
310	328	52	S
311	45	80	N
313	290	90	
313	290	90	
315	325	77	S
315	27	77	S
317	60	72	N
317	356	90	
317	290	61	S
317	82	86	N
320	43	90	
321	320	80	N
321	57	65	N
323	45	86	N
328	65	85	N
328	350	82	N
329	328	90	
329	30	51	N
330	318	84	N
330	295	72	S
331	82	75	N
333	64	90	
336	60	90	
336	328	78	S
345	300	76	S
355	275	88	N
360	280	83	N
361	290	90	
362	290	86	N
362	20	60	N
408	290	80	S
417	290	80	S
699	290	73	S
706	50	65	N
719	30	70	N
719	320	70	S
720	325	90	
720	50	72	N
721	50	55	N
721	310	75	S
726	60	65	N
726	295	80	S
728	40	63	S
733	30	60	N
733	300	76	S
745	280	85	S
745	55	62	N
750	290	76	S
751	40	90	
751	320	90	
754	285	90	
755	40	67	N
757	285	90	
758	50	83	N
779	60	86	S
785	75	80	S
794	50	90	
797	40	90	
802	40	90	
805	44	90	
805	32	50	N
806	50	90	
806	315	65	N
814	57	90	
814	318	81	N
818	318	90	
818	48	90	
823	316	87	N
837	48	88	N
851	276	90	
854	288	90	
861	288	75	S
867	300	85	S
1025	72	78	N
1088	290	70	S
1149	70	65	S

FOLIATION (S2)

Station	Strike	Dip	Dir
280	350	20	N
281	325	25	N
282	317	29	N
283	50	5	S
287	326	8	S
288	315	11	N
289	40	14	S
290	323	20	N
291	16	6	S
292	345	15	N
293	335	21	N
294	50	14	N
295	16	5	S
297	23	29	S
298	335	16	N
299	325	26	N
300	20	6	S
301	10	9	S
302	50	25	S
303	30	20	S
304	10	20	S
304	352	23	N
305	35	16	S
306	33	14	S
307	27	20	S
308	18	6	S
309	20	11	S
310	348	20	N
311	20	35	S
312	5	25	S
313	23	13	S
314	310	9	N
315	313	10	N
316	31	21	S
317	10	10	S
318	30	15	S
319	312	13	N
320	315	4	N
321	324	13	N
322	317	6	S
323	340	14	N
324	317	5	N
325	28	7	S
326	355	9	N
327	326	8	N
328	316	14	S
329	334	20	N
330	343	20	N
331	357	16	N
332	350	15	S
333	328	25	N
334	328	26	N
335	334	15	N
336	340	24	N
337	30	10	S
338	332	38	N
339	7	30	S
340	345	33	N
341	340	38	N
342	351	39	N
343	210	7	E
345	340	50	N
346	350	30	N
349	56	30	S
351	325	10	N
352	62	10	N
353	318	25	N
354	345	15	N
355	350	20	N
356	310	22	N
357	15	14	S
358	330	4	N
358	350	3	N
359	334	5	N
360	30	17	S
361	16	6	S
361	50	6	S
362	40	16	S
363	16	19	S
364	52	20	S
365	355	19	N
368	348	18	N
369	348	18	N
370	320	14	N
371	350	23	N
374	329	12	N
374	61	10	S
375	345	20	N
376	25	11	S
378	349	23	N
379	322	10	N
380	8	8	S
381	340	8	N
382	350	10	N
383	30	20	S
384	15	23	S
385	325	8	N
386	330	12	N
387	350	15	N
388	15	14	S
389	30	12	S
390	10	13	S
391	16	23	S
392	33	23	S
393	7	10	S
394	10	8	S
395	35	18	S
396	30	18	S
397	328	30	N
398	350	8	N
399	355	10	S
400	6	30	S
401	340	23	N
402	300	23	S
403	340	14	N
404	350	18	N
406	241	14	S
407	330	19	N
408	25	26	S
409	25	25	S
410	55	25	S
411	345	23	N
412	18	11	S
413	25	15	S
414	20	24	S
415	74	28	S
416	20	16	S
418	315	22	N
418	310	10	N
418	40	12	N
419	295	10	S
419	330	10	S

LINEATION (L2)

Station	Trend	Plunge
658	115	12
662	43	6
662	80	15
666	88	14
671	73	42
672	73	22
673	105	8
674	105	3
676	40	12
677	60	15
678	55	12
679	85	16
680	105	21
681	55	15
686	70	12
687	105	15
688	110	6
690	88	28
692	220	0
693	86	12
695	76	8
696	235	10
698	86	5
700	80	18
703	70	16
703	86	20
707	255	2
708	220	12
713	108	14
717	88	28
718	105	10
718	95	20
720	78	9
721	265	6
722	89	2
724	110	10
727	85	27
729	265	5
731	255	0
733	95	5
734	88	6
734	117	2
735	83	12
738	115	6
741	74	16
745	83	8
748	155	6
750	67	10
752	88	5
752	80	7
753	88	0
759	115	18
763	115	2
766	113	16
768	55	10
771	80	3
773	118	10
774	230	10
777	230	0
778	50	5
780	55	26
781	15	10
782	50	6
787	85	26
790	40	0
793	240	8
797	70	15
800	82	11
801	55	15
801	60	5
802	40	5
804	40	0
805	50	0
806	250	2
809	48	8
812	82	4
816	199	13
818	226	11
821	221	4
828	46	5
832	76	13
835	36	10
840	82	5
841	90	13
846	78	5
848	86	8
850	92	10
851	116	5
856	90	4
857	70	24
859	256	3
862	271	5
863	98	17
865	284	11
867	91	7
869	55	29
870	69	17
871	90	21
875	73	21
877	72	5
879	88	21
882	95	14
883	285	20
884	286	20
885	89	14
887	109	10
888	111	11
889	134	28
891	71	9
894	81	29
895	91	6
896	94	27
898	86	25
899	81	29
900	72	14
901	96	2
902	86	23
903	96	25
907	96	11
910	86	20
911	59	12
912	59	12
914	251	9
915	115	5
915	89	9
916	50	31
917	254	27
918	74	16
920	100	10
921	101	15
924	280	2
925	296	8

FOLDS (F2)

Station	Trend	Plunge

JOINTS

Station	Strike	Dip	Dir

FOLIATION (S2)				LINEATION (L2)			FOLDS (F2)			JOINTS			
Station	Strike	Dip	Dir	Station	Trend	Plunge	Station	Trend	Plunge	Station	Strike	Dip	Dir
422	325	25	N	929	246	4							
423	26	27	S	931	272	19							
424	305	10	N	931	257	1							
425	20	35	S	934	61	3							
426	355	40	N	938	212	12							
427	50	20	S	942	75	23							
429	40	20	N	942	67	10							
428	330	15	N	943	53	18							
430	310	8	N	945	236	2							
431	330	6	N	947	85	9							
432	15	18	S	948	37	13							
434	355	5	S	948	59	41							
435	325	10	S	948	31	44							
436	330	12	N	948	258	7							
437	40	10	S	949	76	32							
438	285	10	N	952	93	2							
439	318	15	S	953	82	5							
440	328	22	N	957	81	4							
441	10	10	N	960	70	7							
442	15	15	S	961	54	16							
443	15	18	S	963	76	20							
444	355	30	N	964	276	21							
446	340	25	N	965	63	9							
447	348	28	N	966	108	22							
448	345	24	N	967	52	4							
449	10	17	S	969	94	12							
450	75	10	S	970	74	6							
450	345	10	N	971	48	12							
451	345	16	N	971	74	12							
452	315	13	N	972	233	2							
453	40	30	S	973	31	6							
454	35	27	S	974	299	3							
454	40	30	S	977	53	12							
455	313	15	N	978	18	10							
456	345	8	N	982	49	8							
457	320	12	N	983	235	5							
458	320	5	N	984	65	4							
459	350	10	N	985	95	3							
460	15	15	S	985	55	15							
461	20	26	S	987	200	1							
462	345	22	N	987	210	12							
463	30	12	S	990	89	13							
464	60	10	S	991	67	27							
465	25	15	S	992	245	4							
466	35	11	S	995	84	15							
467	330	16	N	997	206	3							
468	15	2	S	998	45	6							
469	20	14	S	1000	62	9							
470	355	10	N	1001	89	18							
471	30	10	N	1001	78	15							
472	320	20	N	1003	104	34							
473	350	15	N	1004	69	10							
475	20	10	S	1007	80	4							
476	20	25	S	1008	80	9							
477	333	20	N	1009	65	10							
478	315	14	S	1013	257	4							
479	5	10	S	1015	66	4							
480	350	6	N	1018	40	18							
481	350	11	N	1019	248	12							
482	20	14	S	1021	239	2							
483	0	20	E	1023	236	5							
484	20	16	S	1025	262	7							
485	320	12	N	1026	66	11							
486	20	27	S	1029	250	21							
487	0	20	E	1031	55	2							
488	0	10	E	1034	253	4							
489	340	15	N	1034	256	16							
490	340	35	N	1035	239	2							
491	350	36	N	1036	240	5							
492	5	4	S	1038	235	2							
493	345	19	N	1041	21	7							
494	10	25	S	1042	23	6							
496	5	33	S	1043	98	25							
497	45	18	S	1043	42	27							
498	30	23	S	1044	5	5							
499	5	11	S	1045	63	29							
500	30	15	S	1048	42	4							
501	340	6	N	1050	34	12							
502	0	10	E	1051	249	9							
503	18	24	S	1056	88	22							
504	310	6	N	1058	39	2							
505	60	36	S	1060	82	7							
506	30	90		1063	238	4							
506	35	32	S	1064	66	2							
506	35	62	N	1066	217	1							
507	35	18	S	1067	210	1							
508	10	32	S	1071	262	36							
509	40	20	S	1075	239	1							
510	20	90		1077	217	11							
510	20	35	S	1077	69	7							
511	40	10	S	1080	56	4							
512	10	5	N	1082	59	4							
513	330	25	N	1086	100	17							
513	330	50	N	1087	56	7							
514	270	5	N	1088	64	16							
515	310	26	N	1089	71	7							
516	20	15	S	1091	85	14							
518	15	12	S	1092	274	3							
519	315	15	N	1094	107	4							
520	85	20	N	1094	257	6							
521	60	12	N	1096	252	4							
522	50	15	N	1096	221	4							
523	40	5	N	1097	44	7							
524	320	7	S	1097	81	5							
525	30	8	N	1098	45	3							
526	332	12	N	1099	61	16							
529	30	15	N	1100	54	24							
530	340	14	N	1102	57	9							
531	40	25	N	1104	11	2							
532	45	18	S	1105	220	3							
533	25	12	N	1106	19	4							
534	20	7	N	1107	5	5							
535	50	8	S	1109	220	3							
536	345	35	N	1110	29	1							
537	42	36	S	1112	35	2							
538	15	15	N	1113	24	4							
539	10	15	S	1115	41	28							
540	65	10	N	1116	120	18							
541	340	12	N	1116	88	25							
542	340	28	N	1117	58	31							
543	340	20	S	1117	91	32							
544	310	25	N	1118	51	21							
545	320	20	N	1120	57	10							
547	0	15	E	1125	70	15							
548	50	16	S	1126	99	5							
548	40	63	S	1128	43	18							
549	310	26	N	1129	213	5							
550	300	30	N	1130	219	4							
551	305	28	N	1132	208	14							
552	300	20	N	1134	194	6							
553	290	10	N	1135	71	6							
554	300	12	N	1136	48	4							

FOLIATION (S2)

Station	Strike	Dip	Dir
557	30	18	S
558	350	70	S
559	290	45	N
560	330	15	S
561	310	16	N
562	10	15	S
563	330	16	N
564	320	30	N
566	58	38	S
567	350	20	N
568	325	23	N
569	80	16	N
571	10	86	S
573	20	25	N
574	20	90	
576	50	6	S
578	355	10	N
579	320	5	N
580	315	8	S
581	325	17	S
582	28	23	S
583	320	10	N
584	20	64	N
585	320	35	N
586	345	12	N
587	335	15	N
588	335	10	S
589	15	20	N
590	340	25	S
591	10	50	N
592	330	10	N
593	330	33	S
594	20	20	N
595	340	15	N
596	350	15	S
597	40	10	W
598	350	20	S
599	50	35	S
600	5	25	S
601	35	15	S
602	20	10	N
603	54	15	N
604	350	20	S
605	50	5	S
607	300	74	S
607	60	5	S
607	50	12	N
609	340	10	S
610	310	10	N
611	75	10	N
612	350	12	S
613	10	2	S
614	45	20	E
616	342	22	S
617	51	22	E
618	178	12	S
620	50	20	W
621	295	10	N
622	110	20	N
622	310	15	N
623	10	3	N
624	340	12	N
625	320	20	S
626	15	18	N
627	55	4	N
629	355	3	N
630	60	4	N
631	20	15	N
632	320	15	N
633	340	2	N
634	355	23	N
634	330	30	N
637	300	20	S
638	55	15	S
638	10	18	N
639	305	16	S
640	10	50	N
641	350	42	N
642	345	26	S
643	30	36	N
643	320	25	N
644	350	35	N
645	315	19	N
646	305	20	N
647	320	15	S
648	60	45	N
648	295	42	N
649	320	38	N
650	335	32	S
651	310	22	N
652	350	15	S
653	60	15	S
654	305	5	S
655	50	15	S
656	305	20	S
657	290	34	S
658	55	15	S
659	315	10	S
660	2	20	N
661	355	28	N
663	340	42	S
664	320	5	S
666	10	16	N
667	340	5	N
668	340	5	N
669	310	35	S
670	10	35	E
672	0	24	S
673	5	8	N
674	345	12	N
675	350	27	S
676	30	12	N
677	325	16	N
678	335	25	N
679	315	22	S
680	25	24	S
681	20	20	S
682	20	18	N
683	330	42	N
684	350	30	N
685	325	25	N
686	330	15	N
687	320	30	N
688	345	12	S
689	15	30	N
690	315	26	N
691	340	34	N
693	305	18	N
694	280	25	N
695	320	35	S
696	55	10	N
697	340	26	E

LINEATION (L2)

Station	Trend	Plunge
1136	226	18
1137	209	6
1138	38	11
1140	69	4
1145	49	11
1146	227	2
1147	215	7
1149	49	5
1158	89	9
1165	204	9
1166	36	3
1167	49	6
1168	22	7
1171	41	2
1172	206	16
1173	236	20
1175	231	13
1178	199	11
1181	219	11
1183	23	8
1184	213	11
1188	226	8
1189	47	2
1190	95	18
1193	71	12
1194	69	6
1196	76	5
1197	89	12
1199	85	7
1200	93	4
1204	270	15
1205	111	2
1206	89	2
1207	110	3
1210	90	21
1212	105	5
1213	109	13
1213	90	6
1213	92	9
1215	76	34
1216	96	3
1218	42	4
1219	90	3
1220	39	10
1221	51	6
1222	225	6
1225	215	1
1227	50	7
1228	234	4
1231	32	4
1232	38	6
1234	218	8
1235	31	1
1238	51	6
1239	206	13
1240	182	12
1246	248	3
1247	84	14
1249	61	21
1250	88	1
1251	80	10
1252	109	7
1253	85	14
1254	70	3
1254	94	17
1255	110	55
1256	87	9
1257	92	2
1258	256	6
1260	76	10
1261	273	5
1263	270	6
1264	60	2
1266	226	8
1270	78	14
1272	70	4
1275	79	6
1277	118	2
1278	89	41
1279	79	4
1280	88	6
1280	79	10
1280	81	5
1281	81	7
1284	77	9
1286	111	23
1287	82	6
1293	78	12
1296	256	27
1297	85	5
1298	94	35
1299	81	9
1300	78	10
1301	70	9
1303	75	6
1306	251	1
1312	95	0
1318	270	6
1322	78	8
1323	70	0
1327	275	10
1330	50	10
1333	274	4
1334	91	16
1335	60	0
1336	263	15
1340	100	6
1342	70	6
1344	120	15
1347	280	15
1348	88	21
1349	96	11
1354	95	14
1355	99	10
1357	87	4
1360	95	2
1361	92	2
1363	265	15
1364	89	16
1365	96	12
1367	99	24
1372	98	19
1373	282	5
1377	225	5
1378	94	10
1379	86	5
1382	42	16
1383	71	9
1385	79	6
1388	50	25
1388	81	21
1389	41	6

FOLDS (F2)

Station	Trend	Plunge

JOINTS

Station	Strike	Dip	Dir

FOLIATION (S2)

Station	Strike	Dip	Dir
700	45	20	N
701	305	10	N
703	358	13	N
704	358	20	S
705	300	19	S
706	80	15	N
707	295	12	S
708	300	20	S
709	45	15	S
710	40	12	N
711	330	10	N
712	355	10	N
713	320	12	S
714	5	15	S
715	320	15	S
716	25	18	N
717	345	28	N
718	348	22	S
718	2	14	S
719	30	20	S
720	36	16	S
722	25	8	N
723	15	5	N
724	340	14	S
725	35	38	N
726	334	12	N
727	348	30	S
728	67	30	S
729	310	12	N
730	5	20	S
732	24	12	N
733	337	20	N
735	325	15	N
736	340	25	N
737	350	14	S
738	277	8	S
739	295	15	N
741	325	18	S
742	55	15	S
743	30	15	S
744	10	10	N
745	330	7	S
746	60	20	N
748	340	22	N
750	345	12	N
752	345	26	S
752	2	35	S
752	15	20	E
753	0	5	S
754	20	16	S
755	40	23	N
756	350	20	S
757	10	10	S
758	355	2	N
759	325	35	N
760	350	20	N
762	300	20	N
763	80	3	N
764	22	9	S
766	340	16	N
767	20	5	N
768	335	14	S
769	28	16	N
770	40	11	S
772	345	12	S
773	12	18	S
774	82	23	S
775	15	5	S
776	84	10	S
777	55	23	S
779	60	6	N
780	308	10	S
781	330	15	S
782	10	8	S
783	15	26	S
785	305	10	S
786	50	6	S
787	20	35	N
788	320	45	S
790	30	15	S
791	15	11	S
792	85	20	S
793	40	5	S
794	10	12	S
795	80	15	S
796	60	14	N
797	310	16	N
798	351	26	S
799	55	15	N
800	355	20	S
801	38	18	S
801	15	40	N
802	318	6	S
804	40	38	N
805	315	9	S
806	320	12	S
807	15	19	N
809	306	7	S
810	10	9	S
811	45	20	S
812	77	18	N
813	340	10	S
814	72	12	S
816	57	10	S
817	31	17	S
818	319	11	S
819	306	42	S
819	37	10	S
819	334	42	S
819	59	15	S
820	309	5	S
821	53	15	S
822	39	19	S
823	45	50	S
824	48	42	N
825	335	18	S
826	8	16	N
827	59	15	N
828	344	13	N
829	342	13	N
830	298	24	S
831	10	26	N
832	312	20	N
833	355	14	S
834	14	8	N
835	12	18	N
836	299	12	N
837	290	16	N
838	46	9	N
839	286	7	S
840	60	76	N
841	350	9	S

LINEATION (L2)

Station	Trend	Plunge
1391	124	16
1392	261	4
1392	70	4
1392	99	4
1393	115	24
1397	99	13
1398	64	8
1399	261	1
1400	61	15
1401	79	8
1402	26	2
1404	71	31
1404	131	26
1408	265	7
1411	46	13
1412	82	9
1419	77	14
1423	54	24
1424	74	17
1425	119	17
1433	225	5
1436	74	12
1437	264	7
1438	260	4
1439	260	3
1441	54	22
1443	72	8
1443	55	5
1443	42	6
1443	74	9
1443	228	8
1444	55	4
1445	104	26
1445	138	13
1446	57	5
1447	22	9
1448	68	24
1450	61	16
1451	86	24
1456	245	2
1458	245	2
1459	205	5
1460	35	11
1462	30	3
1463	30	3
1463	70	5
1464	208	10
1466	20	7
1468	59	0
1471	53	7
1472	88	4
1472	76	8
1472	72	7
1472	56	16
1474	41	18
1475	237	17
1477	64	22
1479	58	6
1480	245	2
1482	71	9
1485	81	5
1486	276	15
1487	86	9
1489	258	1
1491	268	6
1492	275	3
1493	89	5
1495	225	19
1498	251	21
1497	38	6
1498	101	21
1499	59	24
1500	132	26
1501	62	29
1503	21	10
1505	79	10
1506	203	16
1508	76	16
1509	82	13
1510	276	6
1511	96	5
1512	267	1
1513	120	9
1514	125	56
1516	74	26
1521	80	25
1521	232	8
1523	56	4
1524	72	7
1525	89	8
1527	89	15
1528	99	15
1530	60	7
1531	229	8
1532	236	8
1533	114	8
1533	250	4
1534	215	10
1535	85	6
1536	74	25
1537	74	16
1539	61	5
1540	80	3
1542	78	6
1543	264	4
1545	135	16
1548	263	5
1549	92	3
1552	68	6
1556	64	14
1558	245	3
1559		6
1560	226	10
1562	258	10
1563	59	5
1566	58	8
1567	67	7
1569	216	11
1570	251	8
1570	51	8
1572	29	9
1577	101	12
1582	72	8
1585	108	34

FOLDS (F2)

Station	Trend	Plunge

JOINTS

Station	Strike	Dip	Dir

FOLIATION (S2)

Station	Strike	Dip	Dir
842	69	7	S
843	282	6	S
844	40	15	S
845	352	13	S
846	14	10	S
847	10	10	N
847	307	23	S
849	28	16	S
850	289	64	S
851	30	10	N
852	326	23	S
853	76	5	S
854	21	10	S
855	315	7	S
856	2	7	S
857	41	26	N
858	1	15	N
859	342	18	N
861	356	12	N
862	16	10	N
863	321	32	S
864	20	32	E
865	186	13	S
866	285	10	E
867	350	16	S
868	20	20	E
869	358	27	E
870	349	9	E
871	132	15	N
872	21	6	N
873	20	10	N
874	305	18	N
875	354	14	S
876	5	11	S
877	16	10	S
878	10	19	E
879	347	21	S
880	230	29	S
881	49	51	N
882	328	18	E
883	201	14	N
884	304	8	S
885	15	26	N
886	317	34	E
888	192	11	S
889	34	28	S
890	132	8	S
891	292	12	S
892	114	30	N
893	128	7	N
894	350	21	E
895	358	29	S
896	6	21	S
897	55	16	S
898	22	31	E
899	342	29	N
900	342	14	S
901	267	19	S
902	5	10	S
903	31	21	N
904	43	14	N
905	51	12	N
906	317	8	S
907	20	10	E
908	0	40	N
909	306	11	N
910	349	16	N
911	332	22	S
912	29	17	S
913	235	16	S
914	38	14	S
915	47	22	N
916	309	32	E
917	4	34	S
918	44	16	E
919	160	31	N
920	354	15	N
921	326	24	N
922	296	11	E
923	0	34	S
924	86	9	W
925	350	12	E
926	16	16	N
927	288	28	N
928	353	23	N
929	121	16	S
930	9	21	S
931	74	9	N
932	90	18	S
933	95	5	E
935	176	21	S
936	44	11	N
937	343	21	S
938	11	21	E
939	202	15	E
940	16	23	N
941	302	10	E
942	139	15	E
943	296	10	N
944	350	7	E
945	9	3	S
946	49	26	E
947	183	25	N
948	343	10	E
949	191	26	E
950	146	5	S
951	258	20	E
952	189	15	E
953	7	7	N
954	93	18	S
955	85	14	E
956	15	19	E
957	185	25	S
958	21	18	N
959	351	12	E
960	346	7	S
961	6	16	N
962	352	10	N
963	346	20	N
964	347	12	N
965	334	16	S
966	299	5	E
967	342	24	W
968	55	8	N
969	306	9	N
970	322	14	N
971	288	21	W
972	153	7	S
973	26	19	N
974	79	5	S
975	222	3	E
976	17	30	N

LINEATION (L2)

Station	Trend	Plunge

FOLDS (F2)

Station	Trend	Plunge

JOINTS

Station	Strike	Dip	Dir

FOLIATION (S2)				LINEATION (L2)			FOLDS (F2)			JOINTS			
Station	Strike	Dip	Dir	Station	Trend	Plunge	Station	Trend	Plunge	Station	Strike	Dip	Dir
977	337	16	N										
978	42	21	S										
979	185	17	S										
980	58	16	S										
981	42	22	N										
982	55	3	S										
983	47	48	S										
984	50	36	N										
986	95	11	S										
988	240	6	S										
989	22	14	N										
990	356	20	N										
991	342	30	S										
992	24	4	E										
993	6	19	S										
994	49	25	E										
995	190	15	S										
996	342	4	S										
997	214	2	S										
998	334	6	S										
999	29	14	S										
1000	48	16	N										
1001	357	20	N										
1002	334	22	S										
1003	12	37	N										
1004	358	11	S										
1005	46	18	E										
1006	31	15	N										
1007	357	20	E										
1008	151	19	N										
1009	295	15	N										
1010	324	14	N										
1011	324	14	E										
1012	236	17	E										
1012	236	17	N										
1013	11	13	N										
1014	307	5	S										
1015	278	7	E										
1017	185	49	N										
1018	355	19	N										
1019	318	17	S										
1020	22	16	W										
1021	209	4	N										
1022	327	14	W										
1023	130	6	E										
1024	36	3	S										
1025	231	17	N										
1027	900	10	E										
1028	171	12	N										
1030	65	23	N										
1031	68	14	S										
1032	268	22	N										
1033	311	9	N										
1034	355	16	S										
1035	951	16	E										
1037	322	40	S										
1038	56	14	E										
1039	8	13	S										
1040	281	24	N										
1041	326	5	E										
1042	160	10	N										
1043	356	30	E										
1044	169	24	N										
1045	304	26	N										
1046	27	24	E										
1047	185	15	E										
1048	36	25	E										
1049	0	33	N										
1050	350	16	N										
1051	318	11	E										
1052	135	29	S										
1053	21	24	E										
1054	30	42	E										
1055	331	31	N										
1056	356	22	N										
1057	314	15	N										
1058	314	15	N										
1059	70	15	S										
1060	58	17	S										
1061	66	9	E										
1062	223	9	E										
1063	356	16	S										
1064	68	7	S										
1066	80	3	W										
1067	230	13	S										
1068	62	5	N										
1069	56	14	S										
1070	320	15	N										
1071	22	42	S										
1072	230	6	S										
1074	270	32	S										
1075	240	26	S										
1076	270	21	N										
1077	314	11	E										
1077	56	15	N										
1078	80	15	N										
1079	314	20	S										
1080	80	10	S										
1081	220	28	S										
1082	344	6	N										
1083	354	10	E										
1084	5	18	N										
1085	344	15	N										
1086	343	16	N										
1087	356	16	N										
1088	352	17	N										
1089	341	18	S										
1090	5	18	N										
1091	357	15	N										
1092	326	13	E										
1093	204	15	N										
1094	318	21	E										
1095	156	30	N										
1096	15	5	N										
1097	322	7	N										
1098	324	15	N										
1099	350	5	E										
1100	202	30	N										
1101	288	31	N										
1102	339	28	N										
1103	262	10	S										
1104	7	9	S										
1105	75	14	N										
1106	290	17	E										
1110	159	17	S										
1112	54	7	E										
1113	55	5	N										
1114	354	7	N										
1115	283	29	N										
1116	333	27	N										
1116	348	26	N										
1117	332	28	S										

FOLIATION (S2)

Station	Strike	Dip	Dir
1118	58	22	N
1119	289	11	S
1120	324	10	N
1121	288	15	S
1122	18	7	S
1123	329	21	S
1124	336	4	N
1127	348	14	E
1128	351	18	N
1129	299	5	S
1130	298	10	S
1131	300	15	N
1132	325	4	S
1134	16	24	N
1135	339	14	S
1137	292	13	W
1138	197	5	W
1139	359	23	N
1140	346	4	S
1141	4	16	S
1142	4	16	S
1143	51	21	S
1144	126	22	N
1145	356	18	S
1146	18	9	S
1147	90	11	S
1148	48	8	S
1149	85	12	N
1150	265	3	S
1151	48	18	S
1152	35	15	S
1153	4	38	S
1153	80	9	N
1154	336	23	N
1155	302	12	E
1156	20	30	N
1157	288	3	E
1158	45	16	N
1159	318	12	N
1160	308	9	E
1161	308	20	N
1162	277	3	N
1163	318	11	N
1164	344	12	N
1165	355	28	S
1166	34	21	S
1167	9	26	S
1168	32	16	S
1169	260	11	S
1170	31	25	S
1171	54	21	S
1172	310	16	N
1173	10	15	S
1174	290	33	S
1175	290	16	S
1176	70	16	S
1177	330	10	S
1178	81	20	W
1179	352	24	S
1180	9	12	S
1181	79	16	N
1182	314	9	S
1183	330	8	S
1184	263	16	N
1185	345	12	S
1187	71	18	S
1186	89	18	E
1188	216	18	S
1189	215	15	S
1190	50	9	S
1192	41	17	S
1193	38	11	N
1194	328	6	N
1195	322	32	N
1196	217	10	S
1196	11	26	N
1197	324	25	E
1199	162	7	N
1200	102	8	S
1201	55	6	E
1202	3	19	N
1203	99	24	S
1204	326	24	S
1205	288	51	S
1207	42	12	S
1209	16	31	N
1210	352	18	N
1211	346	28	N
1212	284	5	N
1213	270	10	S
1214	94	21	E
1215	335	34	S
1216	278	11	N
1217	319	13	N
1218	315	8	E
1219	325	12	S
1220	12	17	N
1221	314	16	E
1222	180	20	E
1223	21	25	S
1224	265	25	N
1225	340	17	N
1226	235	11	S
1227	240	22	S
1228	47	19	S
1229	220	10	S
1230	69	22	S
1231	195	2	E
1232	20	35	W
1233	239	14	S
1234	290	4	S
1235	35	24	E
1236	0	22	N
1237	309	14	S
1238	240	22	S
1239	274	13	N
1240	346	24	E
1241	191	12	E
1242	198	38	S
1243	11	15	S
1244	56	18	W
1245	72	17	N
1246	311	8	N
1247	338	13	N
1248	336	10	S
1249	335	6	E
1251	155	17	E
1252	5	10	N
1253	134	18	N
1254	336	12	S
1255	18	45	N
1256	44	5	N

LINEATION (L2)

Station	Trend	Plunge

FOLDS (F2)

Station	Trend	Plunge

JOINTS

Station	Strike	Dip	Dir

FOLIATION (S2)				LINEATION (L2)			FOLDS (F2)			JOINTS			
Station	Strike	Dip	Dir	Station	Trend	Plunge	Station	Trend	Plunge	Station	Strike	Dip	Dir
1257	328	17	N										
1258	56	24	S										
1259	9	22	N										
1260	156	18	W										
1261	345	6	N										
1262	304	12	S										
1263	46	11	N										
1264	345	4	E										
1265	32	47	N										
1266	351	16	S										
1267	26	8	S										
1268	226	14	E										
1269	355	33	S										
1270	213	24	S										
1271	47	2	N										
1272	341	8	S										
1273	18	12	S										
1274	290	14	S										
1275	55	10	E										
1279	325	10	N										
1277	319	24	S										
1278	24	41	N										
1279	336	6	S										
1280	22	11	N										
1281	342	35	N										
1281	344	24	S										
1282	12	24	N										
1283	338	11	N										
1284	342	11	N										
1285	346	11	S										
1286	16	23	N										
1287	332	6	N										
1288	85	17	N										
1289	85	10	S										
1290	40	10	S										
1291	95	17	S										
1293	52	31	S										
1294	195	25	S										
1295	10	5	S										
1296	15	16	N										
1297	271	14	S										
1298	280	25	E										
1299	175	25	S										
1300	95	22	N										
1301	15	9	E										
1303	175	10	E										
1304	193	10	S										
1305	80	10	N										
1306	88	27	E										
1307	45	15	W										
1308	145	24	S										
1309	45	27	S										
1310	45	22	S										
1311	75	17	S										
1312	69	23	S										
1313	52	24	E										
1314	185	25	N										
1318	55	4	S										
1319	250	7	S										
1320	155	23	N										
1321	130	10	S										
1322	100	110	E										
1324	0	15	E										
1325	180	19	E										
1327	46	24	N										
1328	120	27	S										
1329	45	20	S										
1330	45	9	E										
1331	80	2	E										
1332	15	11	E										
1334	175	25	E										
1335	60	61	E										
1336	50	28	S										
1338	75	20	E										
1339	170	3	E										
1340	30	14	E										
1341	33	9	E										
1342	55	15	S										
1343	55	11	S										
1344	40	14	S										
1345	66	26	S										
1347	100	20	S										
1348	255	41	S										
1349	50	25	S										
1350	85	25	W										
1351	156	7	S										
1352	40	18	E										
1354	12	19	N										
1355	105	21	S										
1356	207	20	S										
1357	15	5	E										
1358	188	17	W										
1360	17	4	W										
1361	17	4	N										
1362	103	10	W										
1362	10	5	E										
1363	187	25	E										
1364	200	10	S										
1365	215	15	N										
1367	134	12	W										
1368	30	15	E										
1369	27	27	N										
1370	30	18	W										
1371	295	52	S										
1372	190	5	W										
1373	358	24	W										
1374	300	4	S										
1375	34	7	S										
1377	105	6	W										
1378	288	4	S										
1379	265	10	S										
1381	306	21	N										
1382	332	16	N										
1383	336	12	S										
1385	330	14	N										
1387	288	5	N										
1388	356	21	N										
1389	344	6	S										
1390	44	18	N										
1392	324	8	S										
1394	38	12	N										
1395	34	6	N										
1396	312	7	N										
1397	278	15	N										
1398	336	9	N										
1399	336	13	E										
1400	180	18	N										
1401	285	8	N										
1402	294	11	E										
1405	325	23	N										
1406	305	12	N										
1407	318	42	N										

FOLIATION (S2)				LINEATION (L2)			FOLDS (F2)			JOINTS			
Station	Strike	Dip	Dir	Station	Trend	Plunge	Station	Trend	Plunge	Station	Strike	Dip	Dir
1408	325	16	E										
1410	5	20	E										
1411	131	10	E										
1412	41	9	N										
1413	110	9	N										
1414	260	4	N										
1415	190	2	N										
1416	280	21	S										
1416	215	15	N										
1417	315	24	E										
1418	210	38	N										
1419	328	14	N										
1420	320	36	E										
1421	15	20	E										
1422	12	29	N										
1424	354	10	S										
1425	27	21	S										
1426	280	5	N										
1427	99	16	S										
1428	18	12	S										
1429	221	3	N										
1430	359	18	N										
1431	315	21	S										
1432	58	11	S										
1433	342	20	N										
1434	280	11	S										
1435	310	55	S										
1436	8	18	N										
1438	24	7	S										
1439	52	11	N										
1441	283	16	N										
1442	357	16	N										
1443	78	12	S										
1445	6	28	N										
1445	358	28	N										
1446	355	18	S										
1449	32	24	S										
1449	32	24	N										
1450	299	19	S										
1451	10	26	S										
1452	24	14	E										
1456	320	24	S										
1457	71	21	E										
1458	331	29	S										
1459	139	9	E										
1460	145	27	N										
1462	262	6	N										
1464	23	16	S										
1465	47	18	S										
1466	6	11	N										
1467	356	12	N										
1468	114	4	N										
1469	342	17	N										
1470	338	20	N										
1471	351	10	N										
1472	344	6	N										
1472	324	11	N										
1474	330	18	N										
1475	16	30	N										
1477	344	22	N										
1480	270	4	N										
1481	350	26	S										
1482	68	22	S										
1483	28	30	N										
1485	316	22	S										
1486	42	14	N										
1487	292	14	E										
1488	30	20	S										
1489	258	9	S										
1490	6	26	S										
1491	285	10	S										
1492	346	19	N										
1493	342	11	S										
1494	38	17	E										
1495	135	19	S										
1496	318	21	N										
1497	332	17	S										
1498	32	22	S										
1499	11	10	S										
1500	24	34	N										
1501	354	36	N										
1502	352	37	N										
1503	356	33	N										
1504	345	10	S										
1505	230	15	S										
1506	260	27	S										
1507	28	27	N										
1508	339	17	N										
1509	104	24	N										
1510	221	13	N										
1511	335	13	N										
1512	126	19	N										
1513	124	18	N										
1514	297	50	E										
1516	310	30	N										
1517	306	9	S										
1518	90	24	S										
1519	71	19	E										
1520	330	24	N										
1521	345	25	S										
1522	21	7	E										
1524	345	7	N										
1525	336	23	S										
1526	12	10	S										
1527	211	19	N										
1528	286	49	N										
1529	35	6	S										
1530	216	13	N										
1531	4	3	N										
1532	22	24	S										
1533	5	12	S										
1534	55	24	N										
1535	354	6	E										
1536	159	26	S										
1537	24	18	S										
1539	75	5	E										
1540	170	3	N										
1541	100	12	N										
1542	226	22	N										
1543	290	24	N										
1544	115	5	N										
1545	56	27	N										
1546	279	15	N										
1547	115	13	N										
1548	184	10	N										
1549	282	11	N										
1550	326	42	S										
1552	16	10	N										
1553	316	16	N										
1554	300	11	N										
1555	48	15	S										
1556	65	16	E										

FOLIATION (S2)

Station	Strike	Dip	Dir
1557	20	9	N
1558	348	10	N
1559	311	16	S
1560	106	10	N
1561	254	16	S
1562	111	11	E
1563	24	33	S
1564	89	18	N
1566	324	26	N
1567	148	7	S
1568	265	17	S
1569	270	21	S
1570	154	8	N
1572	336	10	N
1573	270	40	N
1575	352	27	N
1574	242	16	S
1576	226	26	N
1577	322	12	S
1578	237	26	S
1579	302	22	N
1580	334	10	N
1581	294	28	N
1582	56	4	N
1583	125	20	S
1584	210	8	S
1585	11	34	S
1586	38	35	S

LINEATION (L2)

Station	Trend	Plunge

FOLDS (F2)

Station	Trend	Plunge

JOINTS

Station	Strike	Dip	Dir

APPENDIX B

ELECTRON MICROPROBE DATA

GARNET ANALYSES

Sample cm126a (R212)

OXIDES WT %	R212(1)	R212(2)	R212(3)	R212(4)	R212(5)	R212(6)	R212(7)	R212(8)	STD. DEV
SIO2	37.29	37.23	37.23	36.89	37.56	37.47	37.44	37.21	0.24
TIO2	0.00	0.00	0.01	0.03	0.00	0.00	0.03	0.03	0.01
AL2O3	20.92	20.90	20.80	20.78	20.82	20.92	20.96	20.72	0.10
CR2O3	0.02	0.00	0.02	0.01	0.01	0.01	0.00	0.01	0.01
MGO	3.10	3.03	3.05	2.61	4.01	3.99	3.92	2.48	0.72
CAO	2.20	2.02	2.13	2.22	2.05	2.05	2.05	2.21	0.08
MNO	5.86	6.04	6.11	5.98	4.45	4.40	4.62	6.01	0.85
FEO	30.07	30.70	30.40	30.84	30.97	30.61	30.71	31.08	0.25
TOTAL	99.47	99.91	99.76	99.35	99.89	99.44	99.75	99.75	

Sample cm126a TR1A

OXIDES WT %	TR1A(1)	TR1A(2)	TR1A(3)	TR1A(4)	TR1A(5)	TR1A(6)	TR1A(7)	TR1A(8)	TR1A(9)	TR1A(10)	TR1A(11)	TR1A(12)	TR1A(13)	TR1A(14)	TR1A(15)	STD. DEV
SIO2	37.42	37.10	37.12	37.02	37.07	37.06	37.12	37.09	37.11	36.97	36.97	37.11	37.01	37.06	37.02	0.10
TIO2	0.03	0.01	0.00	0.02	0.01	0.00	0.00	0.00	0.01	0.00	0.01	0.00	0.00	0.01	0.00	0.01
AL2O3	20.88	20.81	20.88	20.91	20.93	20.88	20.89	21.00	20.95	20.92	20.91	20.84	20.83	20.97	20.82	0.05
CR2O3	0.02	0.00	0.01	0.02	0.01	0.00	0.02	0.02	0.00	0.00	0.04	0.00	0.02	0.01	0.01	0.01
MGO	2.39	2.72	2.79	2.93	2.96	3.02	3.07	3.01	3.07	3.08	3.10	3.17	3.15	3.09	3.09	0.21
CAO	2.27	2.18	2.15	2.11	2.09	1.97	2.00	2.04	2.02	1.96	2.01	2.03	2.02	2.05	2.05	0.06
MNO	6.20	6.39	6.48	6.47	6.71	6.71	6.75	6.70	6.74	6.56	6.69	6.48	6.78	6.65	6.60	0.16
FEO	30.82	30.71	30.44	30.11	30.36	29.93	30.33	30.39	30.28	30.16	30.21	29.78	30.13	30.04	29.98	0.28
TOTAL	100.02	99.92	99.86	99.59	100.13	99.57	100.18	100.25	100.18	99.65	99.93	99.42	99.93	99.88	99.58	

Sample cm126a TR1B

OXIDES WT %	TR1B(16)	TR1B(17)	TR1B(18)	TR1B(19)	TR1B(20)	TR1B(21)	TR1B(22)	TR1B(23)	TR1B(24)	TR1B(25)	TR1B(26)	TR1B(27))	TR1B(28)	TR1B(29)	TR1B(30)	STD. DEV
SIO2	37.12	36.94	37.18	37.02	36.85	37.01	37.00	37.22	36.96	37.14	37.20	37.15	37.25	37.05	37.00	0.33
TIO2	0.00	0.00	0.03	0.00	0.00	0.00	0.02	0.00	0.00	0.00	0.02	0.01	0.00	0.02	0.00	0.01
AL2O3	21.05	20.77	20.89	20.80	21.69	20.87	20.91	20.81	20.85	20.90	20.89	20.81	20.84	20.84	20.69	0.23
CR2O3	0.01	0.02	0.00	0.00	0.00	0.00	0.00	0.00	0.02	0.02	0.00	0.00	0.00	0.00	0.00	0.01
MGO	3.13	3.14	3.06	3.11	2.89	3.05	3.07	2.98	2.97	2.96	2.93	2.94	2.78	2.88	2.96	0.20
CAO	2.06	2.04	2.02	2.06	1.74	2.07	2.11	2.14	2.10	2.10	2.08	2.08	2.14	2.21	2.17	0.10
MNO	6.64	6.68	6.57	6.46	5.55	6.72	6.57	6.65	6.56	6.67	6.45	6.59	6.44	6.41	6.49	0.28
FEO	30.23	30.04	29.95	29.96	29.36	30.07	29.94	30.07	29.90	30.23	30.15	30.22	30.38	30.62	31.01	0.36
TOTAL	100.24	99.63	99.69	99.43	97.08	99.78	99.61	99.86	99.37	100.04	99.73	99.80	99.83	99.83	99.71	

Sample cm427 TR121

OXIDES WT %	TR121(25)	TR121(26)	TR121(27)	TR121(28)	TR121(29)	TR121(30)	TR121(31)	STD. DEV
SIO2	36.71	36.92	37.09	37.07	37.14	36.59	36.72	0.25
TIO2	0.00	0.00	0.00	0.02	0.02	0.04	0.05	0.02
AL2O3	20.85	20.94	20.74	20.76	20.81	20.63	20.64	0.08
CR2O3	0.05	0.00	0.04	0.00	0.00	0.01	0.00	0.02
MGO	2.82	2.92	3.18	3.10	3.10	2.11	2.09	0.56
CAO	1.88	1.80	2.38	2.30	2.32	1.79	1.75	0.33
MNO	5.58	5.40	4.20	4.56	4.89	6.25	6.29	0.97
FEO	31.85	31.81	32.03	32.21	31.83	32.12	31.85	0.16
TOTAL	99.74	99.79	99.68	100.10	100.11	99.53	99.40	

Sample cm427 TR128

OXIDES WT %	TR128(1)	TR128(1)	TR128(1)	TR128(1)	TR128(1)	TR128(1)	TR128(1)	STD. DEV
SIO2	36.26	36.87	36.93	36.74	36.60	36.67	36.96	0.16
TIO2	0.00	0.02	0.00	0.01	0.03	0.03	0.00	0.01
AL2O3	20.43	20.80	20.62	20.73	20.72	20.72	20.87	0.09
CR2O3	0.00	0.00	0.00	0.00	0.03	0.02	0.00	0.01
MGO	2.54	2.53	2.43	2.62	2.57	2.58	2.25	0.15
CAO	1.77	1.78	1.74	1.86	1.90	1.77	1.77	0.07
MNO	5.00	5.18	5.15	5.11	5.23	5.13	5.17	0.05
FEO	33.01	32.92	33.18	32.91	32.91	33.32	33.18	0.18
TOTAL	99.00	100.07	100.05	99.98	99.99	100.23	100.18	

Sample cm677 TR2(5)

OXIDES WT %	TR2(5)A	TR2(5)B	TR2(5)C	TR2(5)D	TR2(5)E	TR2(5)A	TR2(5)F	TR2(5)G	TR2(5)H	TR2(5)I	TR2(5)J	TR2(5)K	TR2(5)L	TR2(5)M	TR2(5)N	TR2(5)O	TR2(5)Q
SIO2	37.22	37.16	36.96	36.64	36.78	36.95	36.90	35.11	37.13	37.03	37.13	36.93	37.03	36.84	36.76	36.95	36.83
TIO2	0.04	0.00	0.00	0.03	0.01	0.00	0.01	0.00	0.01	0.02	0.00	0.03	0.01	0.01	0.02	0.00	0.00
AL2O3	20.93	20.91	20.68	20.63	20.50	20.53	20.57	20.72	20.64	20.69	20.62	20.67	20.69	21.00	20.63	20.64	20.86
CR2O3	0.04	0.00	0.01	0.00	0.00	0.00	0.01	0.00	0.03	0.00	0.00	0.00	0.00	0.06	0.03	0.01	0.02
MGO	2.45	2.74	2.86	2.92	2.87	2.86	2.83	2.79	2.83	2.95	2.88	2.91	2.88	2.93	2.90	2.85	2.86
CAO	0.68	0.64	0.67	0.73	0.96	1.07	1.10	1.01	1.10	1.09	1.18	1.11	1.12	0.73	0.70	0.65	0.74
MNO	1.41	1.86	1.94	2.16	2.14	2.23	2.23	2.04	2.17	2.09	2.19	2.22	2.22	2.26	2.20	2.04	1.74
FEO	37.98	37.11	36.88	36.42	36.14	36.21	36.18	37.22	36.33	36.37	36.10	36.23	36.04	36.37	36.03	36.58	37.03
TOTAL	100.73	100.42	100.00	99.53	99.39	99.87	99.83	98.89	100.25	100.23	100.11	100.11	99.99	100.20	99.26	99.71	100.08

Sample cm677 TR2(5)

OXIDES WT % TR2(5)R	TR2(5)S	TR2(5)T	TR2(5)U	TR2(5)V	TR2(5)W	TR2(5)X	TR2(5)Y	TR2(5)Z	STD_DEV
SIO2	36.80	36.69	37.03	37.12	36.59	36.56	36.93	36.67	36.59	0.40
TIO2	0.01	0.01	0.03	0.00	0.00	0.03	0.00	0.02	0.00	0.01
AL2O3	20.63	20.66	20.67	20.84	20.62	20.50	20.76	20.67	20.56	0.13
CR2O3	0.01	0.00	0.00	0.01	0.04	0.03	0.00	0.00	0.03	0.02
MGO	2.49	2.69	2.48	2.57	2.43	2.45	2.90	2.81	2.59	0.18
CAO	0.69	0.71	0.71	0.71	0.73	0.72	0.80	0.67	0.67	0.19
MNO	1.41	1.58	1.15	1.40	1.28	1.27	2.17	1.90	1.37	0.38
FEO	37.80	37.05	37.66	37.78	37.88	38.04	36.25	37.19	37.34	0.69
TOTAL	99.84	99.37	99.94	100.41	99.58	99.58	99.81	99.92	99.14	

Sample12-2-4 R2(32)

OXIDES WT % R2(32)1	R2(32)2	R2(32)3	R2(32)4	R2(32)5	R2(32)6	R2(32)7	STD_DEV
SIO2	36.38	36.58	37.06	37.18	36.95	36.93	37.19	0.13
TIO2	0.01	0.02	0.00	0.00	0.02	0.00	0.03	0.01
AL2O3	20.47	20.48	20.96	20.92	20.89	21.09	20.97	0.08
CR2O3	0.00	0.00	0.01	0.00	0.03	0.02	0.04	0.01
MGO	2.60	2.87	4.11	3.96	4.14	3.01	3.01	0.58
CAO	2.54	2.31	1.66	1.61	1.66	2.06	2.01	0.21
MNO	8.29	8.21	6.77	7.52	7.05	8.39	8.15	0.69
FEO	28.67	29.06	26.26	26.81	29.36	28.62	29.07	0.40
TOTAL	99.16	99.54	98.89	100.00	100.12	100.33	100.47	

Sample12-2-4 R2(34)

OXIDES WT % R2(34)1	R2(34)2	R2(34)3	R2(34)4	R2(34)5	R2(34)6	R2(34)7	R2(34)8	R2(34)9	R2(34)10	R2(34)11	R2(34)12	R2(34)13	R2(34)14	STD_DEV
SIO2	36.82	37.33	36.99	37.48	37.33	37.23	37.17	37.37	37.42	37.27	37.25	36.72	37.31	36.96	0.22
TIO2	0.00	0.00	0.00	0.03	0.01	0.00	0.00	0.00	0.02	0.02	0.01	0.01	0.03	0.03	0.01
AL2O3	20.58	20.99	20.94	20.83	21.02	21.18	21.11	20.98	21.04	20.91	20.78	20.71	20.82	20.65	0.16
CR2O3	0.02	0.05	0.00	0.01	0.04	0.02	0.06	0.02	0.00	0.01	0.05	0.05	0.03	0.03	0.02
MGO	2.80	3.67	3.90	4.08	4.17	4.05	4.22	3.78	3.54	2.48	2.88	2.89	2.94	3.13	0.61
CAO	2.47	1.78	1.88	1.75	1.82	1.89	1.51	1.73	1.72	3.39	2.37	2.35	2.34	1.96	0.51
MNO	8.05	7.82	7.44	6.87	6.65	7.05	6.72	7.81	8.34	7.94	7.89	8.19	8.05	8.44	0.65
FEO	29.17	28.70	29.13	29.17	29.25	29.05	29.48	28.86	28.32	28.86	29.14	28.87	28.78	28.98	0.29
TOTAL	99.91	100.33	100.27	100.23	100.30	100.27	100.26	100.55	100.40	100.87	100.35	99.79	100.30	100.18	

Sample cm501 TR1

OXIDES WT %	TR1(1)	TR1(2)	TR1(3)	TR1(4)	TR1(5)	TR1(6)	TR1(7)	TR1(8)	TR1(9)	TR1(10)	TR1(11)	TR1(12)	TR1(13)	TR1(14)	TR1(15)	TR1(16)	TR1(17)	TR1(18)	TR1(19)	TR1(20)	STD_DEV
SIO2	36.41	36.64	36.53	36.83	36.78	36.79	36.85	36.89	36.79	36.78	36.97	36.44	36.32	36.59	36.42	36.58	36.71	36.67	36.52	36.95	0.13
TIO2	0.01	0.00	0.00	0.00	0.03	0.02	0.00	0.03	0.02	0.00	0.01	0.02	0.04	0.11	0.03	0.02	0.00	0.00	0.00	0.04	0.01
AL2O3	20.35	20.44	20.51	20.68	20.65	20.64	20.74	20.70	20.59	20.56	20.68	20.31	20.47	20.62	20.64	20.67	20.51	20.60	20.60	20.47	0.08
CR2O3	0.00	0.01	0.01	0.02	0.00	0.01	0.00	0.05	0.04	0.00	0.04	0.03	0.00	0.03	0.06	0.02	0.05	0.00	0.03	0.02	0.02
MGO	2.43	2.80	2.88	3.01	3.06	3.07	3.14	3.13	3.08	3.14	3.13	3.41	3.22	3.14	3.06	3.03	2.96	2.95	2.86	2.80	0.10
CAO	1.43	1.29	1.27	1.21	1.24	1.18	1.17	1.19	1.20	1.20	1.15	1.12	1.12	1.10	1.13	1.20	1.23	1.25	1.29	1.34	0.04
MNO	3.52	3.52	3.59	3.57	3.60	3.60	3.52	3.67	3.53	3.65	3.59	3.50	3.70	3.61	3.66	3.62	3.65	3.70	3.52	3.63	0.05
FEO	35.33	34.77	34.74	34.74	34.37	34.42	34.44	34.45	34.52	34.79	34.24	34.68	34.80	34.86	34.74	34.75	34.65	34.73	34.90	35.28	0.17
TOTAL	99.50	99.47	99.53	100.05	99.73	99.73	99.85	100.11	99.77	100.10	99.80	99.51	99.66	100.06	99.77	99.90	99.78	99.91	99.72	100.34	

Sample cm501 TR1

OXIDES WT %	TR1(21)	TR1(22)	TR1(23)	TR1(24)	TR1(25)	TR1(26)	TR1(27)	TR1(28)	TR1(29)	TR1(30)	TR1(31)	TR1(32)	TR1(33)	TR1(34)	TR1(35)	TR1(36)	TR1(37)	TR1383)	TR1(39)	TR1(40)	STD_DEV
SIO2	36.84	36.52	36.38	36.57	36.73	36.86	36.63	36.63	36.70	36.92	36.78	37.09	36.56	36.94	36.90	37.11	36.86	37.12	36.82	36.82	0.16
TIO2	0.08	0.00	0.00	0.01	0.01	0.01	0.00	0.02	0.00	0.02	0.02	0.00	0.02	0.02	0.01	0.03	0.04	0.01	0.01	0.05	0.01
AL2O3	20.77	20.71	20.58	20.54	20.55	20.51	20.52	20.47	20.49	20.55	20.55	20.78	20.45	20.68	20.58	20.66	20.63	20.69	20.64	20.63	0.04
CR2O3	0.00	0.00	0.01	0.00	0.00	0.00	0.01	0.02	0.01	0.03	0.03	0.03	0.00	0.05	0.00	0.04	0.03	0.00	0.02	0.04	0.01
MGO	2.50	2.83	2.87	2.94	2.97	3.03	2.99	3.03	3.09	3.08	3.11	3.08	3.14	3.11	3.11	3.10	3.12	3.08	3.10	3.10	0.08
CAO	1.36	1.29	1.27	1.21	1.22	1.26	1.21	1.27	1.25	1.20	1.17	1.16	1.08	1.11	1.09	1.19	1.16	1.11	1.16	1.09	0.03
MNO	3.52	3.44	3.50	3.61	3.62	3.60	3.53	3.65	3.53	3.51	3.48	3.58	3.51	3.68	3.56	3.64	3.69	3.62	3.72	3.65	0.06
FEO	35.05	34.68	34.73	34.69	34.72	34.74	34.73	34.28	34.36	34.60	34.79	34.66	34.74	34.76	34.61	34.27	34.40	34.47	34.80	34.59	0.18
TOTAL	100.13	99.47	99.33	99.57	99.81	100.01	99.62	99.36	99.44	99.91	99.93	100.35	99.50	100.34	99.86	100.03	99.92	100.09	100.08	99.97	

Sample cm501 TR1(6)

OXIDES WT %	TR1(6)1	TR1(6)2	TR1(6)3	TR1(6)4	TR1(6)5	TR1(6)6	TR1(6)7	TR1(6)8	TR1(6)9	TR1(6)10	TR1(6)11	TR1(6)12	TR1(6)13	STD_DEV
SIO2	36.67	36.71	37.00	36.81	36.83	36.95	36.96	36.74	36.70	36.96	36.95	37.10	37.07	0.10
TIO2	0.00	0.00	0.00	0.00	0.00	0.00	0.04	0.02	0.01	0.06	0.06	0.01	0.00	0.02
AL2O3	20.75	20.82	20.79	20.74	20.66	20.86	20.71	20.75	20.52	20.77	20.87	20.63	20.68	0.07
CR2O3	0.00	0.00	0.00	0.06	0.04	0.00	0.00	0.01	0.02	0.00	0.02	0.01	0.03	0.02
MGO	2.40	2.45	2.58	2.77	2.88	2.97	3.04	3.00	3.07	3.05	3.04	3.02	3.08	0.17
CAO	1.29	1.28	1.34	1.48	1.33	1.44	1.57	1.52	1.57	1.49	1.56	1.44	1.55	0.10
MNO	3.60	3.56	3.40	3.40	3.45	3.51	3.59	3.56	3.59	3.55	3.51	3.61	3.60	0.08
FEO	35.20	35.04	34.84	34.67	34.54	34.25	34.60	34.07	33.95	34.71	33.96	33.91	33.84	0.29
TOTAL	99.90	99.86	99.94	99.93	99.73	99.97	100.51	99.67	99.44	100.58	99.98	99.72	99.85	

Sample cm175 TR1(20)

OXIDES WT %	TR1 (20) 1	TR1 (20) 2	TR1 (20) 3	TR1 (20) 4	TR1 (20) 5	TR1 (20) 6	TR1 (20) 7	TR1 (20) 8	TR1 (20) 9	TR1 (20) 10	TR1 (20) 11	TR1 (20) 12	TR1 (20) 13	TR1 (20) 14
SIO2	37.55	36.59	36.76	36.87	36.96	36.90	37.03	36.90	37.24	37.34	36.98	36.81	37.07	37.04
TIO2	0.00	0.00	0.00	0.00	0.00	0.01	0.01	0.03	0.00	0.02	0.02	0.02	0.02	0.01
AL2O3	21.23	20.99	20.90	20.94	20.75	21.05	20.84	20.76	20.82	21.27	20.73	20.73	21.04	20.82
CR2O3	0.03	0.00	0.03	0.01	0.00	0.00	0.02	0.01	0.00	0.00	0.04	0.03	0.00	0.00
MGO	2.35	2.63	2.79	2.80	2.91	2.91	2.94	2.87	2.90	2.76	2.94	2.96	2.91	2.98
CAO	1.07	0.98	1.08	1.26	1.34	1.25	1.29	1.42	1.21	1.14	1.21	1.14	1.21	1.16
MNO	3.75	4.08	4.37	4.23	4.41	4.45	4.53	4.51	4.36	4.44	4.40	4.18	4.47	4.38
FEO	34.94	34.59	34.08	33.68	33.73	33.70	33.41	33.52	33.11	33.67	33.59	33.21	32.95	33.48
TOTAL	100.92	99.87	100.01	99.79	100.11	100.27	100.07	100.02	99.65	100.55	99.91	99.08	99.66	99.86

OXIDES WT %	TR1 (20) 18	TR1 (20) 17	TR1 (20) 19	TR1 (20) 20	TR1 (20) 21	TR1 (20) 22	TR1 (20) 23	TR1 (20) 24	TR1 (20) 25	TR1 (20) 26	TR1 (20) 28	TR1 (20) 29	TR1 (20) 30	STD DEV
SIO2	36.97	36.79	37.13	36.99	36.94	36.95	37.21	37.02	37.03	36.93	37.01	36.80	36.22	0.94
TIO2	0.02	0.00	0.02	0.00	0.02	0.01	0.00	0.00	0.00	0.01	0.00	0.01	0.04	0.03
AL2O3	20.91	20.80	20.91	20.76	20.64	20.85	20.94	21.00	20.81	20.85	20.85	20.85	20.29	0.66
CR2O3	0.00	0.00	0.00	0.00	0.03	0.02	0.00	0.02	0.01	0.00	0.00	0.00	0.02	0.01
MGO	2.93	2.95	2.93	2.96	2.87	2.90	2.82	2.89	2.88	2.89	2.71	2.63	2.32	0.02
CAO	1.16	1.20	1.23	1.22	1.25	1.25	1.21	1.23	1.22	1.17	1.12	1.06	1.13	0.04
MNO	4.50	4.32	4.35	4.53	4.44	4.37	4.36	4.30	4.45	4.33	4.17	4.14	3.71	0.03
FEO	33.69	33.52	33.58	33.55	33.88	33.11	33.26	33.70	33.50	33.79	33.91	34.45	35.16	0.16
TOTAL	100.18	99.38	100.14	100.01	100.07	99.46	99.83	100.16	99.90	99.97	99.77	99.95	98.89	

BIOTITE ANALYSES

Sample cm126a TR1(31)

OXIDES WT %	TR1(31)40	TR1(31)41	STD. DEV
SIO2	35.09	35.02	0.05
TIO2	3.90	3.53	0.26
AL2O3	17.53	17.75	0.15
MGO	7.96	8.03	0.12
MNO	0.18	0.13	0.04
FEO	21.03	20.89	0.10
CAO	0.00	0.00	0.00
NA2O	0.19	0.16	0.02
K2O	9.83	9.63	0.15
H2O	3.82	3.80	0.01
F	0.14	0.17	0.02
CL	0.04	0.03	0.01
TOTAL	99.82	99.14	

Sample cm126a R2(12)

OXIDES WT %	R2(12)9	R2(12)10	R2(12)11	R2(12)12	R2(12)13	STD. DEV
SIO2	34.90	34.88	34.88	35.01	35.29	0.18
TIO2	3.52	2.85	2.84	3.51	3.06	0.34
AL2O3	17.54	17.85	17.40	17.61	18.47	0.42
MGO	7.89	8.24	8.38	8.22	7.81	0.24
MNO	0.15	0.09	0.14	0.06	0.06	0.04
FEO	21.20	20.85	21.34	21.27	20.11	0.51
CAO	0.00	0.00	0.00	0.00	0.00	0.00
NA2O	0.17	0.14	0.14	0.18	0.17	0.02
K2O	9.69	9.59	9.62	9.79	9.15	0.25
H2O	3.84	3.77	3.82	3.86	3.86	0.04
F	0.05	0.18	0.06	0.07	0.03	0.06
CL	0.04	0.03	0.01	0.04	0.01	0.01
TOTAL	99.00	98.48	98.58	99.61	98.02	

Sample cm126a R2(12)

OXIDES WT %	R2(12)23	R2(12)24	R2(12)25	R2(12)26	R2(12)27	STD. DEV
SIO2	35.05	35.03	34.86	35.48	35.25	0.24
TIO2	3.28	3.36	3.28	3.43	3.33	0.06
AL2O3	17.85	17.96	18.05	18.30	18.21	0.18
MGO	8.01	7.96	7.85	7.96	8.01	0.07
MNO	0.19	0.19	0.17	0.16	0.20	0.01
FEO	20.75	21.09	20.10	20.84	20.10	0.45
CAO	0.00	0.00	0.00	0.00	0.00	0.00
NA2O	0.21	0.23	0.20	0.22	0.16	0.03
K2O	9.74	9.83	9.58	9.83	9.72	0.07
H2O	3.80	3.83	3.70	3.91	3.75	0.10
F	0.17	0.53	0.30	0.03	0.30	0.19
CL	0.02	0.04	0.04	0.05	0.02	0.02
TOTAL	99.08	99.67	98.14	100.01	99.05	

Sample cm427 R2(6)

OXIDES WT %	R2(6)40	R2(6)41	R2(6)42	STD. DEV
SIO2	34.92	34.41	34.70	0.26
TIO2	3.58	3.48	3.49	0.05
AL2O3	17.27	17.11	17.40	0.14
MGO	7.83	7.67	7.55	0.14
MNO	0.17	0.12	0.21	0.05
FEO	21.98	22.73	22.22	0.38
CAO	0.00	0.00	0.00	0.00
NA2O	0.11	0.15	0.18	0.03
K2O	9.67	9.51	9.65	0.09
H2O	3.71	3.66	3.67	0.02
F	0.31	0.35	0.37	0.03
CL	0.06	0.07	0.06	0.01
TOTAL	99.61	99.24	99.49	

Sample cm427 R2(6)

OXIDES WT %	R2(6)32	R2(6)33	STD. DEV
SIO2	35.38	35.11	0.19
TIO2	3.41	3.29	0.08
AL2O3	18.29	17.99	0.21
MGO	8.10	8.16	0.05
MNO	0.13	0.10	0.02
FEO	20.01	20.30	0.20
CAO	0.00	0.00	0.00
NA2O	0.18	0.16	0.01
K2O	9.21	9.72	0.36
H2O	3.78	3.70	0.06
F	0.22	0.36	0.10
CL	0.06	0.06	0.00
TOTAL	98.78	98.97	

Sample cm427 TR1(22)

OXIDES WT %	TR1(22)11	TR1(22)12	TR1(22)13	TR1(22)14	STD. DEV
SIO2	35.08	35.28	35.34	35.62	0.13
TIO2	3.11	3.25	3.22	3.24	0.07
AL2O3	19.04	18.31	18.04	18.19	0.52
MGO	8.15	8.34	8.62	8.57	0.23
MNO	0.14	0.06	0.17	0.07	0.06
FEO	19.59	20.32	19.93	20.16	0.37
CAO	0.00	0.00	0.00	0.00	0.00
NA2O	0.18	0.19	0.18	0.15	0.01
K2O	9.16	9.42	9.58	9.60	0.21
H2O	3.82	3.75	3.75	3.84	0.04
F	0.14	0.32	0.29	0.16	0.09
CL	0.07	0.06	0.06	0.05	0.01
TOTAL	98.48	99.30	99.19	99.68	

Sample cm427 TR1(28)

OXIDES WT %	TR1(28)8	TR1(28)9	TR1(28)9	STD. DEV
SIO2	34.17	34.24	35.15	0.55
TIO2	3.30	3.33	3.42	0.07
AL2O3	17.24	17.46	17.99	0.39
MGO	7.77	8.15	7.96	0.19
MNO	0.11	0.14	0.12	0.02
FEO	20.22	21.36	21.46	0.69
CAO	0.00	0.00	0.00	0.00
NA2O	0.13	0.17	0.14	0.02
K2O	9.34	9.42	9.54	0.10
H2O	3.58	3.79	3.73	0.11
F	0.37	0.05	0.33	0.17
CL	0.07	0.07	0.08	0.01
TOTAL	96.29	98.19	99.93	

Sample cm677 TR2(5)

OXIDES WT %	TR2(5)AA	TR2(5)BB	TR2(5)CC	TR2(5)DD	TR2(5)EE	TR2(5)FF	TR2(5)GG	STD. DEV
SIO2	34.75	34.94	35.05	35.06	35.04	35.36	35.22	0.19
TIO2	2.60	1.79	1.86	2.11	2.14	2.35	1.73	0.58
AL2O3	18.65	19.33	18.97	18.84	19.23	18.91	19.20	0.48
MGO	7.91	8.52	8.57	8.15	8.44	8.23	8.48	0.43
MNO	0.00	0.01	0.04	0.00	0.06	0.04	0.01	0.01
FEO	21.18	20.64	20.70	20.77	20.55	20.67	20.72	0.38
CAO	0.00	0.00	0.00	0.00	0.00	0.00	0.00	0.00
NA2O	0.30	0.32	0.31	0.32	0.37	0.37	0.34	0.02
K2O	9.28	9.05	9.16	9.07	9.10	9.10	9.19	0.16
H2O	3.62	3.68	3.65	3.68	3.79	3.79	3.75	0.04
F	0.50	0.43	0.48	0.40	0.23	0.23	0.31	0.08
CL	0.05	0.04	0.05	0.04	0.04	0.04	0.04	0.01
TOTAL	98.84	98.75	98.85	98.45	99.01	99.09	98.99	

Sample cm677 PP(24)

OXIDES WT %	PP(24)E	PP(24)F	STD. DEV
SIO2	33.24	34.71	1.04
TIO2	2.78	2.82	0.03
AL2O3	17.91	18.90	0.70
MGO	8.21	7.52	0.49
MNO	0.02	0.03	0.01
FEO	22.22	21.02	0.85
CAO	0.00	0.00	0.00
NA2O	0.19	0.25	0.04
K2O	8.03	8.88	0.60
H2O	3.65	3.67	0.01
F	0.22	0.38	0.11
CL	0.06	0.07	0.00
TOTAL	96.53	98.25	

Sample12-2-4 R2(34a)

OXIDES WT %	R2(34a)6	R2(34a)7	R2(34a)8	R2(34a)9	R2(34a)10	STD. DEV
SIO2	35.28	35.08	35.42	35.09	35.20	0.14
TIO2	2.77	2.30	2.49	1.89	1.67	0.34
AL2O3	17.73	17.99	17.99	18.27	18.50	0.19
MGO	9.88	9.77	9.83	9.74	9.43	0.07
MNO	0.14	0.16	0.18	0.10	0.12	0.02
FEO	19.46	19.51	19.72	18.47	18.11	0.03
CAO	0.00	0.00	0.00	0.00	0.00	0.00
NA2O	0.19	0.18	0.18	0.12	0.11	0.01
K2O	9.55	9.60	9.77	8.62	8.37	0.03
H2O	3.84	3.76	3.75	3.71	3.69	0.06
F	0.09	0.25	0.34	0.25	0.24	0.11
CL	0.09	0.06	0.06	0.07	0.08	0.02
TOTAL	98.81	98.65	99.73	98.33	96.51	

Sample12-2-4 R2(34b)

OXIDES WT %	R2(34b)16	R2(34b)17	R2(34b)18	R2(34b)19	STD. DEV
SIO2	35.84	35.41	35.34	35.20	0.30
TIO2	2.52	2.65	2.82	2.67	0.09
AL2O3	18.11	17.62	17.65	17.62	0.35
MGO	9.56	9.70	9.55	9.46	0.10
MNO	0.14	0.16	0.14	0.03	0.01
FEO	19.12	19.87	19.85	20.16	0.53
CAO	0.00	0.00	0.00	0.00	0.00
NA2O	0.17	0.19	0.17	0.19	0.01
K2O	9.39	9.74	9.77	9.60	0.25
H2O	3.81	3.86	3.72	3.74	0.04
F	0.20	0.08	0.37	0.29	0.08
CL	0.09	0.07	0.08	0.07	0.02
TOTAL	98.64	99.34	99.48	99.03	

Sample12-2-4 R2(34c)

OXIDES WT %	R2(34)20	R2(34c)21	STD. DEV
SIO2	35.42	35.90	0.33
TIO2	2.01	2.01	0.00
AL2O3	18.30	18.60	0.21
MGO	10.14	10.05	0.06
MNO	0.13	0.17	0.03
FEO	19.13	19.13	0.00
CAO	0.00	0.00	0.00
NA2O	0.21	0.14	0.05
K2O	9.56	9.73	0.12
H2O	3.86	3.74	0.08
F	0.08	0.41	0.23
CL	0.10	0.08	0.01
TOTAL	98.94	99.97	

Sample12-2-4 R2(34d)

OXIDES WT %	R2(34d)22	R2(34d)23	STD. DEV
SIO2	35.78	35.06	0.51
TIO2	2.26	2.94	0.48
AL2O3	18.10	17.28	0.58
MGO	9.68	9.61	0.05
MNO	0.21	0.22	0.01
FEO	19.26	20.44	0.84
CAO	0.00	0.00	0.00
NA2O	0.16	0.17	0.00
K2O	9.44	9.83	0.28
H2O	3.62	3.75	0.10
F	0.60	0.27	0.23
CL	0.08	0.08	0.00
TOTAL	99.18	99.86	

Sample cm501 TR1(4b)

OXIDES WT %	TR1(4b)14	TR1(4b)15	TR1(4b)16	TR1(4b)17	TR1(4b)18	STD. DEV
SIO2	34.50	34.67	35.60	34.98	34.88	0.12
TIO2	2.40	2.47	2.38	2.50	2.50	0.05
AL2O3	18.24	17.89	18.55	18.58	18.48	0.25
MGO	9.40	8.89	8.85	8.58	8.61	0.36
MNO	0.16	0.15	0.10	0.06	0.01	0.01
FEO	20.13	20.91	19.53	19.75	20.10	0.55
CAO	0.00	0.00	0.00	0.00	0.00	0.00
NA2O	0.18	0.14	0.20	0.17	0.16	0.03
K2O	9.39	9.02	9.58	9.48	9.56	0.26
H2O	0.00	0.00	0.00	0.00	0.00	0.00
F	0.46	0.30	0.15	0.35	0.14	0.11
CL	0.09	0.08	0.03	0.07	0.05	0.01
TOTAL	94.96	94.53	94.97	94.45	94.49	

Sample cm501 TR1(4a)

OXIDES WT %	TR1(4a)27	TR1(4a)28	TR1(4a)29	STD. DEV
SIO2	35.24	34.72	35.05	0.37
TIO2	2.47	2.60	2.58	0.09
AL2O3	17.95	17.86	17.97	0.06
MGO	8.97	8.94	8.85	0.02
MNO	0.09	0.08	0.07	0.01
FEO	20.03	20.46	20.74	0.31
CAO	0.00	0.00	0.00	0.00
NA2O	0.17	0.14	0.18	0.02
K2O	9.36	9.55	9.29	0.13
H2O	3.82	3.80	3.77	0.02
F	0.12	0.12	0.22	0.00
CL	0.01	0.03	0.03	0.01
TOTAL	98.21	98.29	98.73	

Sample cm501 TR1(4)

OXIDES WT %	TR1(4)30	TR1(4)29a	TR1(4)31	TR1(4)32	STD. DEV
SIO2	34.45	35.05	35.21	33.36	0.42
TIO2	2.25	2.30	2.50	1.82	0.04
AL2O3	17.48	17.45	17.72	18.07	0.01
MGO	9.17	9.09	9.11	9.36	0.05
MNO	0.14	0.08	0.07	0.05	0.04
FEO	21.04	20.90	20.11	22.30	0.10
CAO	0.00	0.00	0.00	0.00	0.00
NA2O	0.13	0.16	0.15	0.13	0.02
K2O	9.01	9.47	9.45	7.35	0.33
H2O	3.60	3.62	3.68	3.76	0.02
F	0.45	0.49	0.39	0.01	0.03
CL	0.05	0.03	0.02	0.04	0.01
TOTAL	97.73	98.64	98.42	98.26	

Sample cm175 TR1(20a)

OXIDES WT %	TR1(20a)3	TR1(20a)4	TR1(20a)5	TR1(20a)6	TR1(20a)7	TR1(20a)8	TR1(20a)9	STD. DEV
SIO2	35.11	33.17	35.12	35.36	35.18	35.14	34.95	0.76
TIO2	2.87	2.45	2.14	1.81	1.83	1.67	2.56	0.45
AL2O3	18.22	17.55	18.68	18.97	18.87	18.90	18.36	0.51
MGO	8.86	8.25	8.98	9.27	9.16	9.30	8.75	0.37
MNO	0.05	0.06	0.03	0.04	0.05	0.09	0.09	0.03
FEO	20.63	23.99	20.30	20.39	20.18	19.70	20.46	1.43
CAO	0.00	0.00	0.00	0.00	0.00	0.00	0.00	0.00
NA2O	0.29	0.28	0.28	0.30	0.29	0.32	0.28	0.01
K2O	9.36	8.65	9.36	9.23	9.28	9.39	9.07	0.26
H2O	3.84	3.63	3.76	3.91	3.79	3.70	3.73	0.09
F	0.14	0.32	0.27	0.00	0.20	0.38	0.29	0.13
CL	0.03	0.04	0.05	0.06	0.05	0.05	0.05	0.01
TOTAL	99.39	98.39	98.97	99.33	98.88	98.64	98.60	

Sample cm175 TR1(20b)

OXIDES WT %	TR1(20b)10	TR1(20b)11	STD. DEV
SIO2	35.09	35.25	0.11
TIO2	1.50	1.48	0.02
AL2O3	18.90	19.17	0.19
MGO	9.23	8.94	0.21
MNO	0.08	0.10	0.01
FEO	20.68	19.55	0.80
CAO	0.00	0.00	0.00
NA2O	0.22	0.31	0.06
K2O	8.76	9.10	0.24
H2O	3.73	3.69	0.03
F	0.31	0.40	0.06
CL	0.06	0.03	0.02
TOTAL	98.57	98.01	

PLAGIOCLASE ANALYSES

Sample cm126a TR1(31)

OXIDES WT%	TR1(31)37	TR1(31)38	TR1(31)39	STD. DEV.
SIO2	59.66	59.27	59.65	0.22
BAO	0.14	0.00	0.00	0.08
AL2O3	25.94	25.82	25.44	0.26
CAO	7.63	7.54	7.48	0.09
FEO	0.08	0.03	0.18	0.07
NA2O	7.34	7.27	7.35	0.04
K2O	0.06	0.11	0.06	0.03
TOTAL	100.85	100.04	100.13	

Sample cm126a R2(13)

OXIDES WT%	R2(13)28	R2(13)31	R2(13)32	R2(13)33	R2(13)34	R2(13)35	R2(13)36	STD. DEV.
SIO2	60.47	59.73	59.57	60.10	59.63	59.27	59.12	0.46
BAO	0.00	0.00	0.11	0.00	0.00	0.02	0.00	0.04
AL2O3	25.13	25.95	25.94	25.15	25.67	25.88	26.31	0.44
CAO	6.84	7.53	7.70	6.94	7.66	7.86	8.00	0.48
FEO	0.18	0.05	0.07	0.13	0.15	0.07	0.08	0.05
NA2O	7.79	7.20	7.20	7.75	7.22	7.17	6.83	0.34
K2O	0.07	0.08	0.11	0.08	0.10	0.16	0.12	0.03
TOTAL	100.26	100.55	100.70	100.15	100.43	100.23	100.44	

Sample 427 R1(21)

OXIDES WT%	R1(21)15	R1(21)16	R1(21)17	R1(21)18	R1(21)19	R1(21)20	STD. DEV.
SIO2	62.09	60.12	62.51	60.84	60.52	60.75	1.28
BAO	0.14	0.00	0.08	0.00	0.01	0.08	0.07
AL2O3	23.76	24.68	23.84	24.70	24.84	24.79	0.51
CAO	5.32	6.57	5.14	6.35	6.38	6.37	0.78
FEO	0.00	0.00	0.02	0.00	0.00	0.03	0.01
NA2O	8.57	7.99	8.42	7.77	7.95	7.86	0.30
K2O	0.10	0.15	0.08	0.13	0.15	0.15	0.03
TOTAL	100.00	99.51	100.09	99.80	99.85	100.04	

Sample cm427 TR1(21)

OXIDES WT%	TR1(21) 21	TR1(21) 22	TR1(21) 23	TR1(21) 24	STD. DEV.
SIO2	61.31	61.11	61.64	61.16	0.27
BAO	0.00	0.00	0.02	0.08	0.01
AL2O3	24.94	23.76	24.15	24.75	0.60
CAO	6.41	5.69	5.87	6.44	0.38
FEO	0.17	0.08	0.01	0.05	0.06
NA2O	7.94	8.30	8.28	7.86	0.20
K2O	0.03	0.06	0.06	0.11	0.02
TOTAL	100.80	99.02	100.02	100.45	

Sample-677 PP(26)

OXIDES WT%	PP(26)G	PP(26)H	PP(26)I	PP(26)J	PP(26)K	PP(26)L	PP(26)M	PP(26)N	STD. DEV.
SIO2	65.90	65.65	65.78	65.61	65.41	65.67	65.59	65.94	0.17
BAO	0.00	0.00	0.08	0.00	0.00	0.00	0.05	0.22	0.05
AL2O3	21.81	21.71	21.92	21.78	21.59	21.85	21.85	22.03	0.10
CAO	2.49	2.49	2.59	2.56	2.48	2.65	2.58	2.57	0.06
FEO	0.08	0.03	0.07	0.02	0.02	0.01	0.01	0.11	0.03
NA2O	10.25	10.12	9.97	10.04	9.75	9.93	10.01	10.01	0.14
K2O	0.07	0.08	0.09	0.08	0.06	0.07	0.07	0.05	0.01
TOTAL	100.58	100.09	100.52	100.09	99.30	100.19	100.15	100.95	

Sample-677 PP(26)

OXIDES WT%	PP(26)43	PP(26)44	PP(26)45	PP(26)46	STD. DEV.
SIO2	64.36	63.64	64.05	64.04	0.37
BAO	0.00	0.11	0.00	0.06	0.06
AL2O3	22.55	22.19	22.08	22.32	0.25
CAO	3.83	3.92	3.67	3.86	0.13
FEO	0.12	0.20	0.06	0.07	0.07
NA2O	9.53	9.42	9.52	9.32	0.06
K2O	0.07	0.08	0.05	0.12	0.01
TOTAL	100.48	99.55	99.43	99.79	

Sample 12-2-4 R2(34)

OXIDES WT%	R2(34)1	R2(34)2	R2(34)3	R2(34)4	R2(34)5	STD. DEV.
SIO2	60.06	59.97	60.00	60.32	60.66	0.05
BAO	0.08	0.00	0.00	0.07	0.02	0.05
AL2O3	25.03	25.05	24.89	25.30	25.03	0.09
CAO	6.69	6.86	6.85	7.03	6.59	0.09
FEO	0.14	0.15	0.05	0.03	0.05	0.06
NA2O	7.85	7.83	7.70	7.67	7.78	0.08
K2O	0.06	0.11	0.19	0.13	0.12	0.05
TOTAL	99.94	99.98	99.67	100.54	100.25	

Sample 12-2-4 R2(34)

OXIDES WT%	R2(34)24	R2(34)25	R2(34)26	R2(34)27	R2(34)28	STD. DEV.
SIO2	60.15	60.21	60.36	60.51	60.40	0.10
BAO	0.01	0.07	0.04	0.00	0.00	0.03
AL2O3	25.50	25.18	25.25	25.06	24.94	0.18
CAO	7.03	6.85	6.78	6.59	6.74	0.13
FEO	0.04	0.00	0.04	0.05	0.11	0.02
NA2O	7.58	7.68	7.67	7.83	7.74	0.05
K2O	0.11	0.11	0.07	0.10	0.08	0.02
TOTAL	100.43	100.08	100.20	100.15	100.01	

Sample cm501 TR1(2)

OXIDES WT%	TR1(2)43	TR1(2)44	TR1(2)45	TR1(2)46	STD. DEV.
SIO2	64.36	63.64	64.05	64.04	0.37
BAO	0.00	0.11	0.00	0.06	0.06
AL2O3	22.55	22.19	22.08	22.32	0.25
CAO	3.83	3.92	3.67	3.86	0.13
FEO	0.12	0.20	0.06	0.07	0.07
NA2O	9.53	9.42	9.52	9.32	0.06
K2O	0.07	0.08	0.05	0.12	0.01
TOTAL	100.48	99.55	99.43	99.79	

Sample cm501 TR1(4)

OXIDES WT%	TR1(4)21	TR1(4)22	TR1(4)23	TR1(4)24	TR1(4)25	TR1(4)26	STD. DEV.
SIO2	63.99	64.18	63.77	64.15	64.14	63.73	0.20
BAO	0.01	0.04	0.00	0.04	0.07	0.13	0.02
AL2O3	22.36	22.27	22.21	22.58	22.28	21.81	0.07
CAO	3.80	3.57	3.74	3.89	3.72	3.62	0.11
FEO	0.08	0.14	0.14	0.04	0.15	0.03	0.03
NA2O	9.41	9.65	9.52	9.35	9.46	8.95	0.12
K2O	0.09	0.08	0.05	0.07	0.04	0.71	0.02
TOTAL	99.73	99.93	99.42	100.13	99.86	98.96	

Sample175 R1(21)

OXIDES WT%	R1(21)14	R1(21)15	R1(21)16	R1(21)17	R1(21)18	R1(21)19	STD. DEV.
SIO2	65.64	63.53	64.75	63.83	63.75	63.06	1.06
BAO	0.00	0.05	0.14	0.02	0.00	0.00	0.07
AL2O3	21.90	22.86	22.42	23.08	23.20	22.96	0.48
CAO	2.81	3.91	3.28	4.08	4.10	4.08	0.55
FEO	0.03	0.04	0.01	0.02	0.02	0.01	0.01
NA2O	10.12	9.53	9.85	9.23	9.29	9.17	0.30
K2O	0.02	0.03	0.04	0.14	0.19	0.18	0.01
TOTAL	100.53	99.95	100.49	100.41	100.54	99.45	

MUSCOVITE ANALYSES

Sample cm126a R2(12)

OXIDES WT %	R2(12)14	R2(12)15	R2(12)16	R2(12)17	STD. DEV
SIO2	45.28	43.49	44.83	45.43	0.86
TIO2	1.01	0.71	0.94	1.01	0.14
AL2O3	33.79	35.90	34.02	33.69	0.14
MGO	0.69	0.50	0.63	0.68	0.09
MNO	0.03	0.00	0.00	0.06	0.03
FEO	2.98	5.15	3.23	2.90	1.07
CAO	0.00	0.00	0.00	0.00	0.00
NA2O	0.50	0.40	0.46	0.47	0.04
K2O	9.47	7.05	8.61	9.43	1.13
H2O	4.41	4.23	4.38	4.41	0.09
F	0.00	0.15	0.00	0.00	0.07
CL	0.00	0.00	0.00	0.01	0.01
TOTAL	98.15	95.58	97.10	98.10	

Sample cm126a TR1(33)

OXIDES WT %	TR1(33)18	TR1(33)19	TR1(33)20	TR1(33)21	TR1(33)22	STD. DEV
SIO2	45.60	45.31	45.08	44.96	45.05	0.18
TIO2	1.22	1.25	1.26	1.23	1.18	0.34
AL2O3	33.66	33.42	33.73	33.93	33.44	0.42
MGO	0.67	0.73	0.65	0.68	0.72	0.24
MNO	0.00	0.05	0.00	0.00	0.04	0.04
FEO	2.92	3.03	2.83	2.95	2.95	0.51
CAO	0.00	0.00	0.00	0.00	0.00	0.00
NA2O	0.53	0.53	0.55	0.53	0.51	0.02
K2O	9.71	9.92	10.02	9.53	9.93	0.25
H2O	4.41	4.42	4.41	4.31	4.40	0.04
F	0.05	0.00	0.00	0.21	0.00	0.08
CL	0.00	0.00	0.00	0.01	0.00	0.01
TOTAL	98.77	98.65	98.52	98.32	98.22	

Sample 427 R2(6a)

OXIDES WT %	R2(6a)37	R2(6a)38	STD. DEV
SIO2	45.88	45.85	0.03
TIO2	1.12	1.20	0.06
AL2O3	34.82	34.92	0.07
MGO	0.69	0.73	0.03
MNO	0.02	0.00	0.02
FEO	1.54	1.68	0.09
CAO	0.00	0.00	0.00
NA2O	0.52	0.54	0.01
K2O	10.00	9.99	0.01
H2O	4.41	4.44	0.02
F	0.14	0.09	0.03
CL	0.00	0.00	0.00
TOTAL	99.16	99.43	

Sample 427 R2(6b)

OXIDES WT %	R2(6b)34	R2(6b)35	R2(6b)36	STD. DEV
SIO2	46.02	45.38	45.91	0.45
TIO2	0.96	1.14	1.05	0.13
AL2O3	34.97	34.89	34.79	0.06
MGO	0.70	0.69	0.68	0.01
MNO	0.00	0.00	0.02	0.00
FEO	1.69	1.48	1.61	0.15
CAO	0.00	0.00	0.00	0.00
NA2O	0.53	0.53	0.57	0.00
K2O	10.00	10.05	10.11	0.03
H2O	4.44	4.45	4.48	0.01
F	0.10	0.00	0.03	0.07
CL	0.00	0.00	0.02	0.00
TOTAL	99.41	98.59	99.25	

Sample cm677 PP(24)

OXIDES WT %	PP(24)A	PP(24)B	PP(24)C	PP(24)D	STD. DEV
SIO2	45.82	45.93	45.77	45.90	0.08
TIO2	0.97	0.81	0.89	0.82	0.07
AL2O3	35.83	35.78	36.00	35.98	0.11
MGO	0.62	0.64	0.62	0.63	0.01
MNO	0.00	0.02	0.00	0.00	0.01
FEO	1.33	1.30	1.10	1.20	0.11
CAO	0.00	0.00	0.00	0.00	0.00
NA2O	0.86	0.89	0.90	0.91	0.02
K2O	8.94	8.97	8.92	8.98	0.03
H2O	4.50	4.50	4.44	4.45	0.03
F	0.00	0.00	0.11	0.11	0.06
CL	0.01	0.00	0.01	0.00	0.00
TOTAL	98.86	98.84	98.75	98.98	

Sample12-2-4 R2(34)

OXIDES WT %	R2(34)11	R2(34)12	R2(34)13	R2(34)14	R2(34)15	STD. DEV
SIO2	45.20	45.60	45.30	45.20	45.00	0.18
TIO2	1.02	1.07	1.05	1.03	1.10	0.34
AL2O3	33.32	33.61	33.34	33.23	32.87	0.42
MGO	0.79	0.71	0.74	0.81	0.78	0.24
MNO	0.00	0.01	0.03	0.01	0.00	0.04
FEO	2.90	2.75	2.93	2.74	3.05	0.51
CAO	0.00	0.00	0.00	0.00	0.00	0.00
NA2O	0.62	0.65	0.61	0.62	0.58	0.02
K2O	10.47	10.49	10.41	10.49	10.36	0.25
H2O	4.41	4.43	4.41	4.34	4.38	0.04
F	0.00	0.02	0.00	0.13	0.00	0.06
CL	0.00	0.00	0.02	0.01	0.01	0.01
TOTAL	98.72	99.35	98.84	98.61	98.10	

Sample cm501 TR1(1)

OXIDES WT %	TR1(1)47	TR1(1)48	TR1(1)49	TR1(1)50	STD. DEV
SIO2	45.48	45.61	45.53	45.43	0.08
TIO2	0.93	0.97	0.93	0.87	0.04
AL2O3	34.67	34.47	34.44	34.52	0.10
MGO	0.71	0.71	0.75	0.74	0.02
MNO	0.00	0.02	0.00	0.00	0.01
FEO	1.54	1.51	1.62	1.44	0.07
CAO	0.00	0.00	0.00	0.00	0.00
NA2O	1.05	1.08	1.04	1.09	0.02
K2O	9.73	9.89	9.89	9.84	0.08
H2O	4.45	4.45	4.44	4.37	0.04
F	0.00	0.00	0.00	0.14	0.07
CL	0.00	0.01	0.01	0.02	0.01
TOTAL	98.58	98.73	98.66	98.46	

Sample 175 R1(21)

OXIDES WT %	R1(21)21	R1(21)22	R1(21)23	STD. DEV
SIO2	45.47	46.02	46.20	0.38
TIO2	0.81	0.79	0.86	0.04
AL2O3	35.33	35.68	35.69	0.20
MGO	0.65	0.67	0.67	0.01
MNO	0.00	0.00	0.00	0.00
FEO	1.17	1.23	1.15	0.04
CAO	0.00	0.00	0.00	0.00
NA2O	0.84	0.91	0.93	0.05
K2O	9.29	9.33	9.11	0.11
H2O	4.38	4.50	4.43	0.06
F	0.14	0.00	0.18	0.09
CL	0.01	0.00	0.00	0.01
TOTAL	98.10	99.13	99.21	

REFERENCES CITED

Achaibar, J., 1983, A petrologic and geochemical study of some amphibolite bodies in the Smith River allochthon, Virginia [M.S. thesis]: Knoxville, University of Tennessee, 93p.

Achaibar, J., and Misra, K. C., 1984, Amphibolites of the Smith River allochthon, southwest Virginia, southern Appalachians: Geological Society of America Abstracts with Programs, v. 16, p. 121.

Aleinikoff, J.N., Zartman, R.E., Rankin, D.W., Lyttle, P.T., Burton, W.C., and McDowell, R.C., 1991, New U–Pb zircon ages for rhyolite of the Catoctin Formation and Mount Rogers Formations— more evidence for two pulses of Iapetan Rifting in the central and southern Appalachians: Geological Society of America Abstracts with Programs, v. 23, p. 2.

Badger, R. L., 1989, Geochemistry and petrogenesis of the Catoctin volcanic province, central Appalachians [Ph.D. dissert.]: Blacksburg, Virginia Polytechnic Institute and State University, 337 p.

Badger, R. L., 1992, Stratigraphic characterization and correlation of volcanic flows within the Catoctin Formation, central Appalachians: Southeastern Geology, v. 32, p.175–196.

Badger, R.L., and Sinha, A.K., 1988, Age and Sr isotopic signature of the Catoctin volcanic province: Implications for subcrustal mantle evolution: Geology, v. 16, p. 692–695.

Badger, R.L., and Sinha, A.K., 1991, Nature of Precambrian mafic magmatism within the Appalachian orogen: Geological Society of America Abstracts with Programs, v. 23, p.5.

Basaltic Volcanism Study Project, 1981, Ocean–floor basaltic volcanism, *in* Basaltic volcanism on the terrestrial planets: New York, Pergamon Press, p. 132–160.

Bell, T. H., 1978, Progressive deformation and reorientation of fold axes in a ductile mylonite zone: The Woodroffe thrust: Tectonophysics, v. 44, p. 285–320.

Bentley, R. D., and Neathery, T. N., 1970, Geology of the Brevard zone and related rocks of the Inner Piedmont of Alabama: Alabama Geological Society, Eighth Annual Field Trip Guidebook, 119 p.

Bentley, R.D., and Reynolds, J.W., 1975, Geology of the Lineville East, Ofelia, Wadley North, and Mellow Valley quadrangles, Alabama: Alabama Geological Survey Bulletin 109, 120 p.

Berthé, D., Choukroune, P., and Jegouzo, P., 1979, Orthogneiss, mylonite and non–coaxial deformation of granites: The example of the South Armorican shear zone: Journal of Structural Geology, v. 1, p. 31–42.

Bird, J. M., and Dewey, J. F., 1970, Lithosphere plate–continental margin tectonics and the evolution of the Appalachian orogen: Geological Society of America Bulletin, v. 81, p. 1031–1060.

Blackburn, W. H., 1969, Zoned and unzoned garnets from the Grenville Gneisses around Gananoque, Ontario: Canadian Mineralogist, v. 9, p. 691–698.

Bland, A. E., 1978, Trace element geochemistry of volcanic sequences in Maryland, Virginia, and North Carolina and its bearing on the tectonic evolution of the central Appalachians [Ph.D. dissert.]: Lexington, University of Kentucky, 328 p.

Bobyarchick, A. R., 1984, A late Paleozoic component of strike–slip in the Brevard zone, southern Appalachians: Geological Society of America Abstracts with Programs, v. 16, p. 126.

Bobyarchick, A. R., Edelman, S. H., and Horton, J. W., Jr., 1988, The role of dextral strike–slip in the displacement history of the Brevard zone, *in* Secor, D. T., ed., Southeastern Geological Excursions: Geological Society of America Southeastern Section Field Trip Guidebook, p. 53–154.

Bohlen, S. R., Wall, V. J., and Boettcher, A. L., Geobarometry in granulites, in S. K. Saxena, ed., Kinetics and Equilibrium in Mineral Reactions, New York, Springer–Verlag, p. 141-171

Brown, W.R., 1958, Geology and mineral resources of the Lynchburg quadrangle, Virginia: Virginia Division of Mineral Resources Bulletin 74, 99 p.

Brown, W. R., 1970, Investigations of the sedimentary record in the Piedmont and Blue Ridge of Virginia, *in* Fisher, G. W., Pettijohn, F. J., Reed, J. C., Jr., and Weaver, K. N., eds., Studies in Appalachian geology: Central and southern: New York, Wiley–Interscience, p. 336-349.

Brun, J. P., and Burg, J. P., 1982, Combined thrusting and wrenching in the Ibero–Armorican arc: A corner effect during continental collision: Earth and Planetary Science Letters, v. 61, 319-332.

Bryan, W. B., Thompson, G., Frey, F. A., and Dickey, J. S., 1976, Inferred settings and differentiation in basalts from the Deep Sea Drilling Project: Journal of Geophysical Research, v. 81, p. 4285 – 4304.

Bryant, B., and Reed, J. C., Jr., 1970, Geology of the Grandfather Mountain window and vicinity, North Carolina and Tennessee: U. S. Geological Survey Professional Paper 615, 190 p.

Burg, J. P., Iglesias, M., Laurent, Ph., Matte, Ph. and Ribiero, A. 1981, Variscan intracontinental deformation: the Coimbra–Cordoba shear zone (SW Iberian Peninsula): Tectonophysics, v. 78, 161–177.

Butler, R. J., 1971, Comparative tectonics of some Alpine and Southern Appalachian structures: Southeastern Geology, v. 12, 203–221.

Butler, J. R., 1990, Metamorphism, *in* Horton, J. W., Jr., and Zullo, V. A., eds., The Geology of the Carolinas, Carolina Geological Society Fiftieth Anniversary Volume: Knoxville, The University of Tennessee Press, p. 127–141.

Carreras, J., Estrada, A., and White, S., 1977, The effects of folding on the c– axis fabric of a quartz mylonite: Tectonophysics, v. 39, p. 3–24.

Chatterjee, N. D., and Johannes, W., 1974, Thermal stability and standard thermodynamic properties of synthetic 2M1–muscovite, $KAl_2AlSi_3O_{10}(OH)_2$: Contributions to Mineralogy and Petrology, v. 48, p. 89–114.

Christie, J. M., 1963, The Moine thrust zone in the Assynt region, northwest Scotland: University of California Publications in the Geological Sciences, v. 40, p. 345-419.

Clarke, J. W., 1952, Geology and mineral resources of the Thomaston quadrangle, Georgia: Georgia Geological Survey Bulletin, v. 59, 103 p.

Cobbold, P. R., and Quinquis, H. 1980. Development of sheath folds in shear regimes: Journal of Structural Geology, v. 2, p. 119-126.

Cobbold, P. R., 1977, Description and origin of banded deformation structures I: Regional strain, local perturbations, and deformation bands: Canadian Journal of Earth Science, v. 14, p. 1721–1731.

Conley, J. F., 1978, Geology of the Piedmont of Virginia—Interpretation and problems, *in* Contributions to Virginia Geology—III: Virginia Division of Mineral Resources Publication 7, p. 115–149.

Conley, J. F., and Henika, W. S., 1973, Geology of the Snow Creek, Martinsville East, Price, and Spray quadrangles, Virginia: Virginia Division of Mineral Resources, Report of Investigations 33, 71 p.

Cook, F. A., Albaugh, D. S., Brown, L. D., Kaufman, S., Oliver, J. E., and Hatcher, R. D., Jr. 1979. Thin–skinned tectonics in the crystalline southern Appalachians: COCORP seismic–reflection profiling of the Blue Ridge and Piedmont: Geology, v, 7, p. 563–568.

Costain, J. K., Hatcher, R. D., Jr., and Çoruh, C., 1989, Appalachian ultradeep core hole (ADCOH) Project site investigation regional seismic lines and geologic interpretation, *in* Hatcher, R. D., Jr., Viele, G. W., and Thomas, W. A., eds., The Appalachian–Ouachita orogen in the United States: Boulder, Colorado, Geological Society of America, The Geology of North America, v. F-2, Plate 8.

Coward, M. P., and Potts, G. J., 1983, Complex strain patterns developed at the frontal tips and lateral tips to shear zones and thrust zones: Journal of Structural Geology, v. 5, p.383–399.

Culshaw, N. G., Corrigan, D., Drage, J. and Wallace, P., 1988, Georgian Bay geological synthesis: Key Harbour to Dillon, Grenville province of Ontario: Geological Survey of Canada Paper 88–1B, p. 129–133.

Dabbagh, A. E., 1975, Geology of the Skyland and Dunsmore Mountain quadrangles, North Carolina [Ph.D dissert.]: Chapel Hill, University of North Carolina, 228 p.

Davis, T. L., and Tabor, J. R., 1989, Preliminary report on detailed mapping of the western Inner Piedmont, Cliffield Mountain quadrangle and surrounding area, North and South Carolina: Geological Society of America Abstracts with Programs, v. 21, p. A11.

Davis, T.L., Tabor, J. R., and Hatcher, R.D., Jr., 1989, Orogen–parallel to orogen–oblique ductile deformation and possible late Paleozoic (?) ductile deformation of the western Piedmont, southern Appalachians: Geological Society of America Abstracts with Programs, v. 21, A65.

Davis, T. L., Tabor, J. R., and Hatcher, R. D., Jr., 1990, Geologic mapping in the Columbus Promontory, western Piedmont: Polyphase development of a crystalline thrust complex: Geological Society of America Abstracts with Programs, v. 22, p. 10.

Davis, T. L., Liu, A., Tabor, J. R., and Hatcher, R. D., Jr., 1990, Possible late Proterozoic(?) ductile front exposed in the Columbus Promontory, North Carolina: Implications for emplacement of the Blue Ridge–Piedmont thrust sheet, southern Appalachians and the kinematics of Paleozoic Africa–North America collision: Geological Society of America Abstracts with Programs, v. 22, p. 225.

Davis, T. L., Hatcher, R. D. Jr., Liu, A., and Tabor, J. R., 1991a, Structural development of a progressively deformed crustal–scale shear zone, southern Appalachian Inner Piedmont, U. S. A.: The geometry of naturally deformed rocks (John Ramsay Meeting), Mitteilugen aus den Geologische Institut ETH Zürich, Neue Folge, p. 119–120.

Davis, T. L., Hatcher, R. D. Jr., Liu, A., and Tabor, J. R., 1991b, Southern Appalachian western Inner Piedmont: A progressive crustal–scale shear zone: Geological Society of America Abstracts with Programs, v. 23, p. A138.

Dell'Angelo, L. N., and Tullis, J., 1989, Fabric development in experimentally sheared quartzites: Tectonophysics, v. 169, p. 1–21.

Dennis, A. J., and Secor, D. T., Jr., 1987, A model for the development of crenulations in shear zones with applications from the southern Appalachian Piedmont: Journal of Structural Geology, v. 9, p. 809–817.

Dennis, A. J., 1991, Is the central Piedmont suture a low–angle normal fault?: Geology, v. 19, p. 1081–1084.

Drake, A. A., Jr., Sinha, A. K., Laird, J., and Guy, R. E., 1989, The Taconic orogen, *in* Hatcher, R. D., Jr., Thomas, W. A., and Viele, G. W., eds., The Appalachians–Ouachitas Orogen in the United States: Boulder, Colorado, Geological Society of America, The Geology of North America, v. F–2, p. 101–178.

Edelman, S. H., Liu, A., and Hatcher, R. D., Jr., 1987, Brevard zone in South Carolina and adjacent areas: An Alleghanian orogen–scale dextral shear zone reactivated as a thrust fault: Journal of Geology, v. 95, p. 793–806.

Eggers, M. R., 1983, Petrology, structure and geochemistry of the Kimsey Bald mafic complex, North Carolina [M.S. thesis]: Columbia, University of South Carolina, 72 p.

Eisbacher, G. H., 1970, Deformation mechanics of mylonitic rocks and fractured granites in Cobequid Mountains, Nova Scotia: Geological Society of America Bulletin, v. 81, p. 2009–2020.

Ellis, M., and Watkinson, A. J., 1987, Orogen–parallel extension and oblique tectonics: The relation between stretching lineations and relative plate motions: Geology, v. 15, p. 1022–1026.

Erlank, A. J., and Kable, E. J. D., 1976, The significance of incompatible elements in Mid–Atlantic Ridge basalts from 45° N with particular reference Zr/ Nb: Contributions to Mineralogy and Petrology, v. 54, p. 281–291.

Espenshade, G. H., 1954, Geology and mineral deposits of the James River–Roanoke River manganese district, Virginia: U. S. Geological Survey Bulletin 1008, 155 p.

Essene, E. J., 1989, The current status of thermobarometry in metamorphic rocks, *in* Daly, J.S., Cliff, R. A., and Yardley, B. W. D., eds., Evolution of Metamorphic belts: Geological Society of London Special Publication 43, p. 1–44.

Evans, C. A., and Mosher, S., 1986, Microstructures and sense of shear in the Brevard zone, southern Appalachians: Geological Society of America Abstracts with Programs, v. 18, p. 596.

Evans, D. J., and White, S. H., 1984, Microstructural and fabric studies from the rocks of the Moine Nappe, Eriboll, NW Scotland: Journal of Structural Geology, v. 6, p. 369–389.

Ferry, J. M., and Spear, F. S., 1978, Experimental calibration of Fe and Mg between biotite and garnet: Contributions to Mineralogy and Petrology, v. 66, p. 113–117.

Floyd, P. A., and Winchester, J. A., 1 975, Magma type and tectonic setting discrimination using immobile elements: Earth and Planetary Science Letters, v. 27, p. 211–215.

Ganguly, J., and Saxena, S. K., 1984, Mixing properties of aluminosilicate garnets: Constraints from natural and experimental data, and applications to geothermo–barometry: American Mineralogist, v. 69, p. 88–97.

Gee, D. G., 1978, Nappe displacement in the Scandanavian Cledonides: Tectonophysics, v. 47, p. 393–419.

Gee, D. G., and Sturt, B. A., 1983, Comments on the stratigraphic / structural evolution of Scandanavia, *in* P. E. Schenk, ed.,: Regional trends in the geology of the Appalachian–Caledonian–Hercynian–Mauritanide Orogen, p. 113–115.

Ghent, E. D., and Stout, M. Z., 1981, Geobarometry and geothermometry of plagioclase–biotite–garnet–muscovite assemblages: Contributions to Mineralogy and Petrology, v. 76, p. 92–97.

Gillon, K. A., 1989, The geology of the eastern Blue Ridge thrust sheets in the vicinity of Helen, Georgia, *in* Fritz, W. J., Hatcher, R. D., Jr., and Hopson, J. L. eds.: Georgia Geological Society Guidebook, v. 9, p. 133–169.

Glover, L., III, and Wang, P., 1992, The Ultramafic–mafic association of the Virginia Blue Ridge: Early Paleozoic ophiolitic melange or part of the Late Precambrian rift facies?: Geological Society of America Abstracts with Programs, v. 24, p. 17.

Goldberg, S. A., Butler, J. A., and Fullagar, P. D., 1986, The Bakersville dike swarm: Geochronology and petrogenesis of Late Proterozoic basaltic magmatism in the southern Appalachian Blue Ridge: American Journal of Science, v. 26, p. 403–430.

Goldsmith, R., Milton, D. J., and Horton, J. W., Jr., 1988, Geologic map of the Charlotte 1 degree x 2 degree quadrangle, North Carolina and South Carolina: U. S. Geological Survey Map I–1251–E, scale 1:250,000.

Griffin, V. S., Jr., 1967, Geology of the Six Mile quadrangle, South Carolina: South Carolina Division of Geology MS–14, scale 1:24,000.

Griffin, V. S., Jr., 1969, Migmatitic Inner Piedmont belt of northwestern South Carolina: South Carolina Division of Geology, Geology Notes, v. 13, p. 87–104.

Griffin, V. S., Jr., 1971a, The Inner Piedmont belt of the southern crystalline Appalachians: Geological Society of America Bulletin, v. 82, p. 1885–1898.

Griffin, V. S., Jr., 1971b, Stockwork tectonics in the Appalachian Piedmont of South Carolina: Geologische Rundschau, v. 60, p. 868–886.

Griffin, V. S., Jr., 1974a, Analysis of the Piedmont in northwest South Carolina: Geological Society of America Bulletin, v. 85, p. 1123–1138.

Griffin, V. S., Jr., 1974b, Geology of the Walhalla quadrangle, South Carolina: South Carolina Division of Geology MS–19, scale 1:24,000.

Guidotti, C. V., 1984, Micas in metamorphic rocks, *in* Bailey, S. W., ed., Micas: Mineralogical Society of America Reviews of Mineralogy, v. 13, p. 357–467.

Hadley, J. B., and Nelson, A. E., 1971, Geologic map of the Knoxville quadrangle, North Carolina, Tennessee, and South Carolina: U.S. Geological Survey Miscellaneous Geologic Investigations Map I–654, scale 1:250,000.

Hanmer, S., 1988, Ductile thrusting at mid–crustal levels, southwestern Grenville Province: Canadian Journal of Earth Science, v. 25, p. 1049–1059.

Harper, S. B., and Fullagar, P. D., 1981, Rb–Sr ages of granitic gneisses of the Inner Piedmont belt of northwestern North Carolina and southwestern South Carolina: Geological Society of America Bulletin, v. 92, p. 864–872.

Hatcher, R. D. Jr., 1969, Stratigraphy, petrology, and structure of the low rank belt and part of the Blue Ridge of northwesternmost South Carolina: South Carolina Division of Geology, Geologic Notes, v. 13, p. 105–141.

Hatcher, R. D. Jr., 1970, Stratigraphy of the Brevard zone and Poor Mountain area, northwestern South Carolina: Geological Society of America Bulletin, v. 81, p. 933–940.

Hatcher, R. D., Jr., 1971a, Geology of the Rabun and Habersham Counties, Georgia: A reconnaissance study: Georgia Department of Mines, Mining, and Geology Bulletin 83, 48 p.

Hatcher, R. D. Jr., 1971b, Stratigraphic, petrologic, and structural evidence in favor of a thrust solution to the Brevard problem: American Journal of Science, v. 210, p. 177–202.

Hatcher, R. D. Jr., 1972, Developmental model for the southern Appalachians: Geological Society of America Bulletin, 83, p. 2735-2760.

Hatcher, R. D. Jr., 1973, Basement versus cover rocks in the Blue Ridge of northeast Georgia, northwestern South Carolina and adjacent North Carolina: American Journal of Science, v. 273, p. 671–685.

Hatcher, R. D. Jr., 1977, Macroscopic polyphase folding illustrated by the Toxaway dome, eastern Blue Ridge, South Carolina–North Carolina: Geological Society of America Bulletin, v. 88, p. 1678–1688.

Hatcher, R. D. Jr., 1978a, Tectonics of the western Piedmont and Blue Ridge, southern Appalachians: Review and speculation: American Journal of Science, v. 279, p. 276–304.

Hatcher, R. D. Jr., 1978b. The Alto allochthon: A major tectonic feature of the Piedmont of northeast Georgia: Georgia Geological Survey Bulletin 93, p. 83–86.

Hatcher, R. D., Jr., 1979, The Coweeta Group and Coweeta syncline: Major features of the North Carolina–Georgia Blue Ridge: Southeastern Geology, v. 21, p. 17–29.

Hatcher, R. D. Jr., 1987, Tectonics of the southern and central Appalachian internides: Annual Review of Earth and Planetary Sciences, v. 15, p. 337–362.

Hatcher, R. D., Jr., 1988, Sauratown Mountains window—Problems and regional perspective, *in* Hatcher, R.D., Jr., ed., Structure of the Sauratown Mountains, North Carolina: Carolina Geological Society Guidebook, p. 1–19.

Hatcher, R. D., Jr., 1989, Tectonic synthesis of the U.S. Appalachians, Chapter 14, *in* Hatcher, R. D., Jr., Thomas, W. A., and Viele, G. W., eds., The Appalachian–Ouachita orogen in the United States: Boulder, Colorado, Geological Society of America, The Geology of North America, v. F–2, p. 511–535.

Hatcher, R. D., and Acker, L. L., 1984, Geology of the Salem quadrangle, South Carolina: South Carolina Geological Survey, MS–26, 23 p., scale 1/24,000.

Hatcher, R. D., Jr., and Butler, J. R., 1979, Guidebook for southern Appalachian field trip in the Carolinas, Tennessee, and northeastern Georgia: International Geologic Correlation Program Project 27, University of North Carolina, Chapel Hill, 117 p.

Hatcher, R. D., Jr., and Goldberg, S. A., 1990, The Blue Ridge Geologic Province, *in* Horton, J. W., Jr., and Zullo, V. A., eds., The Geology of the Carolinas, Carolina Geological Society Fiftieth Anniversary Volume: Knoxville, The University of Tennessee Press, p. 11–35.

Hatcher, R. D., Jr., and Hooper, R. J., 1991, Evolution of crystalline thrust sheets in the internal parts of mountain chains, *in* McClay, K.R., ed., Thrust Tectonics: Chapman and Hall, London, p. 217–234.

Hatcher, R. D., Jr., Howell, D.E., Talwani P., and Zeitz, I., 1977, Eastern Piedmont fault system: Speculations on its extent: Geology, v. 5., p. 636–640.

Hatcher, R. D.Jr., and Odom, A. L., 1980, Timing of thrusting in the southern Appalachians, USA: Model for orogeny?: Journal of the Geological Society of London, v. 137, p. 321–327.

Hatcher, R. D., Jr., and Zietz, I., 1980, Tectonic implications of regional aeromagnetic and gravity data from the southern Appalachians, *in* Wones, D. R., ed., Proceedings, The Caledonides in the U.S.A.: Blacksburg, Virginia Polytechnic Institute and State University Department of Geological Sciences Memoir 2, p. 235–244.

Hatcher, R. D., Jr., Hooper, R. J., Petty, S. M., and Willis, J. D., 1984, Structure and chemical petrology of three southern Appalachian mafic–ultramafic complexes and their bearing upon the tectonics of emplacement and origin of Appalachian ultramafic bodies: American Journal of Science, v. 284, p. 484–506.

Hatcher, R. D., Jr., Osberg, P. H., Robinson, Peter, and Thomas, W. A., 1990, Tectonic map of the U.S. Appalachians: Geological Society of America, Geology of North America, v. F–2, plate 1, scale 1/2,500,000.

Hatcher, R. D., Jr., Thomas, W. A., Geiser, P. A., Snoke, A. W., Mosher, S., and Wiltschko, D. V. 1989, Alleghanian orogen, *in* Hatcher, R. D., Jr., Thomas, W. A., and Viele, G. W., The Appalachian-Ouachita orogen in the United States: Boulder, Colorado, Geological Society of America, The Geology of North America. v. F–2, p. 233–318.

Heyn, T., 1984, Stratigraphic and structural relationships along the southwestern flank of the Sauratown Mountains anticlinorium [M.S. thesis]: Columbia, University of South Carolina, 192 p.

Heyn, T., 1988, Geology of the hinge zone of the Sauratown Mountains anticlinorium, North Carolina, *in* Hatcher, R.D., Jr., ed., Structure of the Sauratown Mountains window, North Carolina: Carolina Geological Society Guidebook, p. 20–50.

Higgins, M. W., and McConnell, K. I., 1978, The Sandy Springs Group and related rocks in the Georgia Piedmont–Nomenclature and stratigraphy, *in* Short Contributions to the Geology of Georgia: Georgia Geologic Survey Bulletin 83, p. 50–55.

Higgins, M. W., Atkins, R. L., Crawford, T. J., Crawford, R. F. III, and Cook, R. B., 1984, A brief excursion through two stacks that comprise most of the crystalline terrane of Georgia and Alabama: Georgia Geological Society, 19th Annual Field Trip, 48 p.

Higgins, M. W., Atkins, R. L., Crawford, R.F., III, and Cook, R.B., 1988, A new interpretation of the stratigraphy, tectono–stratigraphy, structure, and evolution of the southernmost part of the Appalachian orogen, Georgia and Alabama: U. S. Geological Survey Professional Paper1475, 173 p.

Hodges, K. V., and Crowley, P. D., 1985, Error estimation and empirical geothermobarometry for pelitic systems: American Mineralogist, v. 70, p. 702–709.

Hodges, K. V., and Spear, F. S., 1982, Geothermometry, geobarometry, and the Al_2SiO_5 triple point at Mt. Moosilauke, New Hampshire: American Mineralogist, v. 67, p. 1118–1134.

Holdaway, M.J., 1971, Stability of andalusite and the aluminum silicate phase diagram: American Journal of Science, v. 271, p. 97–131.

Holdsworth, R. E., 1990, Progressive deformation structures associated with ductile thrusts in the Moine Nappe, Sutherland, Northern Scotland: Journal of Structural Geology, v. 12, p. 443–452.

Hollister, L.S., (1966), Garnet zoning: an interpretation based on the Rayleigh fractionation model: Science, v. 154, p. 1647–1651.

Hopson, J. L., 1989, Structure, stratigraphy, and petrogenesis of the Lake Burton mafic–ultramafic complex, *in* Fritz, W. J., Hatcher, R. D., Jr., and Hopson, J. L., eds.,: Georgia Geological Society Guidebook, v. 9, p. 93–110.

Hopson, J. L., and Hatcher, R. D. Jr., 1988, Structural and stratigraphic setting of the Alto allochthon, northeast Georgia: Geological Society of America Bulletin, v. 100, p. 339–350.

Horton, J. W., Jr., 1974, Geology of the Rosman area, Transylvania County, North Carolina [M.S. thesis]: Chapel Hill, University of North Carolina, 63 p.

Horton, J. W., Jr., 1982., Geologic map of the Rosman quadrangle, North Carolina: North Carolina Department of Natural Resources and Community Development Map 185–NE, scale 1/24,000.

Horton, J. W., Jr., and Butler, J. R., 1986, The Brevard fault zone at Rosman, Transylvania County, North Carolina: Geological Society of America Centennial Field Trip Guide–Southeast Section, p. 251–256.

Horton, J. W., Jr., and McConnell, K. I., 1990, The western Piedmont, *in* Horton, J. W., Jr., and Zullo, V. A., eds., The Geology of the Carolinas, Carolina Geological Society Fiftieth Anniversary Volume: Knoxville, The University of Tennessee Press, p. 36–58.

Horton, J. W., Jr., Drake, A. A., Jr., and Rankin, D. W., 1989, Tectonostratigraphic terranes and their paleozoic boundaries in the central and southern Appalachians, *in* Dallmeyer, R. D., ed., Terranes in the Circum–Atlantic Paleozoic orogens: Geological Society of America Special Paper 230, p. 213–245.

Hubbard, M. S., 1989, Thermobarometric constraints of the main central thrust zone and Tibetan slab, eastern Himalaya: Journal of Metamorphic Geology, v. 7, p. 19–30.

Hudleston, P. J., 1983, Strain patterns in an ice cap and implications for strain variations in shear zones: Journal of Structural Geology, v. 5, p. 455–464.

Humphris, S. E., Thompson, G., Schilling, J. G., and Kingsley, R. A., 1985, Petrological and geochemical variations along the Mid–Atlantic Ridge between 46° S and 32° S: influence of the Tristan da Cuhna manlte plume: Geochimica et Cosmochimica Acta, v. 49, p. 1445–1464.

Hurst, V. J., 1973, Geology of the southern Blue Ridge belt: American Journal of Science, v. 273, p. 643–670.

Hurst, V. J., and Jones, L.M., 1973, Origin of amphibolites in the Cartersville–Villa Rica area, Georgia: Geological Society of America Bulletin, v. 84, p. 905–912.

Irvine, T. N., and Baragar, W. R. A., 1971, A guide to the chemical classification of common rocks: Canadian Journal of Earth Science, v. 8, p. 523–548.

Jessell, M. W., 1988a, Simulation of fabric development in recrystallizing aggregates — I: Description of the model: Journal of Structural Geology, v. 10, p. 771–778.

Jessell, M. W., 1988b, Simulation of fabric development in recrystallizing aggregates —II: Example of model runs: Journal of Structural Geology, v. 10, p. 779–794.

Jessell, M. W., and Lister, G. S., 1990, A simulation of the temperature dependence of quartz fabrics, *in* Knipe, R. J., and Rutter, E. H., eds., Deformation mechanisms, rheology and tectonics: Special Publication of the Geological Society of London 54, p. 353–362.

Jonas, A. I., 1932, Structure of the metamorphic belt of the southern Appalachians: American Journal of Science, v. 24, p. 228–243.

Keith, A., 1905, Description of the Mount Mitchell quadrangle (North Carolina–Tennessee): U.S. Geological Survey Geologic Atlas, Folio 124, 10 p.

Keith, A., 1907, Description of the Pisgah quadrangle (North Carolina–South Carolina): U. S. Geological Survey Geologic Atlas, Folio 147, 8 p.

Kerrick, D. M., 1990, The fibrolite problem, *in* Kerrick, D. M., ed., The Al_2SiO_5 polymorphs: Mineralogical Society of America Reviews of Mineralogy, v. 22, p. 207–222.

King, P. B., 1955, A geologic cross-section across the southern Appalachians, an outline of the geology in the segment in Tennessee, North Carolina, and South Carolina. *in* Russell, R. J., ed., Guides to southeastern geology: Geological Society of America Annual Meeting, p. 332–373.

Klaper, E. M., 1988, Quartz c–axis fabric development and large–scale post–nappe folding (Wandfluhhorn fold, Penninic nappes): Journal of Structural Geology, v. 10, p. 795–802.

LaGarde, J. L., and Michard, A., 1986, Stretching normal to the regional thrust displacement in a thrust–wrench shear zone, Rehamna Massif, Morocco: Journal of Structural Geology, v.8, p. 483–492.

Law, R. D., 1987, Heterogeneous deformation and quartz crystallographic fabric transitions: Natural examples from the Moine thrust zone at the Stack of Glencoul, northern Assynt: Journal of Structural Geology, v. 9, p. 819–834.

Leake, B. E., 1964, The chemical distinction between ortho– and para–amohibolites: Journal of Petrology, v. 5, p. 238–254.

Leg 135 Scientific Party, 1992, Evolution of Backarc basins: ODP Leg 135, Lau Basin: EOS, Transactions of the American Geophysical Union, v. 73, p. 241–247.

Lemmon, R. E., 1973, Geology of the Bat Cave and Fruitland quadrangles and the origin of the Henderson Gneiss, western North Carolina [Ph.D. dissert.]: Chapel Hill, University of North Carolina, 145 p.

Lemmon, R. E., 1982, Evidence for an Acadian tectonic event in the western Inner Piedmont, North Carolina: Geological Society of America Abstracts with Programs, v. 14, p. 34.

Lemmon, R. E., and Dunn, D. E., 1973a, Geologic Map and mineral resources of the Bat Cave quadrangle, North Carolina: North Carolina Department of Natural Resources and Community Development Map GM 202 NW, scale 1/24,000.

Lemmon, R. E., and Dunn, D. E., 1973b, Geologic Map and mineral resources of the Fruitland quadrangle, North Carolina: North Carolina Department of Natural Resources and Community Development Map GM 202–NW, scale 1/24,000.

Lemmon, R. E., and Dunn, D. E., 1975, Origin and geologic history of the Henderson Gneiss from Bat Cave and Fruitland quadrangles, western North Carolina: Geological Society of America Abstracts with Programs, v. 7, p. 509.

Lisle, R.J., 1984, Strain discontinuities within the Seve–Köli Nappe complex, Scandanavian Caledonides: Journal of Structural Geology, v. 6, p. 101–110.

Lister, G. S., and Snoke, A. W., 1984, S-C mylonites: Journal of Structural Geology, v. 6, p. 617–638.

Lister, G. S., and Williams, P. F., 1980, Fabric development in shear zones: Theoretical controls on observed phenomena: Journal of Structural Geology, v. 1, p. 283–297.

Liu, A., 1991, Structural geology and deformation history of the Brevard fault zone, Chauga belt, and Inner Piedmont, northwestern South Carolina and adjacent areas [Ph.D. dissert]: Knoxville, University of Tennessee, 200 p.

Liu, A., Davis, T. L., and Hatcher, R. D., Jr., 1991, Thrusting in orogenic process: Observations from the Chauga belt and Inner Piedmont, southern Appalachians: Geological Society of America Abstracts with Programs, v. 23, p. 59.

Manktelow, N. S., 1987, Atypical textures in quartz veins from the Simplon Fault zone: Journal of Structural Geology, v. 9, p. 995–1006.

McConnell, K. I., 1988, Geology of the Sauratown Mountains anticlinorium: Vienna and Pinnacle 7.5 minute quadrangles, *in* Hatcher, R.D., Jr., ed., Structure of the Sauratown Mountains window, North Carolina: Carolina Geological Society Guidebook, p. 51–66.

McConnell, K. I., and Abrams, C. E., 1984, Geology of the Greater Atlanta region: Georgia Geological Survey Bulletin 96, 127 p.

McSween, H. Y. Jr., and Hatcher, R. D., 1985, Ophiolites(?) of the southern Appalachian Blue Ridge, *in* Woodward, N. B., ed., Field trips in the southern Appalachians: Knoxville, University of Tennessee Studies in Geology 9, p. 144–171.

Meschede, M., 1986, A method of discriminating between different types of mid–ocean ridge basalts and continental tholeiites with the Nb–Zr–Y diagram: Chemical Geology, v. 56, p. 207–218.

Mies, J. W., 1991, Planar dispersion of folds in ductile shear zones and kinematic interpretation of fold–hinge girdles: Journal of Structural Geology, v. 13, p. 281–297.

Misra, K. C., and Conte, J. A., 1991, Amphibolites of the Ashe and Alligator Back Formations, North Carolina: Samples of Late Proterozoic–early Paleozoic oceanic crust: Geological Society of America Bulletin, v. 103, p.737–750.

Misra, K. C., and Keller, F. B., 1978, Ultramafic bodies in the southern Appalachians: A review: American Journal of Science, v. 278, p. 389–418.

Misra, K. C., and McSween, H. Y., Jr., 1984, Mafic rocks of the southern Appalachians: A review: American Journal of Science, v. 284, p. 294–318.

Miyashiro, A., and Shido, F., 1975, Tholeiitic and calc–alkaline series in relation to the behaviors of titanium, vanadium, chromium, and nickel: American Journal of Science, v. 275, p. 265–277.

Mohan, A., Windley, B. F., and Searle, P., 1989, Geothermobarometry and development of inverted metamorphism in the Darjeeling–Sikkim region of the eastern Himalaya: Journal of Metamorphic Geology, v. 7, p. 95–110.

Neilson, M. J., 1988, The structure and stratigraphy of the Tallassee synform, Dadeville, Alabama: Southeastern Geology, v. 29, p. 41–50.

Neilson, M. J., and Stow, S. H., 1986, Geology and geochemistry of the mafic and ultramfic intrusive rocks, Dadeville belt, Alabama: Geological Society of America Bulletin, v. 97, p. 296–304.

Neilson, M.J., Goldberg, S. A., and Steltenpohl, M. G., 1990a, Geologic research in the Inner Piedmont and its borders: Progress 1970–1990, *in* Neilson, M.J., and Steltenpohl, M. G., Bittner, E. I., and Goldberg, S. A., eds., Tectonometamorphic evolution of Alabama's Inner Piedmont and its borders: Alabama Geological Survey Field Trip Guidebook, p. 1–12.

Neilson, M.J., Steltenpohl, M. G., Bittner, E. I., and Goldberg, S. A., 1990b, Tectonometamorphic development of the southernmost Inner Piedmont terrane and its borders, Alabama, *in* Neilson, M.J., and Steltenpohl, M. G., Bittner, E. I., and Goldberg, S. A., eds., Tectonometamorphic evolution of Alabama's Inner Piedmont and its borders: Alabama Geological Survey Field Trip Guidebook, p. 13–42.

Nelson, A. E., 1985, Major tectonic features and structural elements in the northwest part of the Greenville quadrangle, Georgia: U. S. Geological Survey Bulletin 1643, 22 p.

Nelson, A. E., Horton, J. W., Jr., and Clarke, J. W., 1987, Generalized tectonic map of the Greenville 1 degree x 2 degree quadrangle, Georgia, South Carolina, and North Carolina: U. S. Geological Survey Miscellaneous Field Studies Map MF–1898, scale 1:250,000.

Newton, R. C., and Hasleton, H. T., 1981, Thermodynamics of the garnet–plagioclase– Al_2SiO_5–quartz geobarometer, *in* Newton, R.C., Navrotsky, A., and Wood, B. J., eds., Thermodynamics of Minerals and Melts: Springer–Verlag, p. 131–147.

Odom, A. L., and Fullagar, P. D., 1973, Geochronologic and tectonic relationships between the Inner Piedmont, Brevard zone, and Blue Ridge belts, North Carolina: American Journal of Science, v. 273–A, p. 133–149.

Odom, A. L., and Russell, G. S., 1975., The time of regional metamorphism of the Inner Piedmont, North Carolina, and Smith River allochthon: Inference from whole–rock ages: Geological Society of America Abstracts with Programs, v. 7, p. 522–523.

Oldow, J. S., 1990, Transpression, orogenic float, and lithospheric balance: Geology, v. 18, p. 991–994.

Papike, J. J., 1987, Chemistry of rock–forming silicates: Ortho, ring, and single–chain structures: Reviews of Geophysics, v. 25, p. 1483–1526.

Papike, J. J., 1988, Chemistry of rock–forming silicates: Multiple–chain, sheet, and framework structures: Reviews of Geophysics, v. 26, p. 407–444.

Patterson, J. G., 1989, Deformation in portions of the distal continental margin to ancestral North America: An example from the westernmost internal zone, central and southern Appalachian orogen, Virginia: Tectonics, v. 8, p.535–554.

Pavlis, T. L., 1987, The role of strain heating in the evolution of megathrusts: Journal of Geophysical Research, v. 91, p. 12,407–12,422.

Pearce, J. A., 1975, Basalt geochemistry used to investigate past tectonic environments in Cyprus: Tectonophysics, v. 25, p. 41–67.

Pearce, J. A., 1980, Geochemical evidence for for the genesis and eruptive setting of lavas from Tethyn ophiolites, *in* Panayiotou, A., ed., Ophiolites—Proceedings of the International Ophiolite Symposium, Cyprus, Geological Survey Department, p. 261–272.

Pearce, J. A., and Cann, J.P., 1973, Tectonic setting of basic volcanic rocks determined using trace element analysis: Earth and Planetary Science Letters, v. 19, p. 290–300.

Pearce, J.A., and Flower, M. F. J., 1977, The relative importance of petrogenetic variables in magma genesis at accreting margins: A preliminary investigation: Geological Society of London Journal, v. 134, p. 103–127.

Pearce, J. A., and Norry, M. J., 1979, Petrogenetic implications of Ti, Zr, Y, and Nb variations in volcanic rocks: Contributions to Mineralogy and Petrology, v. 69, p. 33–47.

Platt, J. P., and Vissers, R. L. M., 1980, Extensional structures in anisotropic rocks: Journal of Structural Geology, v. 2, p. 397–410.

Quinn, M. J., 1990, Two lithotectonic boundaries in western North Carolina: Geologic interpretation of a region surrounding Sylva, Jackson County [M.S. thesis]: Knoxville, University of Tennessee, 223 p.

Ragland, P. C., Hatcher, R. D., Jr., and Whittington, D., 1983, Juxtaposed Mesozoic diabase dike sets from the Carolinas: A preliminary assessment: Geology, v. 11, p. 394–399.

Ramsay, J. G., 1958, Superimposed folding at Loch Monar, Inverness-Shire and Ross-Shire: Quarterly Journal of the Geological Society of London, v. 113, p. 271-308.

Ramsay, J. G., 1967, Folding and fracturing of rocks: New York, McGraw–Hill.

Ramsay, J. G., and Graham, R. H., 1970, Strain variation in shear belts: Canadian Journal of Earth Science, v. 7, p. 786-813.

Rankin, D. W., 1970, Stratigraphy and structure of Precambrian rocks in northwestern North Carolina, in Fisher, G. W., Pettijohn, F. J., Reed, J. C., Jr., and Weaver, K. N., eds., Studies of Appalachian geology: Central and southern: New York, Wiley–Interscience, p. 227–245.

Rankin, D. W., 1975, The continental margin of eastern North America in the southern Appalachians: The opening and closing of the Proto–Atlantic Ocean. American Journal of Science, v. 275–A, p. 298–336.

Rankin, D. W., 1976, Appalachian salients and recesses: Late Precambrian continental breakup and the opening of the Iapetus Ocean: Journal of Geophysical Research, v. 81, p. 5605–5619.

Rankin, D. W., Espenshade, G. H., and Shaw, K. W., 1 973, Stratigraphy and structure of the metamorphic belt in northwestern North Carolina and southwestern Virginia: A study from the Blue Ridge across the Brevard fault zone to the Sauratown Mountains anticlinorium: American Journal of Science, v. 273–A, p. 1–40.

Rankin, D. W., Drake, A. A. Jr., Glover, L., III, Goldsmith, R., Hall, L. M., Murray, D. P., Ratcliffe, N. M., Read, J. F., Secor, D. T., Jr., and Stanley, R. S., 1989, Pre–orogenic terrranes, *in* Hatcher, R. D., Jr., and Thomas, W. A., and Viele, G. W., eds., The Appalachian–Ouachita Orogen in the United States: Boulder, Colorado, Geological Society of America, The Geology of North America, v. F–2. p. 7–100.

Rast, N., and Kohles, K. M., 1986, The origin of the Ocoee Supergroup: American Journal of Science, v. 286, p. 593–616.

Reed, J. C., Jr., and Bryant, B., 1964. Evidence for strike–slip faulting along the Brevard zone in North Carolina: Geological Society of America Bulletin, v. 75, p. 1177–1196.

Ridley, J., 1986, Parallel stretching lineations and fold axes oblique to a shear displacement direction — A model and observations: Journal of Structural Geology, v. 8, p. 647–654.

Rodgers, J., 1970, The tectonics of the Appalachians: New York, Interscience Publishers, 271 p.

Roper, P. J., and Dunn, D. E., 1973, Superposed deformation and polymetamorphism, Brevard zone, South Carolina: Geological Society of America Bulletin, v. 84, p. 3373–3386.

Roper, P. J., and Justus, P. S., 1973, Polytectonic evolution of the Brevard zone: American Journal of Science, v. 273–A, p. 105–132.

Russell, G. S., Heatherington, A. L., and Mueller, P. A., 1992, Results of zircon analysis from trondjemitic dikes in the Elkahatchee Quartz Diorite, northern Alabama Piedmont: Geological Society of America Abstracts with Programs, v. 24, p. 62.

Saunders, A. D., and Tarney, J., 1984, Geochemical characteristics of basaltic volcanism with back–arc basins, *in* Kokelaar, B. P., and Howells, M. F., eds., Marginal basin geology: volcanic and associated sedimentary and tectonic processes in modern and ancient marginal basins: Geological Society of London Special Paper, v. 16, p. 59–76.

Schilling, J. G., 1975, Rare–earth variation across 'normal' segments of the Reykjanes Ridge, 60° – 53° N, Mid–Atlantic Ridge, 29° S and East Pacific Rise, 2° – 19° S and evidence on the composition of the underlying low velocity layer: Journal of Geophysical Research, v. 80, p. 1459–1473.

Schilling, J. G., Zajec, M., Evans, R., Johnston, T., White, W., Devine, J.D., and Kingsley, R., 1983, Petrologic and geochemical variations along the Mid–Atlantic Ridge from 27°N to 73°N: American Journal of Science, v. 283, p. 510–586.

Schmid, S. M., and Casey, M., 1986. Complete fabric analysis of some commonly observed quartz c–axis patterns: American Geophysical Union Monograph 36, p. 263–286.

Shaw, H. F., and Wasserburg, G. J., 1984, Isotopic constraints on the origin of Appalachian mafic complexes: American Journal of Science, v. 284, p. 319–349.

Shervais, J. W., 1982, Ti–V plots and the petrogenesis of modern and ophiolitic lavas: Earth and Planetary Science Letters, v. 57, p. 101–118.

Shufflebarger, T. E., 1961, Notes on the relationships of Piedmont metasedimentary rocks with emphasis on the Poor Mountain–Chauga River area, Oconee County, South Carolina: South Carolina Division of Geology, Geologic Notes, v. 5, p. 31–38.

Simpson, C., 1986, Determination of movement sense in mylonites: Journal of Geological Education, v. 34, p. 246–261.

Simpson, C., and Schmid, S. M., 1983, An evaluation of criteria to deduce the sense of movement in sheared rocks: Geological Society of America Bulletin, v. 94, p. 1281-1288.

Sinha, A. K., and Glover, L., III, 1978, U/Pb systematics of zircons during dynamic metamorphism: Contributions to Mineralogy and Petrology, v. 66, p. 305–310.

Sinha, A. K., Hewitt, D. A., and Rimstidt, J. D., 1988, Metamorphic petrology and strontium isotope geochemistry associated with the development of mylonites: An example for the Brevard fault zone, North Carolina: American Journal of Science, v. 288–A, p. 115–147.

Sinha, A. K., Hund, E. A., and Hogan, J. P., 1989, Paleozoic accretionary history of the North American plate margin (central and southern Appalachians): Constraints from the age, origin, and distribution of granitic rocks, *in* Hillhouse, J., ed., Deep structure and past kinematics of accreted terranes: American Geophysical Union Monograph Series, p. 219–238.

Sloan, E., 1908, Catalogue of mineral localities of South Carolina: South Carolina Geological Survey, 505 p.

Snoke, A. W., McGrew, A. J., Valasek, P. A., and Smithson, S. B., 198?, A crustal cross–section for a terrain of superimposed shortening and extension: Ruby Mountains–East Humbolt Range metamorphic core complex, Nevada, *in* Salisbury, M. H., and Fountain, D. M., eds., Exposed cross–sections of the continental crust: Dordrecht, Netherlands, Kluwer, p. 103–135.

Spear, F.S., 1989, Relative thermobarometry and P–T paths, *in* Daly, J. S., Cliff, R. A., and Yardley, B. W. D., eds., Evolution of metamorphic belts: Geological Society of London Special Publication 43, p. 63–81.

Spear, F. S., and Peacock, S. M., 1989, Metamorphic pressure–temperature–time paths: American Geophysical Union Short Course in Geology, v. 7, 102 p.

Spear, F. S., Hickmont, D. D., and Selverstone, J., 1990, Metamorphic consequences of thrust emplacement, Fall Mountain, New Hampshire: Geological Society of America Bulletin, v. 102, p. 1344–1360.

Starkey, J., 1979, Petrofabric analysis of Saxony Granulite by optical and x–ray diffraction methods: Tectonophysics, v. 58, p. 201–219.

Steltenpohl, M. G., Neilson, M. J., Bittner, E., Colberg, M. R., and Cook, R. B., 1990, Geology of the Alabama Inner Piedmont terrane: Alabama Geological Survey Bulletin 139, 80 p.

Stieve, A. L., 1989, The structural evolution and metamorphism of the southern portion of the Tallulah Falls dome, northeast Georgia [unpublished Ph. D. thesis]: Columbia, University of South Carolina, 207 p.

Stirewalt, G. L., and Dunn, D. E., 1973, Mesoscopic fabric and structural history of Brevard zone and adjacent rocks, North Carolina: Geological Society of America Bulletin, v. 84, p. 1629–1650.

Stow, S. H., Neilson, M. J., and Neathery, T.L., 1984, Petrography, geochemistry, and tectonic significance of the amphibolites in the Alabama Piedmont: American Journal of Science, v. 284, p. 416–436.

Stuckey, J. L., and Conrad, S. G., 1958, Explanation text for geologic map of North Carolina: North Carolina Department of Conservation and Development Board Bulletin, v. 71, 55 p.

Sun, S. S., and Nesbitt, R.W., 1978, Geochemical regularities and genetic significance of ophiolitic basalts: Geology, v. 6, p. 689–693.

Sun, S. S., and Nesbitt, R.W., and Sharaskin, Y. A., 1979, Geochemical characteristics of mid–ocean ridge basalts: Earth and Planetary Science Letters, v. 44, p. 119–138.

Tabor, J. R., Davis, T. L. and Hatcher, R. D., Jr., 1990. Implications of late deformation in the Columbus Promontory, southern Appalachians, for regional deformation and metamorphism in the Piedmont: Geological Society of America Abstracts with Programs, v. 22, p. 65.

Thomas, W. A., 1976, Evolution of Ouachita–Appalachian continental margin: Journal of Geology, v. 84, p. 323–342.

Thomas, W. A., 1977, Evolution of the Appalachian–Ouachita salients and recesses from reentrants and promontories in the continental margin: American Journal of Science, v. 277, p. 1233–1278.

Thomas, W. A., 1983, Continental margins, orogenic belts, and intracratonic structures: Geology, v. 11, p. 270–272.

Thomas, W. A., 1991, The Appalachian–Ouachita rifted margin of southeastern North America: Geological Society of America Bulletin, v. 103, p. 415–431.

Thompson, A. B., and Algor, J. R., 1977, Model systems for anatexis of pelitic rocks I: Theory and melting reactions in the system $KAlO_2$–$NaAlO_2$–Al_2O_3–SiO_2–H_2O: Contributions to Mineralogy and Petrology, v. 63, p. 247–269.

Thompson, J. B., 1957, The graphical analysis of mineral assemblages in pelitic schists: American Mineralogist, v. 42, p. 842–858.

Tobisch, O. T., and Paterson, S. R., 1988, Analysis and interpretation of composite foliations in areas of progressive deformation: Journal of Structural Geology, v. 10, p. 745–754.

Tobisch, O. T., Fleuty, M. J., Merh, S. S., Mukhopadhyay, and Ramsay, J. G., 1970, Deformational and metamorphic history of Moinian and Lewisian rocks between Strathconon and Glen Affric: Scottish Journal of Geology, v. 6, p. 243-265.

Tracy, R.J., 1982, Compositional zoning and inclusions in metamorphic rocks, *in* Ferry, J. M., ed., Characterization of metamorphism through mineral equilibria: Mineralogical Society of America Review in Mineralogy, v. 10, p. 355–397.

Treloar, P. J., Broughton, R. D., Williams, M. P., Coward, M. P., and Windley, B. F., 1989, Deformation, metamorphism, and imbrication of the Indian plate, south of the main mantle thrust, northern Pakistan: Journal of Metamorphic Geology, v. 7, p. 111–125.

Tull, J. F., and Stow, S.H., 1979, Regional tectonic setting of the Hillabee Greenstone, *in* Tull, J. F., and Stow, S. H., eds., The Hillabee metavolcanic complex and associated rock sequences: Alabama Geological Society 17th Annual Field Trip Guidebook, p. 30–33.

Tull, J. F., Stow, S. H., Long, L., and Hayes–Davis, B., 1978, The Hillabee greenstone: Stratigraphy, geochemistry, structure, mineralization and theories of origin: Mineral and Resource Institute Research Report Series, no. 1, University of Alabama, p. 1–100.

Vauchez, A., 1987, Brevard fault zone, southern Appalachians: A medium–angle, dextral, Alleghanian shear zone: Geology, v. 15, p. 669–672.

Vauchez, A., and Brunel, M., 1988, Polygenetic evolution and longitudinal transport within the Henderson mylonitic gneiss, North Carolina (southern Appalachian Piedmont): Geology, v. 16, p. 1011–1014.

Vauchez, A., Babaie, H. A., and Babaie, A., 1989, Southwestward displacement in amphibolite facies mylonites of the Inner Piedmont near the Brevard fault zone near Atlanta: Geological Society of America Abstracts with Programs, v. 21, p. 67.

Vauchez, A., Kessler, S. F., LeCorche, J. P., and Villeneuve, 1987, Southward extrusion tectonics during the Carboniferous Africa–North America collision: Tectonophysics, v. 142, p. 317–322.

Walter, K. A., 1990, Geochemistry and trace–element models for the petrogenesis of the mafic rocks in the Hayesville thrust sheet, Georgia–North Carolina Blue Ridge [Ph.D., dissert]: Knoxville, University of Tennessee, 224 p.

Watkinson, A. J., 1975, Multilayer folds initiated in bulk plane strain, with the axis of no change perpendicular to the layering: Tectonophysics, v. 28, p. T7–T11.

Wehr, F., and Glover, L., 1985, Stratigraphy and tectonics of the Virginia–North Carolina Blue Ridge: Evolution of a late Proterozoic hinge zone: Geological Society of America Bulletin, v. 96, p. 285–295.

White, S. H., Burrows, S. E., Carreras, J., Shaw, N. P., and Humphreys, F. J., 1980, On mylonites in ductile shear zones: Journal of Structural Geology, v. 2, p. 175-187.

Williams, P. F., and Zwart, H. J., 1977, A model for the development of the Seve–Köli Caledonian nappe complex, *in* Saxena, K. S., and Bhattacharji, S., eds., Energetics of Geological Processes: Springer–Verlag, New York, p. 169–187.

Williams, P. F., 1970, A criticism of the use of style in the study of deformed rocks: Geological Society of America Bulletin, v. 81, p. 3283-3296.

Williams, P. F., 1985, Multiply deformed terrains – Problems of correlation: Journal of Structural Geology, v. 7, p. 269–280.

Wilson, M., 1989, Igneous petrogenesis: London, Unwin–Hyman, 466 p.

Winkler, H. G. F., 1976, Petrogenesis of metamorphic rocks: Springer, 334 p.

Wood, D. A., Joron, J., and Treuil, M., 1979, A re–appraisal of the use of trace elements to classify and discriminate between magma series erupted in different tectonic settings: Earth and Planetary Science Letters, v. 45, p. 326–336.

Woodsworth, G. J., 1977, Homogenization of zoned garnets from pelitic schists: Canadian Mineralogist, v. 15, p. 230–242.

Yanagihara, G. M., Davis, T.L., and Hatcher, R. D., Jr., 1992, Structural relationships in the western Inner Piedmont, North Carolina: Geological Society of America Abstracts with Programs, v. 24. p. 74.

Yardley, 1989, Introduction to Metamorphic Petrology, Essex, Longman, 248 p.

APPENDICES

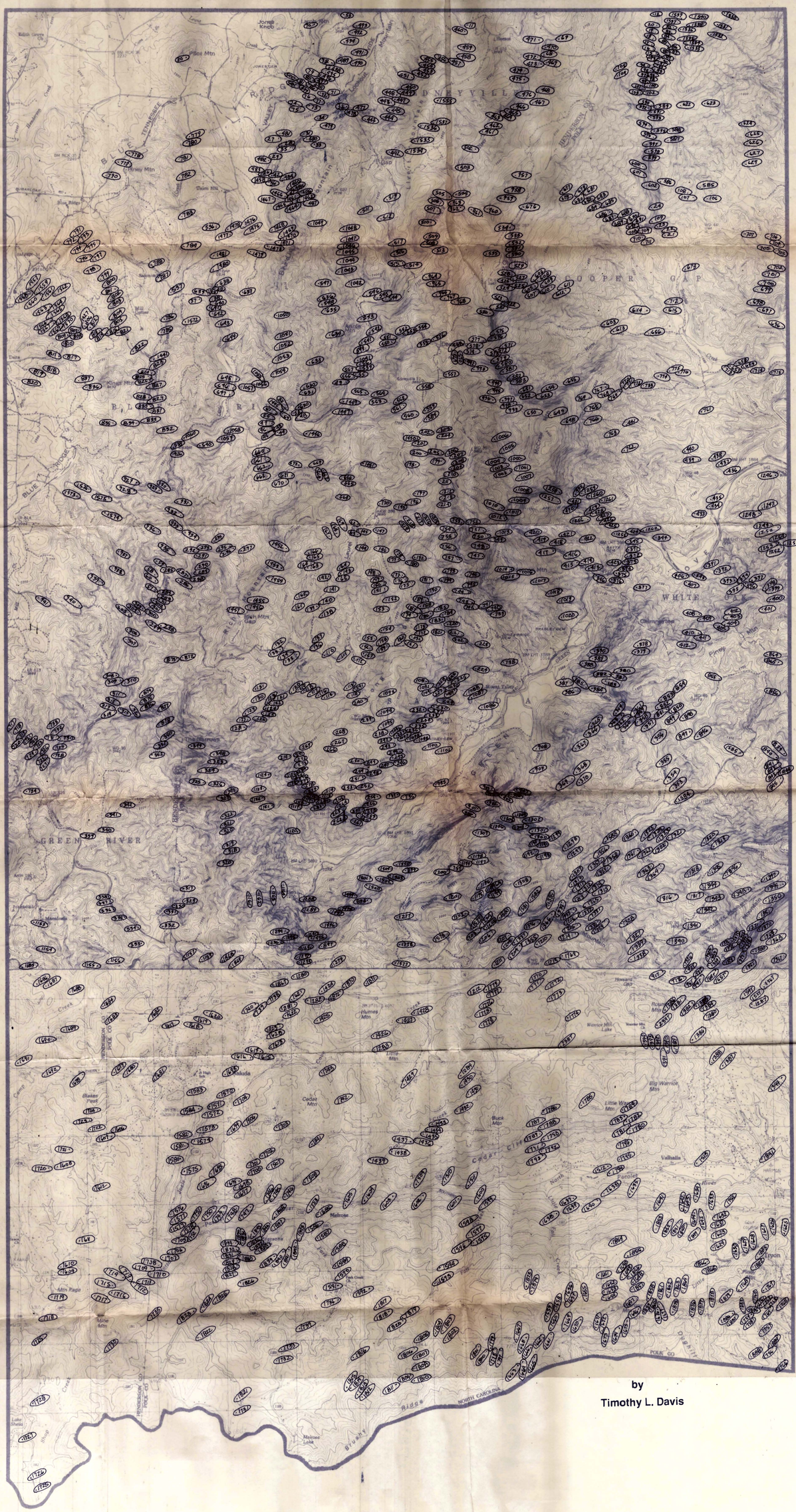
APPENDIX A

STRUCTURAL DATA

VITA

Timothy L. Davis was born on June 11, 1962 in Rensselaer, Indiana. Tim is the son of Michael and Helena Davis and the youngest of six children. Tim lived his entire adolescent and young adult life in Rensselaer. He attended the Rensselaer public schools and graduated from Rensselaer Central High School in May, 1980. In the fall of 1980, Tim began his college career at DePauw University in Greencastle, Indiana. Tim chose to major geology during the first semester of his freshman year, much to the surprise to his father who is also a geologist. Also during his freshman year, Tim joined Sigma Nu Fraternity where he began his friendship with an eclectic group of high – spirited young men who, along with Tim, pursued college life with a vengeance. During his junior year, Tim was introduced to a very interesting redhead named Sally Ann Short on a blind date to an Ohio State football game. Ironically, throughout Tim's young life he had considerable disdain for Ohio State football and red hair. Tim and Sally have been near constant companions since that initial date (Tim and Sally were married on June 20, 1987 in Xenia, Ohio). Tim graduated from DePauw University in May, 1984. In the fall of 1984, Tim started his graduate school career at Bowling Green State University where he pursued an M. S. in geology with a concentration in structural geology. Tim received his M.S. degree from Bowling Green State University in December, 1986. Tim entered the doctoral program at the University of Tennessee in the fall of 1986. Tim received his doctorate in geology from the University of Tennessee on May 14, 1993, ending a process that he and Sally thought would never end! Tim is currently employed with North Carolina Geological Survey in Raleigh, North Carolina. Tim and Sally bought their first house in December, 1992 in an historic area in Raleigh and are enjoying post–graduate school life immensely!

STATION LOCATION MAP OF THE CLIFFIELD MOUNTAIN AND NORTHERN SALUDA $7\frac{1}{2}$ MINUTE QUADRANGLES, HENDERSON AND POLK COUNTIES, NORTH CAROLINA



by

Timothy L. Davis

PLATE II

PLATE III

GEOLOGIC MAP OF THE COLUMBUS PROMONTORY, WESTERN INNER PIEDMONT, NORTH CAROLINA

compiled by

Timothy L. Davis

EXPLANATION

Blue Ridge Rocks

- garnetiferous muscovite schist
- layered muscovite gneiss and schist
- biotite metasandstone
- garnetiferous muscovite – biotite schist

Brevard Fault Zone and Chauga Belt Rocks

Brevard Fault Zone

- porphyroclastic mylonite and mylonite
- phyllonite and mylonite
- marble

Chauga Belt

- Henderson Gneiss (535 Ma *)
- granitic gneiss (438 Ma **)
- Muscovite – biotite gneiss
- Mixed mica gneiss
- Sugarloaf gneiss

Poor Mountain Formation

- amphibolite – amphibole gneiss
- mica – garnet – sillimanite schist
- quartzite
- interlayered amphibolite – quartzite

Inner Piedmont Rocks

Upper Mill Spring complex

- migmatitic biotite gneiss – metagraywacke

Lower Mill Spring complex

- porphyroclastic biotite gneiss – metagraywacke
- amphibolite – amphibole gneiss

Other Rocks

- siliceous cataclasite (flinty crushrock)

STRUCTURAL SYMBOLS

- 6 — strike and dip of foliation
- strike and dip of vertical foliation
- 6 — trend and plunge of mineral lineation
- trend and plunge of horizontal mineral lineation

CONTACTS

- stratigraphic contact

FAULTS

- Tumblebug Creek thrust – teeth on hanging wall
- Sugarloaf Mountain thrust – teeth on hanging wall
- Mill Spring thrust – teeth on hanging wall

DATA SOURCES

1	2	3
4	5	6
	7	

1. Lemmon and Dunn (1973)
2. Lemmon and Dunn (1973)
3. Tabor (unpublished, 1988 - 1990)
4. Lemmon (unpublished, 1975)
5. Davis (this study, 1987 - 1992)
6. Tabor (unpublished, 1988 – 1990)
7. Davis (this study, 1987 – 1992)

* Odom and Fullagar (1973)

** Odom and Russell (1978)

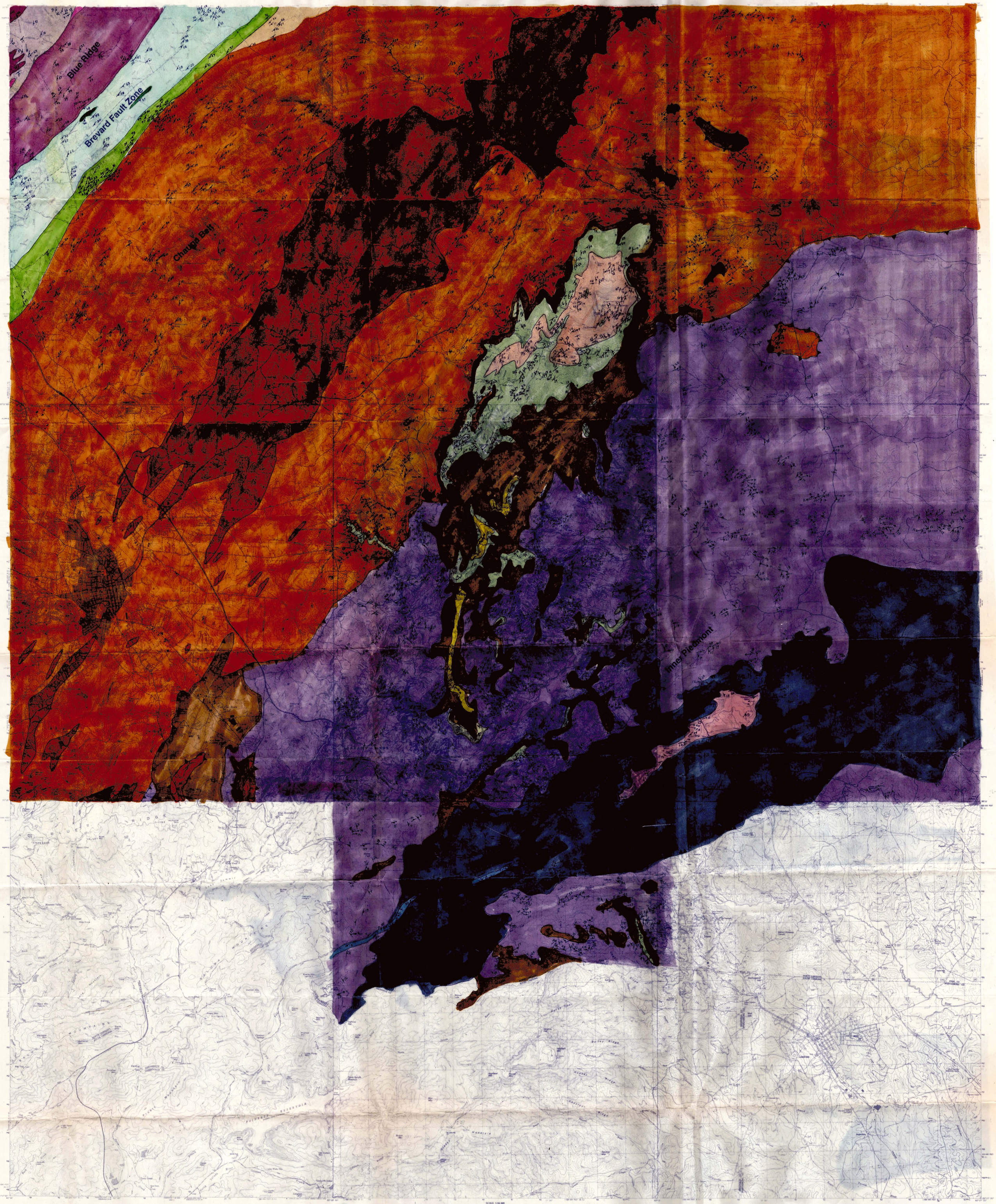


PLATE III